The Role of Sugar-sweetened Water in the Progression of Nonalcoholic Fatty Liver Disease

by

Yuwen Luo

A dissertation submitted to the Graduate Faculty of
Auburn University
in partial fulfillment of the
requirements for the Degree of
Doctor of Philosophy

Auburn, Alabama
December 10, 2016

Keywords: Nonalcoholic fatty liver disease, adipose tissue, fructose, high-fat Western diet, RNA-seq, ORM

Approved by

Michael W. Greene, Chair, Assistant Professor, Nutrition, Dietetics and Hospitality Management
Kevin W. Huggins, Associate Professor, Nutrition, Dietetics and Hospitality Management
Ramesh B. Jeganathan, Associate Professor, Nutrition, Dietetics and Hospitality Management
Robert L. Judd, Associate Professor, Anatomy, Physiology and Pharmacology

Abstract

Nonalcoholic fatty liver disease (NAFLD), which ranges from simple steatosis (fatty liver) to nonalcoholic steatohepatitis (NASH), has become the most common chronic liver disease in both children and adults, paralleling the increased prevalence of obesity and diabetes during the last decades. The rise in NASH prevalence is a major public health concern because there are currently no specific and effective treatments for NASH. In addition, the molecular mechanisms for the progression of steatosis to NASH remain largely undiscovered. To model the human condition, a high-fat Western diet that includes liquid sugar consumption has been used in mice. A high-fat Western diet (HFWD) with liquid sugar [fructose and sucrose (F/S)] induced acute hyperphagia above that observed in HFWD-fed mice, yet without changes in energy expenditure. Liquid sugar (F/S) exacerbated HFWD-induced glucose intolerance and insulin resistance and impaired the storage capacity of epididymal white adipose tissue (eWAT). Hepatic TG, plasma alanine aminotransferase, and normalized liver weight were significantly increased only in HFWD+F/S-fed mice. HFWD+F/S also resulted in increased hepatic fibrosis and elevated collagen 1a2, collagen 3a1, and TGFβ gene expression. Furthermore, HWFD+F/S-fed mice developed more profound eWAT inflammation characterized by adipocyte hypertrophy, macrophage infiltration, a dramatic increase in crown-like structures, and upregulated proinflammatory gene expression. An early hypoxia response in the eWAT led to reduced vascularization and increased fibrosis gene expression in the HFWD+F/S-fed mice. Our

results indicate that the high fat Western diet plus liquid sugar consumption model of obesity is a good model for NAFLD research and likely other clinical conditions associated with adipose tissue dysfunction.

The prevalence of obesity-related NAFLD and limitations of available therapeutic options highlight the need for identifying specific gene and pathway changes that drive progression of NAFLD using state-of-the-art sequencing analysis of human biospecimens or relevant animal models. RNA-seq analysis of a high fat Western diet model of NAFLD revealed differentially expressed genes (DEGs) associated with both HFWD (HFWD vs. Chow; 1065DEGs) and HFWD+F/S (HFWD+F/S vs Chow; 1689 DEGs). However, the addition of liquid sugar consumption resulted in 760 DEGs in the liver of HFWD+F/S-fed mice, which are mainly enriched in small GTPase mediated signal transduction, and lipid homeostasis biological processes. Further, pathway analysis showed pathways in immune response, fibrosis and cancer are major pathways enriched in the livers of HFWD+F/S-fed mice. Our study identified key genes, biological processes and pathway changes in the liver of HFWD+F/S mice and provided a molecular basis for understanding the mechanism through which the addition of liquid sugar promotes the progression of NAFLD.

In addition, RNA-seq analysis also revealed hepatic expression of ORM3 gene was significantly elevated by 20-fold in HFWD+F/S-fed mice. Further validation of ORM3 hepatic expression in an independent dietary treatment experiment confirmed our RNA-seq findings, and found ORM1 and ORM2 hepatic expression was significantly elevated to a similar level as ORM3. Correlation analysis of ORM3 gene expression with NAFLD parameters examined in our recently published study indicated that ORM3 gene expression was significantly positively correlated with body weight, normalized liver weight, and alanine aminotransferase, a marker of

liver dysfunction. Moreover, the gene expression of ORM was also induced in a cellular model of insulin resistance. Furthermore, ORM was observed to promote macrophage polarization toward an anti-inflammatory phenotype. Our observations suggest that ORM might have a protective role in NAFLD by regulate cellular insulin resistance and pro-inflammatory macrophages.

Acknowledgments

I would like to express my deepest gratitude to my advisor, Dr. Michael W. Greene, for his excellent mentorship throughout my course of study. I appreciate his encouragement, freedom to explore, and his insightful interpretations, which inspired me to ask meaningful research questions and motivated me to perform at my best. His patience and support has been an immense help in completing this dissertation. I would also like to thank Dr. Kevin Huggins, Dr. Ramesh Jeganathan, Dr. Robert Judd, and Dr. Richard Curtis Bird for serving on my dissertation committee, and guiding my research. I express my gratitude to Dr. Ann Marie O'Neill for her guidance and help in experiment preparation. I acknowledge and extend gratitude for the financial support received from the Auburn University start-up funds, USDA Hatch Grant and NDHM Graduate Research Award.

I would like to express my deepest gratitude and gratefulness to my husband Mr. Yi Zhang for being a constant source of inspiration and motivation, for his enduring love and immense moral support at every step. I would also like to thank my parents Mr. Jingyuan Luo and Ms. Ruyu Gu for their unconditional love and support. I want to specially mention Dr. Jian Zhang, Mr. Michael Wayne, Ms. Lauren Woodie, and Mr. Bulbul Ahmed for their contribution. I thank my colleagues Mr. Vishal Kothari, Dr. Chen Zheng, Ms. Yueru Li, Ms. Yuxuan Zhang, Ms. Yijing Qi, and Dr. Shraddha Rege. It was a great pleasure studying and working together. I express my sincere gratitude to all faculty members in the Department of Nutrition, Dietetics and Hospitality

Managements, and the College of Veterinary Medicine at Auburn University for giving me this valuable opportunity and excellent atmosphere to conduct my research. Last but not least, I would like to specially mention my dog Brownie for his love and company during my PhD study.

Reference Style

This document is referenced using the citation style of the *Journal of Hepatology*

Table of Contents

List of Tables

List of Figures

Chapter 1: Introduction

Obesity is linked to the pathogenesis of nonalcoholic fatty liver disease (NAFLD), from the seeming benign condition of fatty liver all the way to nonalcoholic steatohepatitis (NASH), which can lead to the more serious clinical conditions of cirrhosis and liver cancer (hepatocarcinoma). The overall prevalence of NASH in the adult US population resembles that of type 2 diabetes [1, 2] and is expected to rise like that of type 2 diabetes [3]. The rise in NASH prevalence is a major public health concern because current treatment options for NAFLD are limited and ineffective [4]. In addition, the molecular mechanisms for the progression of steatosis to NASH remain largely undiscovered. Lack of such knowledge represents an important problem because new therapeutic targets are needed for the treatment of NASH.

NAFLD is believed to be initiated by the accumulation of lipids in the liver (steatosis) and is thought to be a relatively benign state [5]. The diagnosis of NASH is based on the presence of steatosis, inflammation, hepatocyte ballooning, and importantly fibrosis and is still dependent upon a needle biopsy of the liver [6]. In the absence of significant inflammation, there is no risk of liver-related complications in NAFLD patients followed long-term [7]. The exact etiology for transformation of steatosis to NASH remains obscure; however, a classical "two-hit" hypothesis has been proposed to explain progression [8]. Steatosis constitutes the "first hit." Lipid accumulation is regulated by genes involved in lipogenesis, β-oxidation, fatty acid synthesis and uptake, and VLDL export [9]. Pro-inflammatory cytokines (*e.g.* tumor necrosis factor-alpha,

TNFα), oxidative stress, and lipid peroxidation constitute the "second hit" leading to NASH. Later, a further component, or "third hit" has been proposed by Diehl's group [5] suggests that hepatocyte death leads to an inappropriate repair mechanism resulting in the activation of hepatic stellate cells and the production of factors promoting fibrosis. Recently an alternative "non-triglyceride lipotoxicity" hypothesis has been put forward implicating metabolites of free fatty acids in hepatocyte injury and development of NASH [10]. In the lipotoxicity hypothesis model, steatosis is actually protective because it stores lipid in a non-toxic form (i.e. triglyceride). Hepatic free fatty acids and triglyceride deposition are derived from adipocyte stores and *de novo* lipogenesis, which are both regulated by insulin. In insulin resistant states, in which insulin does not work at normal concentrations and is characterized by hyperinsulinemia, inappropriate adipocyte lipolysis and hepatic *de novo* lipogenesis contribute to the development of fatty liver [11]. Hepatic insulin resistance can drive insulin resistance in other insulin target tissues [12] and has been shown to develop in mice fed a high fat diet prior to muscle and adipose tissue insulin resistance [13]. Insulin resistance is also thought to play a central role in the development of NAFLD and NASH in non-obese populations.

High fat diets (typically lard based) are commonly used to model human obesity because they develop increased fat mass, insulin resistance, and hepatic steatosis; however, the progression of NAFLD to steatohepatitis is not observed in these mouse models [14]. The high fat Western diet (HFWD) with liquid fructose/sucrose (F/S) model of obesity in mice was originally developed as a model of NAFLD progression [15-17]. Indeed the presence of liquid fructose in the diet may exacerbate fat deposition, inflammation, oxidative stress, and fibrosis in the liver but maybe not systemic glucose intolerance and insulin resistance [15-17]. Importantly, the HFWD + liquid F/S model of obesity is clinically relevant as it appears to model obese humans with mild NASH

[18]. Given the importance of the HFWD + liquid F/S consumption model of obesity and NAFLD, the purpose of this study was to determine the role of liquid sugar in the progression of NAFLD.

Chapter 2: Review of Literature

2.1 Nonalcoholic Fatty Liver Disease

2.1.1 Introduction and definitions

Nonalcoholic fatty liver disease (NAFLD) is becoming an important public health concern due to its increasing prevalence in parallel with that of obesity and diabetes observed in both children and adult [19]. Hepatic steatosis (the presence of fat in liver parenchyma without inflammation) in the absence of excess alcohol consumption (less than 140g/week in men and 70g/week in women) [20] . NAFLD represents a spectrum of disease, ranging from simple steatosis (>5% fat infiltration, with/without minimal inflammation) to steatohepatitis (the presence of fat in liver parenchyma with inflammation, hepatocyte ballooning and lobular inflammation) through to fibrosis and cirrhosis [21]. Simple steatosis is thought to be a relatively benign state, whereas nonalcoholic steatohepatitis (NASH) represents the advanced form of NAFLD potentially (20%) progressive to fibrosis and cirrhosis over a 15-year time period [22]. NAFLD is strongly associated with features of metabolic syndrome, including obesity, insulin resistance (IR) or type 2 diabetes mellitus (T2DM), and dyslipidemia, it is thus considered the hepatic manifestation of metabolic syndrome [23]. NAFLD is an independent risk factor for cardiovascular disease (CVD) and predicts future events, independently of other risk factors such as age, gender, low density lipoprotein (LDL) cholesterol, smoking and other features of metabolic risk factors [24].

To date, cardiovascular disease remains the leading cause of death in patients with NAFLD, followed by malignancy and liver disease [23]. NAFLD is also associated with increased risk of all-cause mortality, contributed by liver related deaths as well as non-liver related causes such as malignancy, diabetes and coronary artery disease [25].

2.1.2 Prevalence and incidence

The estimates of prevalence and incidence of NAFLD are vary by the population studied (e.g., patients with different ethnicities, sex, and comorbidities) and limited by several biases, such as the lack of sensitivity and specificity of the test used for the diagnosis (abnormal liver enzymes and/or hepatic ultrasound), the relatively short-term follow up of many observational studies and the composite nature of outcomes [26]. Recently, a systemic review of studies regarding to the epidemiology and progression of NAFLD from 1989 to 2015 indicated that the global prevalence of NAFLD is 25.24% with highest prevalence in the Middle East (31.39%) and South America (30.45%) and lowest in Africa (13.48%) [26]. In the US population, the prevalence of hepatic steatosis and NAFLD were 21.4% and 19.0%, respectively, corresponding to estimates of 32.5 million adults with hepatic steatosis and 28.8 million adults with NAFLD nationwide [27]. After adjustment for age, income, education, body mass index (BMI), and diabetes status, NAFLD was more common in men (20.2%) compared to women (15.8%) [27]. Furthermore, ethnic differences in the prevalence of NAFLD have been reported in a study using proteome magnetic resonance spectroscopy of the liver in the U.S.[28]. It revealed a significantly higher prevalence of NAFLD in Hispanics (45%) than in Caucasians (33%) and African Americans (24%). The higher prevalence in Hispanics mirrors the similar higher prevalence of obesity and IR in that group. However, the lower frequency of hepatic steatosis in African Americans was not

explained by factors such as BMI, IR, alcohol, or medication [28]. The prevalence of NAFLD rises substantially when groups with known metabolic risk factors are studied, for example, the overall prevalence of NAFLD in the morbidly obese ranges from 75% to 92% while the prevalence in patients with T2DM is estimated to be between 60% and 70% [26]. The prevalence of NASH is difficult to determine owing to the fact that diagnosis still requires invasive liver biopsy. The results of a systematic review in 2016 placed the prevalence of NASH at 3-5% [29]. In at risk populations, NASH is thought to be present in 25-30% of patients with obesity or T2DM and in 35% of severely obese patients with T2DM [25]. There is no precise data on the incidence rates for NAFLD because of the variation in diagnosis and also due to the fact that a large number of patients may be asymptomatic. Nevertheless, given that the prevalence of obesity in US adults has almost doubled since the early 1960s (1962–48% vs 2010–75%), the incidence of obesity-related NAFLD has almost certainly increased [30].

2.1.3 Natural history

There are a limited number of prospective, longitudinal studies with long-term histologic follow-up of patients with NAFLD. In addition, even liver biopsies are not fully accurate in assessing the severity and progression of disease. In NAFLD, simple steatosis is regarded as the presence of fat in > 5% of hepatocytes, and in about 20-25% of cases, it progresses to NASH and of these patients with NASH, 25-35% will develop fibrosis and subsequently cirrhosis [31] (Fig. 1). Considering available data from community-based and cohort studies, NAFLD is associated with a significantly higher overall mortality compared to the general population, even when cofounders such as metabolic factors are adjusted [32]. In one community-based cohort study of 420 patients from U.S., NAFLD patients had a 34% increase in hazard ratio for overall mortality

[33]. Liver-related disease is the third most common cause of death in large cohorts to patients with NAFLD [33, 34]. A recent meta-analysis also demonstrated that NAFLD increases the risk for all-cause mortality [35]. However, the understanding of natural history is limited by lack of long-term follow-up, difficulties with diagnosis, under-diagnosis, and other confounding factors.

2.1.4 Pathogenesis of NAFLD

2.1.4.1 Two hit hypothesis/current theories

The exact etiology for transformation of steatosis to NASH remains obscure, however, a classical "two hit hypothesis in NAFLD" [Fig. 2. (a)] has been proposed in 1998 by Day et al. to explain progression [8]. The first hit, hepatic triglyceride (TG) accumulation, or steatosis, increases susceptibility of the liver to injury mediated by "second hits", such as inflammatory cytokines/adipokines, mitochondrial dysfunction and oxidation stress, which in turn lead to steatohepatitis and/or fibrosis [8, 36]. However, there is increasing recognition of the role that free fatty acids (FFA) play in directly promoting liver injury, which has led to modification of this theory [Fig.2. (b)]. It is generally accepted that the initiating events in NAFLD are dependent on development of obesity and IR in liver and adipose tissue. In obesity and IR there is an increased influx of FFA to the liver, derived from the non-esterified fatty acid pool (NEFA) via dys-regulation of peripheral lipolysis, de novo lipogenesis (DNL), and dietary fats. These FFA either undergo β-oxidation or are esterified with glycerol to form TGs, leading to hepatic fat accumulation. Accumulation of lipotoxic intermediates such as diacylglycerol (DAG) cause hepatic IR [37]. Increased FFA flux to the liver in turn places hepatocytes under considerable metabolic load and promotes hepatocyte lipotoxicity and endoplasmic reticulum (ER) stress [25]. Actually, the accumulation of TGs within the liver is considered an early adaptive response

through which may be a protective mechanism by preventing the toxic effects of un-esterified FFA [38]. Then, the additive effects of endotoxin-Toll-like receptor 4(TLR4)-induced cytokine release by Kupffer cells (KCs) and immune-mediated hepatocellular injury to induce cellular damage and activate cell death pathways, promoting the transition to NASH [25]. There is now substantial evidence that FFA can directly cause toxicity by increasing oxidative stress and by activation of inflammatory pathways [39]. When increased oxidative stress and inflammation persist, stellate cell activation, collagen deposition and hepatic fibrosis occur [25].

Later, a further component, or "third hit" has been proposed to reflect inadequate hepatocyte proliferation [Fig. 2. (c)]. In the healthy liver, cell death stimulates replication of mature hepatocytes, which replaces the dead cells and reconstitute normal tissue function [5]. However, under NASH condition, oxidative stress inhibits the replication of mature hepatocytes [21]. In chronic liver injury, the development of fibrosis/cirrhosis is dependent on the efficacy of hepatocyte regeneration, and therefore cell death with impaired proliferation of hepatocyte progenitors represents the proposed "third hit" in NAFLD pathogenesis [5].

2.1.4.2 Lipid accumulation/steatosis

Lipid handling in the liver is maintained by a delicate balance among delivery of FFAs to the liver and its usage by either esterification or oxidation, and turnover [25]. The balance was maintained by a complex interplay of hormones, nuclear receptors, intracellular signaling pathways, and transcription factors and is summarized in Fig. 3. FFAs arise in the liver are from three distinct sources: lipolysis (the hydrolysis of FFA and glycerol from TG) within adipose tissue, dietary sources, and DNL [25]. In contrast, FFA may be utilized either through β-oxidation, re-esterification to TG and storage as lipid droplets, or packaged and exported as very

low density lipoprotein (VLDL) [25]. Therefore, liver steatosis, characterized by the accumulation of TGs, can occur as a result of increased fat synthesis, increase fat delivery, decreased fat export, and/or decreased fat oxidation [21]. A study used a multiple-stable-isotope method to establish the relative contribution of lipid accumulation in patients with NAFLD, demonstrating that approximately 60% of liver TG content derived from FFA influx from adipose tissue, 26% from DNL, and 15% from diet [40]. This contrasts with healthy individuals in whom DNL contributes <5% of hepatic TG formation [41].

2.1.4.2.1 FFAs delivery

Dietary fats are first absorbed in the intestinal lumen. The liver is essential for enterocyte hydrolyzed lipid absorption via bile acids. Once absorbed, FFAs which have a chain length of less than 14 carbons enter directly into the portal vein system and are transported to the liver, while FFAs with 14 or more carbons are esterified and packaged into nascent chylomicrons, and released into the circulation via the lymphatic system [42]. Once in the circulation, nascent chylomicrons mature by gaining apolipoprotein E (apoE) and apolipoprotein C2 (apoC2). Gain of apoC2 activates lipoprotein lipase (LPL) which hydrolyzing TG into glycerol and FFAs [42]. FFAs are partially taken up by adipose tissue with the remainder transported in chylomicron remnants and taken up by the liver after binding with the apoE receptor [42]. In addition to dietary FFAs, NEFA pool is another source of hepatic FFAs. In an insulin-resistant state the NEFA pool is greater due to increased adipocyte lipolysis. FFAs are taken up, not only passively but also in a facilitated manner by FATP2 and FATP5 [43]. In mouse hepatocytes, adenovirus-mediated knockdown of FATP2 or genetic deletion of FATP5 significantly decreases the rates of FFA uptake and TG storage [43].

2.1.4.2.2 Hepatic lipogenesis

Liver FFAs, sourced from DNL, the NEFA pool, and dietary fat, are further processed to form TGs for storage, oxidized by mitochondria to create energy and ketones, added to lipoproteins for secretion as VLDL, or used to synthesize phospholipids, depending on ongoing metabolic requirements. Acetyl-CoA carboxylase (ACC), fatty acid synthase (FAS), and stearoyl-CoA desa turase 1(SCD1) are predominant enzymes that catalyze hepatic FFA synthesis, while DNL is tightly controlled on a transcriptional level by insulin and glucose, via Sterol regulatory element-binding protein 1(SREBP-1c) and carbohydrate-responsive element-binding protein (ChREBP), respectively [44]. The activity of lipogenesis is regulated by a nuclear receptor, liver X receptor (LXR) [45]. LXRs controls the expression lipogenic genes such as ACC, FAS, and SCD1 as well as transcription factors SREBP-1c and ChREBP [46].Therefore, LXR plays both a direct and an indirect role in the regulation of lipogenesis. LXR together with ChREBP and SREBP-1c belong to a network of nutrient sensing factors involved in the control of hepatic FA synthesis and thereby TG accumulation. So far, the relative importance of these transcription factors in controlling the synthesis of fat in response to glucose and insulin signals has been difficult to ascertain because they act either independently and/or synergistically to regulate their target genes.

2.1.4.2.3 Hepatic FFA oxidation

FFAs are the most efficient energy yield for homeostasis, compared with other macronutrient subtypes. FFAs may be oxidized in the mitochondria, peroxisomes, or microsomes. However, β-oxidation of FFAs in the mitochondria is the predominant energy source in the fasted state. FFAs

are broken down into acetyl-CoA, which then enters the citric acid cycle. Yet, for FFAs to be used in β-oxidation pathways, they need to be transported from the cytoplasm into the mitochondria, although short- and medium-chain fatty acids simply diffuse across the mitochondrial membrane, long-chain fatty acids (LCFAs) are activated by ayl-CoA-synthetase to acyl-CoA in the cytosol. LCFAs are shuttled across and catalyzed by carnitine palmitoyl transferase 1 (CPT-1) on the outer mitochondrial membrane. Malonyl-CoA, a key intermediary of DNL, is an inhibitor of CPT-1, as is insulin [47]. This step is promoted by PPARα, which also up-regulates FFAs transport proteins and enzymes related to apolipoprotein B (apoB) metabolism [47]. When FFAs are in abundance, acetyl-CoA can be converted into ketone bodies rather than enter the citric acid cycle [47].

2.1.4.2.4 Hepatic glucose metabolism

Carbohydrate intake can also influence FFA metabolism in the liver. Excess glucose is normally stored as glycogen under the influence of insulin. They also can provide the glycerol backbone via triose phosphate or acetyl-CoA, which can be further esterified into TGs or packaged into VLDL via DNL. After a meal, glucose is delivered to the hepatocyte by the portal vein and is taken up by glucose transporter type 2 (GLUT2), independent of insulin signaling. Once in the hepatocyte, glucose is phosphorylated to glucose-6-phosphate by liver glucokinase. Mutation in the glucokinase gene has been implicated in NAFLD pathogenesis. Glycolysis, an insulin dependent 10-step process, metabolizes glucose to pyruvate with a net gain of two ATP and two NADH molecules per glucose molecule. Key enzymes involved in regulation are glucokinase, phosphofructokinase, adenosine monophosphate (AMP), and pyruvate kinase. Pyruvate kinase is activated by phosphoenolpyruvate and limited by ATP abundance. ChREBP induces

transcription of pyruvate kinase in the presence with glucose, while insulin, adrenaline, and glucagon regulate pyruvate kinase via the phosphoinositide 3-kinase (PI3K) pathway (132). Pyruvate undergoes decarboxylation to acetyl-CoA, which is then processed in the metabolic citric acid cycle or utilized in anabolic pathways such as DNL, as mentioned above. Insulin also activates glycogen synthesis via repression of protein kinase A (PKA), an inactivator of glycogen synthase, the key enzyme catalyzing uracil-diphosphate glucose to glycogen. When glucose levels start to wane, the liver provides the body with energy by breaking down and converting glycogen into glucose; during prolonged fasting, hepatic gluconeogenesis occurs, providing glucose-6-phosphate as a substrate for the synthesis of glucose [25].

2.1.4.3 Insulin resistance

In healthy individuals, binding of insulin receptor leads to phosphorylation of several substrates including insulin receptor substrates (IRS)-1, -2, -3, and -4, which propagate the insulin signal [21]. Insulin stimulation of IRS-1 and -2 leads to activation of intracellular PI3K and AKT pathways, which are intimately involved in mediating the metabolic effects of insulin [48]. AKT activation then results in translocation of glucose transporter, GLUT4, containing vesicles to the plasma membrane, thus facilitating glucose uptake. Meanwhile, the expression of key lipogenic genes is increased, with a concomitant decrease in gluconeogenesis gene expression via its regulation of forkhead (FOXO) transcription factor activity.

Insulin has a potent action to suppress adipose tissue lipolysis. However, in situations of IR, this suppression is impaired resulting in an increased efflux of FFA from adipose tissue to liver [49]. Fig.4. summarizes the main processes contributing to IR and hepatic steatosis. Specifically, obesity, recruitment of macrophages to adipocytes, and increased secretion of pro-inflammatory

adipokine (TNFα) lead to the impairment in insulin-mediated suppression of lipolysis in adipocytes. Increased lipolysis in adipose tissue results an increased NEFA pool in NAFLD and thus, the accumulation of intra-myocelluer lipids in skeletal muscle, which interferes with insulin signaling and impairs glucose uptake. The scenario leads to the development of peripheral IR and a compensatory hyperinsulinemia, resulting in increased delivery of FFAs to the liver. Hyperinsulinemia associated with IR leads to: (1) up-regulation of the transcription factor SREBP-1c and ChREBP, which are key transcriptional regulators of genes involved in DNL[44]. Gluconeogenesis is not suppressed by hyperinsulinemia, providing more substrates for DNL. And (2) inhibition of β-oxidation and VLDL assembly thus further promoting buildup of TGs in the liver [48]. In addition, metabolites such as DAG further amplify hepatic IR.

2.1.4.3.1 Liver and insulin resistance

The development of NAFLD is strongly associated with hepatic IR. Animal studies implicated that hepatic IR is activated by FFA, cytokines (TNFα/IL6) and ER stress, and mediated by nuclear factor kappa B (NF-κB) and c-Jun N-terminal kinase (JNK) inflammatory pathways. However, recent data suggest that lipid metabolites themselves can cause IR. DAG is an intermediate in the conversion of FFA into TG. Accumulation of hepatic DAG within cytosolic lipid droplets is associated with increased translocation of the primary novel protein kinase C (PKC) isoform in the liver, PKCε, to the plasma membrane where it binds and inhibits the intracellular kinase domain of the insulin receptor [50]. Similar processes occur in skeletal muscle cells, leading to a more generalized state of IR. In a recent translational study in a group of obese, non-diabetic patients undergoing bariatric surgery, although all patients were obese, there was significant variation in IR; DAG content and PKCε activation were the strongest

predictors of hepatic IR and accounted for 60% of the variability in hepatic insulin sensitivity [51]. PKCδ is another PKC isoform that has been shown to play an important role in the development of hepatic IR in both mice and humans [52]. PKCδ is activated in the liver of obese Zucker rats and mediates diet-induced whole body IR and hepatocyte cellular IR [53]. Mice with liver-specific overexpression of PKCδ developed hepatic IR characterized by decreased insulin signaling, enhanced lipogenic gene expression, and hepatosteatosis [52]. In contrast, PKCδ-null mice fed a high-fat diet (HFD) exhibited increased insulin sensitivity, reduced liver TG accumulation and diminished lipogenic enzymes production [54].

2. 1.4.3.2 Adipose tissue and insulin resistance

Adipose tissue is the major source of FFA and responsible for 60% of TG accumulation. In human, the expansion of adipose tissue results from increased numbers of individual adipocytes (hyperplasia), and from the hypertrophy of adipocytes, in a depot-dependent manner [55]. There is a large individual variation in size and expandability of different adipose tissue, so it is critically important in understanding the relationship between obesity and IR, as adipose tissue is a metabolically active organ that plays a crucial role in regulating insulin sensitivity. Previous studies had suggested that obese individuals often have enlarged adipocytes due to lipid overload [56]. It has been shown that enhanced expansion of subcutaneous fat is correlates with decreased risk of glucose and insulin abnormalities, whereas increased expansion of visceral fat, is associated with IR [57].

2.1.4.3.2.1 Visceral adipose tissue adipokines production

Visceral adipocytes are more likely to be infiltrated with macrophages, undergo inflammation, and secrete inflammation cytokines such as TNFα, interleukin (IL)-6 and monocyte chemoattractant protein 1(MCP-1), all of which blunt adipocyte insulin sensitivity [58]. TNFα is expressed more in visceral fat than subcutaneous fat, and activates two pro-inflammatory pathways: NF-κB and JNK pathway [58]. MCP-1 is an important chemokine for macrophage migration into adipose tissue, which is increased in visceral fat [59]. Conversely, adipokines that repress IR and steatosis show decreased secretion in visceral fat. Adiponectin acts to modulate lipid metabolism and decrease inflammation via AMP-activated protein kinase (AMPK) and PPARα pathway [60]. It also improves insulin sensitivity as a result of mitogen-activated protein kinase (MAPK)-mediated improvement in FA oxidation and decreased liver gluconeogenesis [60]. Patients with NAFLD have been reported to have low adiponectin levels [61]. Mice with steatotic livers have improved insulin sensitivity, decreased steatosis, and lower levels of TNFα when treated with recombinant adiponectin [62]. Leptin is another adipokines that is reported to have a role in hepatic steatosis, as leptin deficient mice (*ob/ob*) become obese, hyperphagic, and diabetic and develop marked steatosis, indicating a role for leptin in prevention of fatty liver either indirectly through central neural pathways or directly via hepatic activation of AMPK [9]. However, obese patients who have a fatty liver also have a high level of leptin, suggesting they may have developed resistance to leptin [9].

2.1.4.3.2.2 Excessive and ectopic lipid deposition

Despite a highly evolved ability of adipose tissue to sequester fat, the storage capacity of single adipocytes is finite [57]. Enlarged adipocytes display IR without much macrophage infiltration into adipose tissue following a short HFD [63]. Thus, even without inflammatory responses,

excess lipid in adipose cells results in IR. One plausible hypothesis is that excess lipid accumulation in adipocyte, and ectopic lipid accumulation in liver and muscle may lead to IR through the formation of metabolically toxic products, for example, ceramide and DAG [50]. These lipotoxic products may activate signaling pathways, for example, one or more of the protein kinase C protein's that negatively impact upon insulin signal transduction [64].

2.1.4.4 Inflammation/steatohepatitis

2.1.4.4.1 Hepatic lipotoxicity

A surplus of FFAs in non-adipose cells may enter deleterious pathways leading to cell dysfunction (lipotoxicity) and apoptotic cell death (lipoapoptosis) [56]. FFA can induce these effects through several mechanisms that may differ across different cell types. In liver, the overloading of hepatocytes with FFAs has been linked to hepatocyte apoptosis and liver injury [65]. SCD1, the enzyme that converts saturated fatty acid (SFA) to monounsaturated fatty acids, plays a key role in lipotoxicity and lipoapoptosis. SCD-1 knockout mice fed an MCD diet accumulated less TG compared with wild-type mice but had increased hepatocyte apoptosis and liver injury [65]. The results support a model in which during the development of NAFLD, overflow of FFAs to the liver is associated with an increase in SCD1 expression and activity resulting in a tilt of the balance towards MUFA formation, TG storage, liver adaptation and development of isolated hepatic steatosis. In contrast, SCD1 deficiency results in hepatic over-accumulation of SFA triggering hepatocellular apoptosis, liver damage and development of NASH [66]. In addition, recent data suggested that free cholesterol (FC), another lipid metabolite, could sensitize hepatocytes to TNFα and Fas-induced apoptosis [67]. TNFα treatment of FC-loaded hepatocytes caused apoptosis and ROS in livers, in part due to

glutathione reduction in mitochondria [67]. It has been reported that FC in the liver increases with disease progression from steatosis to NASH [66]. The mechanisms resulting in overloading FC in NAFLD remain incompletely known but could be related to mitochondrial abnormalities [66]. A recent study highlighted the emerging role of FC in the pathogenesis of human NAFLD by examining the expression of enzymes that regulate cholesterol homeostasis [68]. Both SREBP-2 (a transcriptional factor that plays an important role in cholesterol synthesis) and StAR (a transporter of FC from the external to the internal mitochondrial membranes) were overexpressed in patients with NASH compared to those with simple steatosis. These findings suggest a role of mitochondrial FC in disease progression from steatosis to NASH.

2.1.4.4.2 Inflammatory cytokines

A growing body of evidence supports a central role of inflammatory cytokines in the progression from fatty liver to NASH. Increased levels of FFAs and consequent lipotoxicity, IR, peripheral adipose tissue dysfunction and gut derived endotoxins concur in activating and maintaining the production and release of pro-inflammatory cytokines, both systemically and locally in the liver [69]. The mechanism through inflammatory cytokines contributing to hepatic inflammation is mainly through activation of the Iκκ-β/NF-κB and JNK-AP-1 inflammatory pathways [69]. As previously mentioned, JNK is a member of mitogen activated protein kinases, in addition to impair insulin signaling, is also associated with activation of apoptosis and development of NASH. JNK silencing in animal models leads to decreased steatosis and NASH [70]. NF-κB is a transcription factor and a primary regulator of inflammatory activation, and its inhibitor of κB (IκB) kinase (IKK)2 subunit is the major component required for its activation during the acute inflammatory response [69]. In animal models of HFD-induced steatosis, increased NF-κB

activity is associated with elevated hepatic expression of inflammatory cytokines such as TNF-α, IL6 and interleukin 1-beta (IL1β), and activation of KCs [71]. Liver specific NF-κB inhibition prevents HFD-induced inflammatory gene expression, whereas HFD-induced hyperglycemia and IR can be reproduced by selective over-expression of IKK-β in hepatocytes [71]. Studies in animal models demonstrated that hepatic exposure to increased levels of pro-inflammatory cytokines leads to histological changes typically seen in NASH, such as hepatocyte necrosis and apoptosis, neutrophil chemotaxis, activation of hepatic stellate cells (HSCs) and production of Mallory bodies [69]. Furthermore, serum and hepatic level of TNFα are increased in patients with NASH and correlate with histological severity of liver damage [69].

2.1.4.4.3 Oxidative stress and mitochondrial dysfunction

The role of oxidative stress and mitochondrial dysfunction in NASH is well-established, with more advanced disease correlating with greater degrees of oxidative stress [21]. β-oxidation of short-, medium-, and long-chain fatty acids takes place in the mitochondria under physiological conditions. In the event of hepatocyte FFA overloading, this process become overwhelmed and give rise to reactive oxygen species (ROS) [56]. Meanwhile, physiologically minor pathways such as β-oxidation in the peroxisome, and cytochrome P450-4A- and P450-2A1- mediated ω-oxidation in the ER further increase hepatocyte ROS production [25]. ROS induce oxidative stress, which further results in nuclear and mitochondrial DNA damage, phospholipid membrane disruption by lipid peroxidation, and the subsequent activation of inflammatory pathways [56]. A marker for oxidative stress, 3-nitrotyrosine, was found elevated in liver biopsies with NASH [25]. In addition, structural mitochondrial abnormalities and a reduction in mitochondrial respiratory chain activity have been observed in human studies of NASH [72]. Moreover,

elevated expression and activity of hepatic microsomal FA oxidizing enzyme cytochrome P450 2E1 (CYP2E1) which has been observed in human and animal models of NASH represents a potent source of ROS [21]. Importantly, transgenic over-expression of CYP2E1 activity is associated with oxidative stress, IR and hepatic fat accumulation [21].

2.1.4.4.4 Endoplasmic reticulum stress

Disruption of ER homeostasis, often termed ER stress, has been observed in liver and adipose tissue of humans with NAFLD or obesity, and has implicated in both the development of steatosis and progression to NASH [73]. The ER is an intracellular membranous network where the majority of secreted and membrane proteins are folded. Unfolded proteins can accumulate due to a variety of cellular responses, for example, if excessive FFAs are present. Aggregated unfolded proteins then trigger an adaptive mechanism called the unfolded protein response (UPR), which can lead to the induction of autophagy [73]. The UPR is an adaptive response to reestablish normal homeostasis by cell cycle arrest, transient attenuation of global protein synthesis, folding catalysts, induction of ER-localized chaperone proteins, and ER-associated protein degradation [73]. If this response fails, stress-sensor proteins, including activating transcription factor 6, inositol-requiring enzyme-1 (IRE-1), and Protein Kinase R–like ER kinase (PERK), can trigger apoptosis [73]. Activated IRE1α can interacts with various inflammatory cascades by activation of JNK and IKK-NFκB signaling and production of ROS [73]. Significant increase in ER stress response genes, including CHOP, GADD34, and GRP78, were seen when palmitic acid and stearic acid were incubated with a rat hepatoma cell line followed by mitochondria-dependent apoptosis [74] . Moreover, variable degrees of UPR activation in

biopsies from patients with NAFLD and NASH [66], indicating that ER stress may have a role in human NAFLD.

2.1.4.5 Innate immunity

Innate immune activation is a key factor in triggering and amplifying hepatic inflammation in NAFLD. Endotoxin (LPS), one of the key components of the outer wall of gram-negative bacteria, plays a central role in innate immune responses and has been a focus of research in the promotion of NASH. LPS is delivered directly to the liver via the portal vein and is recognized by TLR4 located on KCs, which are the resident hepatic macrophages. The activation of TLR4 by LPS triggers an essential intracellular inflammatory cascade, including stress-activated and mitogen-activated protein kinases, JNK, p38 and the NF-κB pathways [56]. Therefore, TLR4 has a prominent role in promoting inflammation and liver injury. Mouse models have demonstrated that NASH induced by high-fat, high-fructose and MCD diets lead to enhanced expression of TLR4, with measurable portal endotoxemia. Wild-type mice on standard diets receiving low-dose infusions of LPS also develop a steatohepatitic phenotype, emphasizing the importance of the gut-liver axis in disease pathogenesis [75]. In contrast, TLR4 mutant mice display reduced levels of diet-induced steatosis and hepatic mRNA level of key fibrogenic markers, indicating that inflammation and fibrogenesis are dependent on TLR4-mediated signaling in KCs and HSCs [76]. The exact downstream pathway of TLR-4 that contributes to the pathogenesis of NASH is currently unknown but may include chaperone proteins, transcription factors, and ROS [77]. TLRs comprise a family of pattern recognition receptors that play a key role in the innate immune system and recognize specific invariant motifs on pathogens, including LPS (TLR4), peptidoglycan (TLR2), and unmethylated CpG motifs (TLR9) [77]. NASH research has

generally focused on TLR4, as detailed above. However, the roles of TLR9 and more recently TLR2 are being investigated.

2.1.4.6 Hepatic injury and death

Ultimately, multiple distinct insults combine to induce cellular damage and activate cell death pathways, marking the transition to NASH. Hepatocyte death occurs in the form of either programmed (apoptotic, necroptotic) or accidental (necrotic) cell death. However, recent evidence suggests cross talk between other types of cell death. Typically, cell death has a specific initiating cellular event, distinct signaling transduction pathways and specific cellular events. Terminal events exhibit either breakdown of cellular components with intact plasma membranes (apoptosis) or lytic processes (necrosis). However, there are frequent overlap and crosstalk between modes. Apoptosis is a highly regulated programmed cell death and has been linked with lipotoxic events and fibrogenesis in NAFLD and NASH [77]. In hepatocytes, two distinct pathways execute apoptosis: the extrinsic pathway mediated by death receptors at the cell surface and the intrinsic pathway activated by mechanisms of cell and membrane stress. Death receptors that can initiate the extrinsic pathway include Fas, tumor necrosis factor receptor 1 (TNF-R1), and tumor necrosis factor–related apoptosis–inducing ligand receptors (TRAIL-Rs). FFAs induce up-regulation of Fas and TRAIL-R5 (DR5), both were found higher in patients with NASH than in patients with steatosis [78, 79]. Similarly, both TNFα expression and TNF-R1 expression in liver tissue were increased in NASH patients [80]. In hepatocytes, lysosomal destabilization by FFAs resulted in activation and release of cathepsin B into the cytosol, and stimulate TNFα expression. Cathepsin B deficient mice are unable to induce lysosomal-driven apoptosis and are thus protected against diet-induced NASH (181, 182). Also, silencing of

Cathepsin B prevented FFA-induced mitochondrial dysfunction [81]. Necrosis leads to cell swelling, karyolysis, and cell membrane rupture, an un-programmed form of cell death. Necrosis occurs in ATP depletion and is commonly associated with an inflammatory cell reaction. Both apoptosis and necrosis can occur as a consequence of the same triggering event, possibly representing different ends of a spectrum of cell death [82]. Thus, a third form of programmed cell death, incorporating features of both apoptosis and necrosis, termed necroptosis may also play a role in NASH. Necroptosis shares upstream mediators with apoptosis (receptor-induced) but results in caspase-independent organelle and cellular swelling, which may function as a pathway to enable cell death where apoptosis is inhibited. A recent study showed that NASH livers express high levels of receptor-interacting protein (RIP)-3, which along with RIP-1 forms a complex known as the necrosome, a critical transducer of the necroptotic signal [25]. Finally, a caspase-1 dependent form of programmed cell death known as pyroptosis has been shown to contribute to NASH development in mouse models [77]. Hepatic caspase 1 activation occurs in hepatocytes and tissue macrophages and is mediated by NLRP3 [nucleotide oligomerization domain (NOD)-like receptor family, pyrin domain–containing 3] inflammasomes [25]. Mice deficient in the NLRP3 inflammasome develop less severe liver disease in dietary-induced NASH [83]. Conversely, mice with a constitutively activated NLRP3 inflammasome showed hepatocyte pyroptotic cell death [83].

2.1.4.7 Fibrosis

Fibrosis, and its more advanced form cirrhosis, represents the final common pathway of almost all chronic liver disease including NASH. Advanced fibrosis results in liver failure and increased the risk of hepatocelluar carcinoma (HCC). In NAFLD progression, two distinct

fibrogenic pathways are present in NAFLD [84]. Pericentral fibrogenesis is due to activation of HSCs by damaged hepatocytes. On the other hand, hepatocyte damage could stimulate HPCs proliferation, thus resulting in the appearance of ductular response (DR) [84]. DR then activates portal myofibrolasts (MF), which are responsible of periportal fibrogenesis. Finally, KC/MΦ polarization toward M1 phenotype could be involved in both pathways since M1-MΦs are able to stimulate HSCs and HPCs [84]. Recent evidence indicated that adipokines could contribute to fibrogenesis as well. The most well studied are leptin and adiponectin. Leptin-deficient mice (*ob/ob*) have reduced fibrogenesis, which is reverted with leptin treatment [85]. HSCs express functional leptin receptors and are thus responsive to increased circulating levels of leptin. The leptin activated phenotype of stellate cells occurs through stimulation of proliferation, suppression of apoptosis, increase in collagen 1 and tissue inhibitor of metalloproteinase 1 expression (197), activation of NADPH (nicotinamide adenine dinucleotide phosphate) oxidase and ROS generation, and increase in phagocytosis of apoptotic bodies (198). Interestingly, low mRNA level of leptin was seen in quiescent stellate cells and increase upon activation [86]. Leptin also targets KCs and sinusoidal endothelial cells, increasing TGFβ expression [87]. The compelling experimental evidence for a relationship between leptin and fibrogenesis does not seem to mirror data from human studies; no study has convincingly correlated leptin levels independently with fibrosis progression. Adiponectin has been shown to have anti-fibrotic effects, as adiponectin-deficient mice have more fibrosis when challenged by chronic carbon tetrachloride (CCl4) administration (201). Adiponectin modulates stellate cells by inhibition of pro-inflammatory pathways (NF-κB), reduced TGFβ-induced pro-fibrogenic gene expression, and increased caspase-mediated apoptosis. HSCs express adiponectin receptors and its anti-fibrotic action is mediated through AMPK-mediated pathways (199, 202). As is the case with

leptin, no clear evidence exists linking low levels of adiponectin with fibrosis in human NAFLD, independent of severe IR.

2.1.5 Rodent model of NAFLD

2.1.5.1 An ideal NAFLD animal model

Animal models of NAFLD provide crucial information, not only for elucidating the pathogenesis of NAFLD, but also for helping screening for potential therapeutic targets. Animal models of NAFLD that encompass the general physiological alterations associated with the disease development in humans, (e.g., obesity, IR, NASH, and fibrosis), and also replicate the pathological patterns and histological alterations found in the different stages of the disease in humans would be an ideal experimental model to study the onset of, but also progression of NAFLD to later stages of the disease, like NASH or even fibrosis and cirrhosis. Inadequateness in resembling either the liver pathology or the physiological alterations in animal models of NALFD will make it difficult to translate results found in such laboratory model system to the clinical situation, and subsequently the development of therapeutic or prevention strategies of the disease. Specifically, an appropriate animal model of NAFLD should display not only steatosis, but also inflammation, liver cell injury and, if long enough extended, should also progress to fibrosis. Furthermore, the model should also display metabolic abnormalities like overweight, IR, impaired glucose tolerance, dyslipidemia and altered adipose tissue/adipokines profiles, as well as the impaired innate immune system where are frequently found in patients with NAFLD [88].

2.1.5.2 Dietary animal models of NAFLD

The development of NAFLD usually takes years and results from an interplay of several risk factors like overnutrition and/or an inappropriate dietary pattern (e.g., high fat and/or high sugar intake) as well as inadequate energy expenditure due to a sedentary lifestyle in human patients. Accordingly, one of the most commonly used methods to induce progressive NAFLD in laboratory model is through dietary modifications.

2.1.5.2.1 Methionine- and choline-deficient (MCD) diet

The MCD is still a widely employed diet in NASH animal studies because of its ability to resemble inflammatory and fibrotic aspects of the NAFLD spectrum. The MCD diet normally contains substantial amounts of sucrose (e.g., 40%) and low amounts of fat (10%) but is deficient in methionine and choline, which are essential for hepatic β-oxidation and the production of VLDL [89]. Rodents fed a MCD diet rapidly (e.g., within 1 to 2 weeks) develop hepatic steatosis due to enhanced uptake of FFAs and decreased secretion of VLDL from the liver [90]. After two weeks, the development of steatosis is followed by necrosis and inflammation and then even progresses to periportal and pericentreal fibrosis. In addition, oxidative stress, mitochondrial DNA damage, and changes in cytokines and adipokines occur in this model, all contributing to liver injury in this dietary model [91]. Despite the fact that under the MCD diet rodents develop significantly faster and more pronounced liver damage, and is able to replicate the histological features of NASH and fibrosis observed in human NASH, this dietary feeding regiment has some marked limitations. For instance, animals fed the MCD diet lose weight (up to 40% in 10 weeks), and have low fasting blood glucose and serum insulin levels [9, 91], as well as decreased blood TG and cholesterol, which creating a metabolic profile opposite to the human disease. Therefore, genetically obese mice, such as *ob/ob* and *db/db* mice, are occasionally used as the MCD-fed

animal [9]. The main advantages of the MCD diet are that it is widely available and replicates NASH histological phenotype within a relatively shorter feeding time than other dietary models of NASH. The MCD model also causes more severe inflammation, oxidative stress, apoptosis, and fibrosis than other animal nutritional models of NASH [92]. However, it has been shown in several studies that the responsive of different mouse strains towards the MCD diet induced NAFLD varies considerably [93]. Therefore, the MCD diet is far from optimal to examine the metabolic parameters of NAFLD, and its use to study the development of NALFD should be discouraged.

2.1.5.2.2 High fat diet

Epidemiological studies suggest that a diet rich in fat might be a risk factor for the development of obesity and IR [94]. The increased fat content, e.g., 30%-75% of total calories derived from SFAs (+unsaturated fatty acids), can trigger symptoms of the metabolic syndrome, including obesity, hyperinsulinemia, hypercholesterolemia, and dyslipidemia [94, 95]. Thus, HFD has been proposed to be a useful tool to induce metabolic alterations and obesity-related NAFLD. However, variable results have been obtained with regard to the degree of steatosis, inflammation and fibrosis, and the results really depend on the rodent strain, the fat content of the diet, the composition of the dietary fat, and the duration of treatment [96]. HFD directly provides an excess supply of FAs to the liver, where their storage generates conditions of steatosis. Continued exposure to a HFD can promote inflammation, fibrosis, and HCC [97]. C57BL/6 mice are a particularly good model for studying human metabolic syndrome because these mice develop obesity, hyperinsulinemia, hyperglycemia, and NAFLD when allowed *ad libitum* access to a HFD but still remain lean and physically normal when they are restricted to a

normal chow diet [98]. Chronic administration of a HFD with 60% energy from fat (lard), lead to impaired glucose tolerance, mild steatosis and hepatic inflammation in C57BL/6 mice [99]. However, severe fibrosis and carcinoma, which are characteristics of advanced NASH, do not appear even after prolonged exposure. Indeed, in order to induce NASH, Deng *et al.* has introduced an intragastric feeding model adapted from the model used in alcoholic liver research [100]. In this model, C57BL/6 mice were fed a liquid high fat diet for 9 weeks intragastically resulting in not only hepatic steatohepatitis with beginning fibrosis but also metabolic abnormality such as overweight, IR, increased visceral fat, impaired glucose tolerance and increased expression of adipokines in white adipose tissue [101]. However, this model requires a surgical procedures and a high maintenance of the animals as the diet is administrated through a pump-driven tubing system implanted in the stomach of the animals.

In addition to the amount of dietary fat, the source of fat and the FA composition can significantly impact experimental outcomes. Experimental evidence indicates that dietary SFAs and trans-fatty acids (TFAs) negatively impact liver health, while monounsaturated (MUFA) and polyunsaturated (PUFA) fatty acids are generally thought to be beneficial. A high dietary SFA content is associated with NASH in both mice and humans [102, 103]. SFAs have been shown to initiate hepatocyte apoptosis by activation of JNK stress signaling pathways that respond to prolonged ER and oxidative stress [102]. High level of dietary TFA also promotes steatohepatitis and liver injury in mice through enhanced hepatic lipogenesis [16, 104, 105]. Although the impact of TFA consumption on NAFLD in humans is less clear, its association with IR and cardiovascular disease has been well reported [106, 107]. N-9 oleic acid is the most prevalent MUFA in the diet, and olive oil is one of its major sources (other sources include nuts and avocado). Several studies have demonstrated that a diet high in MUFA decreases oxidized LDL,

LDL cholesterol and TG concentrations, especially when MUFAs replace both saturated fat and high levels of carbohydrates [108-110]. A recent study has demonstrated that in only 6 weeks, an olive oil rich diet, the Mediterranean diet, which contains high levels of MUFAs, promotes a decrease in hepatic steatosis accompanied by an improvement in peripheral insulin sensitivity and a reduction in circulating insulin concentrations in humans [111]. Although the same effect has been observed in mouse models developed NAFLD [65, 112], conflicting results such that dietary MUFAs activate the NF-κB signaling pathway and lead to IR and hepatic steatosis has also been observed [113]. PUFAs can have a pro-inflammatory or anti-inflammatory effect depending on their structure. N-6 PUFAs, such as linoleic acid and arachidonic acid are precursors to potent pro-inflammatory eicosanoids [77]. While, N-3 PUFAs such as alpha-linoleic acid have an anti-inflammatory role and have been found to improve lipid metabolism, reduce hepatic TG accumulation, and ameliorate inflammation pathways involved in NAFLD development and progression [114, 115]. Mechanistically, N-3 PUFA improves NAFLD by activation of PPARs and inhibition of SREBP-1[116]. Activation of PPARs stimulates lipid oxidation and decreases inflammation and IR, which leading to amelioration of hepatic steatosis. Inhibition of SREBP-1 can decease the expression of genes involved in hepatic DNL and thereby reduce liver fat [116]. Patients with NAFLD have been shown to have a lower fish and N-3 PUFA consumption than those without fatty liver [77]. Moreover, lipidomic studies in patients with NAFLD or NASH have consistently demonstrated an association between a high N-6:N-3 ratio with the presence and severity of NAFLD [77]. Currently, manipulating the diet to alter this ratio seems to be an attractive and safe target for the treatment of NASH [77].

Overall, HFD does not produce as severe degrees of liver injury as those found in the MCD diet models and feeding times necessary to achieve more severe damage are markedly longer than

those found for the MCD diet [96]. However, these diets more closely resemble the pathological and molecular alterations found in humans with NAFLD. It is also for this reason that HFDs are commonly combined with genetic animal models of NAFLD (e.g., *ob/ob* mice) in recent years [117].

2.1.5.2.3 High fructose diet

Dietary sugar consumption, in particular sugar-sweetened beverages and the high fructose corn syrup (HFCS) has increased dramatically in the United States since its introduction in 1967, and this increase has occurred roughly in parallel with the increase in obesity and metabolic disease as well as the incidence and severity of NALFD [118]. A large clinical study conducted by the NASH Clinical Research Network showed that dietary fructose consumption was associated with more severe fibrosis (283). Studies giving C57BL/6 mice *ad libitum* access to different mono- and disaccharides in drinking water revealed that fructose had the most damaging effect on the liver [119]. Furthermore, it was shown that fructose in chow (e.g., up to 60% of total calories derived from fructose) or drinking solutions (e.g., 30% fructose solution) lead to dyslipidemia, IR and development of NAFLD even in the absence of obesity [120, 121]. The mechanism of fructose promoting the development of NAFLD mainly involve: 1) fructose promotes DNL and intrahepatic lipid accumulation, as well as inhibition of mitochondrial β-oxidation of LCFAs, which lead to steatosis and 2) fructose promotes protein fructosylation and formation of ROS, which lead to oxidative stress and expression of pro-inflammatory cytokines [122]. Similar to what was reported from HFD models, high fructose diets do not cause liver injury as severe as that found in the MCD diet models, despite more closely resembling pathological and molecular alterations and the dietary patterns found in humans with NAFLD.

2.1.5.2.4 Western diet: combination of fat and sugar

A combination of both fat and fructose-sometimes with slightly elevated cholesterol contents-referred to as Western -style or fast food diet has also been widely used as a dietary model to induce NAFLD in rodents. The addition of the high fructose (55% fructose, 45% glucose in drinking water) to a high fat diet (45% calories from fat, with 30% of the fat in the form of partially hydrogenated vegetable oil) for 16 weeks induced obesity, IR, severe hepatic steatosis with associated necroinflammatory changes in C57BL/6 mice. Although mice displayed molecular markers of fibrosis, overt fibrosis was not striking on histology [16]. Given the importance of fibrosis as an indicator of severity and disease progression in NASH, Kohli *et al* used a high fat high carbohydrate diet (HFHC) (58% of calories from fat + 55% fructose in drinking water) to induce NASH with fibrosis. C57BL/6 mice on an HFHC diet for 16 weeks in addition to developing obesity also had increased hepatic oxidative stress and a NASH-like phenotype with significant fibrosis, which mice on HFD only did not develop [15]. A similar paradigm to obtain hepatocellular injury, inflammation, and fibrosis in NASH using fructose was reproduced in rat model as well [123]. Because fibrosis in patients with NASH typically develops over prolonged periods of time, Charlton *et al*. developed a model of fibrosing NASH by feeding C57BL/6 mice for 6 months a fast food diet consisting of a high-fat diet (40% of energy from fat with 2% cholesterol) and drinking water enriched with HFCS (42g/L). This diet is also known as high fat, fructose and cholesterol (FFC) diet [17]. Mice-fed FFC diet not only become overweight and IR but also developed steatohepatitis with pronounced hepatocellular ballooning and progressive fibrosis, and increased expression of genes involved with fibrosis, inflammation, ER stress and lipoapoptosis. Adipose tissue dysregulation is a key component of

NASH and the inflammation in the liver and adipose tissue is interrelated [124]. Thus, dietary animal models of NAFLD that would resemble clinical conditions associated with adipose tissue dysfunction would be a good model for NAFLD research.

2.1.5.2.5 Atherogenic diet (high cholesterol and cholate)

Dietary with supplemented cholesterol (up to 3% w/w) was originally used for the study of atherosclerosis pathogenesis. However, it was also observed that a high cholesterol diet is an important risk factor for the progression of simple steatosis to NASH in a mouse model [125]. Thus, other studies proposed new animal models fed an atherogenic diet with high levels of cholesterol and cholate, which could both lead to atherosclerosis and NASH. A mouse model showed that an atherogenic diet can induce varied degrees of liver inflammation and augmented collagen gene expression [125]. The atherogenic diet also stimulates the liver to produce TNFα, which increases the inflammatory response and causes the progression of NASH [67]. Mice-fed the atherogenic diet consisting of 1.25% cholesterol and 0.5% cholate presented progressive hepatic steatosis, inflammation, and fibrosis after 6–24 weeks [126]. The addition of 60% fat from cocoa butter in the atherogenic diet accelerated the development of histopathological alterations within 12 weeks. Furthermore, the atherogenic diet induced oxidative stress, dyslipidemia, lipid peroxidation, and HSCs activation in the liver [127]. However, metabolic status analysis of atherogenic diet-fed animals showed an attenuation of the IR factors. In fact, during the course of the experiment, the animals lost 9% body weight, and the TG levels were lower compared with the controls [92, 127]. Thus, although the atherogenic diet enriched with fat can imitate the progression of human NASH, but the metabolic profile is different from human NASH. Therefore, further studies are needed to assess whether changes in fat

composition or addition of other dietary factors can improve the biochemical results of this model to increase its similarities to human NASH.

2.1.5.3 Genetic animal models of NAFLD

A great variety of genetically modified mice have been developed to better understand NASH. These genetic alterations can act diversely in various pathways but all contribute to hepatic lipid accumulation. The main known genetic variation results in increased ingestion of calories, higher hepatic influx of FFAs, increased DNL, and decreased hepatic oxidation of FFAs and TGs [92]. However, an addition of modified diets is frequently required in these models to induce histopathological features of NASH as it is lack of marked inflammation and fibrosis, which represents the major limitation of these models [126]. Nevertheless, NAFLD genetic models have provided us with many important insights into the mechanisms by which lipid metabolism promotes fatty liver disease.

2.1.5.3.1 *ob/ob* Mice (Leptin deficiency)

Ob/ob mice exhibit a spontaneous mutation in the leptin gene (leptin deficient). Leptin, which is secreted as a peptide hormone produced predominantly by adipose tissue, negatively regulates food intake and increases energy expenditure by affecting the hypothalamic-pituitary axis and regulating neuroendocrine mechanisms. Leptin is also involved in the modulation of fibrogenesis and cell death [128]. Because a mutation in the leptin gene causes leptin deficiency and decreased interaction between leptin and its receptor, therefore, the *ob/ob* mice are hyperphagic, extremely obese, and inactive [129]. In addition, these animals have an altered metabolic profile and exhibit hyperglycemia, IR, hyperinsulinemia, and spontaneous development of fatty liver

[130]. In *ob/ob* mice, fat in liver is redistributed from adipose tissue and other non-adipose tissue, Fat accumulation in the liver induced hepatocyte lipotoxicity and lipoapoptosis. However, the utility of the *ob/ob* mouse model is limited by concerns with the development of liver fibrosis. In fact, the *ob/ob* mice are protected against MCD diet-induced fibrosis despite developing similar necroinflammatory lesions as their genetic controls [85]. Because the progression to NASH does not occur spontaneously in this model, a secondary stimulus is necessary such as a MCD or high-fat diet or administration of LPS (endotoxin). Furthermore, leptin mutations are not prevalent in obese subjects or patients with NASH, and leptin levels are not well correlated with the development of NAFLD, which represents a disadvantage of this model [131].

2.1.5.3.2 *db/db* mice (leptin receptor deficiency)

The *db/db* mouse model exhibits a spontaneous mutation in the leptin receptor gene. Although the *db/db* mice exhibit normal or elevated levels of leptin, they are resistant to the effects of leptin. Thus, the *db/db* animals are obese, hyperglycemia, hyperinsulinemia, and develop IR and hepatic steatosis [132]. In addition, they may develop NASH after a second stimulus such as the intake of trans-fat or an MCD diet. In contrast to *ob/ob* mice, *db/db* mice on the MCD diet develop significant liver fibrosis [133]. The phenotype of the *db/db* mice better simulates the conditions of the human metabolic syndrome in many circumstances. However, these mice are limited because they do not spontaneously develop liver fibrosis or NASH without a second stimulus [85].

2.1.5.3.3 Zucker Rats

One of the most commonly used animal models of NAFLD, genetic obesity, and the metabolic syndrome is the genetic model of obese Zucker rats (fa/fa). Zucker rats exhibit a spontaneous mutation in the leptin receptor (fa allele), which decreases the affinity of this receptor for leptin and changes the transduction signal [134]. Zucker rats are homozygous for the fa allele, while heterozygous fa rats (lean) serve as the control. Similar to *ob/ob* and *db/db* mice, Zucker rats develop severe obesity and are hyperleptinemic, hyperphagic, inactive, obese, and insulin resistant (hyperinsulinemia, mild hyperglycemia, and hyperlipidemia) [135]. Hyperlipidemia is characterized by increased VLDL and HDL without significant changes in LDL cholesterol but have reduced expression of the hepatic LDL-receptor [136].

Macro- and microvesicular steatosis is diffusely present in the Zucker model without signs of progression to steatohepatitis [129]. The Zucker rats also display low hepatic Glutathione (GSH) and vitamin E levels and decreased catalase activity [137]. As a result of leptin resistance, increased expression of SREBP-1c and ChREBP may also be observed. The increased expression of SREBP-1c mRNA was accompanied by augmented levels of lipogenic enzymes and TG accumulation in the liver [129].

Similar to *ob/ob* and *db/db* mice, Zucker rats do not present spontaneous development of NASH and require a second stimulus to induce the progression from steatosis to NASH. Because the dietary models (except MCD) more closely resemble the pathogenesis of human NAFLD compared to the genetic models, the use of dietary interventions for genetic models has become more popular. Accordingly, Zucker rats fed with a diet rich in saturated fat (60% of energy supply derived from lard) for 8 weeks developed severe micro- and macrovesicular steatosis and progression to steatohepatitis [138]. Liver injury was accompanied by increased levels of alanine aminotransferase (ALT), TNF-α and TGF-β, higher collagen deposition, and activation of HSCs.

Markers of oxidative stress markers such as lipid peroxidation and protein carbonyl groups were increased, while the hepatic levels of reduced GSH and antioxidant enzymes were diminished [138].

Although Zucker rats partially simulate human metabolic syndrome (obesity, IR, dyslipidemia, hyperinsulinemia, and liver), this animal model still has some disadvantages. Because leptin or leptin receptor mutations are rare in humans, Zucker rats may not reflect the clinical and pathological circumstances of the development of the NAFLD spectrum observed in humans. Furthermore, Zucker rats do not naturally develop steatohepatitis, are resistant to liver fibrosis, and require additional interventions to induce the progression of steatosis to NASH [131].

2.1.5.3.4 SREBP-1C transgenic mice

In mammals, intracellular levels of glucose, FAs and cholesterol are controlled through a feedback regulatory system mediated by a family of transcription factors called SREBPs. SREBP-1c transgenic mice overexpress the transcription factor SREBP-1c in their adipose tissue, have impaired adipose differentiation and develop severe IR and marked hepatic steatosis while the amount of systemic fat tissue is decreased [139]. When SREBP-1c transgenic mice are fed a high-fat diet, pronounced hepatic steatosis can be induced in a few days. Even a standard diet is sufficient to induce steatosis, lobular and perivenular inflammation, and pericellular fibrosis in these animals after a period of 8 weeks [140]. Therefore, the findings are similar to many of the histology features observed in NASH. However, human NAFLD is frequently associated with metabolic syndrome and increased visceral fat, while this animal model develops lipid deposits exclusively in the liver. Consequently, despite the satisfactory pathological features, this model may differ from the clinical context of human NASH [92].

2.1.5.3.5 LDL receptor knock-out mice

NAFLD is a component of the metabolic syndrome and therefore it is frequently associated with hyperlipidemia and atherosclerosis [141]. Low-density lipoprotein receptor knockout ($LDLR^{-/-}$) mouse, a well-known animal model of dyslipidemia and atherosclerosis, was reported to develop NASH-like phenotypes under high-cholesterol or high-fat diet conditions [125, 142-145]. Different from other genetic animal models of NAFLD, $LDLR^{-/-}$ mouse develops many features of the metabolic syndrome when fed a high fat diet, including obesity, IR, and dyslipidemia, as well as local (adipose tissue), systemic inflammation and atherosclerosis[146, 147]. In these mice, as observed in humans, liver steatosis and oxidative stress promoted NASH development. However, 12–24 weeks of dietary treatment is required to induce hepatic fibrosis even under cholesterol diet conditions [143, 144]. There are also no reports on advanced diseases such as cirrhosis or HCC in $LDLR^{-/-}$ mice. Recently, $LDLR^{-/-}$ mice have been described as a suitable model to detect the onset inflammation in NAFLD [143], because $LDLR^{-/-}$mice developed early hepatic inflammation and steatosis when fed a high-fat-high-cholesterol (HFC) diet for 12 weeks, whereas C57Bl/6 mice only developed steatosis.

2.2 RNA-seq

2.2.1 Introduction

The transcriptome is the complete set of transcripts in a cell, and their quantity, for a specific developmental stage or physiological condition [148]. Understanding the transcriptome is essential for interpreting the functional elements of the genome, revealing the molecular constituents of cells and tissues, and also for understanding development and disease. So far, various technologies have been developed to deduce and quantify the transcriptome, including

hybridization- or sequence-based approaches. Hybridization-based approaches typically involve incubating fluorescently labeled cDNA with custom-made microarrays or commercial high-density oligo microarrays. Hybridization-based approaches are high throughput and relatively inexpensive. However, these methods have several limitations, which include: restriction to know regions of genome; a limited dynamic range; high background levels and difficulties in comparing expression levels between experiments [149]. In contrast to microarray methods, sequence-based approaches directly determine the cDNA sequence. Initially, Sanger sequencing of cDNA or EST libraries was used, but this approach is relatively expensive, low throughput and generally not quantitative [150]. Tag-based methods, which have high throughput and provide precise gene expression level, were developed to overcome the limitations of Sanger sequencing. However, a significant portion of the short tags cannot be uniquely mapped to the reference genome, moreover, only a portion of the transcript is analyzed and isoforms are generally indistinguishable from each other [150]. Recently, a novel high-throughput DNA sequencing method termed RNA-seq, was developed to provide a new method for both mapping and quantifying transcriptomes. This method can be used to extend our knowledge of the mechanisms of gene regulation [151], differential gene expression[152-154], alternative splicing events [155], novel genes and transcripts [156], and fusion transcripts [157]. It has been reported that 85% of novel splicing events and 88% of differentially expressed exons have been predicted by RNA-seq [158].

2.2.2 RNA-seq technology and benefits

The RNA-seq method typically consists of identification of suitable biological samples (and replicates), isolation of total RNA, enrichment of nonribosomal RNAs, conversion of RNA to a

library of cDNA fragments with adaptors attached to one or both ends (Fig. 5), sequencing on a high-throughput sequencing platform with or without amplification, generation of single or pair-end reads of 30-400 base pairs (bp) in length, alignment to a reference genome/transcripts, or assembly of these reads, and downstream analysis.

Although RNA-seq is still a technology under active development, it offers several key advantages over existing technologies. First, unlike hybridization-based approaches, RNA-seq is not limited to detecting transcripts that correspond to existing genomic sequence. RNA-seq can reveal the precise location of transcription boundaries, to a single base resolution. Furthermore, 30-bp short reads from RNA-seq give information about how two exons are connected, whereas longer reads or pair-end short reads should reveal connectivity between multiple exons. These factors make RNA-seq useful for studying complex transcriptomes. In addition, RNA-seq can also reveal sequence variations (for example, SNPs) in the transcribed regions [155]. Second, RNA-seq has a very low background, because DNA sequences can be unambiguously mapped to unique regions of the genome. RNA-seq has a large dynamic range of expression levels (>8,000-fold range) since it does not have an upper limit for quantification. However, microarrays lack sensitivity for genes expressed either a low or very high levels and therefore have a much smaller dynamic range (up to a few hundred fold). Also, RNA-seq has been shown to be highly accurate for quantifying expression levels, as determined using qPCR [159]. The results of RNA-seq also show high levels of reproducibility for both technical and biological replicates [159, 160].

Taking all of these advantages into account, RNA-seq is the first sequencing-based method that allows the entire transcriptome to be surveyed in a very high-throughput and quantitative manner. This method not only offers single-base resolution for annotation and also digital gene

expression levels at the genome scale, but more importantly, it has a much lower cost than either tiling microarrays or large-scale Sanger EST sequencing.

2.2.3 Challenges for RNA-seq

2.2.3.1 Library construction

The ideal method for transcriptomics should be able to directly identify and quantify all RNAs, small or large. However, unlike small RNAs [microRNAs(miRNAs), short interfering RNA(siRNAs) and many others], which can be directly sequenced after adaptor ligation, larger RNA molecules must be fragmented into smaller pieces (200 – 500 bp) to be compatible with most deep-sequencing methods. Common fragmentation methods include RNA fragmentation and cDNA fragmentation. Each of these methods creates a different bias in the outcome. Also, some manipulations during library construction complicate analysis of RNA-seq results. For example, many short reads that are identical to each other can be obtained from cDNA libraries that have been amplified, or they could be PCR artifacts. One way to discriminate between these two possibilities is to determine whether the same sequences are observed in different biological replicates. Another key consideration concerning library construction is whether or not to prepare strand-specific libraries. These libraries have the advantage of yielding information about the orientation of transcripts, which is valuable for transcriptome annotation, especially for regions with overlapping transcription from opposite directions; however, strand-specific libraries are currently laborious to produce because they require many more steps[149].

2.2.3.2 Bioinformatics challenges

Like other high-throughput sequencing technologies, RNA-seq faces several informatics challenges, including the development of efficient methods to store, retrieve and process large amounts of data. Once high-quality reads have been obtained, the first task is to map the short reads from RNA-seq to the reference genome or to assemble them into contigs before aligning them to the genomic sequence to reveal transcription structure. However, short transcriptomic reads also contain reads that span exon junctions or that contain poly(A) ends, which cannot be analyzed in the same way. For genomes in which splicing is rare, special attention only needs to be given to poly(A) tails and to a small number of exon-exon junctions. For complex transcriptomes, it is more difficult to map reads that span splice junctions owing to the presence of extensive alternative splicing and transplicing. Although a junction library that contains all the known and predicated junction sequences and map reads within the library could be a partial solution, a computationally simple method to identify novel splicing events that take place between two distant sequences or between exons from two different genes is a challenge for the future. For large transcriptomes, alignment is also complicated by the fact that a significant portion of sequence reads match multiple locations in the genome, however, a paired-end sequencing strategy, in which short sequences are determined from both ends of a DNA fragment, has been developed to extend the mapped fragment length to 200-500 bp and appears to be compatible with most deep-sequencing methods [149, 161].

2.2.3.3 Coverage vs cost

Sequence coverage, or the percentage of transcripts surveyed, is another important issue because it directly affects the cost. In general, the larger the genome, the more complex the transcriptome, the more sequencing depth is required for adequate coverage. Unlike genome-

sequencing coverage, it is less straightforward to calculate the coverage of the transcriptome; this is because the true number and level of different transcript isoforms is not usually known and because transcription activity varies greatly across the genome. The expected relative abundance of RNAs vary widely, with published estimates suggesting that at least 10^5–10^7 orders of magnitude are expected between genes with the lowest and highest expression [162]. Since RNA-seq works by random sampling, a small fraction of highly expressed genes can consume the majority of reads. One consequence of this wide range is that in order to capture a snapshot of the transcriptome that includes rarely expressed genes, an RNA-seq library must be much deeper than one might expect based on the proportion of bases in a genome that are annotated as expressed.

2.3 Acute Phase Proteins

2.3.1 Overview

Acute phase proteins (APPs) are blood proteins primarily synthesized by hepatocytes as part of the acute phase response (APR). The APR is part of the early-defense or innate immune system, which is triggered by different stimuli including injury, trauma, infections, stress, inflammation, as well as neoplasia [163]. The APR results in a complex systemic reaction with the goal of reestablishing homeostasis and promoting healing [164].

APPs are a large and varied group of plasma proteins, which are released into the blood stream in response to a variety of stressors. The changes in the concentrations of APPs are largely due to changes in their production by hepatocytes. All the up-regulated proteins have been called positive APPs, which are further classified as major, moderate, or minor, depending on their concentration. Major proteins represent those that increase 10- to 100-fold, moderate proteins

increase 2- to 10-fold, and minor proteins are characterized by only a slight increase (< 2-fold) [165]. Major proteins are often observed to increase markedly within the first 24–48 h after the triggering event and often exhibit a rapid decline due to their very short half-life. Moderate and minor proteins follow in the magnitude of their response and may both increase more slowly and may be more prolonged in duration, depending on the status of the triggering event [163]. Moderate and minor APPs may also be observed more often during chronic inflammatory processes [166].

The biologic functions of APP are vast; however, the main function of APP is to defend the host against pathological damage, assist in the restoration of homeostasis and in the regulation of different stages of inflammation [167]. For example, C-reactive active protein (CRP) can bind residues and polysaccharides on bacteria, fungi, and parasites to activate complement and phagocytosis. In addition, CRP can both upregulate and downregulate cytokine production and chemotaxis [168, 169]. Serum amyloid A (SAA), has been demonstrated to result in chemotaxis of monocytes, polymorphonuclear cells, and T cells. In addition, SAA has marked inhibitory effects and is assumed to be important in the down regulation of the inflammatory process. Haptoglobin, another positive APP, can bind free hemoglobin released from erythrocytes thereby reducing oxidative damage associated with hemolysis. It has been observed to have bacteriostatic and immunomodulatory effects [170]. The APP α1-acid glycoprotein or orosomucoid (ORM) is considered to be a natural anti-inflammatory and immunomodulatory agent. It exhibits a moderate APR in most species and is more likely to be associated with chronic conditions. Moreover, ORM is one of the most important drug binding proteins in plasma with important pharmacokinetic implications [171]. Further detailed discussion on ORM is covered below in this review. In nearly all animal species and humans, albumin represents the major negative

APP. During the APR, the demand for amino acids for synthesis of the positive APP is markedly increased, which necessitates reprioritization of hepatic protein synthesis. Thus, albumin synthesis is down-regulated and amino acids are shunted into synthesis of positive APP [172]. Transferrin, the iron-binding protein of serum has also been described as a negative APP. The primary role of transferrin is to transport iron safely around the body to supply growing cells. Essentially, all circulating plasma iron is normally bound to transferrin. It renders iron soluble under physiological conditions, prevents iron-mediated free radical toxicity [173]. In addition, transferrin has been observed to inhibit multiplication and growth of certain viral, bacterial and fungal organisms by limiting their access to iron. In summary, positive APP all have multiple functions including modulating the immune system, protein transport, and tissue protection from damage by the inflammatory process.

2.3.2 ORM

2.3.2.1 Introduction

ORM was first described more than 100 years ago by Tokita and Schmid [174], and is considered an unusual protein with a very low pI of 2.8-3.8 and a very high carbohydrate content of 45%. The molecular weight of purified ORM varies from 37 to 54 kDa due to differences in glycosylation extent. ORM is mainly synthesized in the liver and secreted into the circulation, but extra-hepatic synthesis has also been reported [175]. There are two isoforms of ORM in humans, three in mice, and one in rats. The normal level of ORM in rat is 0.1-0.2 mg/ml, in mouse is 0.2-0.4mg/ml, and in human is 0.4-1.2mg/ml of plasma (corresponding 1-3% of plasma protein). During APR, the plasma concentration of ORM rises two to five times. Thus, ORM is considered as a major member of positive APP family. In addition, its glycosylation pattern can

also change depending on the type of inflammation [176]. The biological function of ORM is not completely understood; however, a number of activities *in vitro* and *in vivo* have been described, such as various immunomodulating effects and the ability to bind basic drugs and many other molecules like steroid hormones; the latter leading to the suggestion that ORM might be a member of lipocalin family [176].

2.3.2.2 ORM gene and protein structures

Structures of the genes encoding ORM

ORM shows extensive genetic variation. Human ORM is the product of a cluster of three adjacent genes: AGP-A, AGP-B, and AGP-B′ covering 70kb of the human genome and located on the long arm of chromosome 9. AGP-A gene is actively expressed in human liver and codes for the major component of serum ORM (ORM1, accounting for 75 % of plasma ORM), while the other two identically code for the ORM2 variant [177]. Only AGP-A can be induced by acute-phase stimuli; thus, ORM1 is the unique member that could be considered as the APR in the ORM family. In the rat, there is only one gene for ORM in the genome, which is located on chromosome 5. In the mouse, three genes (AGP-1, AGP-2, and poorly expressed AGP-3) are arranged as a cluster on chromosome 4 encoding ORM1, ORM2, and ORM3, respectively. These genes have an identical structure to the human and rat genes with six exons and five introns [178].

2.3.2.3 The structure of ORM protein

In humans, ORM is a glycoprotein of 41-43 kDa molecular weight, which consists approximately of 45% carbohydrates attached in the form of five complex-type N-linked glycans

[175]. A notable characteristic of ORM is its unusually high solubility in water and in many polar organic solvents. Different forms of ORM can be distinguished in serum depending on the type of glycosylation and multiple amino acid substitutions. The ORM1 precursor is a single polypeptide chain of 201 residues. An N-terminal secretory signal peptide of the first 18 residues is cleaved during the processing of the protein, resulting in a protein with a single polypeptide chain of 183 amino acids, including two disulfide bonds. There are 22 amino acid differences between ORM1 and ORM2 [179]. In addition, at position 32 and 47, other amino acids can be present, probably reflecting polymorphism in the human population. With a molecular weight of 40-44 kDa [180], the mature form of rat ORM is a 187-amino acid protein with only one disulfide bridge, containing six N-linked complex-type oligosaccharides per molecule, sharing 59 % amino acid sequence homology with human ORM. In mice, three forms of ORM each composed of 187 amino acids, are the products of the three main ORM genes, respectively. Among them, ORM1 has five potential glycosylation sites, ORM2 has six sites, and ORM3 has three sites. In spite of these differences, the functional domain of ORM is highly conserved in humans, rats, and mice. Changes in glycosylation of ORM are not restricted to acute inflammatory conditions, but also occur in a wide variety of other pathophysiological conditions like pregnancy, severe rheumatoid arthritis, alcoholic liver cirrhosis and hepatitis [175]. Therefore, different glycoforms of ORM might be used as diagnostic and prognostic markers during clinical therapy. Measuring ORM level and detecting its glycoforms could be more helpful to evaluate the progression of a certain disease than measuring the CRP or SAA concentrations alone.

2.3.2.4 Synthesis of ORM

ORM is predominantly synthesized by hepatocytes and parenchymal cells upon stimulation by pro-inflammatory cytokines [178]. It is then released into the blood and distributed in body fluids, including plasma, mucus, gastric juice, and jejunal fluid. About 60 % of ORM in the body is present in the central compartment and the remainder in a peripheral compartment, most likely the extravascular space. The plasma concentration of ORM is increased in response to various stressful stimuli: physical trauma (such as surgery or wounding), bacterial infection, and nonspecific inflammatory stimuli (such as subcutaneous injection of turpentine, etc.) [175]. The levels of liver ORM mRNA and plasma ORM protein increase 10- to 200-fold within 24 h of experimentally induced inflammation in rats, mice, and rabbits [175].

Extrahepatic production of ORM has been described over the last 40 years. Human breast epithelial cells, type II alveolar epithelial cells, human microvascular endothelial cells, human granulocytes, the monoblastoid cell line THP-1, monocytes, macrophages, polymorphonuclear leukocytes, and granulocytes have been shown to synthesize and secrete ORM. However, ORM was not been found in T and B lymphocytes [175]. Constitutive ORM gene expression has been observed in extrahepatic organs such as lung, breast, kidney, and adipose tissue.

2.3.2.5 Regulation of ORM

Gene expression of ORM is controlled by a combination of the major regulatory mediators such as glucocorticoids, TNFα, IL1β, chemokines (IL8), IL6 and IL6-related cytokines in liver from human, rat, mouse, and rabbit [181-183]. In addition to inflammatory mediators, ORM gene expression can also be regulated by a series of other exogenous and endogenous factors. Repeated administration of phenobarbital (PB) and rifampicin enhances ORM serum levels by a mechanism independent of the inflammatory pathway [184]. Molecules such as retinoic acids

can also increase ORM expression at the transcriptional level in a dose-dependent manner via the activation of the retinoic acid receptor alpha and retinoid X receptor alpha [185]. In addition, the nuclear bile acid receptor, farnesoid X receptor (FXR), expressed in the liver, intestine, vascular wall, pancreas, and kidney [186], can also activate mouse hepatic ORM expression both in vitro and in vivo via a FXR response element upstream of the mouse ORM1 promoter [187]. Although ORM gene regulation is remarkably similar among species, the enhancer sequence and its location are quite variable. In fact, mouse ORM gene induction is more complex, involving both positive and negative transcription factors, which play synergistic roles in the induction of ORM gene transcription during the APR. Additionally, the promoter region of the mouse AGP-1 gene contains a region termed the APR element, which has been shown to mediate the induction of ORM expression in response to LPS instead of glucocorticoid [178].

2.3.1.6 Biological functions of ORM

2.3.1.6.1 Anti-inflammatory and immunomodulatory properties

ORM is considered a natural anti-inflammatory and immunomodulatory agent notably with respect to its anti-neutrophil and anti-complement activity. ORM inhibits mitogen-induced proliferation of lymphocytes and aggregation of platelets as well as chemotaxis, superoxide generation, and aggregation of neutrophils [175, 176, 188]. Addition of ORM to the lymphocyte culture resulted in a 60% decrease in lymphocyte proliferation as well as a 65% decrease in IL2 secretion [189]. ORM1 is also involved in vitamin D-mediated macrophage deactivation [190]. There is a vitamin D response element (VDRE) in the promoter region of ORM1. Vitamin D could induce ORM1 expression in human monocytes and thereafter inhibit pro-inflammatory cytokine (TNF-α, IL-6) expression and promote deactivating marker (MMP9, CD163)

expression [190]. Similarly, ORM1 was reported to lead to an upregulated expression of CD163 and to inhibit the inflammatory process by activating the TLR4/CD4 signaling pathways [191]. Furthermore, ORM was recently observed to regulate inflammation by modulating the polarization of M2 macrophages, which is an anti-inflammatory phenotype of macrophages [192].

ORM also can interfere with cytokine function by inducing the secretion of soluble TNFα receptor and IL-1 receptor antagonist [193]. Human ORM has been shown to induce the secretion of an inhibitor of IL-1 activity, when introduced in culture medium of mouse peritoneal macrophage. Moreover, ORM was synergistic with low concentrations of LPS in the induction of both IL-1 receptor antagonist and IL-1β synthesis [193]. Injection of exogenous ORM was shown to consistently protect mice from lethal shock induced by TNFα [194], and inflammatory hepatitis induced by TNFα and galactosamine [195].

On the other hand, ORM can also induce the release of soluble TNFα, IL1, and IL12 by mononuclear leukocytes both systemically and locally [176]. Since IL1 and TNFα can stimulate ORM production, thus ORM untimely modulate the inflammatory reaction by contributing both anti- and pro-inflammatory signals to cytokine-mediated feedback mechanisms activated by the APR. However, the process is incompletely understood and not fully characterized. Interestingly, ORM transgenic mice displayed higher sensitivity to acute colitis when compared to wild-type mice, with higher local myeloperoxidase levels, higher inflammation scores of the colon, higher systemic levels of IL-6 and serum amyloid P component, and higher amounts of bacteria in organs, showing the pro-inflammatory role of ORM [196].

2.3.1.6.2 Transporting protein

ORM, together with human serum albumin and the lipoproteins, is one of the most important drug-binding proteins in plasma and may have important pharmacokinetic implications in clinical therapy. Generally, ORM has the ability to bind and carry numerous basic and neutral drugs from endogenous and exogenous origin due to its physical-chemical properties (pI = 2.8–3.8) [197]. The basic drugs include dipyridamole, chlorpromazine, vinblastine, imatinib, and UCN-01, tamoxifen and propranolol [178], while the neutral drugs include steroids, diazepam, and carbamazepine [178]. More recently, ORM was found to also bind synthetic steroids (mifepristone), β-blockers, local anesthetics, phenothiazine drugs, anticancer drugs (especially tyrosine kinase inhibitors such as imatinib), and HIV protease inhibitors. ORM can also bind and transport acidic drugs, and its binding is often stereoselective [178]. The binding capacity of a drug mainly depends on the ORM protein conformation, ligand polarity, temperature, pH, and several other amino acid residues lying at the periphery of the hydrophobic domains of ORM. Because the concentration of ORM is relatively low and there is only one drug-binding site in each molecule, molecule transport is both easily saturable and subject to competitive displacement [171]. In addition, the existence of two forms of the same protein in the blood system also has influence on the drug-binding affinity. Recent studies have demonstrated that drugs like methadone, disopyramide, deramciclane, propafenone, and amitriptyline bind selectively to ORM2, as opposed to warfarin, prazosin, imatinib, quinidine, and dipyridamole, which prefer the ORM1 variant [178].

2.3.1.6.3 Regulating metabolism

It has been reported that ORM increases glucose uptake activity in 3T3-L1 adipocytes and relieves hyperglycemia-induced I as well as TNF-α-mediated lipolysis in adipocytes [198].

Accordingly, ORM improved glucose and insulin tolerance in obese and diabetic *db/db* mice [198]. Further, ORM was recently observed to regulate food intake and energy homeostasis via leptin receptor signaling pathway [199]. Administration of exogenous ORM decreased food intake, in HFD-fed C57BL/6 and *ob/ob* mice, which was absent in *db/db* mice. ORM was also found to bind directly to the leptin receptor and activate receptor-mediated JAK2-STAT3 signaling in hypothalamus tissue [199]. Clinical investigation showed the level of circulating ORM correlated positively with BMI, body fat mass, and serum leptin [200]. It also correlated with fasting insulin, HOMA-IR values and C-reactive protein in men [200]. In addition, ORM can be an auspicious biomarker in distinguishing overweight/obese women with metabolic syndrome from those who are metabolically healthy independent of body weight, fat mass, and physical activity/fitness [201].

Figures and figure legends

Figure 1

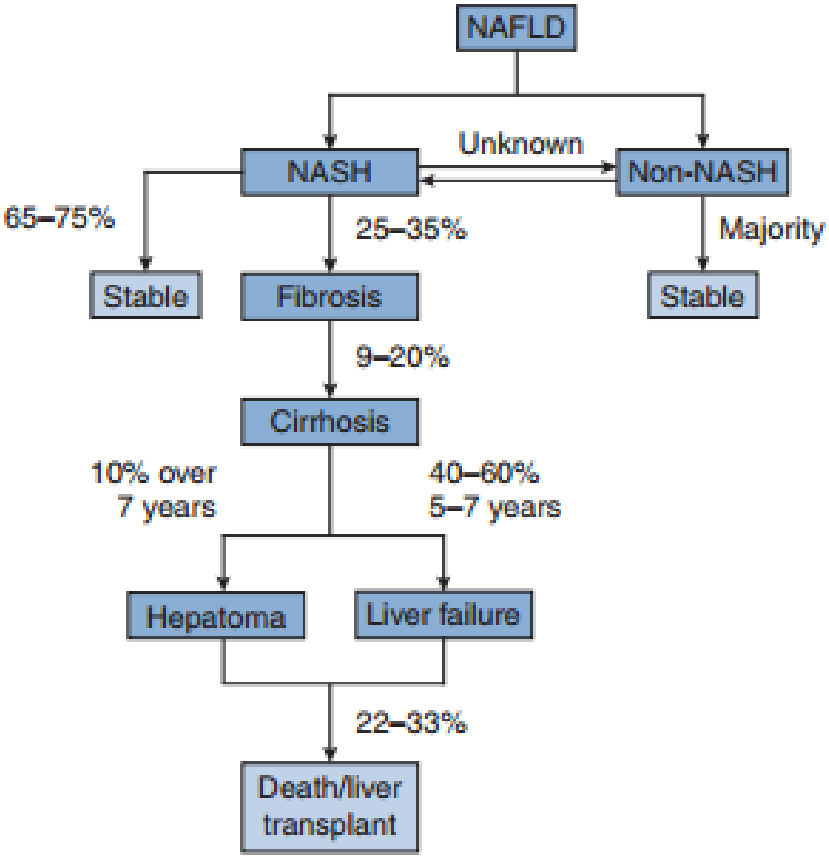

Fig. 1. Natural history of NAFLD [31].

Figure 2

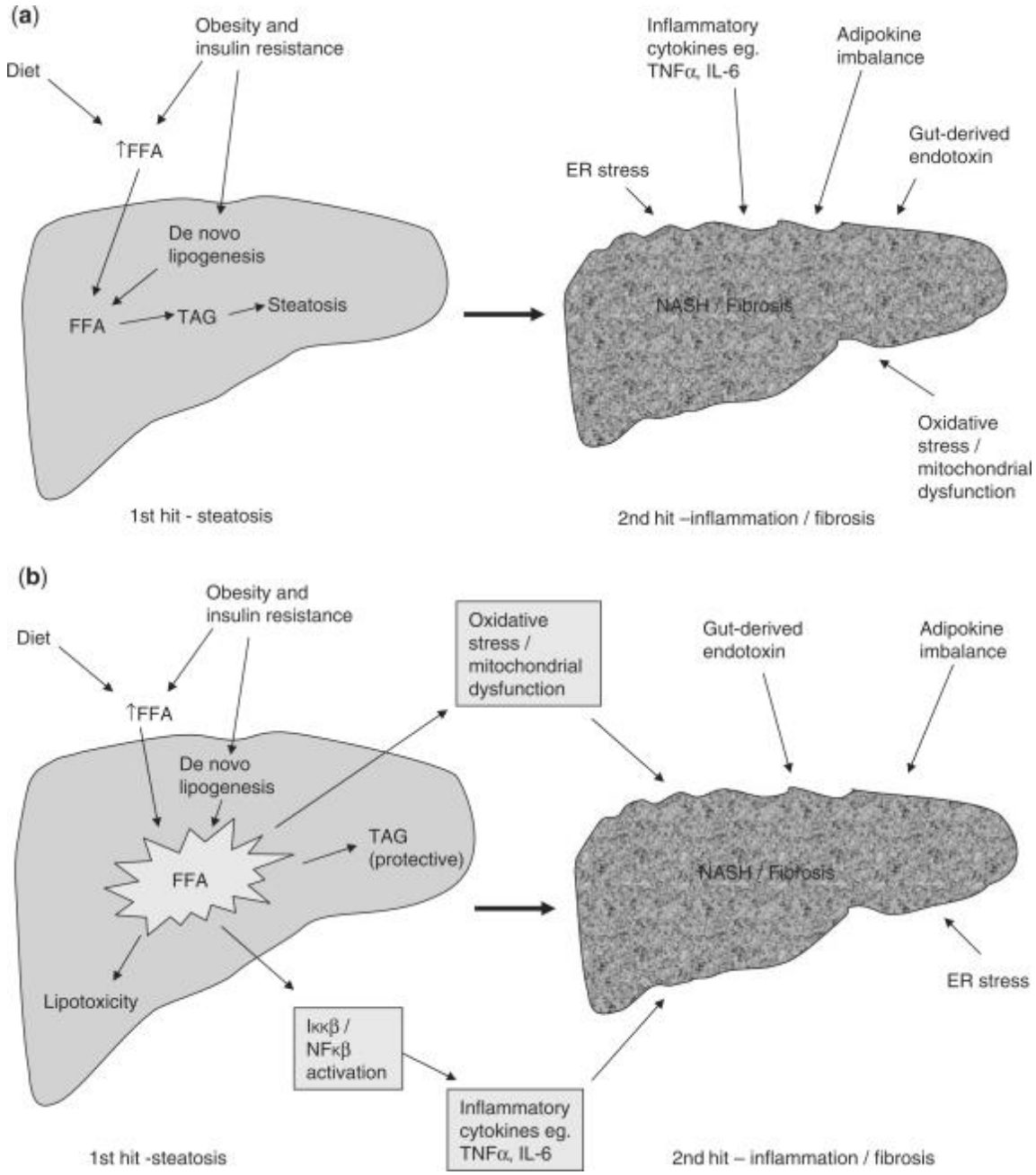
(a)
Diet
Obesity and insulin resistance
↑FFA
De novo lipogenesis
FFA
TAG
Steatosis
1st hit - steatosis
Inflammatory cytokines eg. TNFα, IL-6
Adipokine imbalance
Gut-derived endotoxin
ER stress
NASH / Fibrosis
Oxidative stress / mitochondrial dysfunction
2nd hit –inflammation / fibrosis
(b)
Diet
Obesity and insulin resistance
↑FFA
De novo lipogenesis
FFA
TAG (protective)
Lipotoxicity
Oxidative stress / mitochondrial dysfunction
IκKβ / NFκβ activation
Inflammatory cytokines eg. TNFα, IL-6
Gut-derived endotoxin
Adipokine imbalance
NASH / Fibrosis
ER stress
1st hit -steatosis
2nd hit – inflammation / fibrosis

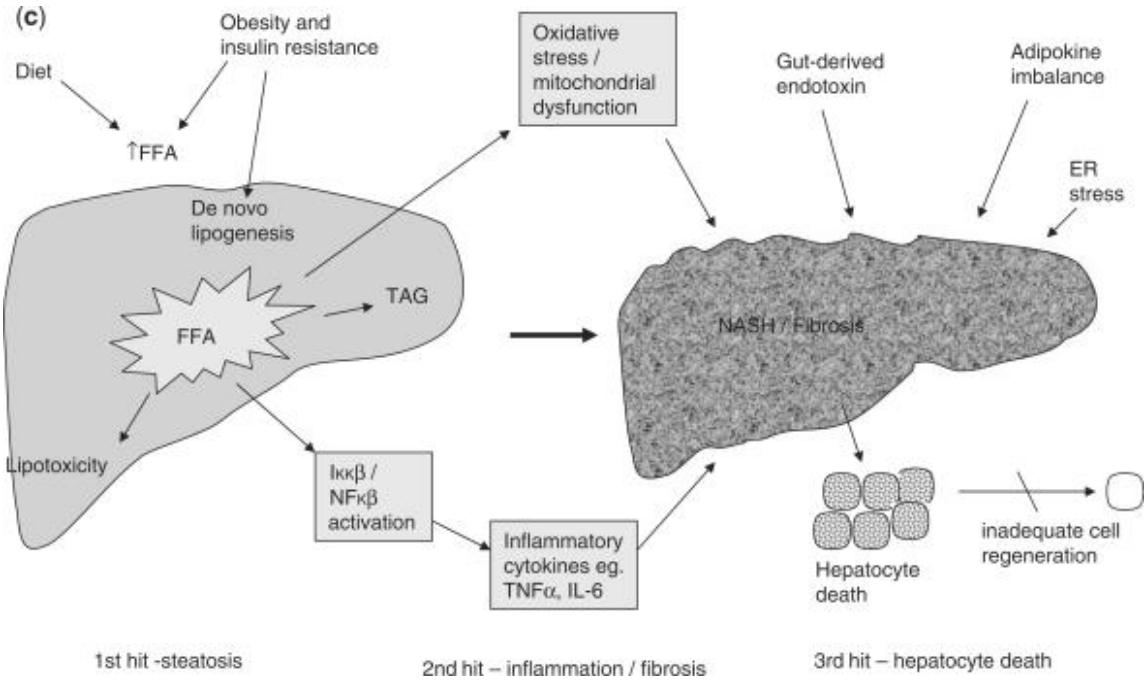

Fig. 2. (**a**) The traditional 2-hit hypothesis: steatosis represents the 'first hit', which then sensitizes the liver to injury mediated by 'second hits', such as inflammatory cytokines, adipokines, oxidative stress and mitochondrial dysfunction, leading to NASH and fibrosis. The presence of high levels of oxidative stress reduces the ability of mature hepatocytes to proliferate, resulting in reduced endogenous liver repair. (**b**) Modified 2-hit hypothesis: the accumulation of FFA alone has been suggested to be sufficient to induce liver damage, without recourse for a second hit. Indeed, rather than being harmful, TG accumulation in the form of steatosis may actually be protective by preventing FFA-induced inflammation and oxidative stress. (**c**) The 3-hit hypothesis: oxidative stress reduces the ability of mature hepatocytes to proliferate, resulting in the recruitment of other pathways of liver regeneration, such as hepatic progenitor cells (HPCs). These cells have the capability of differentiating into both cholangiocytes and hepatocytes and contributing to liver repair. It has been suggested that an inability to mount such a ductular response, as is seen in patients transplanted for NASH who

have denervated livers, may be responsible for a more progressive pattern of liver damage. Thus, impaired proliferation of hepatocyte progenitors represents the proposed ‘third hit’ in NAFLD pathogenesis.[21]

Figure 3

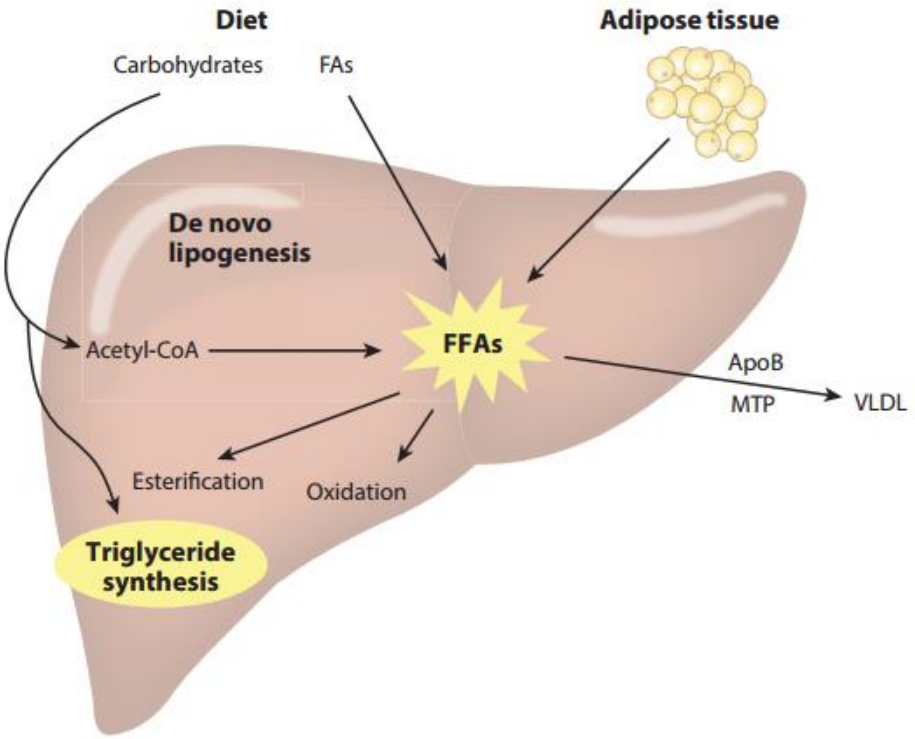

Fig. 3. Lipid handling by the liver. FFAs are delivered to the liver by diet, adipose tissue, and *de novo* lipogenesis (DNL). Dietary carbohydrates contribute to lipogenesis both by entering the citric acid cycle to produce acetyl-CoA for DNL and by providing the glycerol backbone via triose-phosphate. Abbreviations: acetyl-CoA, acetyl coenzyme A; ApoB, apolipoprotein B; FFAs, fatty acids; MTP, microsomal transfer protein; VLDL, very low density lipoprotein [25].

Figure 4

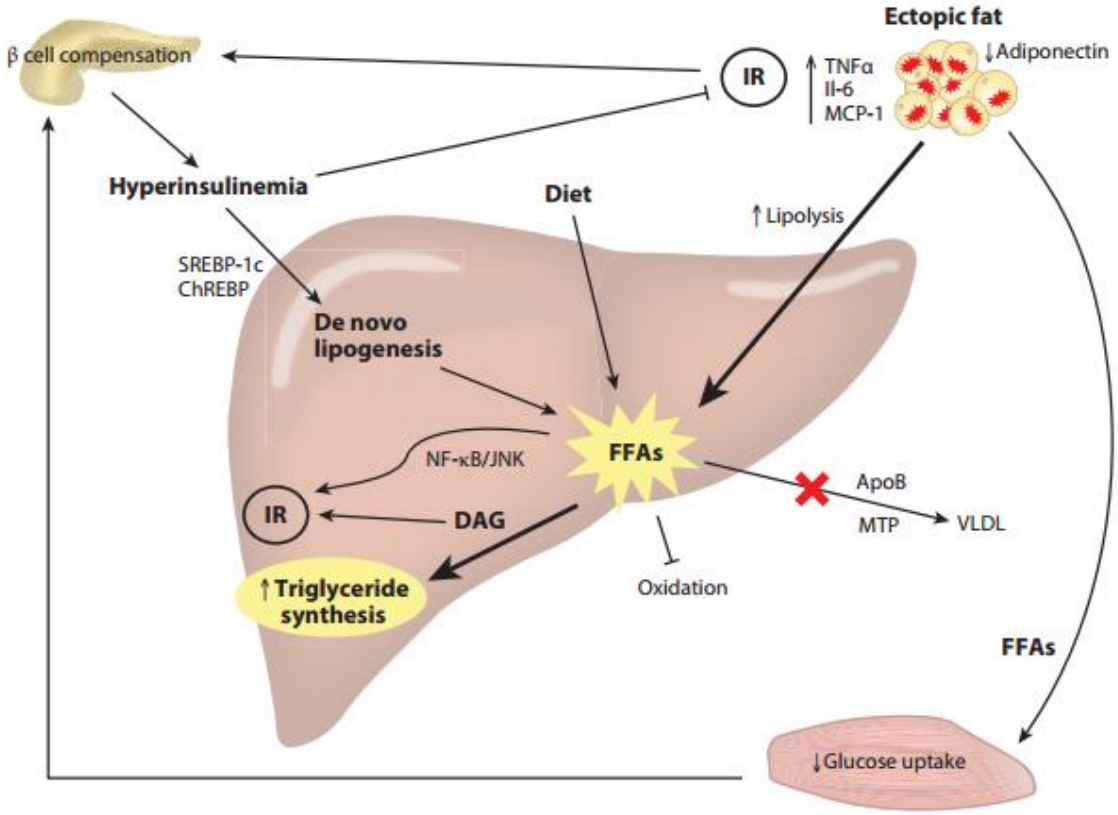

Fig.4 Interorgan links among insulin resistance (IR), dysregulation of hepatic free fatty acid (FFA) flux, and the development of hepatic steatosis. Obesity and the deposition of ectopic fat lead to the recruitment of macrophages; dys-regulated adipokines abrogate insulin signaling. Thus arises an impairment of insulin-mediated suppression of lipolysis, leading to increased flux of FFAs from adipocytes to other tissues (60%). Also, impaired glucose tolerance develops secondary to increased FFA flux to muscles and suppression of glucose uptake. Pancreatic β cells compensate by increasing insulin secretion, leading to hyperinsulinemia. *De novo* lipogenesis is stimulated in the liver, contributing 25% of the altered FFA pool in hepatic steatosis; dietary FFAs contribute the remainder. DAG, a triacylglycerol intermediate, also contributes to hepatic IR. Abbreviations: ApoB, apolipoprotein B; ChREBP, carbohydrate-responsive element–binding protein; Il-6, interleukin 6; MCP-1, monocyte chemoattractant

protein 1; MTP, microsomal transfer protein; NF-κB/JNK, nuclear factor κB/c-Jun N-terminal kinase; SREBP-1c, sterol regulatory element–binding protein 1c; TNFα, tumor necrosis factor α; VLDL, very low density lipoprotein [25].

Figure 5

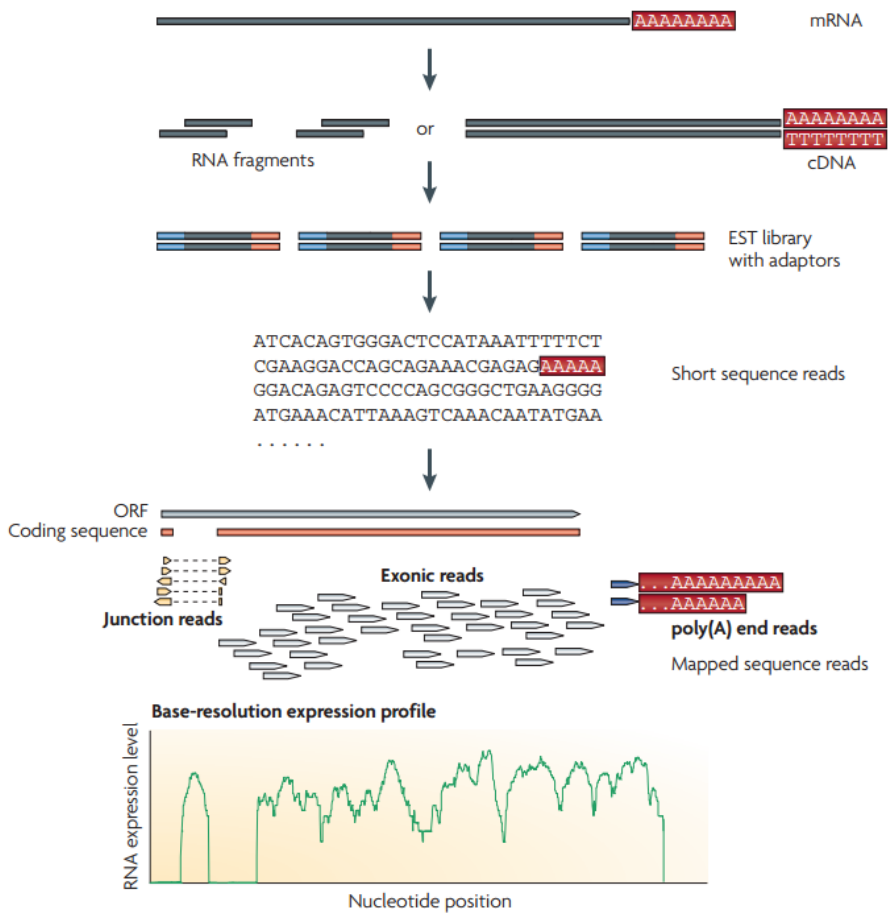

Fig. 5 A typical RNA-seq experiment. Briefly, long RNAs are first converted into a library of cDNA fragments through either RNA fragmentation or DNA fragmentation (see main text). Sequencing adaptors (blue) are subsequently added to each cDNA fragment and a short sequence is obtained from each cDNA using high-throughput sequencing technology. The resulting sequence reads are aligned with the reference genome or transcriptome, and classified as three types: exonic reads, junction reads and poly(A) end-reads. These three types are used to generate a base-resolution expression profile for each gene, as illustrated at the bottom; A yeast ORF with one intron is shown [149]

Chapter 3: Metabolic phenotype and adipose and liver features in a high-fat Western diet-induced mouse model of obesity-linked NAFLD

3.1 Abstract

Nonalcoholic fatty liver disease (NAFLD), an obesity and insulin resistance associated clinical condition - ranges from simple steatosis to nonalcoholic steatohepatitis. To model the human condition, a high-fat Western diet that includes liquid sugar consumption has been used in mice. Even though liver pathophysiology has been well characterized in the model, little is known about the metabolic phenotype (e.g., energy expenditure, activity, or food intake). Furthermore, whether the consumption of liquid sugar exacerbates the development of glucose intolerance, insulin resistance, and adipose tissue dysfunction in the model is currently in question. In our study, a high-fat Western diet (HFWD) with liquid sugar [fructose and sucrose (F/S)] induced acute hyperphagia above that observed in HFWD-fed mice, yet without changes in energy expenditure. Liquid sugar (F/S) exacerbated HFWD-induced glucose intolerance and insulin resistance and impaired the storage capacity of epididymal white adipose tissue (eWAT). Hepatic TG, plasma alanine aminotransferase, and normalized liver weight were significantly increased only in HFWD+F/S-fed mice. HFWD+F/S also resulted in increased hepatic fibrosis and elevated collagen 1a2, collagen 3a1, and TGFβ gene expression. Furthermore, HWFD+F/S-fed mice developed more profound eWAT inflammation characterized by adipocyte hypertrophy, macrophage infiltration, a dramatic increase in crown-like structures, and

upregulated proinflammatory gene expression. An early hypoxia response in the eWAT led to reduced vascularization and increased fibrosis gene expression in the HFWD+F/S-fed mice. Our results demonstrate that liquid sugar consumption induces acute hyperphagia, limits adipose tissue expansion, and exacerbates glucose intolerance and insulin resistance, which are associated with NAFLD progression.

3.2 Introduction

Obesity is linked to the pathogenesis of nonalcoholic fatty liver disease (NAFLD), from the seemingly benign condition of fatty liver to nonalcoholic steatohepatitis (NASH), which can lead to the more serious clinical conditions of cirrhosis and liver cancer (hepatocarcinoma). The overall prevalence of NASH in the adult US population (8%) matches the prevalence of type 2 diabetes [202]. Currently, there are no specific therapeutic treatments for NASH.

Obesity is characterized by expanded adipose tissue. Excessive secretome molecules (adipokines, cytokines, free fatty acids, and other lipid moieties) from adipose tissue may lead to an altered metabolic state with inflammation and insulin resistance and contribute to the progression of NAFLD [203]. Evidence for adipose tissue insulin resistance in obese patients with NAFLD suggests that adipose tissue expansion and/or dysfunction plays a role in NAFLD development and progression [204]. A tight relationship between the expansion of epididymal white adipose tissue (eWAT) and NAFLD development and progression in mice highly responsive to a high-fat diet support this postulate [205].

To gain insight into the pathogenesis of NASH, obesity-linked overnutrition models have been developed based on a Western diet that is high in animal-derived saturated fats and added sugar in the form of fructose and/or sucrose, which mimics the consumption of sugar in adults [206]

and children [207]. Fructose, in the presence of a high-fat diet, may exacerbate fat deposition, inflammation, oxidative stress, and fibrosis in the liver but maybe not systemic glucose intolerance and insulin resistance [15-17]. Increased fructose intake has been associated with increased hepatic fibrosis in patients with NAFLD [208]. The presence of fibrosis in the liver is an important predictor of adverse long-term outcomes, including diabetes and progression to cirrhosis [209].

The high-fat Western diet-plus-liquid sugar consumption model of obesity in mice was originally developed as a model of NAFLD progression [15-17] and appears to model obese humans with mild NASH, as recently reported in a thorough analysis of the liver pathophysiology phenotype [210]. Yet, it may be a good model for other chronic conditions associated with obesity such as diabetes, cardiovascular disease, and Alzheimer's disease. A greater understanding of factors leading to hepatic and adipose tissue dysfunction in NASH and other obesity-linked conditions represents an important area of investigation, because new therapeutic targets are needed for the treatment of NASH and other obesity-linked conditions. Given the importance of the high-fat Western diet + liquid sugar consumption model of obesity, little is known about the development of metabolic dysfunction in the model. In particular, it is not known whether changes in energy expenditure, activity, or food intake underlie the obese phenotype. Furthermore, whether the consumption of liquid sugar exacerbates the development of glucose intolerance, insulin resistance, and adipose tissue dysfunction in the model is also currently in question. To address these gaps in our knowledge, we investigated pathophysiological parameters, including the energy expenditure, activity, food intake, and glucose and insulin tolerance, together with histological parameters and gene expression from hepatic and adipose tissues in mice fed a low- or high-fat Western diet with or without liquid sugar.

3.3 Materials and Methods

3.3.1 Animals

Male C57BL/6NHsd mice from Harlan Laboratories (Somerville, NJ) were housed three per cage in Thoren units in the Bassett Research Institute, an AAALAC accredited animal facility, in 12:12-h light-dark, temperature at 22°C, and humidity-controlled rooms. Mice were provided with standard laboratory chow and water ad libitum in accordance with an Institutional Animal Care and Use Committee approved protocol for 1 wk to allow for acclimatization to the animal facility. No procedures were undertaken that caused more than minimal pain, distress, or discomfort. Mice (*n*= 8, 6 wk old) were then placed for 2 and 12 wk on a low-fat Western diet (LFWD) (Test Diets, Cat. #5TJS) or a high-fat Western diet (HFWD) (Test Diets, Cat. #5TJN) containing ~12% and 40% energy from fat, respectively. The composition of fat in the diets was 30% from lard, 30% from butterfat, and 30% from Crisco. Sugar (42 g/l) was added to the drinking water at a ratio of 55% fructose/45% sucrose (F/S) to mice on the LFWD and HFWD. Mice were euthanized by inhalation of CO_2. Blood samples were immediately drawn from the caudal vena cava. After clotting at room temperature, the sample was centrifuged at 12,000 *g* for 15 min at 4°C. The serum was removed and stored frozen at −80°C until tested. Liver and eWAT were excised, weighed, and flash-frozen in liquid nitrogen or fixed in 10% buffered formalin prior to paraffin embedding. A follow-up study was performed using male C57BL/6NHsd mice (*n* = 8, 6 wk old) from Harlan Laboratories housed one per cage in the Auburn University Veterinary Research Building, an AAALAC accredited animal facility, in 12:12-h light-dark, temperature at 22°C, and humidity-controlled rooms. Mice were provided with standard laboratory chow and water ad libitum in accordance with an Institutional Animal Care and Use Committee approved protocol for 1 wk to allow for acclimatization to the animal facility. The

mice were then placed on the LFWD or HFWD with or without sugar (42 g/l) added to the drinking water at a ratio of 55% fructose/45% sucrose (F/S). Indirect calorimetry was performed at 24 h, 2 wk, and 12 wk following a 24-h acclimation to the metabolic cages. Metabolic data were collected over a 48-h period. The mice were then stimulated with insulin at 2 and 12 wk. A second follow-up study was performed using male C57BL/6NHsd mice (n = 8, 6 wk old) from Harlan Laboratories housed one per cage in the Auburn University Veterinary Research Building. The mice were placed on a chow (Teklad Global Rodent Diet 2018) or HFWD with or without sugar (42 g/l) added to the drinking water at a ratio of 55% fructose/45% sucrose (F/S).

3.3.2 Antibodies and immunoblotting

Polyclonal antibodies to Akt, phospho-Akt (Ser^{473}), phospho-Akt (Thr^{308}), GSK3β, phospho-GSK3β (Ser^{9}), caspase-9 (mouse specific), cleaved caspase-9, caspase-3, cleaved caspase-3 (Asp^{175}), collagen 1, SCD1, and monoclonal antibodies to phospho-JNK (Thr^{183}/Tyr^{185}) were from Cell Signaling Technology (Danvers, MA). Rabbit monoclonal antibodies to $p67^{phox}$ and $p91^{phox}$(NOX2) were from Epitomics (Burlingame, CA). Polyclonal antibodies to $p22^{phox}$ and $p47^{phox}$ were from EMD Millipore (Billerica, MA). A polyclonal antibody to adiponectin was from Abcam (Cambridge, MA). Monoclonal antibodies to α-tubulin were from Sigma (St. Louis, MO). Goat anti-mouse and anti-rabbit peroxidase-conjugated antibodies were from Sigma. Goat anti-rabbit and anti-mouse Alexa fluor 635-conjugated secondary antibodies were from Molecular Probes/Invitrogen (Carlsbad, CA). Goat anti-rabbit and anti-mouse IRDye 650- and IRDye 800-conjugated secondary antibodies were from Li-Cor (Lincoln, NE).

3.3.3 Glucose and insulin tolerance tests and insulin stimulation

A blood sample was drawn from the tail veins of conscious mice for measurements of serum glucose using a FreeStyle FLASH glucometer and strips. Animals were fasted overnight, and a glucose tolerance test (GTT) was performed using 2 g glucose/kg body wt, administered by intraperitoneal injection. Glucose readings were taken at baseline (time = 0) and at 15, 30, 60, and 120 min after injection. One week after the GTT, an insulin tolerance test (ITT) was conducted using Novolin R human insulin at 0.85 U/kg body wt administered by intraperitoneal injection. Animals were fasted (5 h), and serum glucose was tested by tail vein at baseline (time = 0) and at 30, 45, 60, and 90 min after injection. The rate constant for glucose disappearance (K_{ITT}) was calculated using the formula $0.693/t_{1/2}$. The glucose $t_{1/2}$ was calculated from the slope of the least square analysis of the plasma glucose concentration during the linear decay phase. Insulin stimulation was performed in mice fasted overnight and then anesthetized with 2.5% isoflurane gas. Following opening of the abdominal cavity, insulin (12 mU/g) or sterile phosphate-buffered saline (PBS) was injected into the inferior vena cava, and then the liver and eWAT were harvested after 2 and 4 min, respectively, and then flash-frozen in liquid N_2.

3.3.4 Metabolic phenotyping and food intake

Energy expenditure was assessed by indirect calorimetry using a computer controlled system (PromethionM; Sable Systems, Las Vegas, NV). The calorimetry system consists of eight metabolic cages, which are essentially identical to home cages with bedding. Each cage was equipped with water bottles and food hoppers connected to load cells (MM-1, Sable Systems) for food and water intake monitoring. All mice had ad libitum access to food and water throughout the study.

Respiratory gases were measured with an integrated fuel cell oxygen analyzer, spectrophotometric CO_2 analyzer, and capacitive water vapor partial pressure analyzer (GA3m1, Sable Systems). Gas sensors were calibrated prior to each run with 100% N_2 as zero reference and with a span gas containing a known concentrations of 0.993% CO_2 with balance N_2 (AirGas, Opelika, AL). The PromethionM system utilizes a pull-mode, negative pressure system. The multichannel mass flow generator measures and controls air flow (FR8-1, Sable Systems). The in-current flow rate was set at 2,000 ml/min. Water vapor was continuously measured, and its dilution effect on O_2 and CO_2 was compensated for mathematically in the analysis stream [211]. Oxygen consumption ($\dot{V}o_2$) and CO_2 production ($\dot{V}co_2$) were measured for each mouse at 7-min intervals for 1 min. Air reference values are determined after measuring every four cages. Respiratory quotient (RQ) was calculated as the ratio of $\dot{V}co_2$over $\dot{V}o_2$. Energy expenditure was calculated using the Weir equation [212]:

$kcal/h = 60 \times (0.003941 \times \dot{V}o_2 + 0.001106 \times \dot{V}co_2)$.

Activity (ambulatory) was detected with XYZ beam arrays (BXYZ-R, Sable Systems) with a beam spacing of 0.25 cm. To assess activity, consecutive adjacent infrared beam breaks (X, Y, and Z) were scored as an activity count. Data acquisition and system control were coordinated using MetaScreen v. 2.2.8, and the obtained raw data were processed using ExpeData v. 1.8.2 (Sable Systems). The following data analysis scripts (macros) were used for data transformation: Macro 4, data summarized by circadian cycle (6 AM to 6 PM day) and Macro 13, combined metabolic uptake, and activity data acquired from each animal every 8 min.

The changes in weight of the food hoppers in the metabolic cages were not used to assess food uptake due to the observation that mice fed the HFWD consistently pulled food out of the hopper. Therefore, food uptake was assessed by manually weighing the food at 6 AM and 6 PM.

3.3.5 Liver tissue histological and lipid analysis

Paraffin-embedded sections were stained with hematoxylin and eosin and Masson's trichrome, examined in a blinded fashion by a board certified pathologist, and then graded for steatosis by determining the overall percentage of liver parenchyma containing lipid vacuoles, with 0 = none, 1 = mild (<30%), 2 = moderate (30–60%), and 3 = marked (>60%). Inflammation was graded by the presence or absence of inflammatory cells, with 0 = absent, 1 = minimal or focal occasional single clusters of inflammatory cells present in a few microscopic fields, 2 = mild inflammation, 3 = moderate inflammation, and 4 = marked inflammation. The pattern of fibrosis was graded with 0 = none, 1 = portal fibrosis, 2 = periportal fibrosis or rare septa, 3 = septal fibrosis and architectural distortion but not true cirrhosis, and 4 = cirrhosis, widespread fibrosis, and hepatocyte nodule formation. TGs were assayed using a kit from Thermo Scientific (Rockford, IL) and normalized to the protein content measured using the BCA protein assay reagent (Thermo Scientific/Pierce, Rockford, IL).

3.3.6 Adipose tissue histological and CLS enumeration

Paraffin-embedded sections were stained with hematoxylin and eosin and examined in a blinded fashion by a board-certified pathologist. Crown-like structures (CLS) were defined as shrunken adipocytes completely surrounded by morphologically identified macrophages and were counted on hematoxylin and eosin stained slides. Macrophage identification was verified with F4/80 cytoplasmic staining in step sections using rat anti-mouse F4/80 antibody (Abd Serotec, Raleigh, NC; Clone CI:A3-1) with Rodent Block M (BioCare Medical, Concord, CA) to reduce nonspecific staining. The entire surface area of each fat pad was counted to provide a total number of CLS per fat pad.

3.3.7 Adipocyte area

Slides were scanned using the Aperio ScanScope scanner (Vista, CA) and evaluated on VisioPharm software (Hoersholm, Denmark). Briefly, the entire adipocyte section was evaluated at 20× increments, using the following rules, to identify and measure adipocyte area. Objects were identified and counted as adipocytes if *1*) the area was between 500 and 20,000 μm, and *2*) it had a shape factor of 0–0.7, where a shape factor of 1 indicates a straight line and 0 indicates a perfect circle. Approximately 80–90% of the adipocytes were counted for each section.

3.3.8 Liver oxidative stress analysis

Liver samples were flash-frozen and ground in liquid nitrogen. Ground tissue (50–100 mg) was homogenized on ice in PBS pH 7.4 buffer. 4-Hydroxy-2-nonenal (4-HNE) staining was performed using a 4-HNE (HNE11-S) antibody (Alpha Diagnostics, San Antonio, TX). Five random fields per slide were scored, and the results were determined from an average of those scores. NADPH oxidase activity was measured by the lucigenin enhanced chemiluminescence method. Briefly, 50 μg of membrane protein fractionated from frozen liver was added to Krebs-Ringer buffer, pH 7.0, containing 1 mM EGTA, 150 mM sucrose, 5 μM lucigenin, and 100 μM NADPH. Photon emission in terms of relative light units was measured in a luminometer every 30 s for 5 min. There was no measurable activity in the absence of NADPH. Superoxide anion production was expressed as relative chemiluminescence (light) units (RLU)/mg protein. Protein content was measured using the BCA protein assay reagent (Thermo Scientific-Pierce, Rockford, IL).

3.3.9 Alanine aminotransferase assay

The Alanine Aminotransferase-SL Assay (Genzyme Diagnostics) was performed in 96-well plates. The change in absorbance at 340 nm at 37°C was monitored over 12 min using a Molecular Devices Spectramax spectrophotometer and SOFTmax PRO software. Alanine aminotransferase (ALT) was calculated as units/liter using the manufacturer's formula and molar extinction coefficient of NADH. Protein content was determined by the BCA assay. ALT (U/l) was normalized to protein concentration.

3.3.10 Apoptosis analysis

TUNEL-positive cells were detected using the DeadEnd Fluorometric TUNEL system (Promega, Madison, WI) and the manufacturer's recommendations for controls. Propidium iodide (0.25 mg/ml) was used as the counterstain. An average score was generated based on a ratio of positive nuclei to total nuclei in 3 random fields at ×200 magnification.

3.3.11 Measurement of SOD activity

Total SOD activity was measured by determining the ability to inhibit the auto-oxidation of pyrogallol using the method described by Marklund and Marklund [213]. The rate of auto-oxidation was determined by measuring increases in the absorbance at 420 nm. Reaction mixture containing 0.2 mM pyrogallol in 50 mM Tris-cacodylic acid buffer (pH 8.5) and 1 mM diethylenetriamine pentaacetic acid was incubated for 3 min at 25°C. One unit of SOD activity was defined as the amount of the enzyme required to inhibit the rate of pyrogallol auto-oxidation by 50%. SOD activity was expressed as a unit activity per milligram of protein.

3.3.12 Subcellular fractionation

Frozen liver tissue was ground with mortar and pestle in liquid N_2, and then 100–150 mg ground-frozen tissue was placed in a 1.5-ml homogenization buffer containing 10 mM Tris (pH 7.4), 20 mM sucrose, 0.1 mM Na_3VO_4, 100 nM okadaic acid, and 1× protease inhibitor cocktail Set I (Calbiochem/EMD Biosciences, La Jolla, CA) and then precleared by centrifugation at 250 *g* for 5 min at 4°C. Precleared tissue was homogenized by passage through a 25-gauge needle 7–8× on ice in buffer. Homogenates were centrifuged at 100,000 *g* for 30 min at 4°C. The supernatant was removed and designated as the cytosolic fraction. The pellet was resuspended in a buffer containing 10 mM Tris (pH 7.4), 2 mM NaCl, 1% Triton X-100, 0.1 mM Na_3VO_4, 100 nM okadaic acid, and 1× protease inhibitor cocktail (Pierce), incubated on ice for 30 min, and then centrifuged at 100,000 *g* for 30 min at 4°C. The resultant supernatant was transferred to a fresh tube and designated as the Triton-soluble (membrane) fraction.

3.3.13 Western blot analysis

Tissue was lysed with 50 mM HEPES, pH 7.5, 150 mM NaCl, 1% Nonidet P-40, 0.1% SDS, 0.1% sodium deoxycholate, 1 mM NA_3VO_4, 100 nM okadaic acid, and 1× protease inhibitor mixture Set I. Cellular debris was removed by centrifugation at 15,000 rpm for 15 min at 4°C. Protein content of the clarified lysate was determined using bicinchoninic acid (BCA) reagents from Thermo Scientific (Rockford, IL). Isolated proteins were denatured in SDS gel buffer, separated by SDS-PAGE, and immunoblotted. Enhanced chemiluminescence substrate was from GE Healthcare (Piscataway, NJ). Goat anti-rabbit and anti-mouse Alexa fluor 635, horseradish peroxidase-conjugated, IRDye680, and IRDye 800 secondary antibodies were used for detection and quantitation of immunoblots. Membranes were imaged using a Storm PhosphoImager (GE

Healthcare) or LiCor Odyssey scanner, and blots were analyzed by Image Studio 2.0 analytical software (LiCor, Lincoln, NE).

3.3.14 RNA isolation and qRT-PCR

TRIzol reagent (Sigma-Aldrich, St. Louis, MO) was used to isolate total RNA from frozen tissue. RNA quantity and quality were assessed using a bioanalyzer (Agilent 2100 Bioanalyze; Agilent Technologies, Santa Clara, CA) prior to reverse transcription using the RT^2 First Strand Kit (Qiagen, Valencia, CA). PCR was performed in 384-well plates with the RT^2 SYBR Green ROX qPCR Mastermix (Qiagen, Valencia, CA) with gene-specific primers (SABiosciences, Fredrick, MD) using an Applied Biosystems 7900HT Sequence Detection System (Life Technologies, Carlsbad, CA) with a Corbett Robotics CAS-1200 precision liquid handling system for plate set-up. Melting curve analysis was performed to verify product purity. A threshold value of 0.02 was used for the analysis of gene expression. GAPDH was used to normalize ΔCt values.

3.3.15 Statistical analysis

Chemiluminescent and fluorescent signals were directly quantitated using Storm 860 Imager and ImageQuant v. 5.1 software. The absolute integration value of the immunoreactive bands minus background was determined. Statistical significance of gene expression data was analyzed by Student's *t*-test ($\alpha = 0.05$) using the LFWD group as a control. Statistical significance between groups was determined by one-way repeated-measures analysis of variance ($\alpha = 0.05$) using the XLSTAT 2009 program (Addinsoft, New York, NY). Pairwise comparisons were made using the Newman-Keuls test ($\alpha = 0.05$). Statistical significance of frequency distributions was

determined by Kolmogorov-Smirnov test ($\alpha = 0.05$) using the XLSTAT 2009 program (Addinsoft, New York, NY). Analysis of covariance (ANCOVA) comparison tests were used to test if the slopes of the adipocyte area vs. eWAT weight lines differed significantly or not ($\alpha = 0.05$) using the XLSTAT 2009 program (Addinsoft). Statistical significance of the impact of body weight as a covariate on energy expenditure was analyzed by ANCOVA ($\alpha = 0.05$) using the Mouse Metabolic Phenotyping Centers Energy Expenditure Analysis web page [214].

3.4 Results

3.4.1 Effects of diets on body and organ weight and serum metabolites

C57Bl/6N mice aged 6 wk were placed on a LFWD or HFWD with or without 42 g/l F/S in the drinking water for up to 12 wk. The LFWD group served as the control group. The characteristics of mice at the age of 2 and 12 wk are shown in Table 1. Mice fed the HFWD+F/S gained the most weight at 2 and 12 wk ($P < 0.05$). A significant 67% increase in liver weight normalized to body weight from 2 to 12 wk was observed in the HFWD+F/S group compared with <10% in the other groups ($P < 0.05$). Consistent with these results, a disease marker of hepatocyte damage, ALT, was greatest in mice from the HFWD+F/S group at 12 wk ($P < 0.05$). We also found that eWAT weight normalized to body weight at 2 wk was markedly higher in the HFWD+F/S group ($P < 0.05$). However, the greatest increase (132%) in normalized eWAT weight from 2 to 12 wk was observed in the HFWD group, whereas, surprisingly, an 11% decrease was observed in the HFWD+F/S group. Serum glucose was significantly elevated in the HFWD-fed mice at 2 wk but surprisingly along with HFWD+F/S-fed mice not at 12 wk. The lack of an effect of high fat or sucrose feeding on serum glucose has been reported by others in C57Bl/6 mice [215, 216], although this phenomenon is not consistently observed. Unlike serum

levels of glucose and TGs, serum levels of insulin were significantly higher in the HFWD+F/S group compared with all the other groups at both the 2- and 12-wk time points ($P < 0.05$). Taken together, these data indicated that, compared with HFWD-fed mice, HFWD+F/S-fed mice have significantly greater body weight and normalized liver weight with greater liver hepatocyte damage yet limited eWAT expansion.

3.4.2 Effects of diets on energy expenditure, substrate utilization, activity, and food intake

To gain insight into the weight gain observed in the groups, 24-h total energy intake was first assessed in group-housed mice. The HFWD- and HFWD+F/S-fed mice consumed more total calories per day than the other two groups at 2 wk (Table 1). There was no difference in 24-h total energy intake between LFWD-, HFWD-, and HFWD+F/S-fed mice at 12 wk. Interestingly, water consumption was greatest in the LFWD+F/S group at 2 and 12 wk. Next, the metabolic phenotype was assessed at 2 and 12 wk. Circadian energy expenditure, activity, and food consumption were determined using metabolic cages. At 2 wk, no significant differences were observed in total energy expenditure between the diet treatments in the day and night phases (Fig. 6*A left*). Furthermore, no differences in total energy expenditure between the HFWD and HFWD+F/S groups in the day and night phases were observed when analyzed by ANCOVA (data not shown). Total energy expenditure was also not significantly different from the day to the night phase for the LFWD and HFWD groups. In contrast, total energy expenditure was significantly elevated between the day and night phases for the LFWD+F/S and HFWD+F/S groups. Total activity was not significantly different between the diet treatments in the day and night phases (Fig. 6*A right*). To examine the changes in energy expenditure, substrate utilization, and activity over a 24-h period at 2 wk, metabolic cage data were analyzed every 8 min for the

24-h period. As shown in Fig. 6C (*top left* and *right*), no statistical differences were observed in average energy expenditure between the LFWD and LFWD+F/S groups, whereas in the comparison between the HFWD and HFWD+F/S groups average energy expenditure was elevated in the mid-night phase in the HFWD+F/S group. No statistical differences were observed in average substrate utilization between the LFWD and LFWD+F/S groups or the HFWD and HFWD+F/S groups (Fig. 6*C middle*, *left* and *right*). Statistical differences in activity (pedestrian meters) traveled between the LFWD and LFWD+F/S groups were observed in the night phase, with the mice in the LFWD+F/S group showing more activity, although LFWD-fed mice were also observed in the day and night phases to have significantly increased activity (Fig. 6*C bottom left*). In contrast, HFWD+F/S-fed mice were more significantly active at 10 different time points in the night phase compared with the HFWD-fed mice (Fig. 6*C bottom right*). Circadian assessment of food intake, feeding bouts, and rate of food intake indicated that HFWD+F/S-fed mice consumed a great amount of food in the day and night phases at 2 wk (data not shown). However, because mice removed the HFWD from the food hopper in the metabolic cages (data not shown), accurate circadian food intake was not possible in the metabolic cages. Therefore, to examine circadian food intake, an independent study was performed in which the food from chow-, HFWD-, and HFWD+F/S-fed mice was manually measured at zeitgeber time 0 (ZT0) and ZT12 in singly housed mice. As shown in Fig. 6*B*, HFWD+F/S-fed mice, but not HFWD-fed mice, consumed a significantly greater amount of food than the chow-fed mice during the day phase at 2 wk. Food uptake in the HFWD+F/S group was also significantly elevated in the night phase compared with HFWD-fed mice. Thus, our data suggest that consumption of liquid sugar in singly housed HFWD-fed mice results in hyperphagia independently of changes in energy expenditure.

Circadian analysis of mice fed the diets for 12 wk revealed that total energy expenditure in the day phase was significantly elevated in the HFWD and HFWD+F/S groups compared with LFWD and LFWD+F/S fed mice (Fig. 7*A left* and *right*). Consistently, no statistical differences were observed in average energy expenditure and substrate utilization during the day phase for metabolic cage data that were analyzed every 8 min (Fig. 7*C top* and *middle*, *left* and *right*). In the night phase, total energy expenditure was also significantly elevated in the HFWD and HFWD+F/S mice compared with LFWD- and LFWD+F/S-fed mice (Fig. 7*A left*). In contrast, total activity was significantly reduced in the HFWD- and HFWD+F/S-fed mice (Fig. 7*A right*). Analysis of pedestrian meters traveled revealed that LFWD+F/S-fed mice had a greater number of significantly elevated events compared with LFWD-fed mice (Fig. 7*C bottom left*). In contrast, HFWD-fed mice had a greater number of significantly elevated pedestrian meters events than HFWD+F/S fed mice (Fig. 7*C bottom right*). No difference in food uptake was observed in the day phase between chow-, HFWD-, and HFWD+F/S-fed mice, whereas, in contrast, chow-fed mice consumed more food than HFWD- and HFWD+F/S-fed mice in the night phase (Fig. 7*B*). Our data suggest that consumption of sugary drinking water differentially effects activity in longer-term LFWD- and HFWD-fed mice.

Changes in food uptake but not total energy expenditure and total activity at 2 wk suggest an early hyperphagic response in the HFWD-fed mice consuming sugary drinking water. To examine whether the hyperphagic response was acute, manual food uptake was determined in the first 24 h following the change to the HFWD and HFWD+F/S treatments. As shown in Fig. 8*B*, food intake in the day phase but not the night phase in the HFWD+F/S-fed group was significantly elevated compared with the chow- and HFWD-fed groups. Circadian total energy expenditure and activity were also assessed over the 24-h period following the change in the

diets. As shown in Fig. 8, *A*and *B*, there were no significant differences between diet treatment groups in the day and night phases for total energy expenditure and activity.

Analysis of average energy expenditure every 8 min over a 48-h period following the change in the diets revealed few significant events when LFWD and LFWD+F/S groups were compared (Fig. 8*C top left*) and HFWD and HFWD+F/S groups were compared (Fig. 8*C top right*). In contrast, significant reductions were observed in the night phase for RQ in LFWD+F/S-fed mice compared with LFWD-fed mice, whereas RQ in the second day phase following the change in the diets was significantly elevated in the LFWD+F/S-fed mice compared with LFWD-fed treatments (Fig. 8*C middle left*). No significant changes in RQ were observed between the HFWD and HFWD+F/S treatments (Fig. 8*C middle right*). However, more significant pedestrian meter events in the day and night phases were observed in HFWD-fed mice compared with HFWD+F/S-fed mice. These data suggest an early direct effect of liquid F/S consumption on RQ in LFWD-fed mice and food intake and activity independent of energy expenditure in HFWD-fed mice.

3.4.3 Effects of diets on glucose tolerance, insulin resistance, and insulin signaling

To further explore metabolic changes associated with the consumption of liquid sugar in LFWD- and HFWD-fed mice, we performed a glucose tolerance test (GTT) and an insulin tolerance test (ITT) at 2 and 12 wk to assess glucose tolerance and insulin resistance, respectively. Fasting glucose and insulin levels were used to assess insulin sensitivity by using the Quicki score. The GTT performed at 2 wk demonstrated that only mice in the HFWD+F/S group displayed glucose intolerance (Fig. 9, *A* and *C*), whereas both HFWD- and HFWD+F/S-fed mice exhibited glucose intolerance at 12 wk (Fig. 9, *B* and *D*). The ITT at 2 wk demonstrated that the insulin-mediated

reduction in blood glucose was significantly different only at the 45-min time point between the HFWD+F/S group and the LFWD and LFWD+F/S groups (Fig. 9*E*). However, no differences were detected in the glucose disappearance rates (K_{ITT}; Fig. 9*G*) and Quicki score (Table 1). In contrast, the ITT at 12 wk indicated that insulin resistance was greatest in the HFWD+F/S group as reflected by reduced K_{ITT} value compared with other groups (Fig. 9, *F* and *H*), and the Quicki score demonstrated that HFWD+F/S-fed mice were less insulin sensitive than HFWD-fed mice (Table 1). To confirm and expand our findings on insulin resistance, we stimulated mice with insulin at 2 and 12 wk to assess activation of insulin signaling proteins in liver and adipose tissue. As shown in Fig. 10, mice from all diet treatment groups at 2 wk were responsive to insulin. However, we detected a significant reduction in hepatic and adipose phospho-Akt at Ser^{473} and Thr^{308} phosphorylation in the HFWD+F/S group compared with all other diet treatment groups (Fig. 10, *A* and *B*, *top right*). HFWD+F/S-fed mice also had a significantly lower level of phospho-GSK3β-Ser9 in liver but not adipose tissue compared with the other groups (Fig. 10, *A* and *B*,*bottom right*). Insulin stimulation at 12 wk indicated that hepatic Akt-Ser^{473}, Akt-Thr^{308}, and GSK3β-Ser^{9} phosphorylations were significantly increased upon insulin stimulation in all the diet groups (Fig. 11*A*); however, they were blunted by the addition of liquid sugar in LFWD- and HFWD-fed mice (Fig. 11*A*). Consistent with our ITT data, we observed the lowest level of insulin stimulated Akt-Ser^{473}, Akt-Thr^{308}, and GSK3β-Ser^{9} in the liver from mice in the HFWD+F/S group (Fig. 11*A*). Furthermore, insulin failed to stimulate adipose Akt-Ser^{473}, Akt-Thr^{308}, and GSK3β-Ser^{9}phosphorylations in HFWD+F/S-fed mice (Fig. 11*B*). Taken together, our data indicated that consumption of liquid sugar accelerates HFWD-induced glucose intolerance and exacerbates HFWD-induced insulin resistance in mice.

3.4.4 Effects of diets on the hepatic gene expression

Our observation that consumption of liquid sugar differentially effected normalized liver weight, glucose tolerance, and insulin resistance suggested a hepatic effect of liquid sugar consumption. Thus, we examined the temporal changes in expression of hepatic genes regulating lipid metabolism, inflammation, oxidative stress, apoptosis, cell cycle, and fibrosis using quantitative (q)PCR. The hepatic genes were chosen based on major pathological changes observed in NAFLD. To visualize only significant changes to the expression of the genes compared with the LFWD group, we constructed a Venn diagram (Fig. 12*A left*), and fold changes and P values can be found in Supplemental Table S1 (supplemental material can be found in the appendix). Individual lipid metabolism genes were differentially regulated across the groups at 2 wk; however, a small set (8/62) overlapped between the LFWD+F/S, HFWD, and HFWD+F/S groups. We observed that significant reductions in the expression of genes regulating apoptosis occurred in all the diet groups (Fig. 12*A left*, and Supplemental Table S1). For genes regulating cell cycle and oxidative stress, no consistent changes to expression were observed across the treatment groups (Fig. 12*A left*, and Supplemental Table S1). Noticeably, the expressions of genes regulating inflammation were not significantly changed in any of the treatment groups at 2 wk (Supplemental Table S1).

We next investigated the change in expression of the same hepatic genes at 12 wk. Again, a Venn diagram was constructed to represent only significant changes to the expression of genes compared with the LFWD group (Fig. 12A *right*). Analysis of genes regulating lipid metabolism revealed that Acox1, PGC1α, MTTP, PPARα, and Apo C-III were differentially regulated in the LFWD+F/S and HFWD groups (Fig. 12A *right*, and Supplemental Table S2). In contrast, IRS-2 and SREBP-1were significantly reduced only in the HFWD+F/S group. Significant reductions

(>2-fold) in the expression of genes regulating glucose metabolism, G6P and PCK, overlapped between the HFWD and HFWD+F/S groups (Fig. 12A *right*, and Supplemental Table S2). For inflammation associated genes, we observed that TNFα gene expression was significantly increased in all the treatment groups, yet the highest level of expression was observed in the HFWD+F/S group (3.5-fold; Supplemental Table S2). In addition, substantial increases in gene expression of greater than 3-fold in MIP1α was observed exclusively in the HFWD+F/S group (Supplemental Table S2). Significant changes to the expression of cell cycle and apoptosis function genes (BNIP3, GADD45, and FASL) were primarily observed in the HFWD groups (Fig. 12A *right*). Analysis of genes with an oxidative stress function revealed that expression of hepatic Nox4 was significantly decreased only in the HFWD+F/S group (Fig. 12A *right*, and Supplemental Table S2). Furthermore, $gp91^{phox}$and $p67^{phox}$ gene expression was significantly elevated only in the HFWD+F/S group. Analysis of genes with a fibrosis function (collagen 1a2, collagen 3a1, and TGFβ) showed that a significant increase in the expression of these genes occurred only in the HFWD+F/S group (Fig. 12A *right*, and Supplemental Table S2). Taken together, our data demonstrate that significant increases in expression to inflammation, oxidative stress and fibrosis genes are concentrated in the liver from the HFWD+F/S group.

3.4.5 Hepatic steatosis

We investigated the role of sugar in the drinking water on Western diet-induced hepatic steatosis. Histological scoring of stained liver tissue sections from the diet treatment groups at 2 wk revealed that the steatosis score was significantly elevated in the HFWD+F/S group compared with the HFWD+F/S group but not the LFWD and LFWD+F/S groups (Fig. 12, *B* and *C left*). However, the liver TG level was significantly elevated in the HFWD+F/S group compared with

all other dietary treatments (Fig. 12*D left*). At 12 wk, the steatosis score was significantly elevated in the HFWD+F/S groups compared with the LFWD and LFWD+F/S groups, yet statistical significance ($\alpha = 0.05$) was not reached compared with the HFWD group (Fig. 12, *B* and *C right*). In contrast, a significant difference in liver TG level was observed between the HFWD and HFWD+F/S groups (Fig. 12*D right*).

3.4.6 Hepatic inflammation and oxidative stress

The role of sugar in the drinking water on Western diet-induced hepatic inflammation was investigated. Histological examination of stained liver sections at 2 wk indicated an absence in inflammation only in the HFWD group (Fig. 12E left). The HFWD+F/S group had the greatest number of animals with inflammation, although statistical significance ($\alpha = 0.05$) was not reached (Fig. 12*E left*). The inflammation score increased from 2 to 12 wk in all of the diet treatment groups, although there were no significant differences in inflammation score between groups at 12 wk (Fig. 12*E right*). To further investigate hepatic inflammation, JNK phosphorylation was assessed. A significant increase in phospho-JNK was detected only in the HFWD+F/S group (Fig. 12*F*). Taken together, our data do not fully support that hepatic inflammation is concentrated in the HFWD+F/S group.

Next, we examined the role of sugar in the drinking water on hepatic oxidative stress, which is thought to play a key role in progression of NAFLD from steatosis to steatohepatitis [217]. Examination of liver tissue from mice in the LFWD+F/S and HFWD+F/S groups showed significantly elevated staining for 4-HNE, a highly reactive aldehyde generated by exposure of polyunsaturated fatty acids to peroxides and reactive oxygen species (Fig. 13*A*). In contrast, we observed that hepatic total SOD activity was significantly decreased only in the HFWD+F/S

group (Fig. 13*B*). NADPH oxidase subunit protein expression was elevated for $p22^{phox}$ protein and decreased for $p47^{phox}$ and $gp91^{phox}$ across all diet treatments compared with the control diet (Fig. 13*C*). Taken together, our data do not strongly indicate that hepatic oxidative stress is exacerbated by the addition of liquid sugar in HFWD-fed mice.

3.4.7 Hepatic apoptosis

Apoptosis is a characteristic marker for the progression of steatosis to steatohepatitis. It is associated with an inflammatory response and is thought to play a critical role in the development of fibrosis [82]. Analysis of TUNEL-positive hepatocytes in liver sections from mice fed the diets for 12 wk revealed significantly elevated TUNEL-positive hepatocytes in the HFWD+F/S group compared with the LFWD+F/S group. However, the HFWD+F/S group was not significantly different ($\alpha = 0.05$) compared with the LFWD and HFWD groups (Fig. 14*A*). Apoptosis was further examined by assessing caspase-3 and -9 total and cleaved protein levels. A significant increase in total but not cleaved caspase-9 was observed only in the HFWD+F/S group compared with all other groups (Fig. 14*B*). There was no change in total caspase-3 in any of the diet groups. However, cleaved caspase-3 was significantly reduced in the HFWD+F/S groups. Taken together, our data suggest that hepatic apoptosis is modulated by the addition of liquid sugar in HFWD-fed mice.

3.4.8 Hepatic fibrosis

Next, hepatic fibrosis was investigated in the mice fed the diets for 12 wk. Eighty-six percent of the mice in the HFWD+F/S group developed fibrosis compared with only 33% in the LFWD

group (Fig. 14*C*). Furthermore, only HFWD+F/S-fed mice developed the most severe type of fibrosis (Fig. 14*D*). Protein expression of collagen I, an important marker of hepatic fibrosis, was greatest in the HFWD+F/S group, although it did not reach statistical significance at $\alpha = 0.05$ (Fig. 14*E*). Finally, we tallied steatosis, inflammation, and fibrosis scores for each animal to generate a NAFLD total score. As shown in Fig. 14*F*, the HFWD+F/S group had a significantly greater NAFLD total score at 12 wk. Thus, consumption of liquid sugar appears to exacerbate NAFLD in HFWD-fed mice.

3.4.9 Effects of diets on adipose RNA expression

Our observation that eWAT expansion was impaired in the HFWD+F/S group but not the HFWD group (Table 1) suggested that liquid sugar consumption differential affected the eWAT adipose depot in Western diet fed-mice. Thus, we examined, using qPCR, the temporal changes in expression of adipose genes regulating lipid metabolism, inflammation, oxidative stress, apoptosis, and cell cycle, which are known to be modulated by overnutrition [218]. To visualize only significant changes to the expression of the genes, we constructed a Venn diagram (Fig. 15*A left*), while fold changes and *P* values can be found in Supplemental Table S3. Analysis of adipose genes revealed that individual lipid metabolism genes were differentially regulated across the groups at 2 wk. However, a small subset (3/20) of lipid metabolism genes overlapped among the LFWD+F/S, HFWD, and HFWD+F/S groups (Fig. 15*A left*, and Supplemental Table S3). Similar results were observed in the expression of genes regulating oxidative stress (SOD2, Hmox1, NCF, and Nrf2; Fig. 15*A left*, and Supplemental Table S3). For genes regulating inflammation, we observed that only IL-6 gene expression was significantly increased in all of the treatment groups at 2 wk, yet the highest level of expression was observed in the LFWD+F/S

group (3.1-fold; Supplemental Table S3). However, no consistent changes to expression of genes regulating cell cycle and apoptosis were observed across the treatment groups (Fig. 15*A left*, and Supplemental Table S3).

We next investigated the change in expression of the same adipose genes at 12 wk. Again, a Venn diagram was constructed to represent only significant changes to the expression (Fig. 15*A right*). Changes to genes regulating lipid metabolism were concentrated in HFWD and HFWD+F/S groups at 12 wk; however, a unique group (CEBPα, SREBP1, ATGL, and SCD-1) was observed significantly reduced only in the HFWD+F/S group at 12 wk (Fig. 15*A right*, and Supplemental Table S4). Interestingly, adiponectin was also significantly reduced only in HFWD+F/S group at 12 wk (Fig. 15*A right*, and Supplemental Table S4). Consistent with the RNA expression, protein levels of adipose SCD-1, ATGL, and adiponectin were significantly reduced in the HFWD+F/S group compared with control group (Fig. 15, *B* and *C*).

A significant increase (>2-fold) in the expression of genes regulating inflammation (IL1β, MIP1α, and TNFα) overlapped between the HFWD and HFWD+F/S groups (Fig. 15*A right*, and Supplemental Table S4). Similar results were observed in the expression of genes regulating oxidative stress ($p22^{phox}$, $p91^{phox}$, $p47^{phox}$, $p67^{phox}$, Hmox1, and Nrf2) in the HFWD and HFWD+F/S groups at 12 wk (Fig. 15*A right*, and Supplemental Table S4). Furthermore, a significant increase in the expression of genes regulating cell cycle (p21) was also observed in the HFWD and HFWD+F/S groups. Consistent with this, gene expression of GADD45 and cyclin D1 were significantly increased in the HFWD and HFWD+F/S groups, respectively (Fig. 15*A right*, and Supplemental Table S4). No significant changes were observed in the expression of genes regulating apoptosis in any treatment groups at 12 wk (Supplemental Table S4).

Analysis of PKC isoform expression at 12 wk (Fig. 15*A*, *right*, and Supplemental Table S4)

revealed that a significant increase (>2-fold) in the expression of PKCβ and PKCδ overlapped between the HFWD and HFWD+F/S groups, whereas a surprising, significant decrease (>2-fold) in the expression of PKCε was observed only in HFWD+F/S group.

3.4.10 Adipocyte size

To determine whether hypertrophy played a role in fat accumulation in the HFWD and HFWD+F/S groups, we measured adipocyte diameter in the eWAT from mice at 2 and 12 wk. A significant increase was observed at 2 wk in the diameter of eWAT adipocytes in the HFWD+F/S group compared with the LFWD and HFWD groups (Fig. 16, *A* and *B top left*). However, the diameter of eWAT adipocytes at 12 wk in the HFWD+F/S group was not significantly different from those in the HFWD group (Fig. 16, *A* and *B top right*).

3.4.11 Adipose macrophage-containing crown-like structures and inflammation gene expression

We next investigated the inflammatory status of eWAT, since low-level chronic inflammation and macrophage infiltration into WAT is a well-documented phenomenon in obesity [219]. Macrophage infiltration in WAT is characterized by the appearance of crown-like structures (CLS), which constitute proinflammatory macrophages surrounding dying adipocytes [220]. Therefore, to examine whether macrophage infiltration in eWAT is coincident with increased fat pad size and adipocyte hypertrophy, histological analysis using H&E and the macrophage marker F4/80 of eWAT was undertaken to assess CLS. No differences were observed in the number of CLS in the HFWD group compared with the LFWD group (Fig. 16, *A* and *B, bottom*). In contrast, a significant 12-fold increase in CLS was observed in the HFWD+F/S compared

with LFWD and HFWD groups (Fig. 16*B bottom*). The presence of macrophages in the CLS was confirmed using the murine macrophage-specific marker F4/80 (Fig. 16*C*). To investigate the disparity in CLS in eWAT from the HFWD and HFWD+F/S groups, proinflammatory gene expression in the eWAT was determined. As shown in Fig. 16*D*, proinflammatory gene expression was elevated in the HFWD+F/S group. However, only MIP1α was significantly elevated (~15-fold) in the HFWD+F/S group. TNFα gene expression was significantly elevated in the HFWD+F/S groups compared with the LFWD and LFWD+F/S groups, yet statistical significance ($\alpha = 0.05$) was not reached compared with the HFWD group. Taken together with our adipocyte size data, a HFWD induces adipocyte hypertrophy and consumption of liquid sugar exacerbates HFWD-induced adipose tissue inflammation.

3.4.12 Adipose tissue dynamics

Our normalized eWAT and adipocyte diameter data suggested that dynamic changes to the eWAT depot were occurring in the groups and in particular with the HFWD- and HFWD+F/S-fed mice between 2 and 12 wk. To further explore the dynamic changes, we determined the area of the adipocytes in the eWAT from HFWD-, HFWD+F/S-fed mice, and LFWD-fed mice as a control, at 2 and 12 wk and plotted the data by the mean frequency of the area for 2,000 to 12,000 adipocytes per fat pad. As shown in Fig. 17*A left*), the distribution of the frequency of adipocytes was not significantly different from 2 to 12 wk in LFWD-fed mice. In contrast, there was a highly significant shift in the area of adipocytes from 2 to 12 wk in HFWD-fed mice (Fig. 17*A middle*), indicating that 12 wk HFWD-fed mice have larger adipocytes. We also observed that the distribution was significantly different from 2 to 12 wk in HFWD+F/S-fed mice (Fig. 17*A right*). Consistent with the adipocyte diameter data, the distribution of adipocyte area was

shifted in the HFWD+F/S group compared with the LFWD and HFWD groups at 2 wk (data not shown). Taken together, our adipocyte diameter and area data suggest a role for hypertrophy in the expansion of the eWAT from 2 to 12 wk and acceleration in hypertrophy in the HFWD+F/S group.

To further investigate the expansion of the eWAT depots from 2 to 12 wk, we examined the relationship between eWAT average adipocyte area and adipose tissue weight as described by MacDougald's group[221-223]. The correlation between average adipocyte area and adipose tissue weight between treatment groups provided information on the adipocyte number and size [221]. As shown in Fig. 17*B left*, the relationship between average adipocyte area and eWAT weight was virtually identical in LFWD-fed mice from 2 to 12 wk. In HFWD-fed mice the dramatic shift in eWAT weight from 2 to 12 wk was accompanied by a steeper slope in the 12-wk-fed mice compared with the 2-wk-fed mice, although the slopes were not significantly different ($P = 0.053$). However, in HFWD+F/S-fed mice with similar eWAT weights from 2 to 12 wk, there was a significant flatting of the slope in the 12-wk-fed mice compared with the 2-wk-fed mice. When the three diet groups were compared with one another at 2 wk, the HFWD+F/S group was significantly different from the LFWD and HFWD groups (data not shown), whereas all three diet groups were significantly different from one another at 12 wk (data not shown). These data suggest that there was little change in the size of adipocytes in the LFWD group from 2 to 12 wk whereas a slight change in number was accompanied by a significant change in size in the HFWD group. This appears to be different from that observed in the HFWD+F/S group based on the change in slope from 2 to 12 wk.

To gain insight into the mechanism mediating the dynamic difference occurring in the eWAT between the HFWD- and HFWD+F/S-fed mice, we next examined expression of genes

regulating hypoxia, angiogenesis, and fibrosis, which play important roles in adipose tissue expansion in the eWAT [224, 225]. In 2-wk-fed mice, HIF1α, a master regulator of the hypoxia response [226], showed significantly elevated expression in both HFWD and HFWD+F/S groups compared with the LFWD and LFWD+F/S groups; however, no differences were detected between the HFWD and HFWD+F/S groups (Fig. 17*C top left*). In contrast, gene expression of a HIF1α target, lysyl oxidase (LOX), was significantly increased only in the HFWD+F/S group (Fig. 17*C top middle*). Examination of genes regulating eWAT angiogenesis at 2 wk showed that VEGF gene expression was not significantly different between the diet treatments (Fig. 17*C top left*). However, significantly greater Ang1 gene expression was observed only in the LFWD+F/S-fed mice compared with LFWD-fed mice (Fig. 17*C bottom left*). We next examined in 2-wk-fed mice the gene expression of collagen 1a1 and collagen 6a1, which are considered major extracellular matrix (ECM) components in adipose tissue [227]. Significantly increased expression of collagen 1a1 was observed in both HFWD and HFWD+F/S groups (Fig. 17*C bottom middle*). However, no difference was observed in the gene expression of collagen 6a1 across groups (Fig. 17*C bottom right*). Taken together, our data suggest an early hypoxia response in both HFWD and HFWD+F/S groups, with the potential for greater collagen cross-linking in the HFWD+F/S fed mice and a trend toward greater angiogenesis in LFWD+F/S-fed mice. Examination of gene expression regulating hypoxia, angiogenesis, and fibrosis in the eWAT from 12-wk-fed mice revealed that HIF1α and LOX were significantly greatest in the HFWD+F/S group (Fig. 17*D top left* and *middle*). Furthermore, a significant reduction in the expression of VEGF and Ang1 was also observed in HFWD+F/S group (Fig. 17*D top left* and *bottom right*). In contrast, VEGF was significantly elevated only in the LFWD+F/S group (Fig. 17*D top right*). HFWD+F/S-fed mice had significantly elevated gene expression of

collagen 6a1 at 12 wk (Fig. 17*D bottom middle*). However, collagen 1a1 gene expression at 12 wk in the HFWD+F/S group was not significantly different from those in the HFWD group (Fig. 17*D bottom middle*). Taken together, our data in the eWAT at 12 wk suggest a role for increased hypoxia and fibrosis and reduced angiogenesis in HFWD+F/S-fed mice and a trend toward greater angiogenesis in LFWD+F/S-fed mice.

3.5 Discussion

The metabolic phenotype of the HFWD+F/S model of obesity and NAFLD was explored at 2 and 12 wk to determine the metabolic parameters modulated by the HFWD and F/S treatments. Our observation that F/S consumption in HFWD-fed mice induced hyperphagia at 2 wk in the absence of changes to energy expenditure suggested an early effect of liquid sugar consumption. To examine whether the hyperphagic response was acute, we determined the metabolic phenotype of the HFWD+F/S model at 24 h after the transition to the dietary treatment. Our observation of the hyperphagic response in the day phase at 24 h in HFWD+F/S fed mice suggests an initial circadian disruption to the normal feeding pattern that has previously been reported in high-fat-fed mice [228]. Consistent with the changes in diet, a reduction in substrate utilization was observed in HFWD- and HFWD+F/S-fed mice at 24 h that persisted at 2 wk. After 12 wk of HFWD feeding (with and without F/S), we observed differences in energy expenditure, total activity, and substrate utilization with the LFWD- and LFWD+F/S-fed mice. The data from 12 wk HFWD-fed mice (with and without F/S) are consistent with the phenotype associated with HFD-induced obesity that has previous been reported [229, 230].

As we expected, the HFWD resulted in a large increase in normalized eWAT weight at 12 wk. HFWD+F/S-fed mice, despite showing the highest normalized eWAT weight at 2 wk, had

significantly less normalized eWAT after 12 wk, which indicated that the capacity of the eWAT to expand was impaired in the HFWD+F/S group. Our results are in agreement with a recently study demonstrating that the capacity of the eWAT to expand in high-fat diet-fed C57Bl/6 mice is impaired in mice that achieve a mass of around 40 g [231]. Interestingly, van Beek et al. [231] did not observe impaired expansion of the subcutaneous and mesenteric depots. It will be important to examine in future studies whether subcutaneous and mesenteric depot expansion is also not impaired in HFWD+F/S-fed mice. Impairment in adipose tissue expansion has been found to be a critical factor in the development of insulin resistance [232], whereas enhanced adipose tissue expandability can lead to an improvement in insulin sensitivity [233]. Thus, we questioned whether the consumption of sugary drinking water exacerbates high-fat diet-induced insulin resistance, which has not been clearly established in previous studies [15, 16]. In our study, HFWD+F/S-fed mice were more glucose intolerant and insulin resistant than HFWD-fed mice. Importantly, our results are consistent with epidemiological [234] and human studies [235].

The capacity of adipose tissue to form new adipocytes (hyperplasia), which accumulate excess energy, can prevent ectopic lipid deposition in critical organs including visceral adipose tissue, liver, and muscle [57, 225, 236]. Adipose tissue expansion can also result from an increase in the size (hypertrophy) of adipocytes in a depot-dependent fashion [57, 225, 236]. Thus, we determined whether hypertrophy contributed to adipose tissue accumulation in the HFWD and HFWD+F/S groups. Changes to eWAT adipocyte size and area in the HFWD+F/S group at 2 wk suggested a role for hypertrophy in the adipose tissue expansion. At 12 wk, the change in eWAT adipocyte diameter was similar between the HFWD- and HFWD+F/S-fed mice. A significant shift in the distribution of the eWAT adipocyte area confirmed these results. When hyperplasia

in addition to hypertrophy was examined as described by MacDougald's group [221], we observed differential changes to the relationship between average adipocyte area and eWAT weight in HFWD- and HFWD+F/S-fed mice from 2 to 12 wk (a steeper slope vs. a flatter slope, respectively). Thus, there are differences between eWAT adipose dynamics in the mice consuming liquid sugar and a HFWD compared with those just consuming a HFWD. The mechanism by which sugary drink consumption limits expandability of the adipose tissue is not known; however, it has been suggested that fibrosis, accumulation of extracellular matrix, and capillary vascularization may play a role in limiting adipose tissue expansion [224]. Our data suggest that an early hypoxia response in the eWAT leads to reduced vascularization and increased fibrosis in the HFWD+F/S-fed mice. In the HFWD-fed mice, an early hypoxia response was also observed, but it was not accompanied by elevated expression of LOX or Col6a1, although Col1a1 gene expression was elevated at 12 wk. Our observation that Ang1 and VEGF were significantly elevated in LFWD+F/S-fed mice compared with LFWD-fed mice at 2 and 12 wk, respectively, suggests that eWAT expands in a healthy manner in LFWD+F/S-fed mice [225]. To assess whether the adipose tissue expansion in our study was consistent with a pathological expansion [219], we examined the inflammatory status of eWAT. Compared with other groups, adipose tissue of HFWD+F/S-fed mice showed more profound inflammation, as shown by a dramatic increase in CLS formation and the expression of MIP-1α and TNFα. It has been proposed that T cell activation and recruitment within adipose tissue is an underlying cause of macrophage infiltration and eWAT inflammation [237, 238]. Whether T cell activation and recruitment within adipose tissue mediates eWAT inflammation in mice consuming liquid sugar with a HFWD is not known.

In the present study, HFWD+F/S-fed mice had a significantly higher normalized liver weight, hepatic TG concentration, serum ALT level, and histological steatosis grade at as early as 2 wk compared with the other groups, which suggested that NAFLD progression was more pronounced in the HFWD+F/S-fed mice. Consistent with this conclusion, hepatic gene expression of proinflammatory molecules was markedly increased in the HFWD+F/S group, as were phospho-JNK protein levels. Finally, in our study, 86% of the mice in the HFWD+F/S group developed fibrosis of varying degrees, and the most severe type of fibrosis was observed in the HFWD+F/S-fed mice. Increased hepatic expression of genes regulating fibrosis (collagen 1a2, collagen 3a1, and TGFβ) and protein expression of collagen I was observed in HFWD+F/S-fed mice. Taken together, our data confirm and expand upon the work that consumption of liquid sugar in Western diet-fed mice leads to hepatic dysfunction. Thus, the combination of liquid sugar and high-fat accelerates liver disease from steatosis toward NASH.

Even though fructose is well known to be lipogenic, it is not known whether chronic consumption of a sugary drink containing fructose and sucrose leads to NAFLD in mice fed a LFWD. Our results indicate that substrate utilization in the day and night phases is acutely affected in mice consuming the liquid sugar. Furthermore, consumption of a fructose and sucrose sugary drink leads to robust changes in lipid metabolism gene expression in liver and adipose tissues. However, glucose tolerance, insulin resistance, liver dysfunction, and adipose inflammation were not modulated in the LFWD+F/S group, suggesting that F/S alone is not responsible for the changes we observed.

A strength of our study was the analysis of metabolic data and NAFLD at two time points. The study design allowed us to assess metabolic, histological, and gene expression changes over time in adipose and liver tissues. We found that HFWD+F/S resulted in significant obesity, insulin

resistance, steatosis, and adipocyte hypertrophy as early as 2 wk, and inflammatory and fibrotic changes that were not observed in mice fed HFWD at 12 wk. Importantly, because we assessed adipose tissue at two time points, we were able to observe dynamic histological and gene expression changes, which correlated with the severity of hepatic dysfunction. Our observation that adiponectin was reduced at the gene expression and protein levels in the HFWD+F/S group suggests that adiponectin may be a potential link between adipose tissue dysfunction and NAFLD progression. This hypothesis is consistent with the known role of adiponectin in modulating steatosis, inflammation, and fibrosis [239]. However, further experimentation is required to determine whether a reduction in adiponectin mediates the effects of the HFWD+F/S combination in NAFLD progression.

A limitation of our study was that adipose tissue depot expansion was assessed only in eWAT. It is not known whether adipose tissue expansion in other depots is modulated by consumption of liquid sugar in HFWD-fed mice. Other limitations include a lack of baseline body and organ weight, serum parameters, and insulin sensitivity measurements and the length of our study (12 wk). It is possible that we would have observed greater hepatic fibrosis development in the animals if the diet treatment had been for a longer duration.

Finally, our study suggests a model (Fig. 18) in which the combination of a HFWD with F/S in the drinking water can induce hyperphagia and circadian disruption of the feeding cycle in the absence of changes in energy expenditure, which modulates adipose tissue expansion and dysfunction leading to hepatic steatosis, inflammation, glucose intolerance, insulin resistance, and hepatic fibrosis that is consistent with progression to NASH. In conclusion, our data indicate that the high fat Western diet plus liquid sugar consumption model of obesity is a good model for NAFLD research and likely other clinical conditions associated with adipose tissue dysfunction.

Tables

Table 1 Body and organ weight, serum parameters, and insulin sensitivity measurements in mice.

	LFWD	HFWD	LFWD + F/S	HFWD + F/S
Weights				
Whole Body				
2 wk	25.2 ± 0.3[a]	27.3 ± 1.1[b]	28.2 ± 0.7[b]	33.5 ± 0.8[c]
12 wk	32.3 ± 0.6[a]	37.0 ± 1.3[b]	33.6 ± 0.8[a]	46.4 ± 1.1[c]
Liver (g)				
2 wk	1.19 ± 0.06[ab]	1.13 ± 0.08[a]	1.18 ± 0.04[ab]	1.41 ± 0.04[b]
12 wk	1.48 ± 0.06[a]	1.55 ± 0.11[a]	1.50 ± 0.10[a]	3.09 ± 0.20[b]
eWAT (g)				
2 wk	0.48 ± 0.04[a]	0.75 ± 0.13[b]	0.77 ± 0.11[b]	1.50 ± 0.10[c]
12 wk	1.17 ± 0.14[a]	2.31 ± 0.11[b]	1.43 ± 0.18[a]	1.83 ± 0.11[c]
Liver/Body wgt				
2 wk	0.047 ± 0.002	0.041 ± 0.001	0.042 ± 0.001	0.042 ± 0.001
12 wk	0.046 ± 0.001[a]	0.042 ± 0.002[a]	0.044 ± 0.002[a]	0.070 ± 0.002[b]
eWAT/Body				
2 wk	0.019 ± 0.001[a]	0.027 ± 0.004[a]	0.027 ± 0.004[a]	0.045 ± 0.002[b]
12 wk	0.036 ± 0.004[a]	0.062 ± 0.002[b]	0.042 ± 0.004[a]	0.040 ± 0.003[a]
Serum				
Glucose (mg/dL)				
2 wk	180 ± 5[a]	203 ± 12[b]	140 ± 9[c]	166 ± 7[a]
12 wk	205 ± 8[a]	136 ± 3[b]	154 ± 5[b]	147 ± 9[b]
Triglyceride (mg/mg protein)				
2 wk	37.5 ± 2.3	39.3 ± 3.6	28.9 ± 3.2	36.8 ± 2.6
12 wk	38.4 ± 3.4	38.3 ± 2.7	41.1 ± 4.0	52.6 ± 8.9
Insulin				
2 wk	1.52 ± 0.15[a]	1.54 ± 0.22[a]	1.66 ± 0.43[a]	3.27 ± 0.46[b]
12 wk	2.15 ± 0.50[a]	2.54 ± 0.56[a]	1.69 ± 0.24[a]	5.15 ± 1.41[b]
ALT (U/mg protein)				
2 wk	24.5 ± 5.6	32.3 ± 7.0	16.6 ± 3.0	24.7 ± 3.5
12 wk	28.1 ± 3.8[a]	37.2 ± 12.2[a]	42.7 ± 13.0[a]	130.6 ± 12.3[b]
Insulin				
Quicki				
2 wk	0.393 ± 0.008[ab]	0.390 ± 0.014[ab]	0.425 ± 0.022[a]	0.364 ± 0.012[b]
12 wk	0.366 ± 0.010[ab]	0.390 ± 0.014[a]	0.390 ± 0.008[a]	0.330 ± 0.014[b]
Food Intake				
Food kcal/d				
2 wk	13.33 ± 0.46[ab]	14.55 ± 0.42[a]	12.14 ± 0.53[bc]	14.98 ± 0.51[a]
12 wk	16.58 ± 0.48[a]	15.47 ± 1.12[a]	11.49 ± 0.34[b]	17.14 ± 0.80[a]
Water g/d				
2 wk	2.24 ± 0.07[a]	2.18 ± 0.13[a]	3.45 ± 0.16[b]	2.67 ± 0.29[a]
12 wk	2.16 ± 0.09[ac]	1.96 ± 0.26[a]	4.37 ± 0.32[b]	3.04 ± 0.41[c]
Water kcal/d				
2 wk	0.00 ± 0.00[a]	0.00 ± 0.00[a]	0.58 ± 0.03[b]	0.45 ± 0.05[c]
12 wk	0.00 ± 0.00[a]	0.00 ± 0.00[a]	0.73 ± 0.05[b]	0.50 ± 0.09[c]

Total kcal/d				
2 wk	13.33 ± 0.46[ac]	14.55 ± 0.42[bc]	12.72 ± 0.53[a]	15.43 ± 0.53[b]
12 wk	16.58 ± 0.48[a]	15.47 ± 1.12[a]	12.22 ± 0.36[b]	17.64 ± 0.81[a]

Wgt, weight; ALT, alanine aminotransferase; d, day
Values represents the means ± SEM for n= 5-10
Data was analyzed by ANOVA and pair-wise comparisons were made using Newman-Keuls test
Different letters indicate significantly different values at $P < 0.05$.

Figures and figure legends

Figure 6

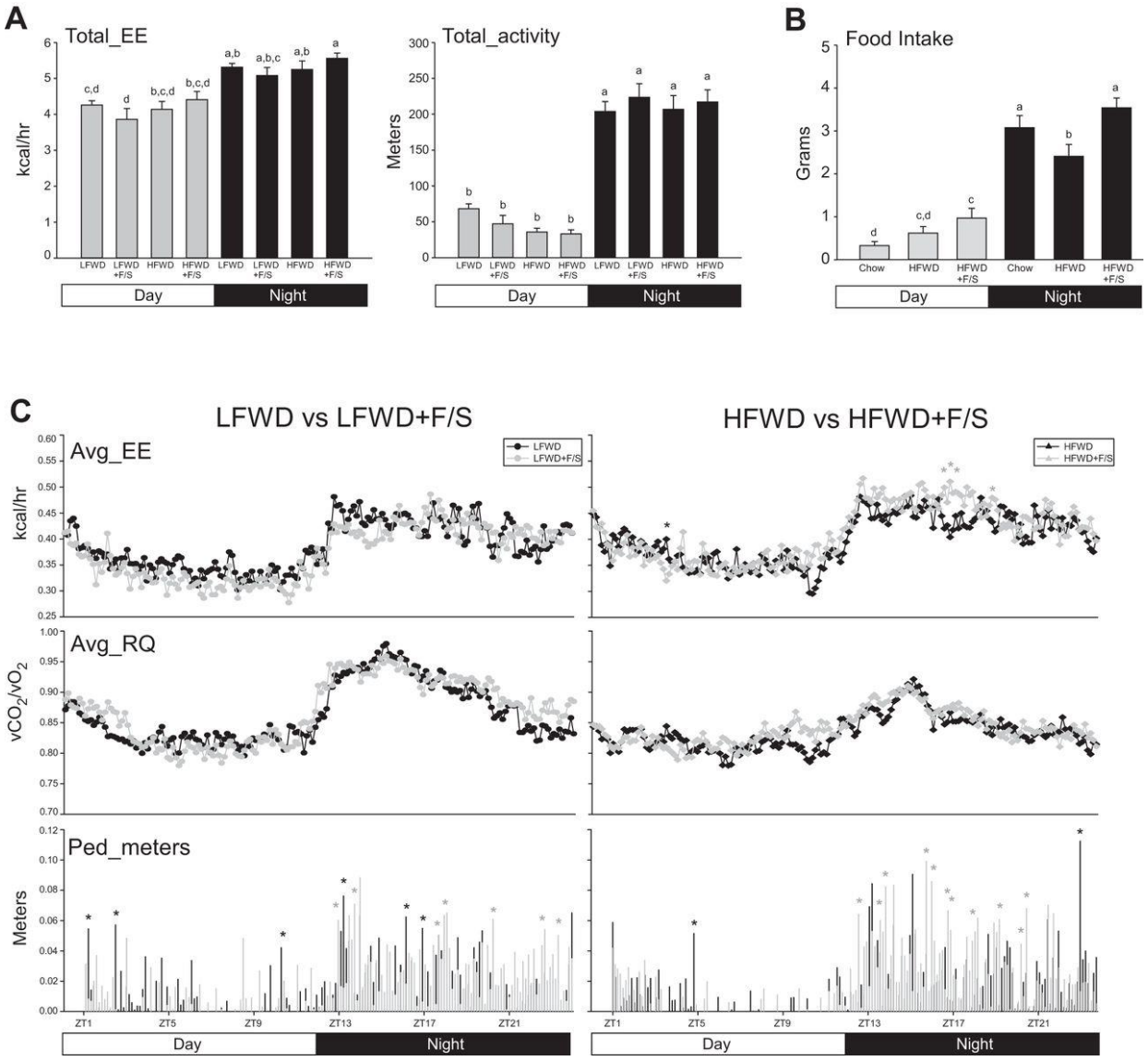

Fig. 6 Metabolic phenotype at 2 wk. *A*: mean ± SE circadian analysis of total energy expenditure (Tot_EE) (*left*) and total activity (*right*) for day and night phases over a 48-h period in mice fed

low-fat Western diet (LFWD), high-fat Western diet (HFWD), LFWD+F/S (sugary drink - fructose and sucrose), or HFWD+F/S. *B*: circadian analysis of food intake in chow, HFWD, and HFWD+F/S groups. *A* and *B*: different letters indicate significantly different values at $P < 0.05$. *C*: means ± SE of average energy expenditure (Avg_EE), average respiratory quotient (Avg_RQ), and pedestrian meters (Ped_meters) every 8 min during the 24-h period for LFWD vs. LFWD+F/S (*left*) and HFWD vs. HFWD+F/S (*right*) groups. Black stars, significant increases ($P < 0.05$) in LFWD and HFWD groups over LFWD+F/S and HFWD+F/S groups (*left* and *right*, respectively); gray stars, significant increases ($P < 0.05$) in LFWD+F/S and HFWD+F/S groups over LFWD and HFWD groups (*left* and *right*, respectively).

Figure 7

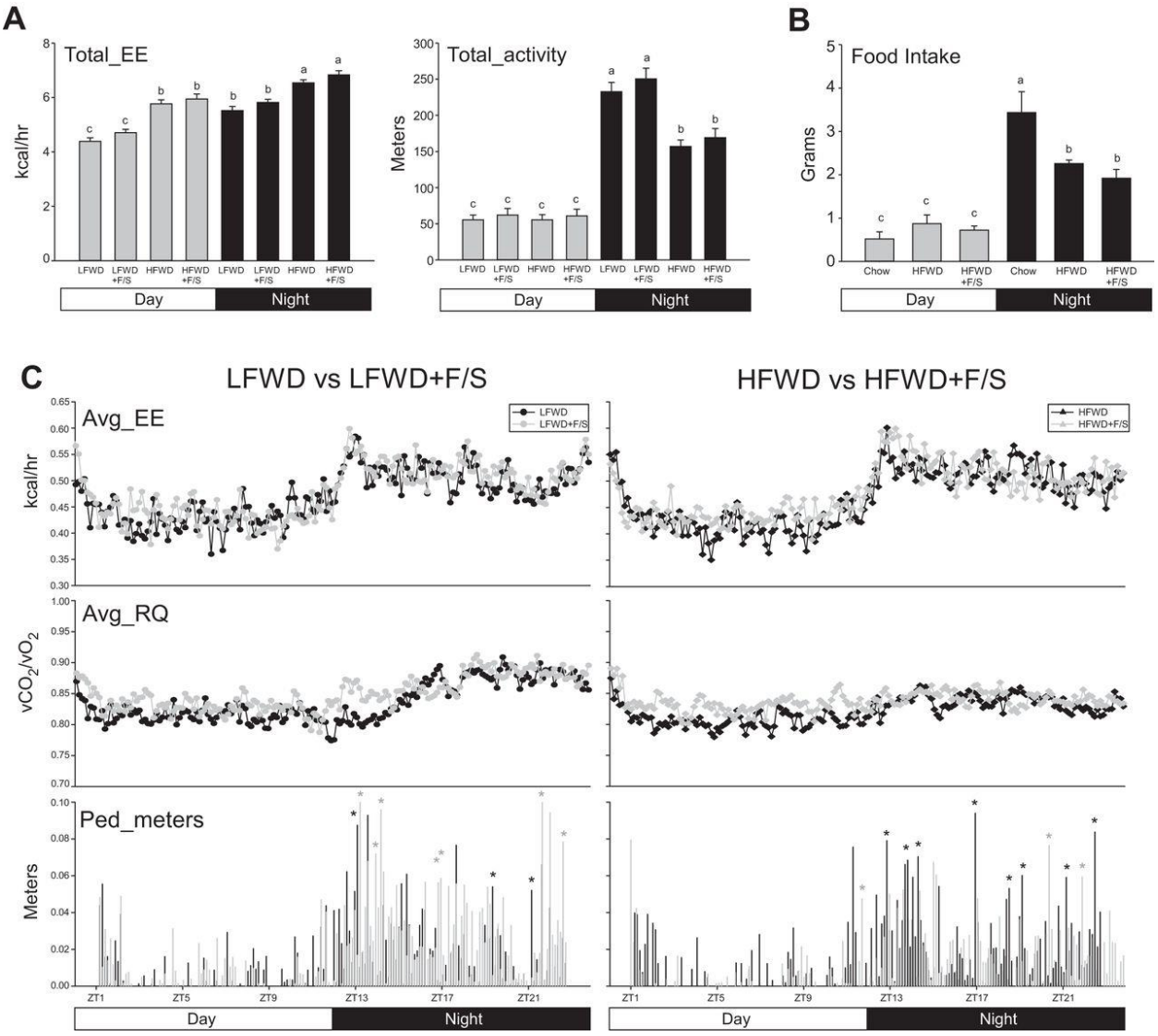

Fig. 7 Metabolic phenotype at 12 wk. A. Mean ± SE circadian analysis of total energy expenditure (Tot_EE) (*left*) and total activity (*right*) for day and night phases over a 48-hperiod in mice fed LFWD, HFWD, LFWD+F/S, or HFWD+F/S. *B*: circadian analysis of food intake in chow, HFWD, and HFWD+F/S groups. *A* and *B*: different letters indicate significantly different values at $P < 0.05$. *C*: means ± SE of Avg_EE, Avg_RQ, and Ped_meters every 8 min during the 24-h period for LFWD vs. LFWD+F/S (*left*) and HFWD vs. HFWD+F/S (*right*) groups. Black

stars, significant increases ($P < 0.05$) in LFWD and HFWD groups over LFWD+F/S and HFWD+FS groups (*left* and *right, respectively*); gray stars, significant increases ($P < 0.05$) in LFWD+F/S and HFWD+FS groups over LFWD and HFWD groups (*left* and *right, respectively*).

Figure 8

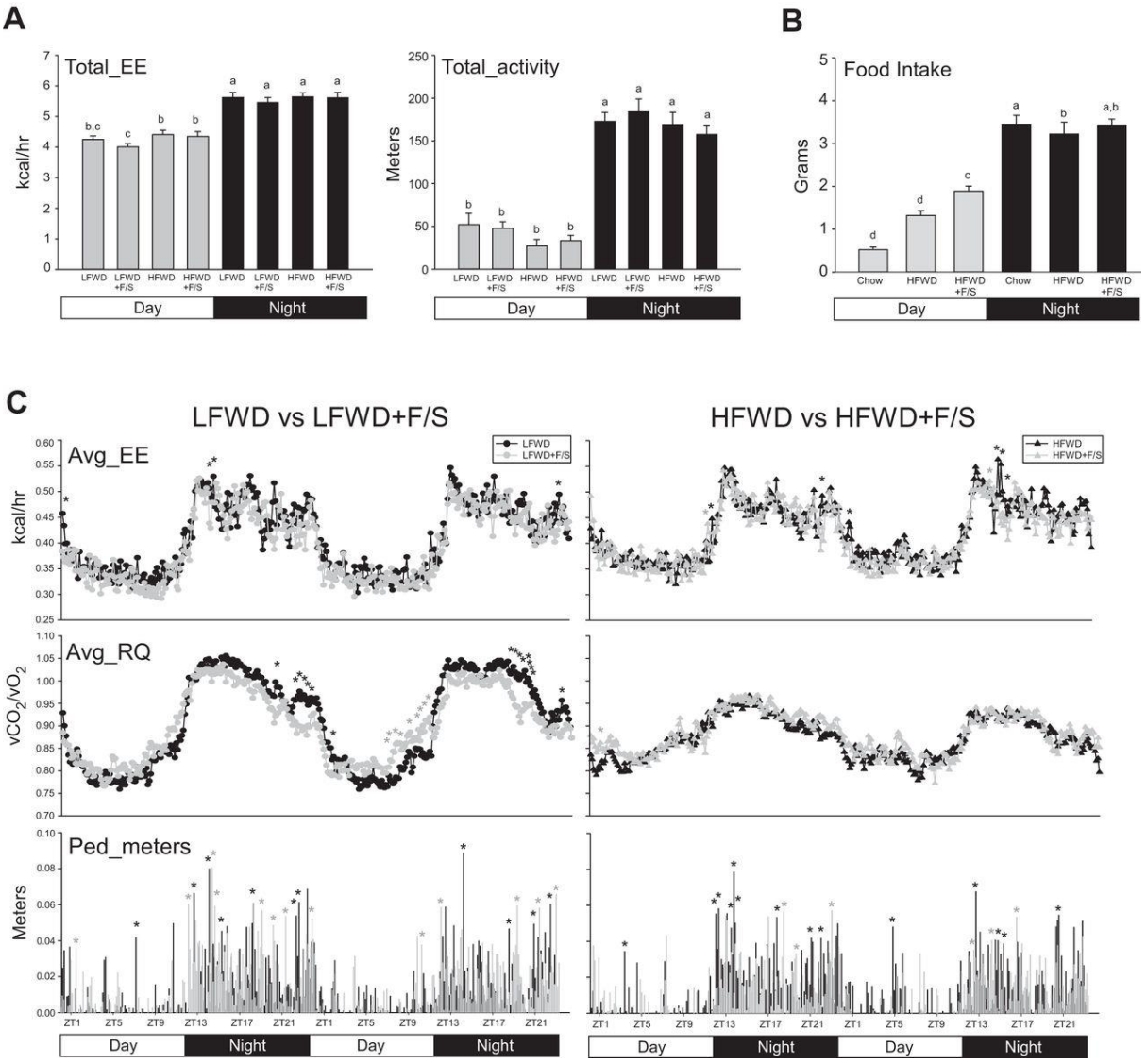

Fig. 8 Metabolic phenotype after 24 h on the diets. *A*: mean + SE circadian analysis of Tot_EE (*left*) and total activity (*right*) for day and night phases over a 24-period in mice fed LFWD, HFWD, LFWD+F/S, or HFWD+F/S. *B*: circadian analysis of food intake in chow, HFWD, and HFWD+F/S groups. *A* and *B*: different letters indicate significantly different values at $P < 0.05$. *C*: means + SE of Avg_EE, Avg_RQ, and Ped_meters every 8 min during the 48-h period for LFWD vs. LFWD+F/S (*left*) and HFWD vs. HFWD+F/S (*right*) groups. Black stars,

significant increases ($P < 0.05$) in LFWD and HFWD groups over LFWD+F/S and HFWD+F/S groups (*left* and *right*, respectively); gray stars, significant increases ($P < 0.05$) in LFWD+F/S and HFWD+FS groups over LFWD and HFWD groups (*left* and *right*, respectively).

Figure 9

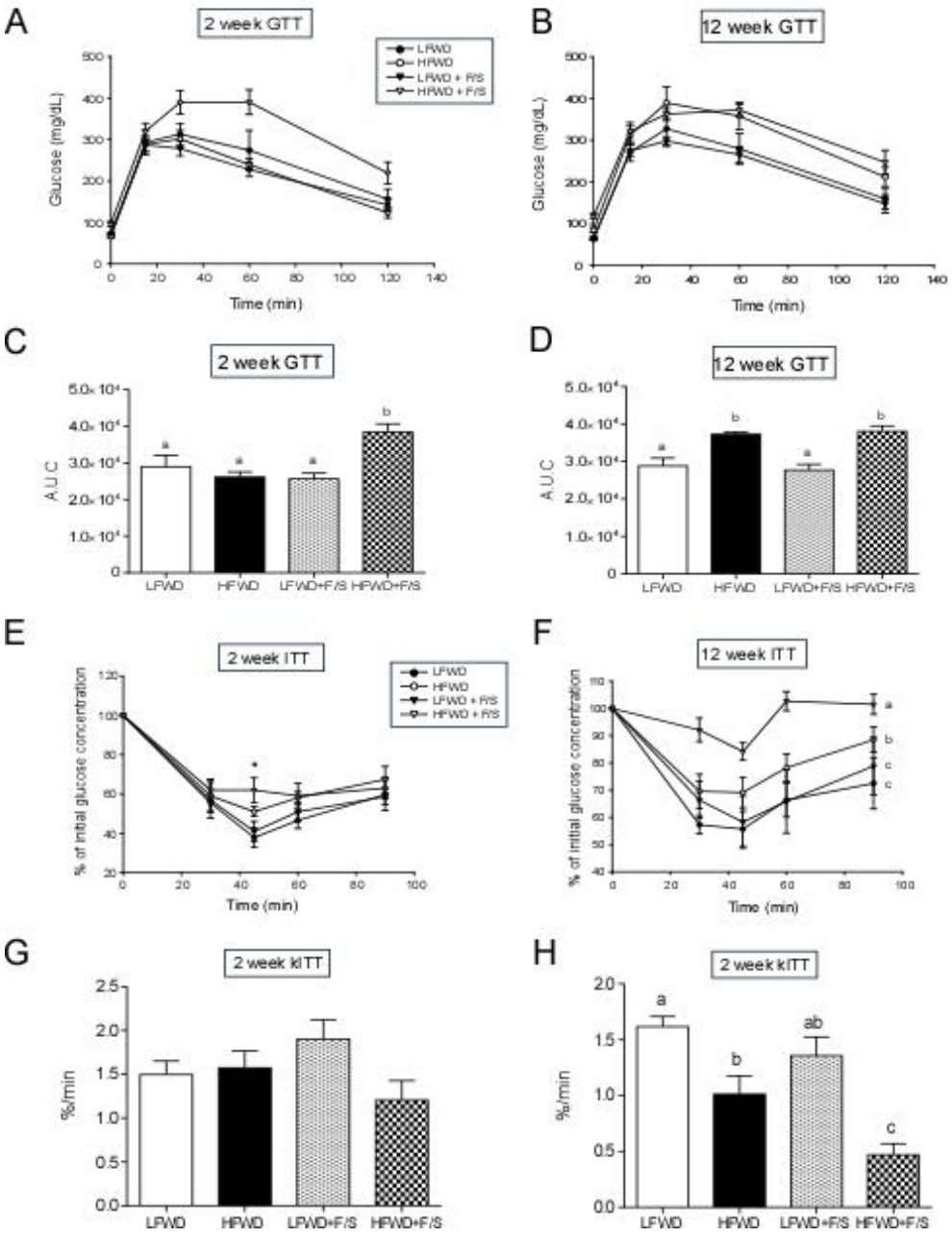

Fig. 9 Glucose and insulin tolerance. *A* and *B*: mean glucose concentration in GTT curves at 2 wk (*A*) and 12 wk (*B*). *C* and *D*: means ± SE of area under the curve (AUC) calculated for each GTT curve at 2 wk (*C*) and 12 wk (*D*). *E* and *F*: %reduction in mean glucose concentration in ITT curves at 2 wk (*E*) and 12 wk (*F*). *G* and *H*: means ± SE of plasma glucose disappearance

rate (K_{ITT}) during ITT at 2 wk (*G*) and 12 wk (*H*). Different letters indicate significantly different values at $P < 0.05$. *Significantly different value at $P < 0.05$ in HF+S group over LF and LF+S groups.

Figure 10

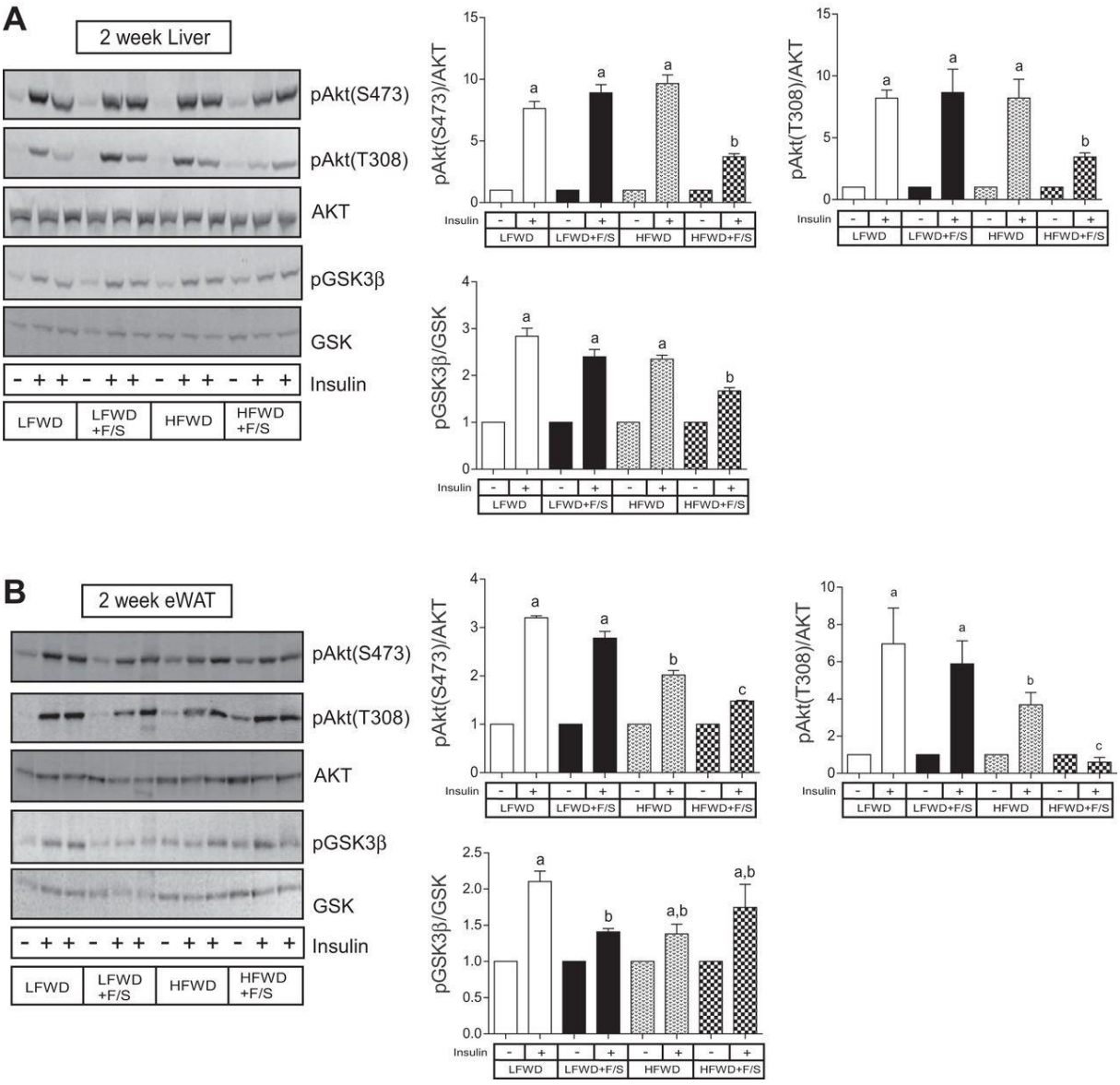

Fig. 10 Hepatic and adipose insulin signaling at 2 wk. *A* and *B*: insulin-stimulated hepatic Akt Ser^{473} (S473), Akt Thr^{308} (T308), and GSK3β Ser^{9} (pGSK3β) phosphorylation, total Akt, and GSK3β representative blots (*A*) and means ± SE (*B*) of insulin-stimulated LFWD-fed mice. *C* and *D*: insulin-stimulated adipose AktS473, AktT308, and GSK3β phosphorylation, total Akt, and GSK3β representative blots (*C*) and means ± SE (*D*) of insulin-stimulated LFWD-fed

mice. AktS473 and -T308 phosphorylations were normalized to total Akt; GSK3β phosphorylation was normalized to total GSK. Different letters indicate significantly different values at $P < 0.05$.

Figure 11

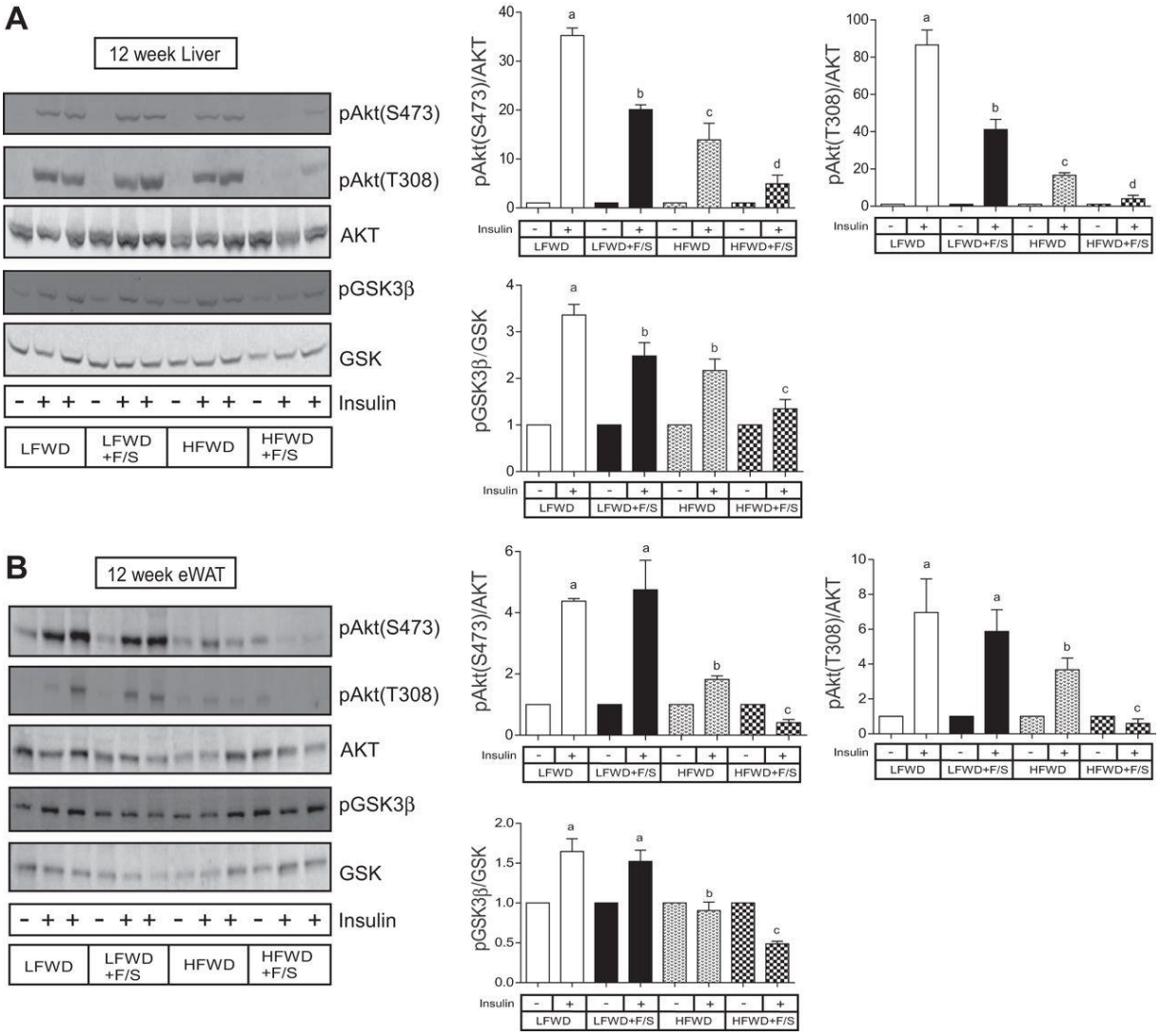

Fig. 11 Hepatic and adipose insulin signaling at 12 wk. *A* and *B*: insulin-stimulated hepatic AktS473, AktT308, and GSK3β pGSK3β phosphorylation, total Akt, and GSK3β representative blots (*A*) and means ± SE (*B*) of insulinstimulated LFWD-fed mice. *C* and *D*: insulin-stimulated adipose AktS473, AktT308, and GSK3β phosphorylation, total Akt, and GSK3β representative blots (*C*) and - means ± SE (*D*) of insulin-stimulated LFWD-fed mice. AktSer473 and -T308

phosphorylations were normalized to total Akt; GSK3β phosphorylation was normalized to total GSK. Different letters indicate significantly different values at $P < 0.05$.

Figure 12

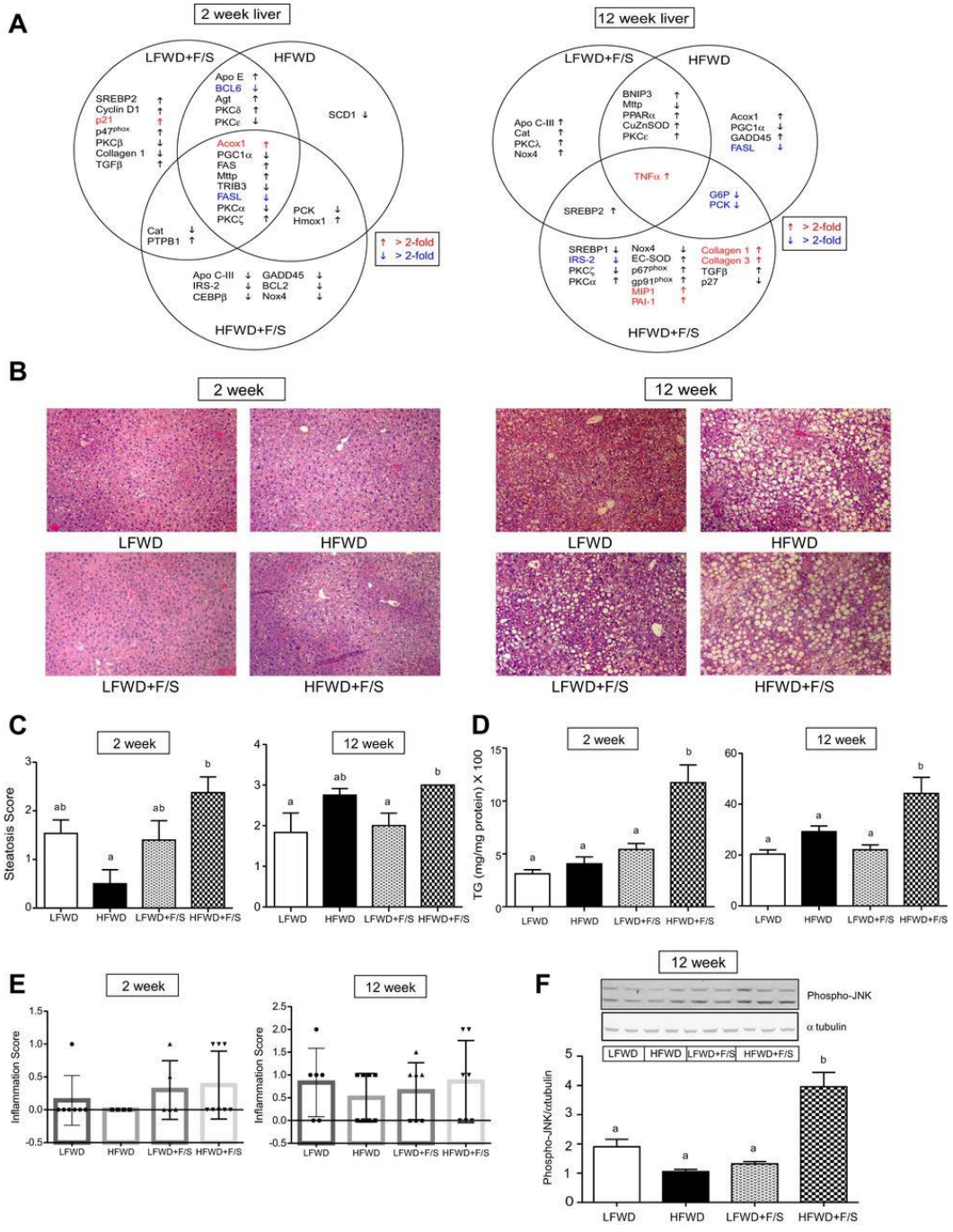

Fig. 12 Hepatic gene expression, steatosis, triglyceride accumulation and inflammation. *A*: hepatic gene expression determined by qRT-PCR at 2 and 12 wk. Arrows indicate significant differences in expression vs. LFWD-fed mice at each time point (red and blue texts represent >2-

fold increases and decreases, respectively). *B*: hematoxylin and eosin (H&E)-stained liver sections at 2 and 12 wk. *C*: steatosis scoring of H&E-stained liver sections at 2 and 12 wk. *D*: quantitation of hepatic triglyceride content is shown as means ± SE at 2 and 12 wk. *E*: inflammation scoring of H&E-stained liver sections is shown as mean ± SE at 2 and 12 wk. *F*: phospho-JNK and α-tubulin expression at 12 wk. Shown are representative blot and quantitation of protein expression (means ± SE) of phospho-JNK normalized to α-tubulin. Different letters indicate significantly different values at $P < 0.05$.

Figure 13

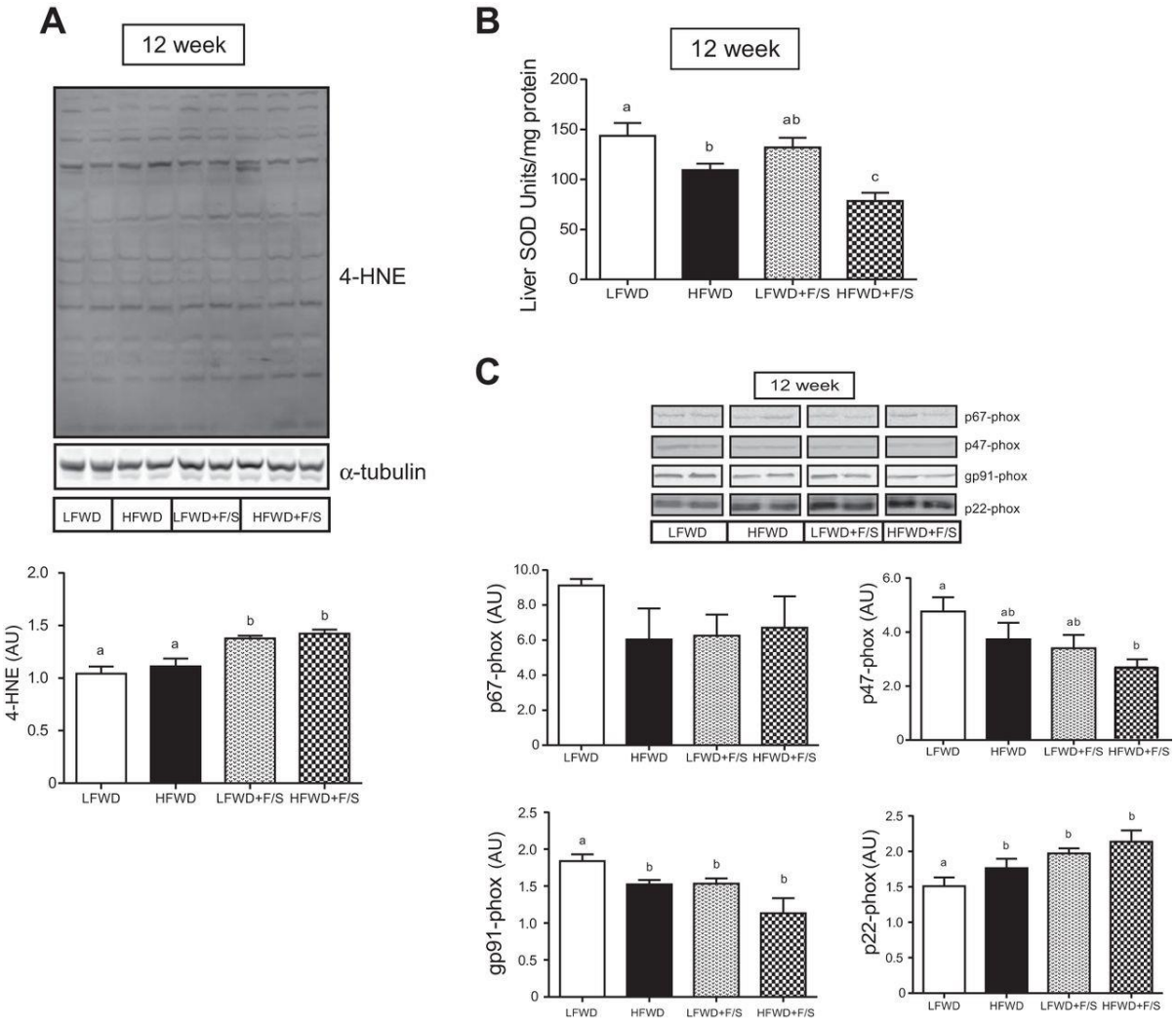

Fig. 13 Markers of hepatic oxidative stress and apoptosis. *A*: 4-HNE-stained liver section (*top*) and quantitation (mean ± SE) in arbitrary units (AU) (*bottom*). *B*: quantitation of hepatic SOD is shown as mean ± SE. *C*: hepatic NADPH oxidase subunit protein expression. Representative immunoblots are shown (*top*) and quantitation of immunoreactive bands minus background is shown as means ± SE in arbitrary units (AU) (*bottom*). Different letters indicate significantly different values at $P < 0.05$.

Figure 14

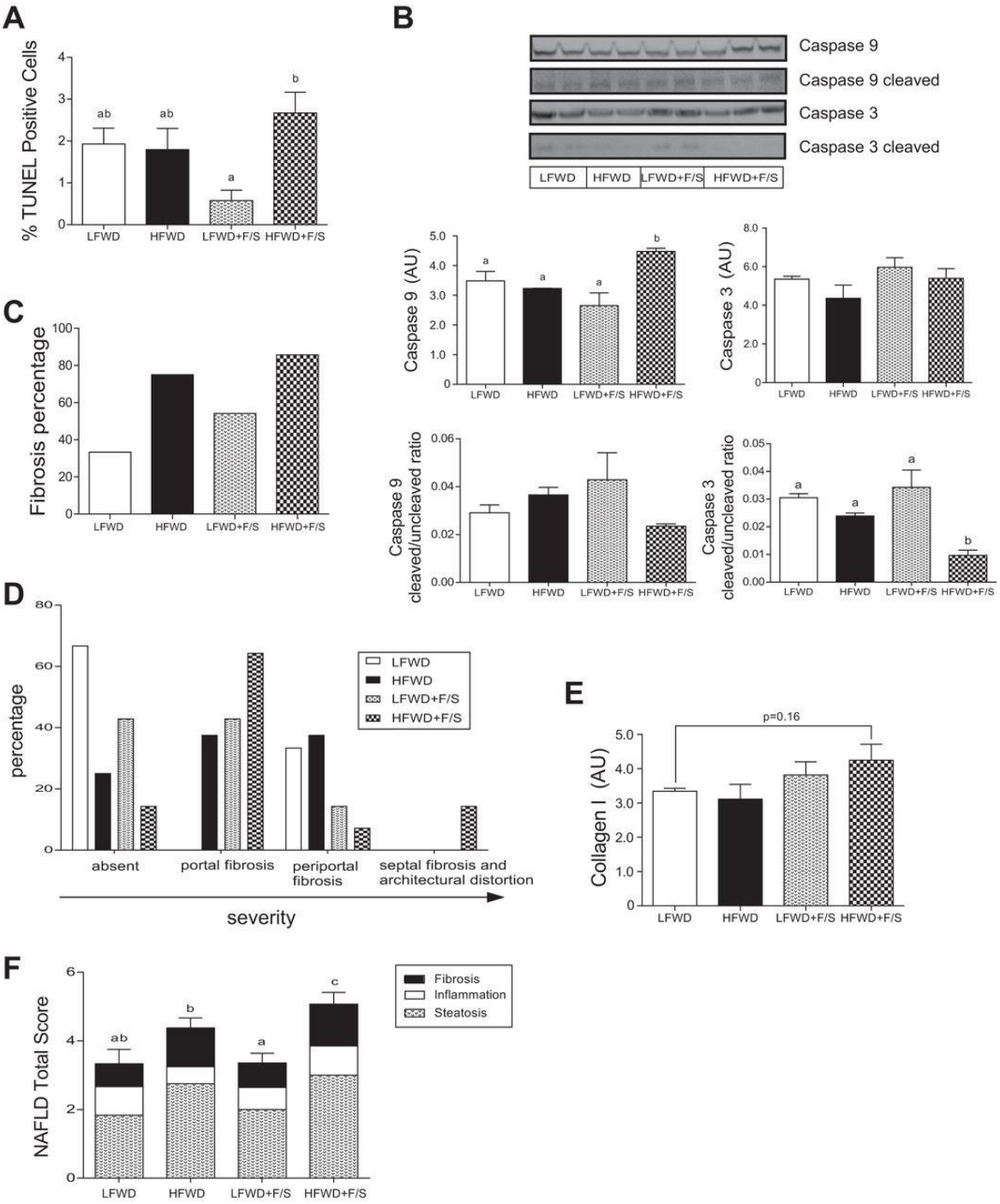

Fig. 14 Markers of hepatic apoptosis, apoptosis-related protein expression, fibrosis, and fibrosis-related protein expression. *A*: TUNEL staining of liver is shown as mean ± SE at 12 wk. *B*:

assessment of caspase cleavage. Representative immunoblots are shown (*top*) and quantitation of immunoreactive bands minus background is shown as means ± SE in AU (*bottom*). *C*: fibrosis scoring of Masson's trichrome-stained liver fibrosis section is shown as percentage by treatment groups. *D*: fibrosis scoring of Masson's trichrome-stained liver fibrosis section is shown as percentage by fibrosis location. *E*: collagen I expression. Quantitation of protein expression is shown as means ± SE in AU. *F*: NAFLD total score at 12 wk is shown as means ± SE. Different letters indicate significantly different values at $P < 0.05$.

Figure 15

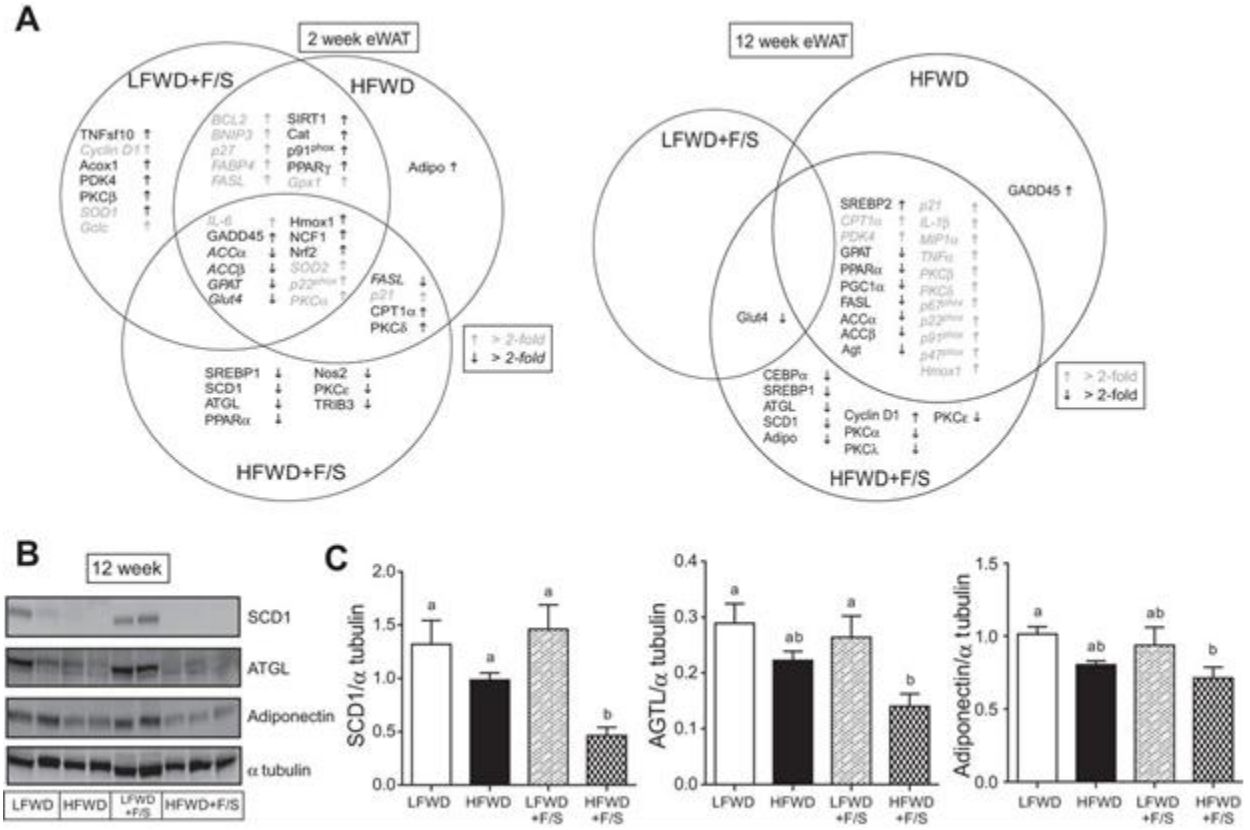

Fig. 15 Epididymal white adipose tissue (eWAT) gene and protein expression. *A*: adipose gene expression at 2 and 12 wk. Arrows indicate significant differences in expression vs. LFWD-fed mice at each time point (italicized text represents >2-fold differences, with gray text representing upregulated genes). *B* and *C*: SCD1, ATGL, adiponectin, and α-tubulin expression. Representative immunoblots are shown (*B*); quantitation of immunoreactive bands relative to α-tubulin is shown as means ± SE (*C*). Different letters indicate significantly different values at $P < 0.05$.

Figure 16

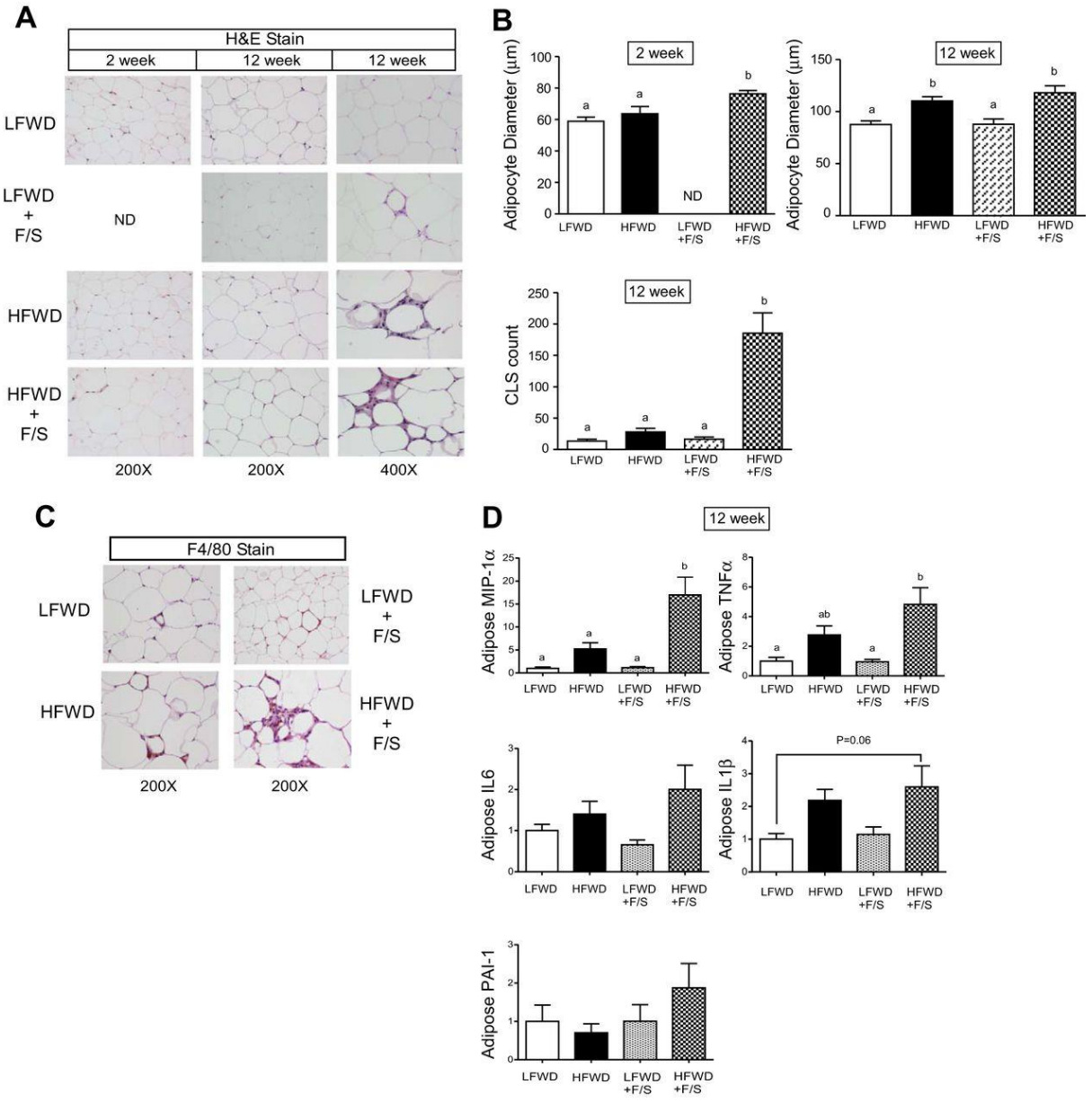

Fig. 16 eWAT inflammation and adipocyte size. *A*: H&E-stained adipose tissue sections at 2 and 12 wk. Shown are representative images at ×200 *left* and *middle*) and ×400 (*right*). *B*: quantitation of adipocyte size (*top*) and crown-like structures (CLS) (*bottom*) are shown as means ± SE at 2 and 12 wk. *C*: F4/80-stained eWAT macrophages at 12 wk. *D*: normalized gene

expression of eWAT proinflammatory genes and fold changes (means ± SE) relative to LFWD at 12 wk. Different letters indicate significantly different values at $P < 0.05$. ND, not determined.

Figure 17

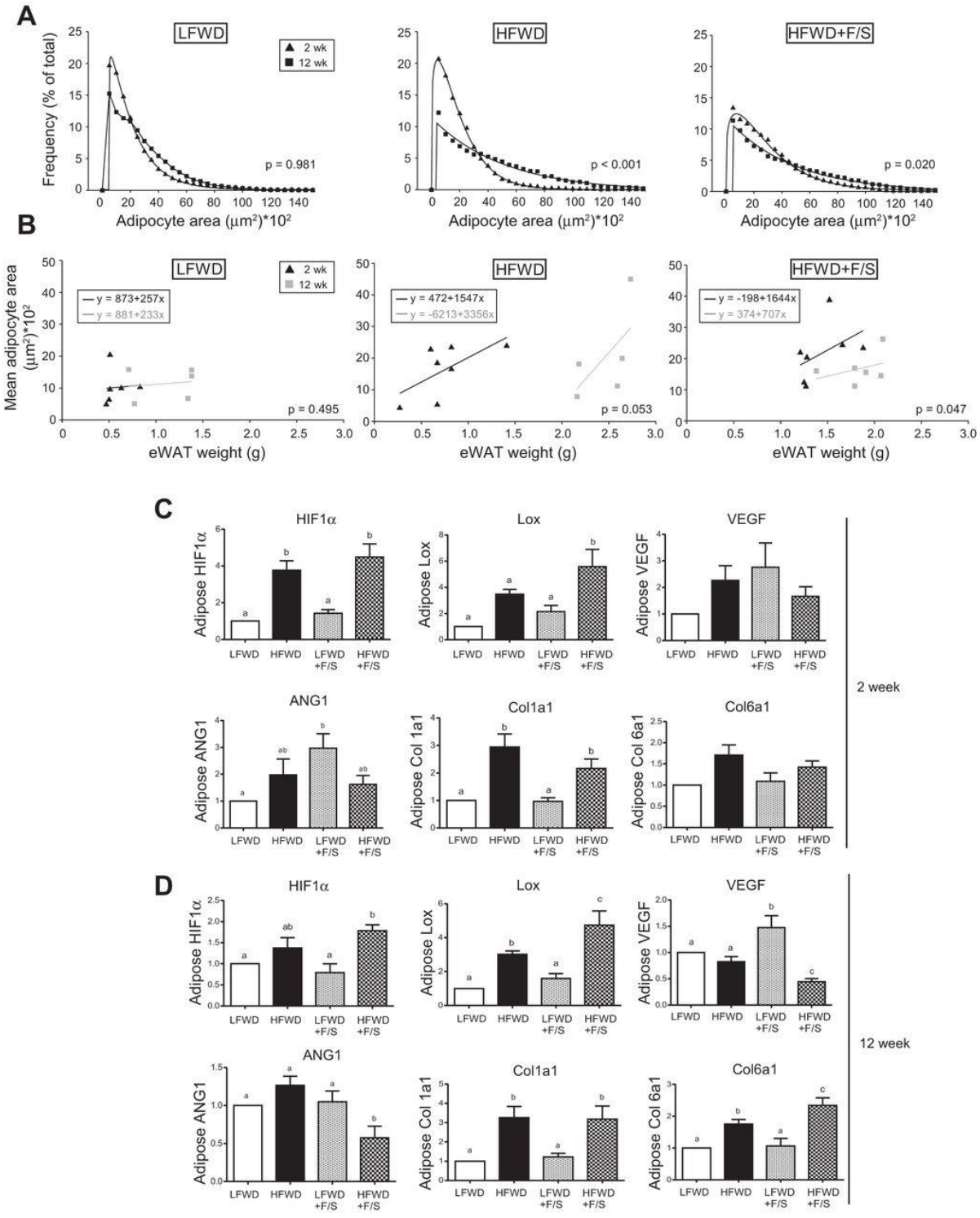
A
LFWD
HFWD
HFWD+F/S
2 wk
12 wk
Frequency (% of total)
p = 0.981
p < 0.001
p = 0.020
Adipocyte area (μm²)*10²
B
Mean adipocyte area (μm²)*10²
y = 873+257x
y = 881+233x
y = 472+1547x
y = -6213+3356x
y = -198+1644x
y = 374+707x
p = 0.495
p = 0.053
p = 0.047
eWAT weight (g)
C
HIF1α
Lox
VEGF
ANG1
Col1a1
Col6a1
Adipose HIF1α
Adipose Lox
Adipose VEGF
Adipose ANG1
Adipose Col 1a1
Adipose Col 6a1
LFWD
HFWD
LFWD +F/S
HFWD +F/S
2 week
D
12 week

Fig. 17 eWAT adipocyte size distribution and fibrosis and angiogenesis gene expression. *A*: frequency of adipocyte area from 0 to 1,500 μm^2 in increments of 500 μm^2 is shown as the mean at 2 and 12 wk. *P* values for the Kolmogorov-Smirnov test for sample distribution are shown. *B*: relationship between mean adipocyte area and eWAT weight at 2 wk (black triangles) and 12 wk (gray squares). Linear regression was performed separately for samples collected at 2 wk (black lines) and 12 wk (gray lines). Line equations and *P* values for differences in slopes are shown. *C*: normalized gene expression of eWAT fibrosis and angiogenesis genes and fold changes (means ± SE) relative to LFWD. Different letters indicate significantly different values at $P < 0.05$.

Figure 18

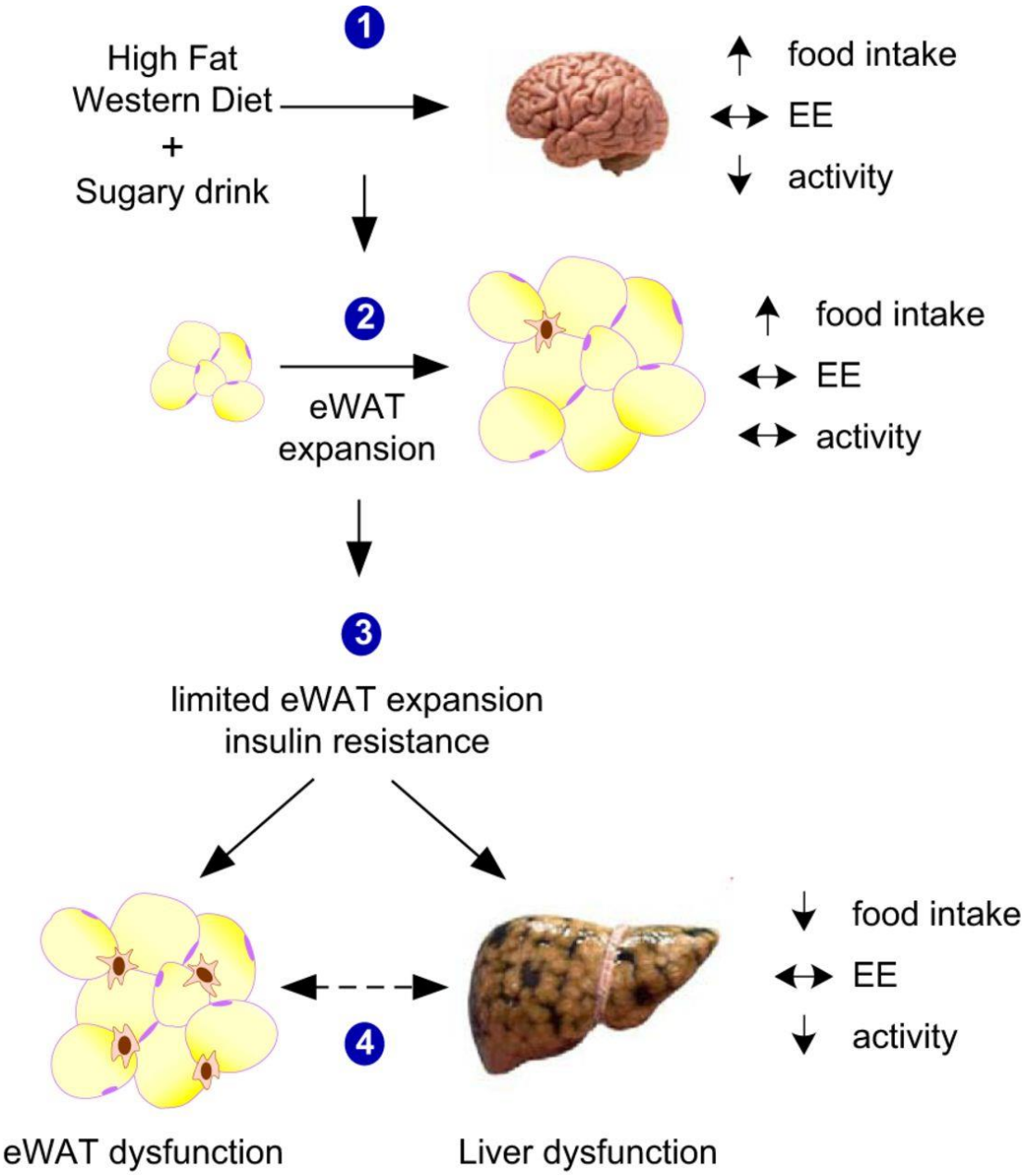

Fig. 18 Model of the metabolic and pathophysiological effect of consuming a HFWD + sugary drinking water in mice. Events are*1*) acute hyperphagic response to consumption of the diet in the absence of changes to energy expenditure is observed at 24 h and after 2 wk on the diet; *2*) rapid eWAT expansion; *3*) inability of eWAT to further expand, coupled with liver and adipose insulin resistance; and *4*) adipose and liver dysfunction characterized by inflammation and

progression to nonalcoholic steatohepatitis (NASH), respectively. The interaction between dysfunctional adipose tissue and the liver is still not fully known (dashed line).

Chapter 4: Role of liquid sugar in regulating the hepatic transcriptome in a high fat Western diet model of NAFLD

4.1 Abstract

Nonalcoholic fatty liver disease (NAFLD), which ranges from simple steatosis (fatty liver) to nonalcoholic steatohepatitis (NASH), has become the most common chronic liver disease in both children and adults, paralleling the increased prevalence of obesity and diabetes during the last decades. The rise in NASH prevalence is a major public health concern because there are currently no specific and effective treatments for NASH. In addition, the molecular mechanisms for the progression of steatosis to NASH remain largely undiscovered. The prevalence of obesity-related NAFLD and limitations of available therapeutic options highlight the need for identifying specific gene and pathway changes that drive progression of NAFLD using state-of-the-art sequencing analysis of human biospecimens or relevant animal models. This study uses a high fat Western diet (HFWD) together with liquid sugar [fructose and sucrose (F/S)]-fed mice to investigate genomic changes involved in the development and progression of NAFLD. In our study, the combination of a HFWD with F/S in the drinking water exacerbated HFWD-induced obesity, hyperinsulinemia, hyperglycemia, hepatic steatosis and inflammation that is consistent with progression to NASH. RNA-seq analysis revealed differentially expressed genes (DEGs) associated with both HFWD (HFWD vs. Chow; 1065DEGs) and HFWD+F/S (HFWD+F/S vs Chow; 1689 DEGs). However, the addition of liquid sugar consumption resulted in 760 DEGs in

the liver of HFWD+F/S-fed mice, which are mainly enriched in small GTPase mediated signal transduction, and lipid homeostasis biological processes. Further, pathway analysis showed pathways in immune response, fibrosis and cancer are major pathways enriched in the livers of HFWD+F/S-fed mice. Taken together, this study identified key genes, biological processes and pathway changes in the liver of HFWD+F/S mice and provided a molecular basis for understanding the mechanism through which the addition of liquid sugar promotes the progression of NAFLD.

4.2 Introduction

Nonalcoholic fatty liver disease (NAFLD) has become the most common chronic liver disease in both children and adults [240], paralleling the increased prevalence of obesity and type 2 diabetes during the last decades [202]. The NAFLD spectrum ranges from simple steatosis (fatty liver) to nonalcoholic steatohepatitis (NASH), which can lead to more serious clinical conditions of cirrhosis and liver cancer (hepatocarcinoma). However, current treatment options for NAFLD are limited and ineffective [4]. In addition, the molecular mechanisms for the progression of steatosis to NASH remain largely undiscovered. The prevalence of obesity-related NAFLD and limitations of available therapeutic options highlight the need for identifying specific gene and gene pathway changes that drive progression of NAFLD using state-of-the-art sequencing analysis of human biospecimens or relevant animal models.

This study uses a high fat Western diet together with liquid sugar-fed mice, as a NASH model to investigate genomic changes involved in the development and progression of chronic liver disease. In order to mimic the consumption of sugar in adults [206] and children [207], obesity-linked overnutrition models have been developed based on added sugar in the form of fructose

and/or sucrose. Fructose, a highly lipogenic sugar, may contribute to the development and severity of NAFLD by promoting de-novo lipogenesis, insulin resistance, oxidative stress, inflammation and possibly fibrosis [241]. The high fat Western diet with liquid sugar consumption model of obesity in mice was originally developed as a model of NAFLD progression [15-17], and has been recently reported to model obese humans with mild NASH [210]. Our group recently has shown that 12 wk of a high fat Western diet (HFWD) with liquid sugar (fructose and sucrose) in the drinking water feeding can induce obesity and insulin resistance, as well as NASH and liver fibrosis in C57BL/6 mice, which represents a good model to investigate the mechanism underlying the progression of NAFLD [242].

Microarray technology has been applied to study the expression of genes in nonalcoholic fatty liver disease progression in animal models [243, 244] and humans [245-247], however, it contains limitations such as: restriction to known regions of genome; a limited dynamic range; and difficulties in comparing expression levels between experiments [149]. Here, we have used a more comprehensive, sensitive, quantitative and unbiased approach, next-generation RNA sequencing (RNA-seq), which measures the RNA expression profile more accurately over a greater dynamic range than microarray-based technologies [149]. With this technology, we were able to provide a global view of the hepatic transcriptome responses to the consumption of liquid sugar in mice fed a HFWD diet, and demonstrate the main biological processes and pathways involved in the progression of NAFLD.

4.3 Materials and Methods

4.3.1 Animals

Male C57BL/6NHsd mice from Harlan Laboratories (Somerville, NJ) were housed one per cage in the Auburn University Veterinary Research Building, an AAALAC accredited animal facility,

in 12:12-h light-dark, temperature at 22°C, and humidity-controlled rooms. Mice were provided with standard laboratory chow and water *ad libitum* in accordance with an Institutional Animal Care and Use Committee approved protocol for 1 wk to allow for acclimatization to the animal facility. No procedures were undertaken that caused more than minimal pain, distress, or discomfort. After the one-week acclimation period, mice (*n*= 8, 6 wk old) remained on the standard chow diet or received a high-fat Western diet (HFWD) (Test Diets, Cat. #5TJN) containing ~12% and 40% energy from fat, respectively, with or without sugar (42 g/L) added to the drinking water at a ratio of 55% fructose/45% sucrose (F/S). The composition of fat in the diets was 30% from lard, 30% from butterfat, and 30% from Crisco. Mice were euthanized by inhalation of CO_2. Blood samples were immediately drawn from the caudal vena cava. After clotting at room temperature, the sample was centrifuged at 12,000 *g* for 15 min at 4°C. The serum was removed and stored frozen at −80°C until tested. Liver and eWAT were excised, weighed, and were immersed in RNAlater (Life Techonologies, Carlsbad, CA) and stored at -80°C until used for RNA extraction or fixed in 10% buffered formalin prior to paraffin embedding.

4.3.2 Liver tissue histological and lipid analysis

Paraffin-embedded sections were stained with hematoxylin and eosin examined in a blinded fashion by a board certified veterinary pathologist. NAFLD was scored using a general scoring system for rodent models, which is based on the human NAS (NAFLD activity score) grading criteria [248]. Briefly, micro- and macro-vesicular steatosis were separately scored and the severity was graded, based on the percentage of the total area affected, into the following categories: 0 (<5%), 1 (5–33%), 2 (34–66%) and 3 (>66%). The level of hepatocellular

hypertrophy, defined as cellular enlargement more than 1.5 times the normal hepatocyte diameter, was scored, based on the percentage of the total area affected, into the following categories: 0 (<5%), 1 (5–33%), 2 (34–66%) and 3 (>66%). Hepatic inflammation was analyzed by counting the number of inflammatory foci per field at × 100 magnification (view size 3.1 mm^2) in five different fields per specimen. NAFLD score was calculated for each liver biopsy based on the sum of scores for steatosis, hypertrophy and inflammation. TGs were assayed using a kit from Thermo Scientific (Rockford, IL) and normalized to the protein content measured using the BCA protein assay reagent (Thermo Scientific/Pierce, Rockford, IL).

4.3.3 RNA extraction

RNeasy Plus Universal Kits (Qiagen, Valencia, CA) was used to isolate total RNA from frozen liver and adipose tissue following the manufacturer's protocol. RNA quantity and quality were assessed using a bioanalyzer (Agilent 2100 Bioanalyze; Agilent Technologies, Santa Clara, CA).

4.3.4 RNA-seq library preparation and sequencing

We randomly selected four mice from chow, five mice from HFWD and HFWD+F/S respectively, to isolate total RNA from liver and adipose tissue for RNA-seq analysis. All RNA-seq procedures were performed at the Genomic Services Laboratory (GSL), HudsonAlpha Institute for Biotechnology. Initial QC quantification of the extracted total RNA was done by using Qubit Fluorometer (Invitrogen), and the quality of the extracted RNA was evaluated using an Agilent 2100 Bioanalyzer.

Five hundred ng of total RNA was taken for proceeding to downstream RNA-seq applications. First, ribosomal RNA (rRNA) was removed using Ribo-Zero™ Gold (Yeast) kit (Epicenter,

Madison, WI) using manufacturer's recommended protocol. Immediately after the rRNA removal the RNA was fragmented and primed for the first strand synthesis using the NEBnext First Strand synthesis module (New England BioLabs Inc., Ipswich, MA). The second strand synthesis was then performed using the NEBnext Second Strand synthesis module. Following this the samples were taken into standard library preparation protocol using NEBNext® DNA Library Prep Master Mix Set for Illumina® with slight modifications. Briefly, end-repair was done followed by A-tailing and custom adapter ligation. Post-ligated materials were individually barcoded with unique in-house Genomics Service Laboratory (GSL) primers and amplified through 12 cycles of PCR. Library quantity was assessed by Qubit 2.0 Fluorometer, and the library quality was estimated by utilizing a DNA 1000 chip on an Agilent 2100 Bioanalyzer. Accurate quantification of the final libraries for sequencing applications was determined using the qPCR-based KAPA Biosystems Library Quantification kit (Kapa Biosystems, Inc., Woburn, MA). Each library was diluted to a final concentration of 12.5 nM and pooled equimolar prior to clustering. Paired-End (PE) sequencing (50 million per sample, 100bp) was on an Illumina HiSeq2500 sequencer (Illumina, Inc.).

4.3.5 Processing of RNA-seq Reads

Approximately 50 million, 100bp, PE reads were generated from each sample. Further downstream analysis of the sequenced reads from each sample was performed as per our unique in-house pipeline. Briefly, quality control checks on raw sequence data from each sample will be performed using FastQC (Babraham Bioinformatics, London, UK). Raw reads were mapped to the reference mouse genome mm9 using TopHat v2.0 [249, 250] with two mismatches allowed and other default parameters. The alignment metrics of the mapped reads was estimated using

SAMtools [251]. Aligned reads were then imported onto the commercial data analysis platform, Avadis NGS (Strand Scientifics, CA, USA). After quality inspection, the aligned reads were filtered on the basis of read quality metrics where reads with a base quality score less than 30, alignment score less than 95, and mapping quality less than 40 were removed. Remaining reads were then filtered on the basis of their read statistics, where missing mates, translocated, unaligned and flipped reads were removed. The reads list was then filtered to remove duplicates. Samples were grouped and quantification of transcript abundance was done on this final read list using Trimmed Means of M-values (TMM) [252] as the normalization method. Differential expression of genes were calculated on the basis of fold change (using default cut-off $\geq \pm 2.0$) observed between dietary treatments, and the *p-value* of the differentially expressed gene list was estimated by *z-score* calculations using determined by Benjamini Hochberg FDR correction of 0.05 [253]. Spearman correlation was used to generate the heat map. Tissue specific gene expression was compared between liver and adipose tissue to confirm the specificity of the hepatic transcriptome analysis. Volcano plots, used to illustrate up- and downregulated gene expression events, were generated for each diet comparison using GraphPad Prism 6 (La Jolla, CA). Venn diagrams were created to identify differentially expressed genes between each diet comparison.

The data set (GSE89296) is available at NCBI Gene Expression Omnibus database (www.ncbi.nlm.nih.gov/geo).

4.3.6 Gene Set Enrichment, Biological and Network Analysis

Gene enrichment analyses were performed using 1) Gene ontology (GO) [254]; 2) Ingenuity Pathway Analysis (IPA)(http://www.ingenuity.com/); 3) Kyoto Encyclopedia of Genes and

Genomes (KEGG) [255]; and 4) Protein Analysis Through Evolutionary Relationships (Panther)[256] to identify the most significantly affected unique canonical pathways, biological functions and networks between each diet comparison.

4.3.7 qPCR

The same RNA used to generate cDNA libraries for RNA-seq was also used to validate RNA-seq by qPCR. Reverse transcription was performed using the RT^2 First Strand Kit (Qiagen, Valencia, CA). qPCR was performed with RT^2 SYBR Green qPCR Mastermix (Qiagen, Valencia, CA) and gene-specific primers (SABiosciences, Fredrick, MD) using MyiQ Real-Time PCR systems (Bio-Rad, Hercules, CA). After amplification, melt curve analysis was performed to confirm the specificity of the reaction. All measurements were performed in triplicate. GAPDH was used as a reference gene to normalize gene expression. The $2^{\wedge-\Delta\Delta CT}$ method was used to analyze the qPCR data and measure relative expression differences [257].

4.3.8 Statistical analysis

Statistical analysis was performed using GraphPad Prism 6 (La Jolla, CA). The results are presented as means ± SEMs. Statistical significance of gene expression data was analyzed by Student's *t*-test ($\alpha = 0.05$) using the chow group as a control. Statistical significance between groups was determined by one-way analysis of variance ($\alpha = 0.05$) followed by Newman-Keuls test ($\alpha = 0.05$). Linear regression was performed to compare gene expression results [$\log_2$(fold-change)] obtained by RNA-seq and qPCR.

4.4 Results

4.4.1 Effects of diets on body and organ weight and serum metabolites

C57l/6N mice aged 6 wk were placed on a chow or HFWD with or without 42 g/L (fructose and sucrose) F/S in the drinking water for up to 12 wk. The chow group served as the control group. The characteristics of mice at the age of 12 wk are shown in Table 2. Mice fed the HFWD+F/S gained the most weight at 12 wk, which is 44 % and 12 % higher than the control and HFWD group, respectively ($P< 0.05$). Liver weight normalized to body weight at 12 wk was also markedly higher in the HFWD+F/S group (48% vs control, and 19% vs HFWD). As expected, eWAT weight normalized to body weight at 12 wk was significantly higher in the HFWD+F/S group compared to the chow group ($P<0.05$), however, a 5% decrease was observed when compared to the HFWD. These findings are consistent with our previous observation that adipose tissue expansion was limited by the addition of liquid sugar in HFWD-fed mice [242]. Moreover, plasma fasting glucose level was significantly elevated in the HFWD+F/S-fed mice compared with all the other groups at 12 wk ($P<0.05$). Taken together, these data indicated that, compared with chow and HFWD-fed mice, HFWD+F/S-fed mice are hyperglycemic and have a significantly greater body weight and normalized liver weight, yet limited eWAT expansion.

4.4.2 Hepatic steatosis, hypertrophy, and inflammation

We investigated the role of liquid sugar in the drinking water on Western diet induced hepatic steatosis, hypertrophy, and inflammation which are the key features of NASH [258]. Histological scoring of stained liver tissue sections from the diet treatment groups at 12 wk revealed that both HFWD and HFWD+F/S-fed mice demonstrated substantial steatosis as indicated by greater

macro- and micro-vesicular steatosis scores as well as hepatocellular hypertrophy compared with the control group (Fig. 19A). However, the greatest steatosis (macrosteatosis and microsteatosis) and hypertrophy scores were observed in the HFWD+F/S group (Fig. 19B). Confirming the histological impression, liver TG level at 12 wk was significantly elevated in the HFWD+F/S group compared with all other dietary treatment (Fig. 20A). Moreover, the inflammation score, evaluated by counting the number of inflammatory cell aggregates was greatest in HFWD+F/S group, yet there was no significant difference between groups at 12 wk (Fig. 20B). Finally, we tallied steatosis, hypertrophy, and inflammation scores for each animal to generate a NAFLD total score, which is a validated histological NAFLD scoring system in rodent [248]. As shown in Fig. 20C, the HFWD+F/S group had a significantly greater NAFLD total score at 12 wk. Thus, consumption of liquid sugar appears to exacerbate NAFLD in HFWD-fed mice.

4.4.3 Gene expression analysis by RNA-seq

4.4.3.1 High-throughput sequencing reads

To obtain a global view of the hepatic transcriptome responses to the consumption of liquid sugar in mice fed a HFWD diet, we performed high-throughput sequencing of the liver transcriptomes. Adipose transcriptome was also assessed to serve as a control. Finally, we obtained approximately 150, 149, and 141 million high quality clean reads from the liver of chow, HFWD, and HFWD+F/S-fed mice, respectively. In these high quality reads, approximately 41%, 43%, and 46% reads can be mapped to annotated mouse unique genes in chow, HFWD, and HFWD+F/S group, respectively (Table 3). In addition, ~40% of mapped reads were aligned to protein-coding exonic regions, 19% to untranslated regions (UTR), ~27% to intergenic regions and ~13% to intron regions (Table 3). Cluster analysis detecting pairwise

correlations between samples based on the spearman correlation coefficient showed well-defined tissue segregation, and independent diet group cluster based on transcript expression profiles in liver and adipose tissue, respectively (Fig. 21). Furthermore, RNA-seq analysis of tissue-specific genes also showed a high tissue-specificity. Liver specific genes *Alb, Hamp, Apoa1, Ahsg and Fetub* encoding albumin (ALB), Hepcidin Antimicrobial Peptide (HAMP), Apolipoprotein A1(APOA1), Alpha-2-HS-Glycoprotein (AHSG) and Fetuin B (FETUB) are substantially expressed in liver (Fig. 22A), while adipose specific genes *Adipoq, Lep, Lpl and Slc2a4* encoding adiponectin (ADIPOQ), leptin, (LEP), lipoprotein lipase (LPL) and GLUT4 (Slc2a4) are highly expressed in the adipose tissue (Fig. 22B). Taken together, these data confirm the specificity of the hepatic transcriptome analysis.

4.4.3.2 Differentially expressed genes and top-fold change genes

To identify differentially expressed genes (DEGs) in the livers of chow, HFWD and HFWD+F/S-fed mice, we used Trimmed Means of M-values (TMM) as the normalization method to detect significant DEGs, based on fold change (≥ 2), between groups [259]. Volcano plots (Fig. 23, A-C) were generated to illustrate up- and down-regulated gene expression events for each comparison (HFWD vs chow, HFWD+F/S vs chow, and HFWD+F/S vs HFWD). In total, 1065 genes were differentially expressed (≥ 2-fold) in the HFWD-fed compared to chow-fed mice ($P < 0.05$) (Fig. 23A). Expression was upregulated for 685 genes and downregulated for 380 genes in the HFWD-fed as compared to chow-fed mice. When liquid sugar was added to the HFWD, 1689 genes were differentially expressed (≥ 2 folds) in the HFWD+F/S-fed when compared with chow-fed mice ($P < 0.05$), including 288 downregulated and 1401 upregulated (Fig. 23B). Overall, 760 differentially expressed hepatic genes were identified in HFWD+F/S-

fed mice as compared to HFWD-fed mice (Fig. 23C). Of these 760 DEGs, expression was upregulated for 651 and downregulated for 109 genes in the HFWD+F/S- vs HFWD-fed mice. Based on the high-throughput sequencing analysis, the top 10 fold changes in genes upregulated and downregulated respectively in HFWD vs chow, HFWD+F/S vs chow and HFWD+F/S vs HFWD comparisons are shown in Figure 23, D-F. *Cyp2b9*, a member of the cytochrome P450 superfamily which catalyzes the oxidation of organic substances, was the top upregulated hepatic gene in both HFWD (~23-fold) and HFWD+F/S (~72-fold) when compared to chow group (Fig. 23, D and E). Other top upregulated genes in both HFWD and HFWD+F/S as compared to chow include *cidea* (Cell Death-Inducing DFFA-like Effector A), *kbtbd11* (Kelch Repeat and BTB Domain Containing 11), *osbpl3* (Oxysterol Binding Protein Like 3), and *Klhl31*(Kelch Like Family Member 31). Cidea and Osbpl3 have been found to play an important role in lipid metabolism [260, 261]. However, the role of *kbtbd11* and *klhl31* in liver has yet to be elucidated. Regarding the top fold change genes that were downregulated, we observed that *Col20a1* was significantly downregulated by 46-fold in HFWD-fed mice and was also downregulated by 36-fold in HFWD+F/S-fed mice (Fig. 23, D and E). *Gpr110*, *wdr37*, *Akap9* and *USP24* were additional top fold change genes downregulated in the liver of both HFWD- and HFWD+F/S-fed mice as compared to chow. Interestingly, *ddx60, stk17b, fzd5, and trdv5*, which are primarily involved in immune-related processes, were in the top 10-fold change genes upregulated in HFWD+F/S- vs HFWD-fed mice, while *Xlr4b*, *Col6a6* and *Fam47e* were the top 3 fold changes of the downregulated genes (Fig. 23F).

In order to visualize the overlap of DEGs domains for a three-way comparison, a Venn diagram was generated (Fig. 24). In all, 38 DEGs were common to each group. Upon considering DEGs uniquely expressed between dietary treatments, the HFWD+F/S versus chow comparison

resulted in greater number of DEGs compared to the HFWD versus chow comparison (720 vs. 252, respectively). Interestingly, 655 DEGs were found to overlap between the HFWD+F/S versus chow and HFWD versus chow comparisons. We observed 326 DEGs uniquely expressed between the HFWD+F/S versus HFWD comparison. A total of 276 DEGs were observed between the HFWD+F/S versus chow and HFWD+F/S versus HFWD comparisons which suggests that these DEGs are uniquely regulated by liquid sugar.

4.4.4 Gene Ontology (GO) enrichment analysis of DEGs

To gain further insights into the biological functions of DEGs, we performed GO analysis by querying each DEG identified in the livers of chow, HFWD, and HFWD+F/S-fed mice against the GO database. GO analysis of significant DEGs between HFWD- and chow-fed mice revealed that the top enriched biological processes affected by HFWD feeding including ion transport, lipid localization, and immune response (Fig. 25), while biological processes enriched by HFWD+F/S feeding compared to chow feeding are: oxidation reduction, cell death and apoptosis, and lipid metabolism (Fig. 26). The enriched biological processed affected by the consumption of liquid sugar were also investigated and were found to be mainly involved in the regulation of small GTPase mediated signal transduction, and lipid homeostasis, such as glycerolipid metabolic process, glycerophospholipid metabolic process and phospholipid metabolic process (Fig. 27).

4.4.5 IPA pathway analysis

Ingenuity IPA pathway analysis was performed to further elucidate the biological function of the DEGs identified in the liver of HFWD- and HFWD+F/S-fed mice. The top IPA pathways significantly enriched in the liver of HFWD-fed mice including G-protein coupled receptor signaling, immune-related pathways and pathways involved in cholesterol biosynthesis (Fig. 25), while significantly enriched IPA pathways in HFWD+F/S- vs chow-fed mice were closely correlated with immune-, oxidative stress- and inflammatory responses (Fig. 26). Interestingly, the addition of liquid sugar in HFWD-fed mice resulted in mainly fibrosis, cancer and immune reponse-related pathways enriched, such as *basal cell carcinoma signaling*, *PDGF signaling*, *regulation of epithelial mesenchymal transition pathway*, *Wnt/β-catenin signaling*, *NF-κB signaling*, *Regulation of IL2 expression*, *colorectal cancer metastasis signaling*, *thyroid cancer signaling*, and *ovarian cancer signaling* (Fig. 27)

4.4.6 Overlapping pathways

To further understand the importance of pathway interactions and to screen key pathways for significant roles in NAFLD induced by HFWD+F/S feeding, we used Kyoto Encyclopedia of Genes and Genomes (KEGG) and Protein Analysis Through Evolutionary Relationships (PANTHER) analysis to identify the overlapping pathways enriched at HFWD+F/S vs chow and HFWD+F/S vs HFWD comparisons. As shown in Table 3, the pathways that were significantly enriched by the consumption of liquid sugar in liver of HFDW-fed mice included *pathways in cancer*; *cell cycle*; *T cell receptor signaling pathways*, *PDGF signaling pathway*, as well as *T cell activation*.

4.4.7 Validation of RNA-seq results by qPCR

To validate the differentially expressed genes identified by RNA-seq expression analysis, we randomly selected 8 genes (*DDX60, stk17b, kcnb2, cidea, Htrcr2, Col6a6, TCF7, and bmp1*) from those differentially expression patterns and genes of interest based on their function, for qPCR validation (Fig. 28A). The $\log_2$ fold correlation of RNA-seq (*y* axis) and qPCR (*x* axis) using the $\log_2$ fold change measure of the genes differentially expressed from chow-, HFWD- and HFWD+F/S-fed mice are shown in Fig. 28. qPCR results were significantly correlated with the RNA-seq results by linear regression analysis (R^2= 0.96, P values <0.0001) (Fig. 28B). Thus, the RNA-seq results were confirmed by the qPCR results, indicating the reliability and accuracy of the RNA-seq expression analysis.

4.5 Discussion

In this study we used a more comprehensive, sensitive, quantitative and unbiased approach (RNA-seq), to provide a global view of the hepatic transcriptome responses to the consumption of liquid sugar in mice fed a HFWD diet, and demonstrate the main DEGS, biological processes and pathways involved in the progression of NAFLD.

As we expected, F/S consumption in HFWD-fed mice resulted in a large increase in body weight as well as normalized liver weight at 12 wk. Moreover, HFWD+F/S-fed mice also had a significantly less normalized eWAT weight, which indicated that the capacity of the eWAT to expand was impaired in the HFWD+F/S group. These results are in agreement with our recently published study [242] and another study [231]. Impairment in adipose tissue expansion has been found to be a critical factor in the development of insulin resistance [232]. Indeed, we have shown that HFWD+F/S-fed mice were more glucose intolerant and insulin resistant than HFWD-

fed mice [242]. We also observed that 12 wk consumption of liquid sugar exacerbated HFWD-induced hyperglycemia. These results are consistent with epidemiological [234] and human studies [235]. Histological scoring of stained liver tissue sections from the diet treatment groups at 12 wk revealed HFWD+F/S group has the greatest steatosis, hypertrophy, inflammation and total NAFLD score, indicating that the combination of liquid sugar and high-fat accelerates liver disease from steatosis toward NASH. Taken together these results confirm the validity of our model used to explore global changes in the hepatic transcriptome induced by HFWD and HFWD+F/S feeding in mice.

RNA sequencing is a state-of-the-art approach, which provides a far more precise measurement of levels of transcripts in a relatively unbiased way [149]. With this technology, we are able to detect a total of 1065, 1689 and 760 DEGs in the comparisons of HFWD vs chow, HFWD+F/S vs chow and HFWD+F/S vs HFWD, respectively, with the majority of DEGs upregulated in each diet comparison. Our observation that genes expressed by liver from chow, HFWD, and HFWD+F/S clustered separately indicated that each diet had a unique transcriptomic signature. Based on the high throughput sequencing analysis, we also showed the top 10-fold changes of genes upregulated and downregulated, respectively, in the comparisons of HFWD vs chow, HFWD+F/S vs chow and HFWD+F/S vs HFWD. The top upregulated hepatic gene in the HFWD+F/S vs chow comparison was *cyp2b9*, which belongs to the superfamily of cytochrome p450. Cyp450s are heme-containing membrane-bound enzymes that metabolize steroids and fatty acids. Increased hepatic Cyp2b mRNA have been shown to be elevated in diabetes and high-fat feeding [262], as well as in mice fed high fructose corn syrup [263]. Hepatic *Cidea* was also significantly upregulated in HFWD+F/S (44-fold) as compared to chow group. Overexpression of *Cidea* in mouse liver resulted in increased hepatic lipid accumulation and the

formation of large lipid droplets [264]. In contrast, mice deficient in *Cidea* showed increased metabolic rates and resistance to obesity when on a high fat diet or in *ob/ob* mice [261, 264]. Thus, the combination of liquid sugar and high-fat promotes upregulation of lipid metabolism-related genes. We observed that *Col20a1* was significantly downregulated by 37-fold in HFWD+F/S-fed mice, indicating that extracellular matrix remodeling has been modulated in HFWD+F/S group. Importantly, *col20a1* has been reported to be downregulated in ob/ob mice [265]. However, the role of *Col20a1* in the progression of NAFLD remains to be elucidated. Interestingly, we found largely unknown and markedly DEGs including *DDX60*, *GM5921*, *Xlr4b* in HFWD+F/S vs HFWD comparison. Future studies focused on these markedly differentially expressed hepatic genes with largely unknown effects on the progression of NAFLD will provide new insights into the molecular mechanism of NAFLD.

In the present study, fewer DEGs were observed in the HFWD vs chow comparison compared to the HFWD+F/S versus chow comparison, suggesting that liquid sugar consumption induces changes in the hepatic transcriptome. Indeed, 602 DEGs representing 326 DEGs uniquely observed in the liver of HFWD+F/S-fed and 276 DEGs common to the HFWD+F/S versus chow and HFWD+F/S versus HFWD comparisons provide compelling evidence that the combination of HFWD and liquid sugar has a profound effect on the DEGs in liver.

The spectrum of NAFLD ranges from simple fatty liver to NASH, and an innate and adaptive immune responses have been reported to play important roles in this transition by triggering and amplifying hepatic inflammation [266]. Kupffer cells (KCs), the resident macrophages in liver, are a major component of hepatic innate immune cells, and can inhibit dendritic cell (DC)-induced T cell activation under steady state conditions. Upon activation by bacterial-antigens, such as lipopolysaccaride (LPS), KCs contribute to the liver injury through proinflammatory

cytokines release as well as modulate the differentiation and activation of various immune cells, including T cells [266]. In a large cohort study of NAFLD, the peripheral circulating LPS level was reported to be increased in patients with NAFLD [267]. Moreover, the depletion of KCs has been found to attenuate methionine- and choline-deficient diet (MCD) and HFD-induced liver injury, steatosis, and proinflammatory monocyte infiltration in mice [268]. T cells, which can be activated by KCs, are one of major types of lymphocytes involved in adaptive immunity. In NASH patients and animal models, CD4(+) and CD8(+) T cell infiltration was increased [269, 270]. In human liver biopsies taken from NAFLD/NASH patients, CD4(+) and CD8(+) T cell infiltration was positively correlated with NASH progression [270]. In our study, overlapping pathway analysis in the liver with the HFWD+F/S vs chow and HFWD+F/S vs HFWD comparisons indicated that *T cell activation* and *T cell receptor signaling pathways* are significantly enriched in HFWD+F/S group, suggesting the possible contribution of immune responses in modulating hepatic inflammation in NASH. CD4(+) T cells may promote hepatic inflammation through upregulation of interferon-gamma (IFN-γ) and CD40 ligand, both of which have been shown to be associated with inflammation in liver [269]. However, the role of CD8(+) T cells in NASH progression is not clearly understood and requires further research. Hepatic fibrosis, and its more advanced form cirrhosis, represents the final common pathway of almost all chronic liver disease including NASH. In healthy livers, acute liver injury leads to injury repair arising by replication of mature hepatocytes [271]. However, in NAFLD, the presence of ongoing liver injury is associated with high levels of oxidative stress, which reduce the ability of these mature hepatocytes to proliferate [271]. Thus, other pathways of liver regeneration, such as hepatic progenitor cells (HPCs) proliferation, are activated [21]. The activation of HPCs proliferation has been confirmed in both rodent models and human studies

[272], and is considered as a liver's adaptive response to oxidative stress [84]. The proliferation of HPCs, stimulated by damage hepatocytes and upregulated by *Wnt/β-catenin pathway*, resulted in the appearance of a ductular response. The extent of a ductular response has been found to be strongly and independently correlated with the degree of fibrosis in liver biopsy specimens of human NASH [84]. Possible mechanisms for this include: 1) ductular response can produce fibrogenic factors such as TGFβ and PDGF, which in turn can activate portal myofibroblasts and hepatic stellate cells (HSCs) to produce type 1 and 3 collagen; 2) In parallel, the HPCs could differentiate towards cholangiocytes, which can further undergo epithelial-mesenchymal transition to myofibroblasts, contributing to the portal myofibroblasts pool [84]. Thus, in the progression of NAFLD, the prolonged hepatocyte apoptosis and injury induced by oxidative stress can trigger the proliferation and activation of HPCs [273]. This determined the appearance and expansion of ductular response which can activate fibrogenesis and angiogenesis processes leading to portal fibrosis [274]. In the present study, IPA pathway analysis of HFWD+F/S vs HFWD showed significantly enriched *PDGF signaling*, *regulation of epithelial mesenchymal transition pathway*, and *Wnt/β-catenin signaling*, which are thought to be actively involved in the generation of portal fibrosis in NAFLD (Fig. 27). Moreover, *PDGF signaling* was further identified in the overlapping pathways enriched in the HFWD+F/S vs chow and HFWD+F/S vs HFWD comparisons by PANTHER analysis (Table 4). Our data indicated that the combination of liquid sugar and high-fat activated a series of fibrosis pathways, which might promote the portal fibrosis in NAFLD, a key feature of progressive fibrosis and will subsequently raise the possibility of a second periportal pathway for fibrogenesis in NASH [274].

Hepatocelluar carcinoma (HCC), the most common primary cancer of the liver and the third leading cause of cancer-related death, has been considered the long-term complication of NASH.

It has been reported that 4-22% of HCC in Western countries are attributed to NAFLD [275]. In our study, KEGG enriched pathway analysis identified *Pathways in cancer* as the most enriched overlapping pathway in the HFWD+F/S vs chow and HFWD+F/S vs HFWD comparisons, suggesting an activation of cancer pathways in HFWD+F/S-fed mice. Consistent with this result is the observation that *Liver cancer* is the top pathway enriched in the livers of diabetic *db/db* mice [276] and that a pre-malignant cancer gene expression pattern is observed in patients with steatohepatitis but not steatosis [277]. Consistent with this observation, the *PDGF pathway*, another important pathway implicated in HCC [278], was identified as the most enriched overlapping pathway in the HFWD+F/S vs HFWD and HFWD+F/S vs chow comparisons by PANTHER pathway analysis. PDGF is an angiogenic factor; its gene expression level and plasma protein level have been shown to be increased in HCC tumors and in patients with HCC, respectively [279]. Inhibition of PDGF signaling was found to decrease cell migration *in vitro* and tumor growth *in vivo*, indicating that an important role for PDGF signaling in hepatocyte tumor progression [280]. Moreover, in addition to *Pathways in cancer* and *PDGF pathway*, other HCC related-signaling pathways such as *Wnt/β-catenin signaling*, *NF-κB signaling* and *regulation of epithelial mesenchymal transition pathway* were identified significantly enriched in the HFWD+F/S group by IPA pathway analysis. Our data indicated that the combination of liquid sugar and high-fat initiates a sequence of carcinogenesis pathways such as *pathways in cancer*, *PDGF pathway* and *Wnt/β-catenin signaling*, which may promote the transition from NASH to its end-stage compilation HCC.

In summary, we demonstrated that the combination of a HFWD with F/S in the drinking water exacerbated HFWD-induced obesity, hyperinsulinemia, hyperglycemia, hepatic steatosis and inflammation that is consistent with progression to NASH. More importantly, hepatic

transcriptomic analysis through RNA-seq revealed that pathways in immune response, fibrosis and cancer are major pathways enriched in the livers of HFWD+F/S-fed mice. These results provide a molecular basis for understanding the mechanism through which the addition of liquid sugar promotes the progression of NAFLD.

Tables

Table 2 Body and organ weights, and serum glucose level in mice

	Chow	HFWD	HFWD + F/S
Body weight (g)	30.9 ± 1.3^{a}	39.7 ± 1.2^{b}	44.6 ± 0.8^{c}
Liver weight (g)	1.26 ± 0.05^{a}	2.05 ± 0.22^{b}	2.72 ± 0.22^{c}
Liver/Body weight (%)	4.10 ± 0.10^{a}	5.09 ± 0.43^{ab}	6.06 ± 0.38^{b}
eWAT (g)	1.14 ± 0.20^{a}	2.28 ± 0.12^{b}	2.46 ± 0.09^{b}
eWAT/Body weight (%)	3.57 ± 0.47^{a}	5.80 ± 0.35^{b}	5.54 ± 0.29^{b}
Glucose (mg/dL)	146.5 ± 13.5^{a}	163.7 ± 14.9^{a}	214.4 ± 10.6^{b}

Values represents the means ± SE; n = 8

HFWD, high-fat Western diet; F/S, liquid sugar of fructose and sucrose;

Data was analyzed by ANOVA and pairwise comparisons were made using Newman-Keuls test

Different letters indicate significantly different values at $P < 0.05$.

Table 3 Summary of the sequencing reads alignment to the reference genome

	Chow	**HFWD**	**HFWD + F/S**
All reads	149,452,497	148,805,433	141,153,151
Uniquely mapped reads	60,967, 544	64,190,670	65,496,876
Uniquely mapped rate	0.41	0.43	0.46
Mapping metrics (%)			
Exonic	39	40	42
UTR	18	19	20
Intronic	14	13	13
Intergenic	29	27	26

Table 4 Overlapping Pathway enriched in liver at HFWD+F/S vs Chow and HFWD+F/S vs HFWD as indicated by KEGG and Panther annotation databases.

Annotation	Pathway*	P-value
KEGG	Pathways in Cancer (10, 2.8)	0.008
	Cell Cycle (6, 4.2)	0.012
	T Cell receptor signaling pathway (5, 3.8)	0.039
	Endocytosis (6, 2.7)	0.070
	Regulation of actin cytoskeleton (6, 2.5)	0.089
Panther	PDGF signaling pathway (6, 2.6)	0.072
	T cell activation (5, 3.0)	0.080

* Values within parentheses indicate the number of genes involved in and the fold-enrichment, respectively, of the corresponding pathway.

Figures and figure legends

Figure 19

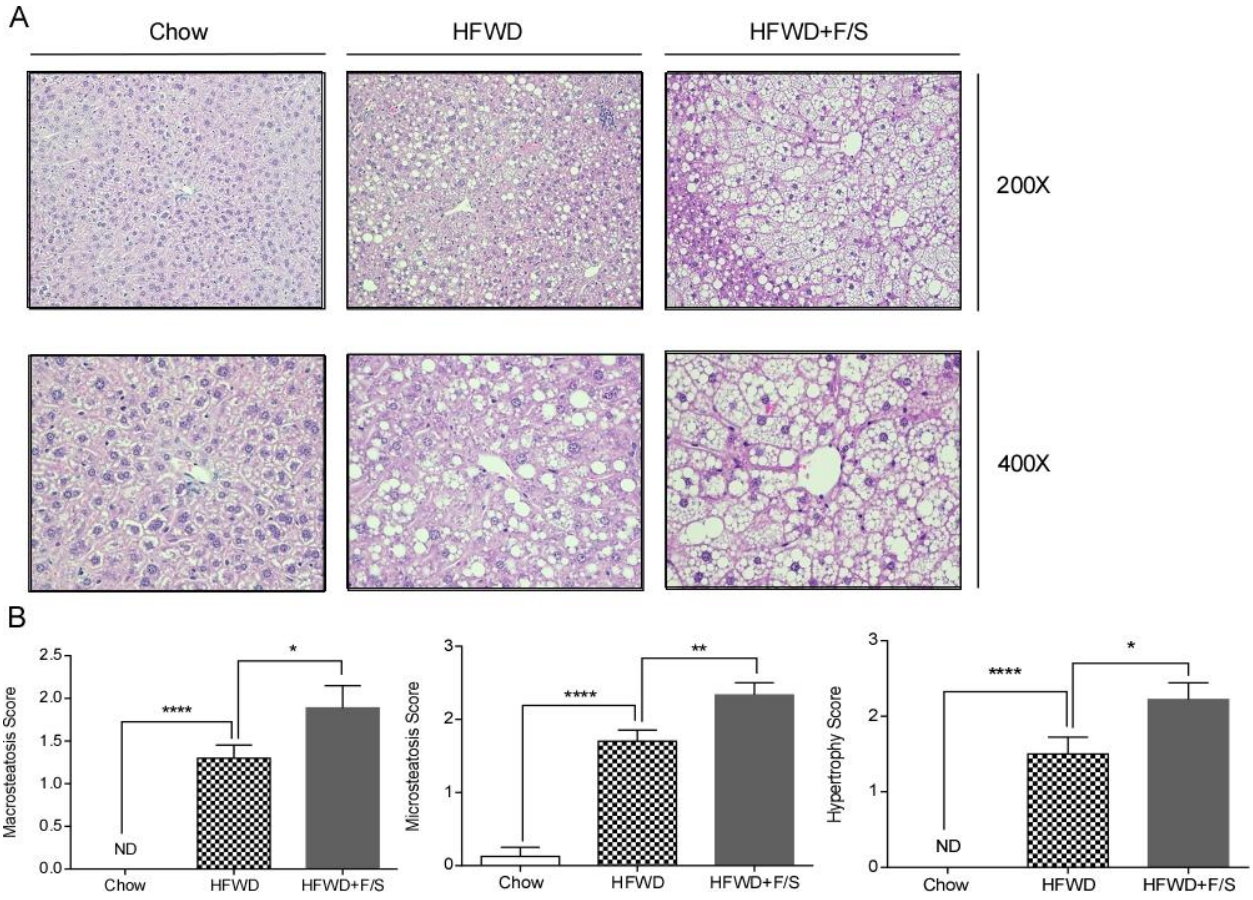

Fig 19 Hepatic steatosis and hypertrophy. (A) Hematoxylin and eosin (H&E)-stained liver section. (B) Steatosis and hypertrophy scoring of H&E-stained liver sections. Data are expressed as means ± SE, n=8 per group. *$P < 0.05$; ****$P < 0.0001$.

Figure 20

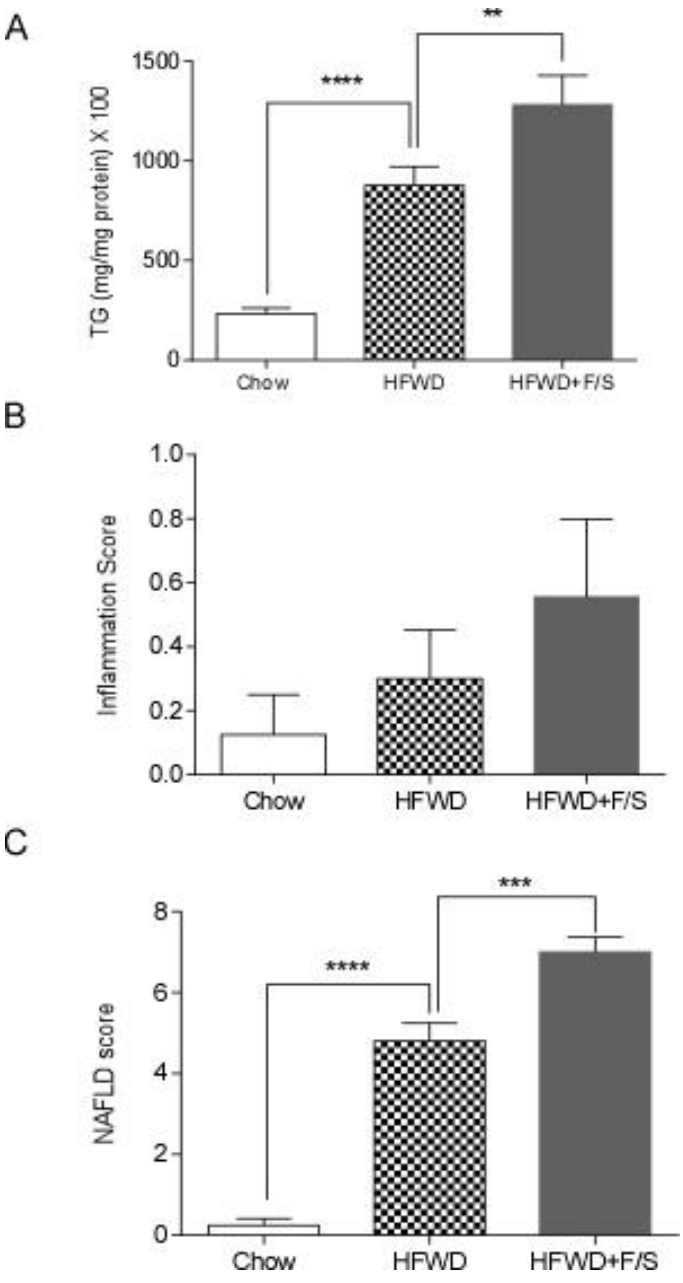

Fig 20 Hepatic triglyceride accumulation and inflammation. (A) Quantitation of hepatic triglyceride content. (B) Inflammation scoring of H&E-stained liver sections. (C) NAFL total score calculated based on the sum of scores for steatosis, hypertrophy and inflammation. Data are expressed as means ± SE, n=8 per group. $^{**}P < 0.01$; $^{***}P < 0.001$; $^{****}P < 0.0001$.

Figure 21

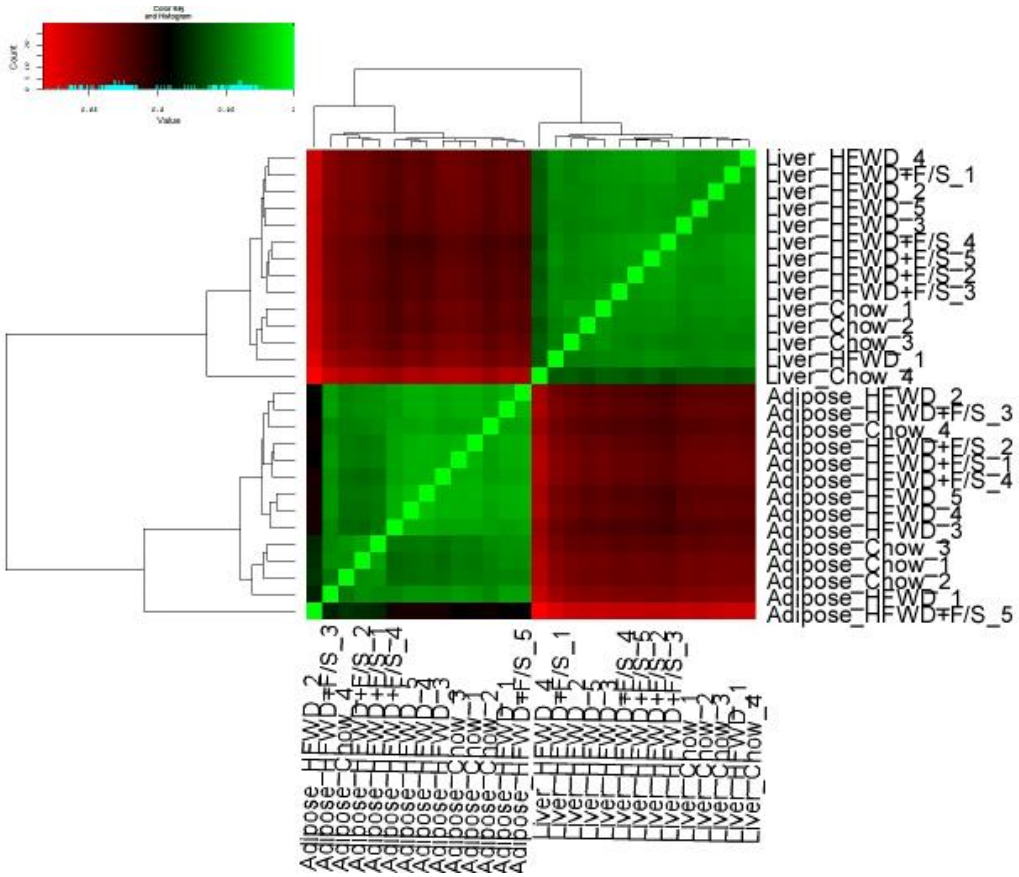

Fig 21 Spearman correlation heat map. Heat map of pairwise correlations between pooled samples based on the Spearman correlation coefficient. Light green represents highest correlation, and red represents lowest correlations.

Figure 22

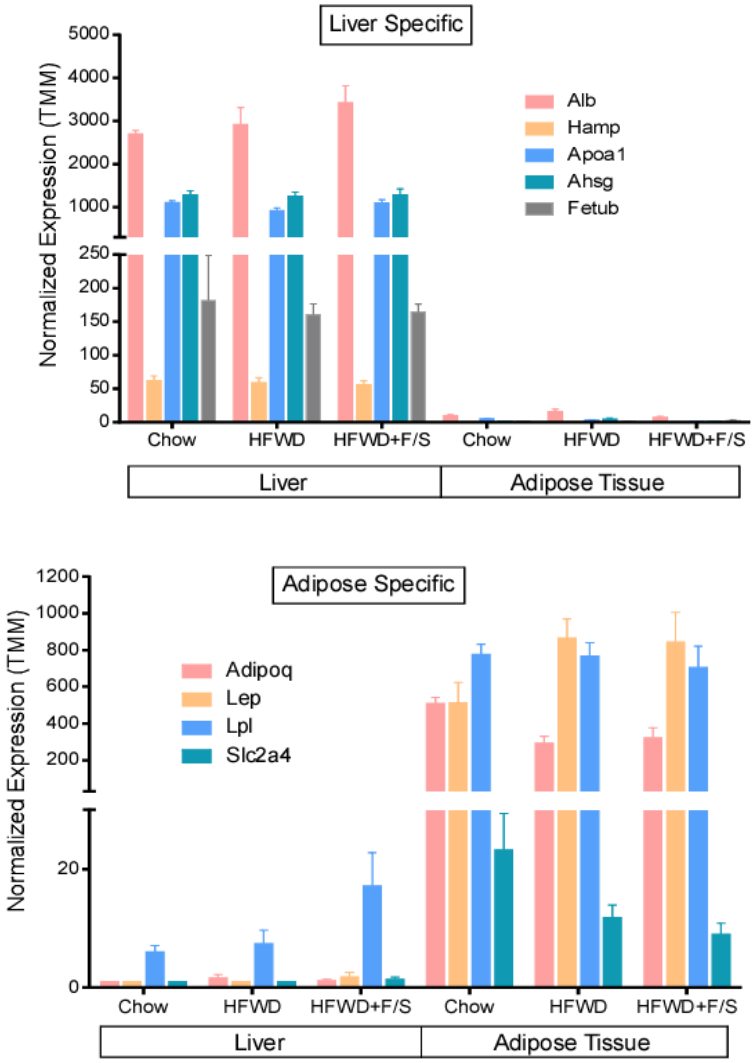

Fig 22 Tissue specificity. (A) Liver specific gene expression in liver and adipose tissue, respectively, expressed as FPKM. Liver specific genes: *Alb, Hamp, Apoa1, Ahsg and Fetub* encoding albumin (ALB), Hepcidin Antimicrobial Peptide (HAMP), Apolipoprotein A1(APOA1), Alpha-2-HS-Glycoprotein (AHSG) and Fetuin B (FETUB) (B) Adipose tissue-specific gene expression in liver and adipose tissue, respectively, expressed as RPKM. Adipose specific genes *Adipoq, Lep, Lpl and Slc2a4* encoding adiponectin (ADIPOQ), leptin, (LEP), lipoprotein lipase (LPL) and GLUT4 (Slc2a4).

Figure 23

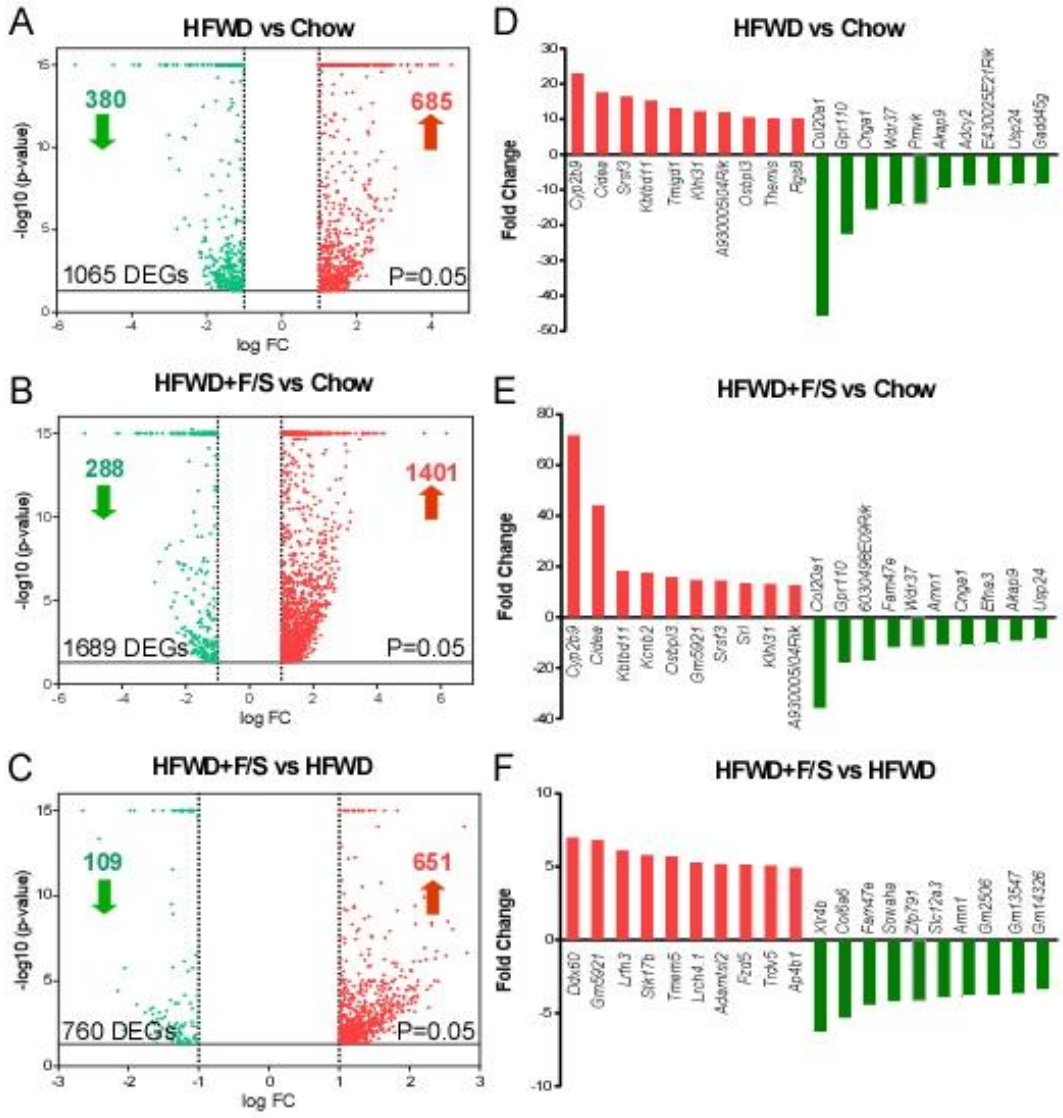

Fig 23 Differentially expressed genes and top fold change genes. Volcano plots (left) illustrating differences in hepatic gene expression between HFWD vs Chow (A), HFWD+F/S vs Chow (B), and HFWD+F/S vs HFWD (C). The horizontal line denotes $P < 0.05$; green denotes genes for which expression was downregulated (fold change ≥ 2); red denotes genes for which expression was upregulated (fold change ≥ 2). For each comparison, the total number of differentially expressed genes (DEGs) is given (# value). The number of DEGs that were downregulated (green) or upregulated (red) are shown. Bar graphs (right) presenting top 10 downregulated

genes (green) and upregulated genes (red) respectively in HFWD vs Chow comparison (D), HFWD+F/S vs Chow comparison (E); and HFWD+F/S vs HFWD comparison (F).

Figure 24

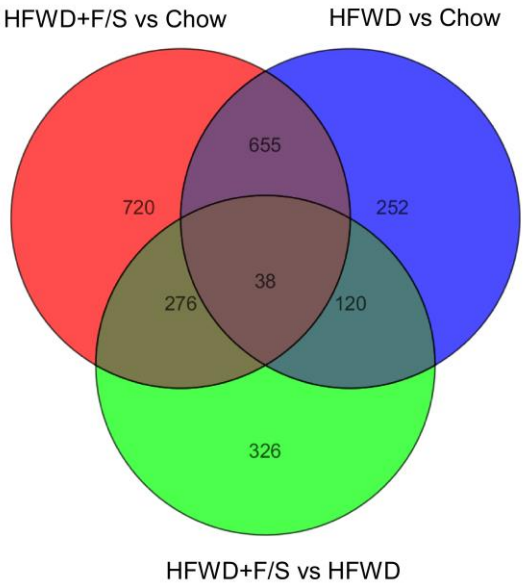

Fig 24 Unique and overlapping differential expressed genes. Venn diagram illustrating the numbers of unique and overlapping DEGs between HFWD vs Chow (blue), HFWD+F/S vs Chow (red), and HFWD+F/S vs HFWD (green).

Figure 25

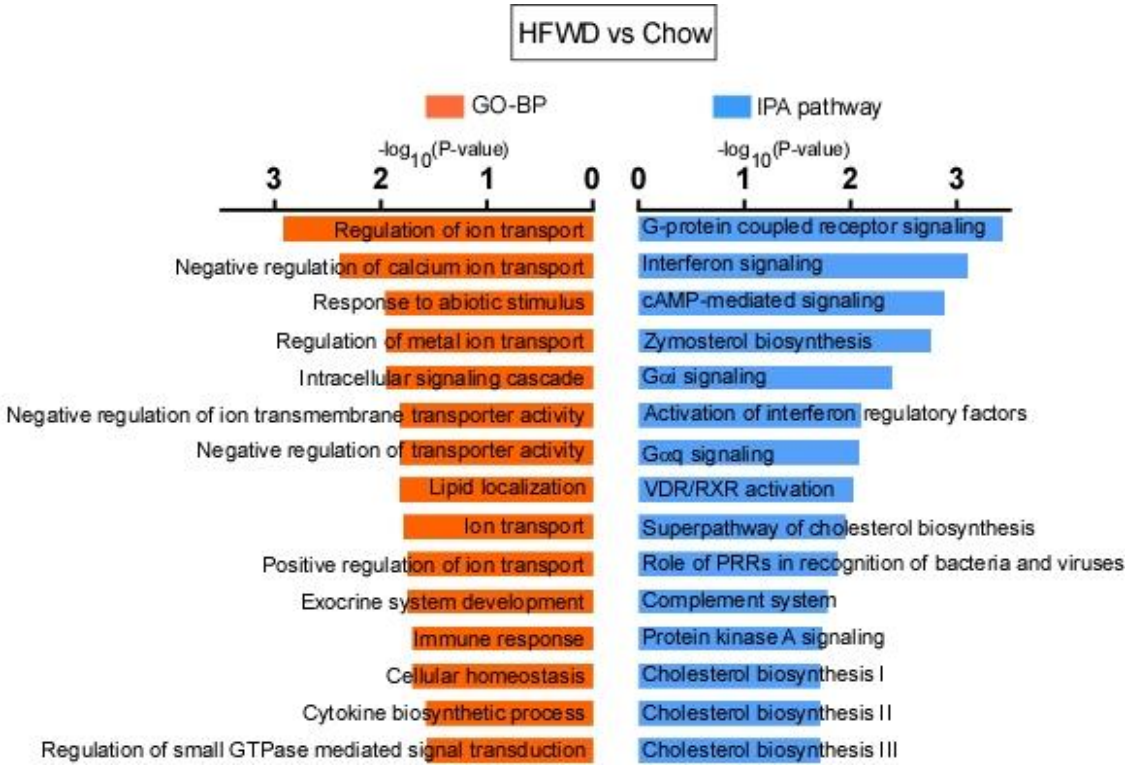

Fig 25 Gene ontology biological process and IPA pathway analysis of DEGs in HFWD vs Chow comparison. Top 15 significant gene ontology biological process (GO-BP) (orange) and IPA pathways (light blue) enriched between HFWD vs Chow. The vertical axis represents the GO category or pathway category, and the horizontal axis represents the $-\log_2$ (*P*-value).

Figure 26

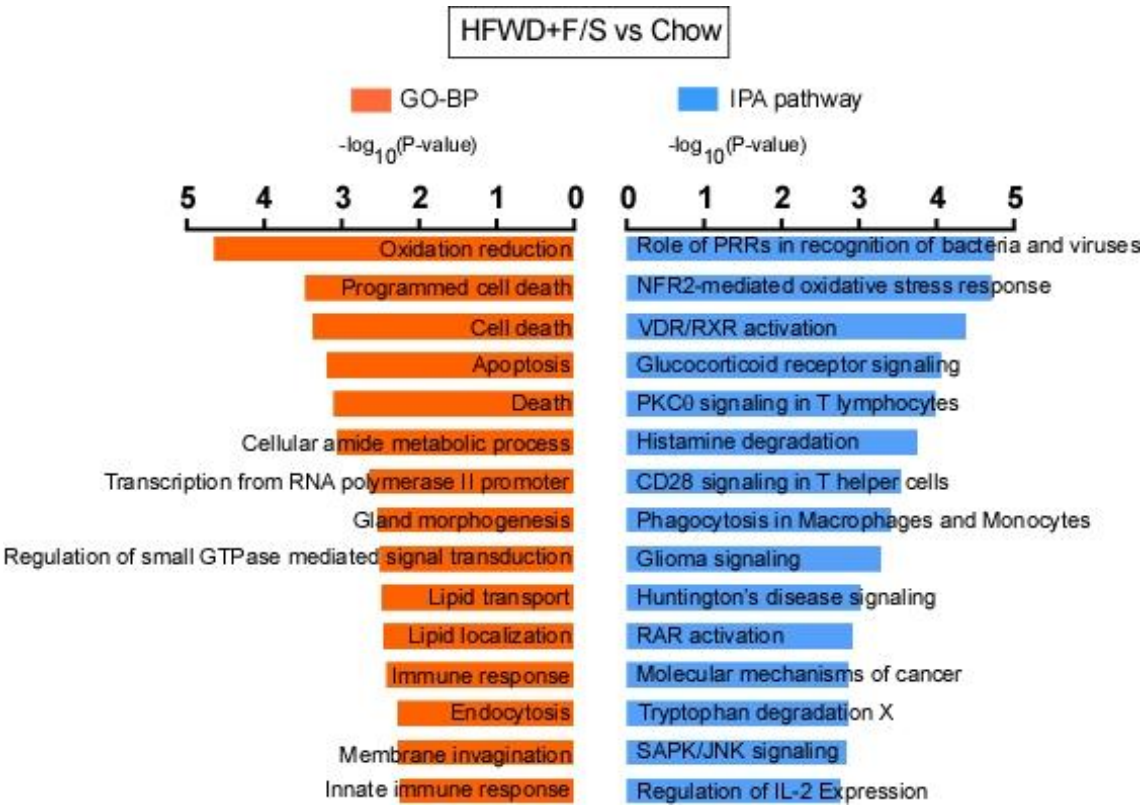

Fig 26 GO-BP and IPA pathway analysis of DEGs in HFWD+F/S vs Chow comparison. Top 15 significant GO-BP (orange) and IPA pathways (light blue) enriched between HFWD+F/S vs Chow. The vertical axis represents the GO category or pathway category, and the horizontal axis represents the $-\log_2$ (*P*-value).

Figure 27

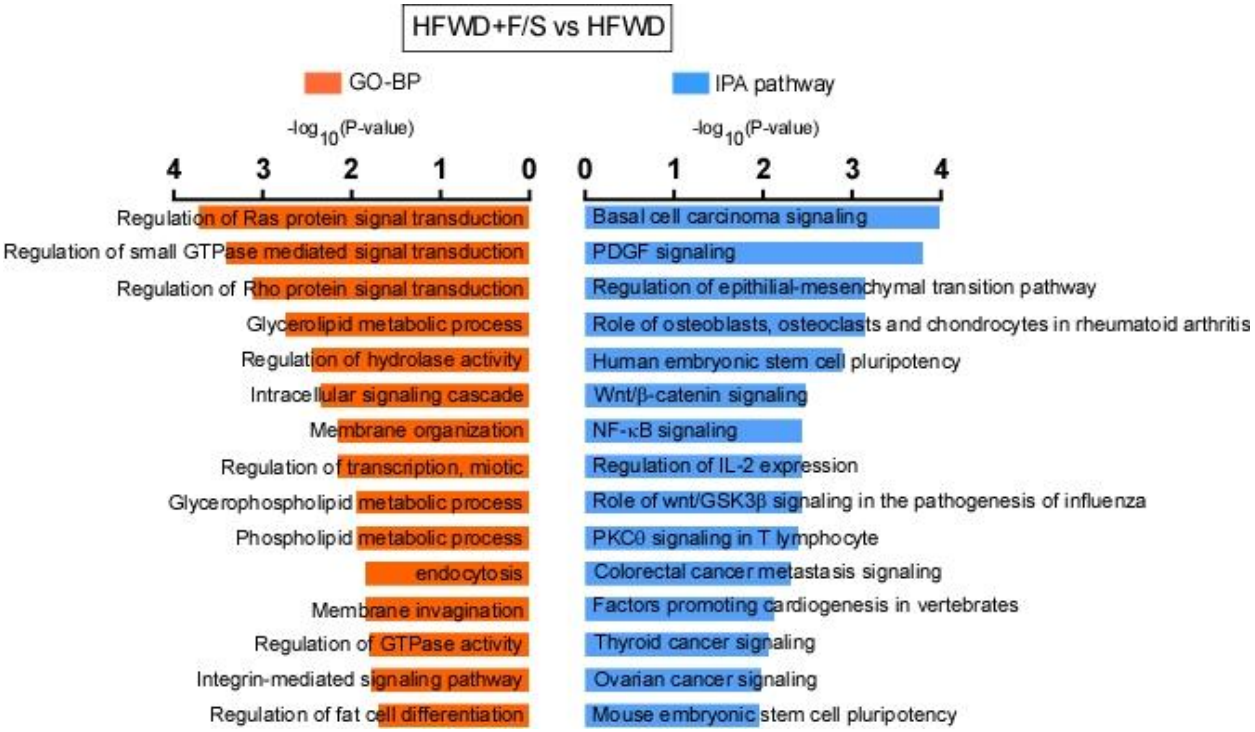

Fig 27 GO-BP and IPA pathway analysis of DEGs in HFWD+F/S vs HFWD comparison. Top 15 significant GO-BP (orange) and IPA pathways (light blue) enriched between HFWD+F/S vs HFWD. The vertical axis represents the GO category or pathway category, and the horizontal axis represents the $-\log_2$ (*P*-value).

Figure 28

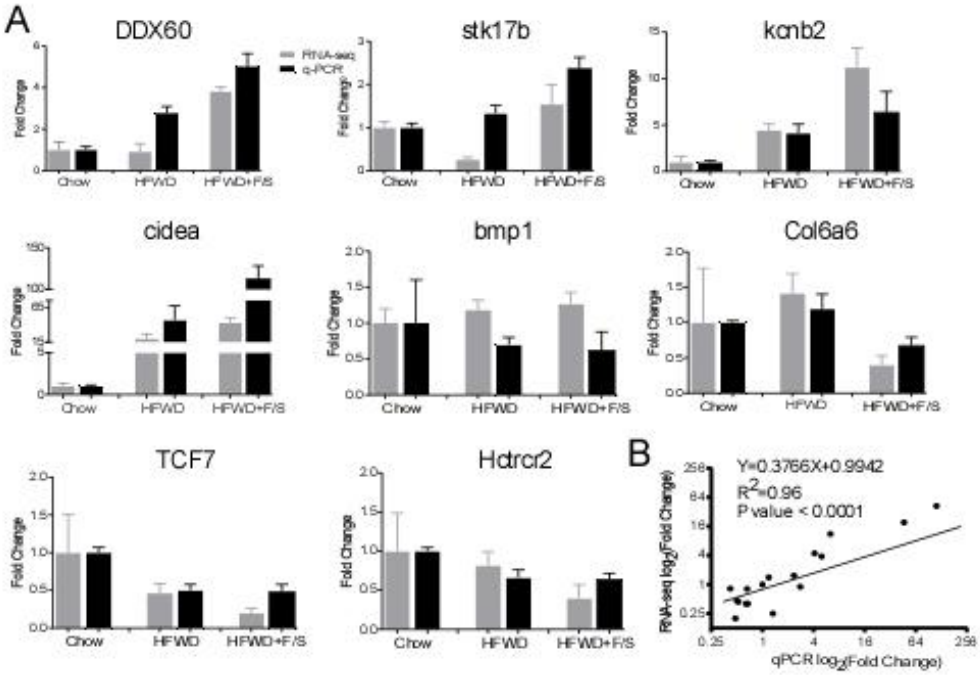

Fig 28 Validation of RNA-seq results by qPCR. (A) normalized gene expression of 8 randomly selected hepatic genes by RNA-seq (grey bars) and qPCR (black bars) respectively. Data are expressed as fold change (means ± SE) relative to chow, n = 8 per group. (B) Regression plot indicating the relationship between qPCR results [log_2 (fold change); X-axis] and the corresponding data from RNA-seq analysis [log_2 (fold change); Y-axis].

Chapter 5: Orosomucoid is induced in a high fat Western diet model of NAFLD and promotes macrophage polarization toward an anti-inflammatory phenotype

5.1 Abstract

Orosomucoid (ORM), also called α-1 acid glycoprotein, is one of the most abundant plasma proteins. As a member of the acute phase protein family, it is produced in the liver and secreted into plasma in response to tissue injury, infection, and inflammation. In this study, RNA-seq analysis of a high fat Western diet model of NAFLD revealed hepatic expression of ORM3 gene was significantly elevated by 20-fold. Further validation of ORM3 hepatic expression in an independent dietary treatment experiment confirmed our RNA-seq findings and found that ORM1 and ORM2 hepatic expression were significantly elevated to similar levels as ORM3. Correlation analysis of ORM3 gene expression with NAFLD parameters indicated that ORM3 gene expression was significantly positively correlated with body weight, normalized liver weight, and alanine aminotransferase, a marker of liver dysfunction. Moreover, the expression of ORM genes was also induced in a cellular model of insulin resistance. ORM was also observed to promote macrophage polarization toward an anti-inflammatory phenotype. Taken together, we suggest that ORM might have a protective role in NAFLD by regulating cellular insulin resistance and pro-inflammatory macrophages.

5.2 Introduction

Nonalcoholic fatty liver disease (NAFLD), an obesity and insulin resistance-associated clinical condition, ranges from simple steatosis to nonalcoholic steatohepatitis (NASH) which can lead to the more serious clinical conditions of cirrhosis and liver cancer (hepatocarcinoma). NAFLD has become the most common chronic disease in both children and adults [240], because the overall prevalence of NASH resembles that of obesity and type 2 diabetes [202]. There are currently no specific therapeutic treatments for NASH. In addition, the mechanisms underlying the progression of NAFLD are not known. Lack of such knowledge represents an important problem because new therapeutic targets are needed for the treatment of NASH. Knowledge of the genes regulating pathological changes associated with NAFLD progression is crucial; because in order for new liver-directed therapeutic options to treat NAFLD and NASH to be developed, it is necessary that the mechanistic details of NAFLD progression be determined so that new mechanisms of causation are identified.

We recently demonstrated, in a model of Western diet-induced obesity that consumption of liquid fructose and sucrose (F/S) exacerbates NAFLD [242]. Mice fed a high fat Western diet (HFWD) with liquid F/S are more obese, glucose intolerant, insulin resistant and have a significant higher NAFLD score than mice fed only the HFWD [242]. Furthermore, HWFD+F/S-fed mice developed an early hypoxia response in the eWAT led to reduced vascularization and increased fibrosis gene expression. Hypoxia in obese adipose tissue plays an important role in the development of whole-body insulin resistance by inducing local inflammation and the release of proinflammatory cytokines [281]. Recently, increasing evidence supported a key role of hypoxia in the progression of NAFLD. Animals prone to develop NASH, exposed to a continuous hypoxia, displayed increased expression in genes involved in hepatic lipogenesis

(such as SREBP-1c, ACC1, ACC2) and decreased expression of genes involved in β-oxidation [282]. Taken together, our results confirmed and extended the conclusion that the HFWD with liquid F/S animal model is a good model of NAFLD progression.

ORM protein, also known as α-1 acid glycoprotein, is one of the most abundant plasma proteins, accounting for about 1% of all plasma proteins [175, 176]. As a member of the acute phase reactant protein family, it is expressed in hepatocytes and secreted into the plasma under stressful conditions such as tissue injury, infection, and inflammation [175]. There are two isoforms of ORM in humans, three in mice, and one in rats. The biological function of ORM is not completely understood, however, a number of functions *in vitro* and *in vivo* have been described, such as immunomodulatory function, barrier function, and carrier function [175, 176]. Recently, it has been reported that ORM1 isoform integrates inflammatory and metabolic signals to protect adipose tissue from severe inflammation and metabolic dysfunction [198], and can regulate inflammation by modulating the polarization of M2 phenotype macrophages [192]. So far, the functions of the three isoforms found in mice have not been fully established. Further, little is known about the role of ORM proteins in NAFLD progression and the regulation of cellular insulin responsiveness in the major insulin target tissues. Thus, there exists a gap in our understanding of the role of ORM proteins in metabolic parameters linked to NAFLD. Here, we demonstrate that expression of the ORM genes is induced in a high fat Western diet model of NAFLD as well as in a cellular model of insulin resistance. Also, in agreement with previous findings, we demonstrated that ORM can regulate inflammation by polarizing macrophages to the M2 phenotype. Thus, we suggest that ORM might have a protective role in NAFLD by regulating cellular insulin resistance and pro-inflammatory macrophages.

5.3 Materials and Methods

5.3.1 Animals

Male C57BL/6NHsd mice from Harlan Laboratories (Somerville, NJ) were housed one per cage in the Auburn University Veterinary Research Building, an AAALAC accredited animal facility, in 12:12-h light-dark, temperature at 22°C, and humidity-controlled rooms. Mice were provided with standard laboratory chow and water *ad libitum* in accordance with an Institutional Animal Care and Use Committee approved protocol for 1 wk to allow for acclimatization to the animal facility. No procedures were undertaken that caused more than minimal pain, distress, or discomfort. After the one-week acclimation period, mice (*n*= 8, 6 wk old) remained on the standard chow diet or received a high-fat Western diet (HFWD) (Test Diets, Cat. #5TJN) containing ~12% and 40% energy from fat, respectively, with or without sugar (42 g/L) added to the drinking water at a ratio of 55% fructose/45% sucrose (F/S). The composition of fat in the diets was 30% from lard, 30% from butterfat, and 30% from Crisco. Mice were euthanized by inhalation of CO_2. Liver were excised, weighed, and were immersed in RNAlater (Life Techonologies, Carlsbad, CA) and stored at -80°C until used for RNA extraction. An independent study was also performed using male C57BL/6NHsd mice from Harlan Laboratories (Somerville, NJ) housed three per cage in Thoren units in the Bassett Research Institute, an AAALAC accredited animal facility, in 12:12-h light-dark, temperature at 22°C, and humidity-controlled rooms. Mice were provided with standard laboratory chow and water *ad libitum* in accordance with an Institutional Animal Care and Use Committee approved protocol for 1 wk to allow for acclimatization to the animal facility. No procedures were undertaken that caused more than minimal pain, distress, or discomfort. Mice (*n*= 8, 6 wk old) were then placed for 2 and 12 wk on a low-fat Western diet (LFWD) (Test Diets, Cat. #5TJS) or a high-fat Western diet

(HFWD) (Test Diets, Cat. #5TJN) containing ~12% and 40% energy from fat, respectively. The composition of fat in the diets was 30% from lard, 30% from butterfat, and 30% from Crisco. Sugar (42 g/l) was added to the drinking water at a ratio of 55% fructose/45% sucrose (F/S) to mice on the LFWD and HFWD. Mice were euthanized by inhalation of CO_2. Liver were excised, weighed, and were immersed in RNAlater (Life Techonologies, Carlsbad, CA) and stored at -80°C until used for RNA extraction.

5.3.2 RNA extraction

RNeasy Plus Universal Kits (Qiagen, Valencia, CA) were used to isolate total RNA from frozen liver and adipose tissue following the manufacturer's protocol. RNA quantity and quality were assessed using a bioanalyzer (Agilent 2100 Bioanalyze; Agilent Technologies, Santa Clara, CA).

5.3.3 RNA Sequencing, Data Processing, and Analysis

Methods as previously described (4.3.4)

5.3.4 qPCR

The same RNA used to generate cDNA libraries for RNA-seq was also used to validate RNA-seq by qPCR. Reverse transcription was performed using the RT^2 First Strand Kit (Qiagen, Valencia, CA). qPCR was performed with RT^2 SYBR Green qPCR Mastermix (Qiagen, Valencia, CA) and gene-specific primers (SABiosciences, Fredrick, MD) using MyiQ Real-Time PCR systems (Bio-Rad, Hercules, CA). After amplification, melt curve analysis was performed to confirm the specificity of the reaction. All measurements were performed in triplicate. GAPDH was used as a reference gene to normalize gene expression. The $2^{\wedge-\Delta\Delta CT}$ method was used to analyze the qPCR data and measure relative expression differences [257].

5.3.5 Cell culture and treatment

The mouse hepatocyte cell line AML12 and mouse macrophage cell line RAW264.7 were purchased from the American Type Culture Collection and cultured in DMEM medium (Life Technologies, Grand Island, NY) supplemented with 10% fetal bovine serum (FBS) (Atlanta Biologicals, Flowery Branch, GA) and 1% penicillin-streptomycin solution (Cellgro, Manassas, VA). Cells were maintained at 37° C in a 5% CO_2 atmosphere. For cellular insulin resistance induction, AML12 cells were serum deprived for 12 h in DMEM containing 0.2% BSA, and then treated with 1) TNFα at 10, 20, 50, 100 ng/ml for 16 h; or 2) free fatty acid with palmitate at 0.4 and 0.9 mM for 16h, and then stimulated with insulin for 2 min. For hypoxic incubation, AML12 cells were incubated at 37°C in 95% air and 5% CO_2 or placed in a hypoxic chamber flushed for 10 min with gas mixture consisting of 1% O_2, 5% CO_2, and 94% N_2. Cell lysates were analyzed by immunoblotting.

5.3.6 Macrophage polarization

For induction of M1-polarized TAMs, RAW 264.7 cells were cultured in complete medium with 10% FBS and 10 ng/ml LPS plus 100 IU/ml IFN-γ for 24h. For M2-polarized macrophages, 20 ng/ml IL-4 was used instead of LPS and IFN-γ to stimulate macrophages for 24h. Untreated RAW 264.7 cells were used as controls [283].

5.3.7 Antibodies and immunoblotting

Polyclonal antibodies to Akt and phospho-Akt (Ser^{473}) were from Cell Signaling Technology (Danvers, MA). Goat anti-rabbit and anti-mouse IRDye 650- and IRDye 800-conjugated secondary antibodies were from Li-Cor (Lincoln, NE).

5.3.8 Western blot analysis

Tissue was lysed with 50 mM HEPES, pH 7.5, 150 mM NaCl, 1% Nonidet P-40, 0.1% SDS, 0.1% sodium deoxycholate, 1 mM NA_3VO_4, 100 nM okadaic acid, and 1× protease inhibitor mixture Set I. Cellular debris was removed by centrifugation at 15,000 rpm for 15 min at 4°C. Protein content of the clarified lysate was determined using bicinchoninic acid (BCA) reagents from Thermo Scientific (Rockford, IL). Isolated proteins were denatured in SDS gel buffer, separated by SDS-PAGE, and immunoblotted. Enhanced chemiluminescence substrate was from GE Healthcare (Piscataway, NJ). Goat anti-rabbit and anti-mouse Alexa fluor 635, horseradish peroxidase-conjugated, IRDye680, and IRDye 800 secondary antibodies were used for detection and quantitation of immunoblots. Membranes were imaged using a Storm PhosphoImager (GE Healthcare) or LiCor Odyssey scanner, and blots were analyzed by Image Studio 2.0 analytical software (LiCor, Lincoln, NE).

5.3.9 Statistical analysis

Fluorescent signals were directly quantitated using Image Quant v. 5.1 software. The absolute integration value of the immunoreactive bands minus background was determined. Statistical analysis was performed using GraphPad Prism 6 (La Jolla, CA). The results are presented as means ± SEMs. Statistical significance of gene expression data was analyzed by the Student's *t*-test ($\alpha = 0.05$) compared to control. Statistical significance between groups was determined by one-way analysis of variance ($\alpha = 0.05$) followed by the Newman-Keuls test ($\alpha = 0.05$).

5.4 Results

5.4.1 Hepatic gene expression of ORM in a high fat Western diet model of NAFLD

C57Bl/6N mice aged 6 wk were placed on a chow or HFWD with or without 42g/L F/S in the drinking water for up to 12 wk. The chow fed mice served as the control group. In our recently

published study [242], we have shown that mice fed a HFWD with liquid F/S are more obese, glucose intolerant, insulin resistant and have a significant higher NAFLD score than mice on HFWD only. To obtain a global view of the hepatic transcriptome responses to the consumption of liquid sugar in mice fed a HFWD diet, we performed high-throughput sequencing of liver transcriptomes (data presented in Chapter 2). A gene with approximately 20-fold and 5-fold increases in expression in the HFWD+F/S group compared to chow and HFWD groups, respectively, was the gene ORM3; a gene in the ORM family (Fig.29A). To validate our RNA-seq data on the expression of ORM3, qPCR was performed on hepatic RNA isolated from mice fed the chow, HFWD and HFWD+F/S diets for 12-weeks. Consistent with our RNA-seq data, ORM3 expression was elevated approximately 5-fold in HFWD+F/S fed mice compared to HFWD fed mice (Fig. 29B). In addition, ORM2 but not ORM1 hepatic expression was also significantly elevated approximately 2-fold in HFWD+F/S fed mice compared to HFWD fed mice (Fig. 29, C and D). Further validation of ORM3 hepatic expression in an independent dietary treatment experiment using mice fed a LFWD, HFWD and HFWD+F/S diets for 12-weeks confirmed our RNA-seq findings (Fig. 29E). ORM3 expression was upregulated approximately 5-fold in HFWD+F/S-fed mice compared to HFWD fed mice. ORM1 and ORM2 hepatic expression was significantly elevated to a similar level as ORM3 in HFWD+F/S fed mice compared to HFWD fed mice (Fig. 29, F and G).

5.4.2 Gene expression of ORM and NAFLD progression

In order to evaluate the relationship between the expression level of the ORM3 gene and NAFLD progression, we performed a correlation analysis of ORM3 gene expression with NAFLD parameters examined in our recently published study [242]. As shown in Figure 30,

ORM3 gene expression was significantly positively correlated with body weight (P= 0.02), normalized liver weight (P = 0.02), and alanine aminotransferase (ALT) level (P = 0.01), a marker of liver dysfunction. Moreover, the correlation between ORM1 gene expression and ORM2 gene expression with NAFLD parameters was also assessed. ORM1 gene expression is significantly positively correlated with ALT, while ORM2 gene expression is significantly negatively correlated with fibrosis. Taken together, these data suggest that ORM genes are playing roles in diet-induced NAFLD.

5.4.3 Gene expression of ORM in a cellular model of insulin resistance

We have shown that in mice with more progressive NAFLD, the expression of ORM genes are upregulated in the liver. Also, the correlation analysis with ORM expression and NAFLD parameters suggested that ORM1, ORM2, and ORM3 were playing roles in NAFLD progression. As insulin resistance is a critical parameter in obesity-linked NAFLD progression, we used a cellular model of insulin resistance to confirm and expand our observations *in vivo*. First, we induced insulin resistance in AML12 cells (a mouse hepatocyte cell line) using tumor necrosis factor-alpha (TNFα), free fatty acids (FFAs), a combination of TNFα and hypoxia treatment, and a combination of FFA and hypoxia treatment (Fig. 31, A and B). TNFα and FFA have been widely used to induce insulin resistance in cultured cells [53], while hypoxia treatment has been recently shown to induce insulin resistance in adipocytes [284]. In order to test if these treatments can induce insulin resistance in hepatocytes, cells were serum deprived, treated with TNFα (10, 20, 50, and 100 ng/ml) or FFA with palmitate (0.4 and 0.9 mM) with or without hypoxia treatment for 16 h, and then stimulated with insulin for 2 min. Cell lysates were analyzed by immunoblotting. As shown in Fig. 31, A and B, AKT-Ser^{473} phosphorylation was

significantly increased in AML12 hepatocytes upon insulin stimulation in all treatment groups except FFA 0.9 mM + Hypoxia group; however, insulin stimulated AKT-Ser^{473} phosphorylation was blunted by the addition of hypoxia treatment. Furthermore, insulin failed to stimulate AKT-Ser^{473} phosphorylation in AML12 hepatocytes treated with FFA 0.9 mM and hypoxia. Our data indicated that the addition of hypoxia treatment exacerbated TNFα and FFA-induced cellular insulin resistance. We next examined the expression of ORM genes in a cellular model of insulin resistance induced by TNFα (50 and 100 ng/ml) or FFA with palmitate (0.4 and 0.9 mM) together with hypoxia treatment, as substantial cellular insulin resistance was observed in these combination treatment groups. Consistent with our findings *in vivo*, the expression of ORM3 gene was significantly elevated approximately 33-fold and 67-fold in AML12 treated with FFA 0.9 mM + hypoxia and TNFα 100 ng/ml +hypoxia, respectively (Fig. 31C). In addition, the combination of TNFα or FFA with hypoxia treatment induced gene expression of ORM3 in a dose-dependent manner. Similar results were observed in the expression of ORM1 and ORM2 genes as well (Fig. 31, D and E). Taken together, our results demonstrated that the ORM gene expression of is induced in the cellular model of insulin resistance in a dose-dependent manner.

5.4.4 The role of ORM proteins in the pro-inflammatory state of macrophage

Most acute phase proteins function to promote the inflammatory state while others restrain the inflammatory response [163]. Previous studies, primarily with ORM1, suggest that the ORM proteins function to restrain the inflammatory response [178]. As polarization of macrophages in the liver to the M1 phenotype (pro-inflammatory phenotype) plays a role in the progression of NAFLD, we next investigated the role of ORM proteins in the pro-inflammatory state of macrophages. First, we induced M1 and M2 phenotype polarization by stimulating RAW 264.7

cells (a mouse leukaemic monocyte macrophage cell line) with10 ng/ml lipopolysaccharide (LPS) plus 100 IU/ml IFN-γ and 20 ng/ml IL-4 for 24h, respectively [283]. Untreated cells were used as controls. We observed that the gene expression of M1 markers, including monocyte chemoattractant protein-1 (MCP-1), TNFα, and IL-6, were significantly elevated in the M1 phenotype, while the expression of M2 markers, including arginase-1 (Arg1) and Fizz ,were significantly induced in the M2 phenotype (Fig. 32). Our results indicated that M1 and M2 phenotype polarization were successfully induced in RAW 264.7 macrophages. Next, we pretreated RAW 264.7 macrophages with recombinant ORM proteins (30 and 100 μg/ml) for 24 h and then followed previously described protocols. Treatment of macrophages with recombinant ORM protein increased gene expression of the markers of the M2 phenotype, including Arg1 and Fizz (Fig. 33, A and B). Furthermore, treatment with ORM significantly decreased gene expression of the M1 markers MCP1, TNFα and IL6 (Fig. 33, C, D and E). Taken together, our results indicated that ORM directly promotes an anti-inflammatory phenotype in macrophage *in vitro*.

5.5 Discussion

In the present study, we observed a substantial increase in hepatic gene expression of ORM (ORM1, ORM2, and ORM3) in HFWD+F/S-fed mice, which have been observed to be more obese, glucose intolerant, insulin resistant and have a significant higher NAFLD score than mice fed only a HFWD [242]. In humans, the serum concentration of ORM has been observed to be elevated in obese and diabetic patients and has been suggested to be a biomarker for obesity-induced metabolic disorders and inflammation [200, 285, 286]. In mice, ORM is induced in the adipose tissue of genetically and diet-induced obese mice. Adipocyte ORM expression is up-

regulated in response to metabolic signals, including insulin, high glucose, and FFAs, as well as the pro-inflammatory cytokine TNFα [198]. Treatment or overexpression of ORM suppressed pro-inflammatory gene expression and relieved hyperglycemia-induced insulin resistance in adipocytes, while knockdown of ORM1 promoted both basal and TNFα-induced expression pro-inflammatory genes and disrupted insulin-stimulated glucose uptake. Hence, ORM appears to integrate inflammatory and metabolic signals to protect adipose tissue from severe inflammation and metabolic dysfunction [198]. Our observation that hepatocyte gene expression of ORM isoforms were significantly elevated in response to TNFα and FFAs together with hypoxia treatment in a dose-dependent manner in our current study, suggest that ORM isoforms may have a similar protective effect in the liver.

Macrophages are broadly classified as: 1) M1 macrophages which secrete pro-inflammatory cytokines: TNFα, IL-6 and IL-1β and tend to mediate chronic inflammation and 2) M2 macrophages that secrete the anti-inflammatory cytokine IL-10 and tend to resolve inflammation [287]. Polarization of macrophages in the liver to the M1 phenotype plays a role in hepatic insulin resistance [288] and progression of NAFLD. In the present study, ORM was observed to promote macrophage polarization toward an anti-inflammatory phenotype, which is consistent with previous findings [192]. The M2 macrophage inducing activity is considered one of the typical immunosuppressive activities of ORM [192]. In humans, the immune complex, TLR agonists, and CCL2 are known to be involved in the generation of M2 macrophages. Since ORM binds directly to macrophages using CCL5 and siglect5 [289, 290], ORM may directly stimulate monocyte conversion to M2 monocyte, but further studies will be needed to resolve this mechanism.

In summary, RNA-seq analysis of a high fat Western diet model of NAFLD revealed hepatic expression of ORM3 gene was significantly elevated by 20-fold. Further validation of ORM3 hepatic expression in an independent dietary treatment experiment confirmed our RNA-seq findings, and found ORM1 and ORM2 hepatic expression was significantly elevated to a similar level as ORM3. Correlation analysis of ORM3 gene expression with NAFLD parameters examined in our recently published study indicated that ORM3 gene expression was significantly positively correlated with body weight, normalized liver weight, and alanine aminotransferase, a marker of liver dysfunction. Moreover, the expression of ORM was also induced in a cellular model of insulin resistance. Furthermore, ORM was observed to promote macrophage polarization toward an anti-inflammatory phenotype. Taken together, we suggest that ORM might have a protective role in NAFLD by regulate cellular insulin resistance and pro-inflammatory macrophages.

Figures and figure legends

Figure 29

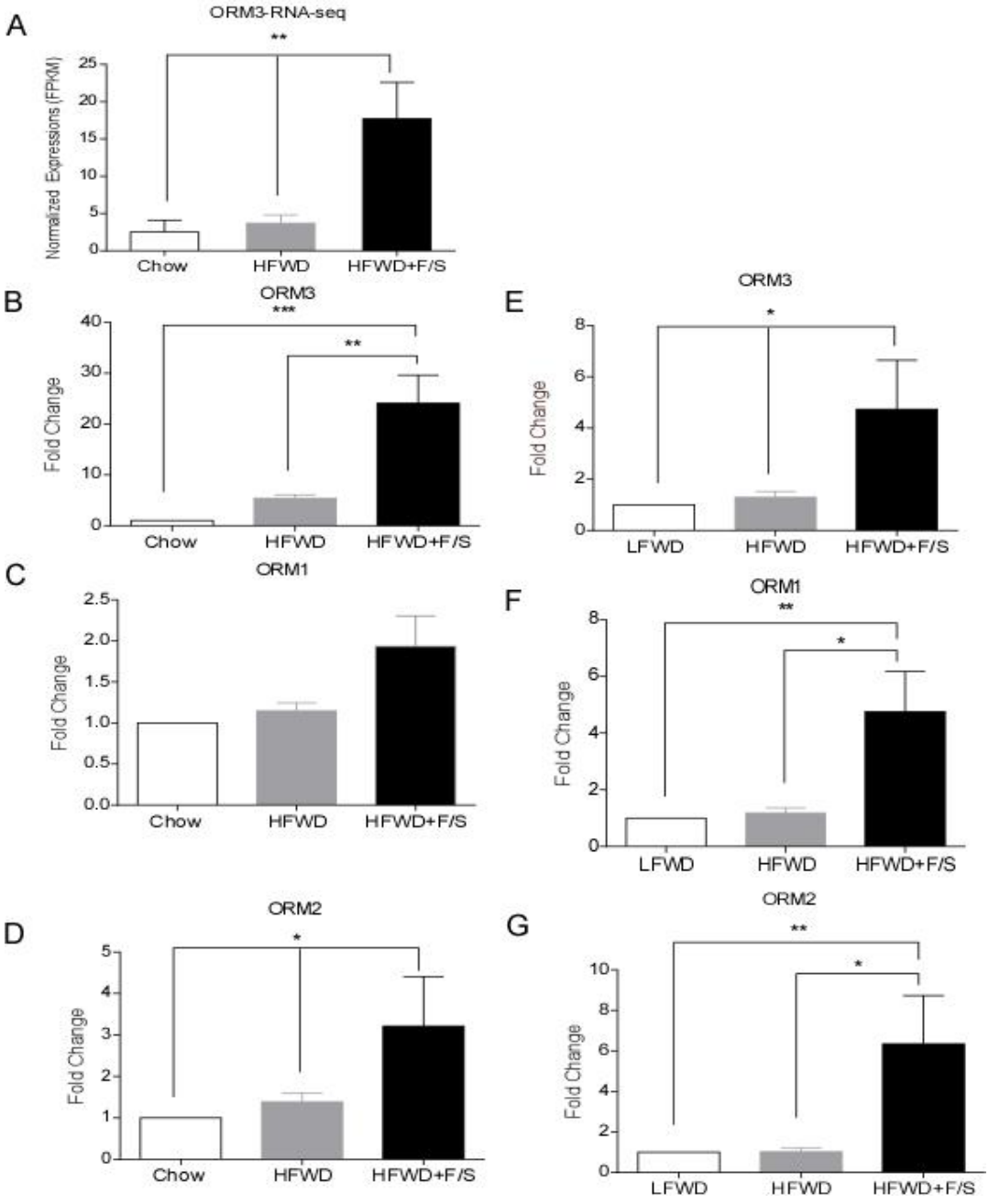

Fig 29 ORM expression in a high fat Western diet model of NAFLD. (A) Fold change in ORM3 gene expression assessed by RNA-seq using liver RNA isolated from mice fed chow, HFWD, or HFWD+F/S for 12 weeks. qPCR validation of ORM3(B), ORM1 (C) and ORM2 (D) mRNA expression. qPCR analysis of ORM3(E), ORM1(F), and ORM2(G) hepatic gene expression in an independent study of 12 week LFWD, HFWD, and HFWD+F/S fed mice. Data are expressed as means ± SE, n=8 per group. $*P < 0.05$; $**P < 0.01$, $***P < 0.001$.

Figure 30

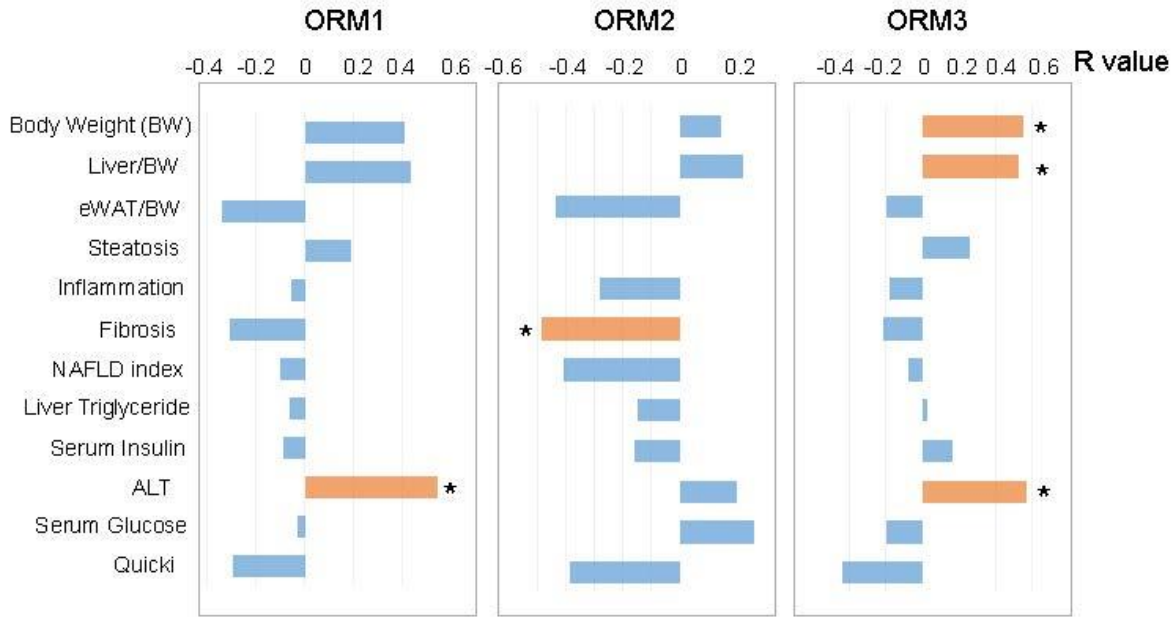

Fig. 30 NAFLD correlation analysis. The correlation of NAFLD parameters was examined in comparison to ORM mRNA expression determined by qPCR. Spearman correlation coefficients (R) are shown. Significant positive (R>1) and negative (R<1) correlations are shown using orange bars and denoted with a * (P <0.05). NALFD parameters were determined in LFWD, HFWD, and HFWD+F/S fed mice.

Figure 31

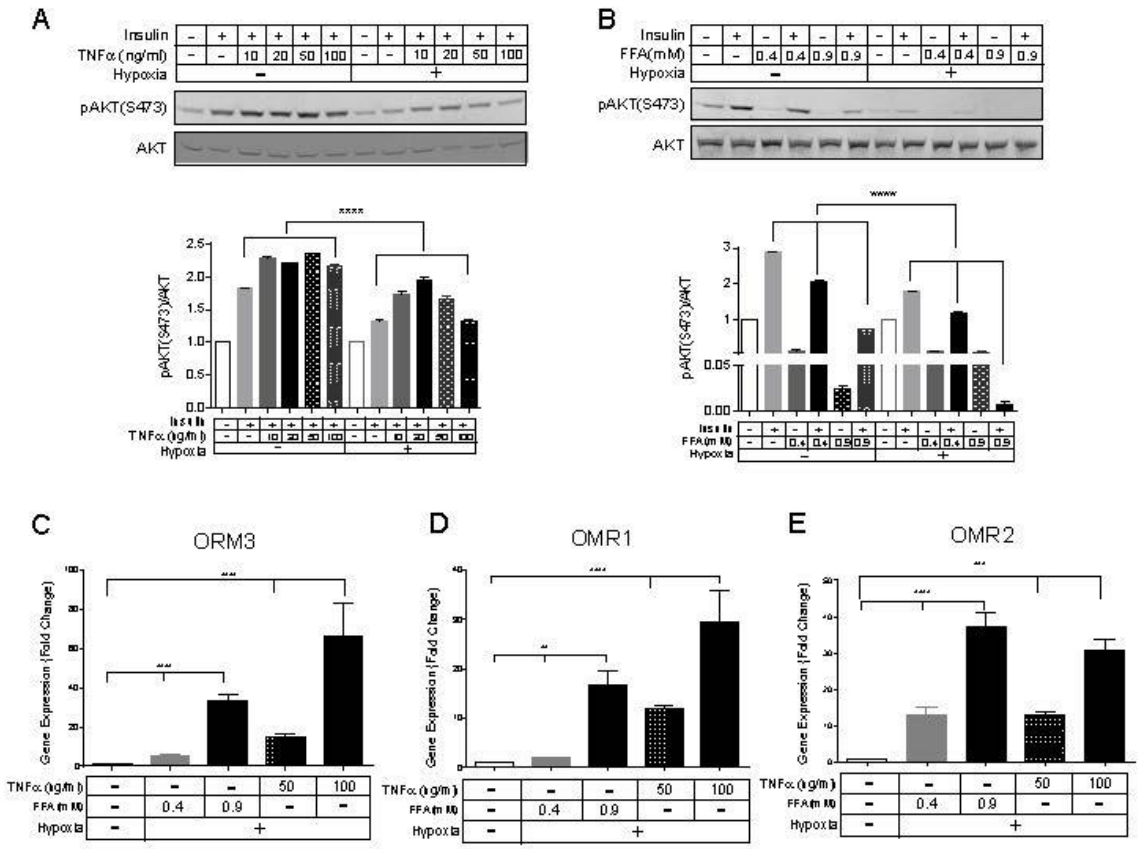

Fig. 31 Gene expression of ORM in cellular model of insulin resistance. (A) Insulin stimulated AKT-Ser^{473} phosphorylation and total AKT representative blots (*upper panel*) and means ± SE (*bottom panel*) in hepatocytes treated with TNFα with or without hypoxia treatment. (B) Insulin stimulated AKT-Ser^{473} phosphorylation and total AKT representative blots (*upper panel*) and means ± SE (*bottom panel*) in hepatocytes treated with FFA with or without hypoxia treatment. Fold change in ORM3(C), ORM1(D), and ORM2(E) gene expression assessed by qPCR in a cellular model of insulin resistance. Data are expressed as means ± SE. $^{**}P$ <0.01, $^{***}P$ <0.001, $^{****}P$ <0.0001.

Figure 32

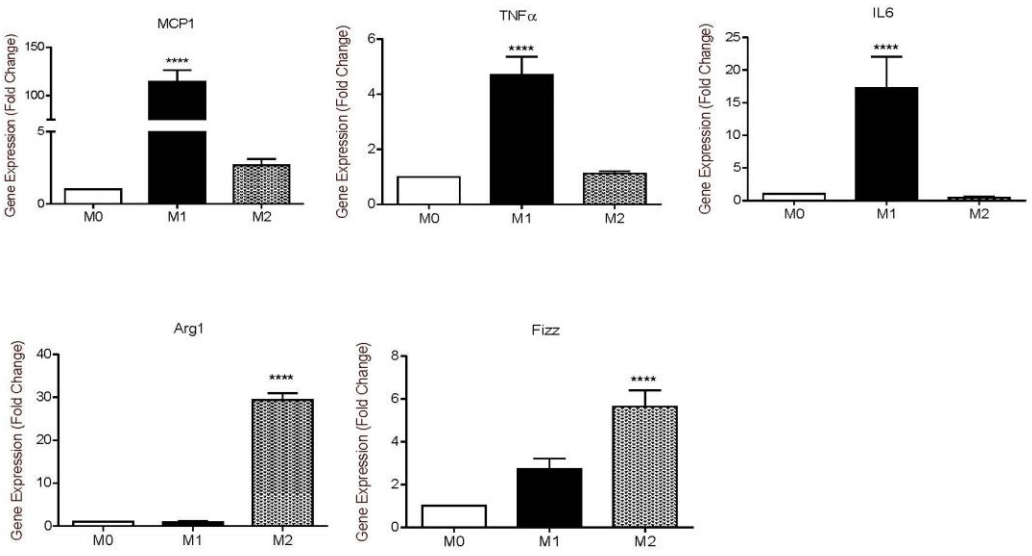

Fig. 32 Fold changes in gene expression of M1 and M2 phenotype markers assessed by qPCR in polarized macrophages relative to control group. Data are expressed as means ± SE. ****P <0.0001.

Figure 33

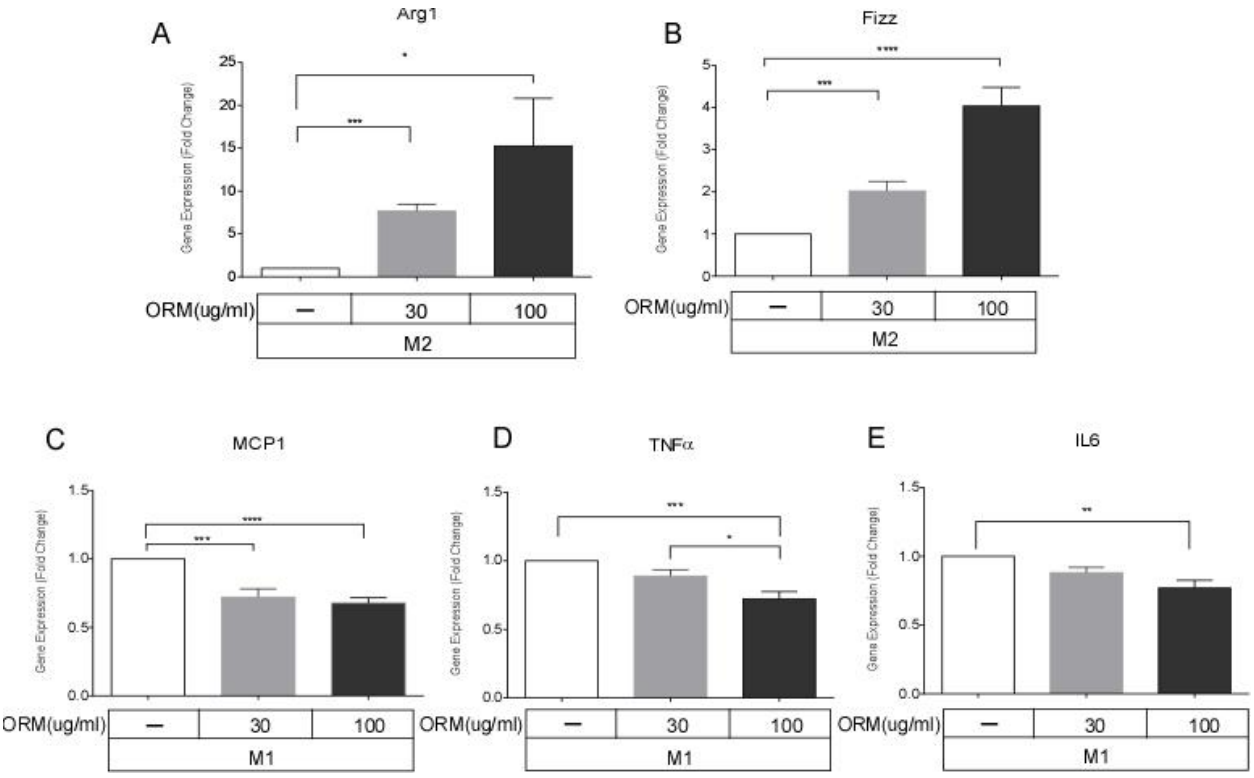

Fig. 33 Fold changes in gene expression of M1 phenotype markers (C, D and E) and M2 phenotype markers (A and B) assessed by qPCR in ORM recombinant protein treated-polarized macrophages relative to the control group. Data are expressed as means ± SE. **P* < 0.05; ***P* <0.01, ****P* <0.001, *****P* <0.0001.

Chapter 6: Summary and conclusion

The high fat Western diet (HFWD) with liquid fructose/sucrose (F/S) model of obesity in mice was originally developed as a model of NAFLD progression. We used this model to investigate the role of liquid sugar in the progression of NAFLD. In our study, liquid sugar induced acute hyperphagia in HFWD-fed mice, yet without changes in energy expenditure. Liquid sugar (F/S) exacerbated HFWD-induced glucose intolerance and insulin resistance and impaired the storage capacity of epididymal white adipose tissue (eWAT). Hepatic TG, plasma alanine aminotransferase, and normalized liver weight were significantly increased only in HFWD+F/S-fed mice. HFWD+F/S also resulted in increased hepatic fibrosis and elevated collagen 1a2, collagen 3a1, and TGFβ gene expression. Furthermore, HWFD+F/S-fed mice developed more profound eWAT inflammation characterized by adipocyte hypertrophy, macrophage infiltration, a dramatic increase in crown-like structures, and upregulated proinflammatory gene expression. An early hypoxia response in the eWAT led to reduced vascularization and increased fibrosis gene expression in the HFWD+F/S-fed mice.

RNA-seq analysis of the high fat Western diet model of NAFLD revealed 760 DEGs in the liver of HFWD+F/S-fed mice, which are mainly enriched in small GTPase mediated signal transduction, and lipid homeostasis biological processes. Further, pathway analysis showed pathways in immune response, fibrosis and cancer are major pathways enriched in the livers of HFWD+F/S-fed mice.

Furthermore, hepatic expression of ORM3 gene was significantly elevated by 20-fold in HFWD+F/S-fed mice through RNA-seq analysis. Further validation of ORM3 hepatic expression in an independent dietary treatment experiment confirmed our RNA-seq findings, and found ORM1 and ORM2 hepatic expression was significantly elevated to a similar level as ORM3 in HFWD+F/S group. Correlation analysis of ORM3 gene expression with NAFLD parameters indicated that ORM3 gene expression was significantly positively correlated with body weight, normalized liver weight, and alanine aminotransferase, a marker of liver dysfunction. Moreover, the gene expression of ORM was also induced in cellular model of insulin resistance. Furthermore, ORM was observed to promote macrophage polarization toward an anti-inflammatory phenotype. Taken together, our results emphasized the importance of liquid sugar in the progression of NAFLD and highlighted key genes, biological processes and pathway changes through which the addition of liquid sugar may promote the progression of NAFLD.

References

[1] Prevention CfDCa. National Diabetes Statistics Report: Estimates of Diabetes and Its Burden in the United States, 2014. Atlanta, GA: US Department of Health and Human Services; 2014.

[2] Williams CD, Stengel J, Asike MI, Torres DM, Shaw J, Contreras M, et al. Prevalence of nonalcoholic fatty liver disease and nonalcoholic steatohepatitis among a largely middle-aged population utilizing ultrasound and liver biopsy: a prospective study. Gastroenterology 2011;140:124-131.

[3] Levi J, Segal L, St. Laurent R, Lang A, Rayburn J. F as in Fat: How Obesity Threatens America's Future 2012: Trust for America's Health and the Robert Wood Johnson Foundation; 2012.

[4] Corrado RL, Torres DM, Harrison SA. Review of treatment options for nonalcoholic fatty liver disease. The Medical clinics of North America 2014;98:55-72.

[5] Jou J, Choi SS, Diehl AM. Mechanisms of disease progression in nonalcoholic fatty liver disease. Seminars in liver disease 2008;28:370-379.

[6] Tiniakos DG. Nonalcoholic fatty liver disease/nonalcoholic steatohepatitis: histological diagnostic criteria and scoring systems. European journal of gastroenterology & hepatology 2010;22:643-650.

[7] Teli MR, James OF, Burt AD, Bennett MK, Day CP. The natural history of nonalcoholic fatty liver: a follow-up study. Hepatology 1995;22:1714-1719.

[8] Day CP, James OF. Steatohepatitis: a tale of two "hits"? Gastroenterology 1998;114:842-845.

[9] Rinella ME, Elias MS, Smolak RR, Fu T, Borensztajn J, Green RM. Mechanisms of hepatic steatosis in mice fed a lipogenic methionine choline-deficient diet. Journal of lipid research 2008;49:1068-1076.

[10] Neuschwander-Tetri BA. Hepatic lipotoxicity and the pathogenesis of nonalcoholic steatohepatitis: the central role of nontriglyceride fatty acid metabolites. Hepatology 2010;52:774-788.

[11] Larter CZ, Chitturi S, Heydet D, Farrell GC. A fresh look at NASH pathogenesis. Part 1: the metabolic movers. Journal of gastroenterology and hepatology 2010;25:672-690.

[12] Samuel VT, Shulman GI. Mechanisms for insulin resistance: common threads and missing links. Cell 2012;148:852-871.

[13] Kleemann R, van Erk M, Verschuren L, van den Hoek AM, Koek M, Wielinga PY, et al. Time-resolved and tissue-specific systems analysis of the pathogenesis of insulin resistance. PloS one 2010;5:e8817.

[14] Schattenberg JM, Galle PR. Animal models of non-alcoholic steatohepatitis: of mice and man. Digestive diseases 2010;28:247-254.

[15] Kohli R, Kirby M, Xanthakos SA, Softic S, Feldstein AE, Saxena V, et al. High-fructose, medium chain trans fat diet induces liver fibrosis and elevates plasma coenzyme Q9 in a novel murine model of obesity and nonalcoholic steatohepatitis. Hepatology 2010;52:934-944.

[16] Tetri LH, Basaranoglu M, Brunt EM, Yerian LM, Neuschwander-Tetri BA. Severe NAFLD with hepatic necroinflammatory changes in mice fed trans fats and a high-fructose corn

syrup equivalent. American journal of physiology Gastrointestinal and liver physiology 2008;295:G987-995.

[17] Charlton M, Krishnan A, Viker K, Sanderson S, Cazanave S, McConico A, et al. Fast food diet mouse: novel small animal model of NASH with ballooning, progressive fibrosis, and high physiological fidelity to the human condition. American journal of physiology Gastrointestinal and liver physiology 2011;301:G825-834.

[18] Machado MV, Michelotti GA, Xie G, de Almeida TP, Boursier J, Bohnic B, et al. Mouse models of diet-induced nonalcoholic steatohepatitis reproduce the heterogeneity of the human disease. PloS one 2015;10:e0127991.

[19] Anderson EL, Howe LD, Jones HE, Higgins JP, Lawlor DA, Fraser A. The Prevalence of Non-Alcoholic Fatty Liver Disease in Children and Adolescents: A Systematic Review and Meta-Analysis. PloS one 2015;10:e0140908.

[20] Chalasani N, Younossi Z, Lavine JE, Diehl AM, Brunt EM, Cusi K, et al. The diagnosis and management of non-alcoholic fatty liver disease: practice guideline by the American Gastroenterological Association, American Association for the Study of Liver Diseases, and American College of Gastroenterology. Gastroenterology 2012;142:1592-1609.

[21] Dowman JK, Tomlinson JW, Newsome PN. Pathogenesis of non-alcoholic fatty liver disease. QJM : monthly journal of the Association of Physicians 2010;103:71-83.

[22] Angulo P. Long-term mortality in nonalcoholic fatty liver disease: is liver histology of any prognostic significance? Hepatology 2010;51:373-375.

[23] Byrne CD, Targher G. NAFLD: a multisystem disease. Journal of hepatology 2015;62:S47-64.

[24] Brea A, Puzo J. Non-alcoholic fatty liver disease and cardiovascular risk. International journal of cardiology 2013;167:1109-1117.

[25] Hardy T, Oakley F, Anstee QM, Day CP. Nonalcoholic Fatty Liver Disease: Pathogenesis and Disease Spectrum. Annual review of pathology 2016;11:451-496.

[26] Younossi ZM, Koenig AB, Abdelatif D, Fazel Y, Henry L, Wymer M. Global epidemiology of nonalcoholic fatty liver disease-Meta-analytic assessment of prevalence, incidence, and outcomes. Hepatology 2016;64:73-84.

[27] Lazo M, Hernaez R, Eberhardt MS, Bonekamp S, Kamel I, Guallar E, et al. Prevalence of nonalcoholic fatty liver disease in the United States: the Third National Health and Nutrition Examination Survey, 1988-1994. American journal of epidemiology 2013;178:38-45.

[28] Pan JJ, Fallon MB. Gender and racial differences in nonalcoholic fatty liver disease. World journal of hepatology 2014;6:274-283.

[29] Vernon G, Baranova A, Younossi ZM. Systematic review: the epidemiology and natural history of non-alcoholic fatty liver disease and non-alcoholic steatohepatitis in adults. Alimentary pharmacology & therapeutics 2011;34:274-285.

[30] Ogden CL, Carroll MD, Kit BK, Flegal KM. Prevalence of obesity and trends in body mass index among US children and adolescents, 1999-2010. Jama 2012;307:483-490.

[31] Mishra A, Younossi ZM. Epidemiology and Natural History of Non-alcoholic Fatty Liver Disease. Journal of clinical and experimental hepatology 2012;2:135-144.

[32] Ong JP, Pitts A, Younossi ZM. Increased overall mortality and liver-related mortality in non-alcoholic fatty liver disease. Journal of hepatology 2008;49:608-612.

[33] Adams LA, Lymp JF, St Sauver J, Sanderson SO, Lindor KD, Feldstein A, et al. The natural history of nonalcoholic fatty liver disease: a population-based cohort study. Gastroenterology 2005;129:113-121.

[34] Soderberg C, Stal P, Askling J, Glaumann H, Lindberg G, Marmur J, et al. Decreased survival of subjects with elevated liver function tests during a 28-year follow-up. Hepatology 2010;51:595-602.

[35] Musso G, Gambino R, Cassader M, Pagano G. Meta-analysis: natural history of non-alcoholic fatty liver disease (NAFLD) and diagnostic accuracy of non-invasive tests for liver disease severity. Annals of medicine 2011;43:617-649.

[36] Day CP. From fat to inflammation. Gastroenterology 2006;130:207-210.

[37] Samuel VT, Petersen KF, Shulman GI. Lipid-induced insulin resistance: unravelling the mechanism. Lancet 2010;375:2267-2277.

[38] Yamaguchi K, Yang L, McCall S, Huang J, Yu XX, Pandey SK, et al. Inhibiting triglyceride synthesis improves hepatic steatosis but exacerbates liver damage and fibrosis in obese mice with nonalcoholic steatohepatitis. Hepatology 2007;45:1366-1374.

[39] Feldstein AE, Werneburg NW, Canbay A, Guicciardi ME, Bronk SF, Rydzewski R, et al. Free fatty acids promote hepatic lipotoxicity by stimulating TNF-alpha expression via a lysosomal pathway. Hepatology 2004;40:185-194.

[40] Donnelly KL, Smith CI, Schwarzenberg SJ, Jessurun J, Boldt MD, Parks EJ. Sources of fatty acids stored in liver and secreted via lipoproteins in patients with nonalcoholic fatty liver disease. The Journal of clinical investigation 2005;115:1343-1351.

[41] Parks EJ. Dietary carbohydrate's effects on lipogenesis and the relationship of lipogenesis to blood insulin and glucose concentrations. The British journal of nutrition 2002;87 Suppl 2:S247-253.

[42] Iqbal J, Hussain MM. Intestinal lipid absorption. American journal of physiology Endocrinology and metabolism 2009;296:E1183-1194.

[43] Hubbard B, Doege H, Punreddy S, Wu H, Huang X, Kaushik VK, et al. Mice deleted for fatty acid transport protein 5 have defective bile acid conjugation and are protected from obesity. Gastroenterology 2006;130:1259-1269.

[44] Sanders FW, Griffin JL. De novo lipogenesis in the liver in health and disease: more than just a shunting yard for glucose. Biological reviews of the Cambridge Philosophical Society 2016;91:452-468.

[45] Zelcer N, Tontonoz P. Liver X receptors as integrators of metabolic and inflammatory signaling. The Journal of clinical investigation 2006;116:607-614.

[46] Ducheix S, Montagner A, Theodorou V, Ferrier L, Guillou H. The liver X receptor: a master regulator of the gut-liver axis and a target for non alcoholic fatty liver disease. Biochemical pharmacology 2013;86:96-105.

[47] Nguyen P, Leray V, Diez M, Serisier S, Le Bloc'h J, Siliart B, et al. Liver lipid metabolism. Journal of animal physiology and animal nutrition 2008;92:272-283.

[48] Postic C, Girard J. Contribution of de novo fatty acid synthesis to hepatic steatosis and insulin resistance: lessons from genetically engineered mice. The Journal of clinical investigation 2008;118:829-838.

[49] Lewis GF, Carpentier A, Adeli K, Giacca A. Disordered fat storage and mobilization in the pathogenesis of insulin resistance and type 2 diabetes. Endocrine reviews 2002;23:201-229.

[50] Samuel VT, Liu ZX, Wang A, Beddow SA, Geisler JG, Kahn M, et al. Inhibition of protein kinase Cepsilon prevents hepatic insulin resistance in nonalcoholic fatty liver disease. The Journal of clinical investigation 2007;117:739-745.

[51] Kumashiro N, Erion DM, Zhang D, Kahn M, Beddow SA, Chu X, et al. Cellular mechanism of insulin resistance in nonalcoholic fatty liver disease. Proceedings of the National Academy of Sciences of the United States of America 2011;108:16381-16385.

[52] Bezy O, Tran TT, Pihlajamaki J, Suzuki R, Emanuelli B, Winnay J, et al. PKCdelta regulates hepatic insulin sensitivity and hepatosteatosis in mice and humans. The Journal of clinical investigation 2011;121:2504-2517.

[53] Greene MW, Burrington CM, Luo Y, Ruhoff MS, Lynch DT, Chaithongdi N. PKCdelta is activated in the liver of obese Zucker rats and mediates diet-induced whole body insulin resistance and hepatocyte cellular insulin resistance. The Journal of nutritional biochemistry 2014;25:281-288.

[54] Frangioudakis G, Burchfield JG, Narasimhan S, Cooney GJ, Leitges M, Biden TJ, et al. Diverse roles for protein kinase C delta and protein kinase C epsilon in the generation of high-fat-diet-induced glucose intolerance in mice: regulation of lipogenesis by protein kinase C delta. Diabetologia 2009;52:2616-2620.

[55] Tchoukalova YD, Votruba SB, Tchkonia T, Giorgadze N, Kirkland JL, Jensen MD. Regional differences in cellular mechanisms of adipose tissue gain with overfeeding. Proceedings of the National Academy of Sciences of the United States of America 2010;107:18226-18231.

[56] Than NN, Newsome PN. A concise review of non-alcoholic fatty liver disease. Atherosclerosis 2015;239:192-202.

[57] Hardy OT, Czech MP, Corvera S. What causes the insulin resistance underlying obesity? Current opinion in endocrinology, diabetes, and obesity 2012;19:81-87.

[58] Arrese M, Cabrera D, Kalergis AM, Feldstein AE. Innate Immunity and Inflammation in NAFLD/NASH. Digestive diseases and sciences 2016;61:1294-1303.

[59] Bruun JM, Lihn AS, Pedersen SB, Richelsen B. Monocyte chemoattractant protein-1 release is higher in visceral than subcutaneous human adipose tissue (AT): implication of macrophages resident in the AT. The Journal of clinical endocrinology and metabolism 2005;90:2282-2289.

[60] Kadowaki T, Yamauchi T, Kubota N, Hara K, Ueki K, Tobe K. Adiponectin and adiponectin receptors in insulin resistance, diabetes, and the metabolic syndrome. The Journal of clinical investigation 2006;116:1784-1792.

[61] Pagano C, Soardo G, Esposito W, Fallo F, Basan L, Donnini D, et al. Plasma adiponectin is decreased in nonalcoholic fatty liver disease. European journal of endocrinology / European Federation of Endocrine Societies 2005;152:113-118.

[62] Xu A, Wang Y, Keshaw H, Xu LY, Lam KS, Cooper GJ. The fat-derived hormone adiponectin alleviates alcoholic and nonalcoholic fatty liver diseases in mice. The Journal of clinical investigation 2003;112:91-100.

[63] Lee YS, Li P, Huh JY, Hwang IJ, Lu M, Kim JI, et al. Inflammation is necessary for long-term but not short-term high-fat diet-induced insulin resistance. Diabetes 2011;60:2474-2483.

[64] Chavez JA, Summers SA. A ceramide-centric view of insulin resistance. Cell metabolism 2012;15:585-594.

[65] Li ZZ, Berk M, McIntyre TM, Feldstein AE. Hepatic lipid partitioning and liver damage in nonalcoholic fatty liver disease: role of stearoyl-CoA desaturase. The Journal of biological chemistry 2009;284:5637-5644.

[66] Alkhouri N, Dixon LJ, Feldstein AE. Lipotoxicity in nonalcoholic fatty liver disease: not all lipids are created equal. Expert review of gastroenterology & hepatology 2009;3:445-451.

[67] Mari M, Caballero F, Colell A, Morales A, Caballeria J, Fernandez A, et al. Mitochondrial free cholesterol loading sensitizes to TNF- and Fas-mediated steatohepatitis. Cell metabolism 2006;4:185-198.

[68] Caballero F, Fernandez A, De Lacy AM, Fernandez-Checa JC, Caballeria J, Garcia-Ruiz C. Enhanced free cholesterol, SREBP-2 and StAR expression in human NASH. Journal of hepatology 2009;50:789-796.

[69] Buzzetti E, Pinzani M, Tsochatzis EA. The multiple-hit pathogenesis of non-alcoholic fatty liver disease (NAFLD). Metabolism: clinical and experimental 2016;65:1038-1048.

[70] Schattenberg JM, Singh R, Wang Y, Lefkowitch JH, Rigoli RM, Scherer PE, et al. JNK1 but not JNK2 promotes the development of steatohepatitis in mice. Hepatology 2006;43:163-172.

[71] Cai D, Yuan M, Frantz DF, Melendez PA, Hansen L, Lee J, et al. Local and systemic insulin resistance resulting from hepatic activation of IKK-beta and NF-kappaB. Nature medicine 2005;11:183-190.

[72] Perez-Carreras M, Del Hoyo P, Martin MA, Rubio JC, Martin A, Castellano G, et al. Defective hepatic mitochondrial respiratory chain in patients with nonalcoholic steatohepatitis. Hepatology 2003;38:999-1007.

[73] Pagliassotti MJ. Endoplasmic reticulum stress in nonalcoholic fatty liver disease. Annual review of nutrition 2012;32:17-33.

[74] Wei Y, Wang D, Pagliassotti MJ. Saturated fatty acid-mediated endoplasmic reticulum stress and apoptosis are augmented by trans-10, cis-12-conjugated linoleic acid in liver cells. Molecular and cellular biochemistry 2007;303:105-113.

[75] Cani PD, Amar J, Iglesias MA, Poggi M, Knauf C, Bastelica D, et al. Metabolic endotoxemia initiates obesity and insulin resistance. Diabetes 2007;56:1761-1772.

[76] Rivera CA, Adegboyega P, van Rooijen N, Tagalicud A, Allman M, Wallace M. Toll-like receptor-4 signaling and Kupffer cells play pivotal roles in the pathogenesis of non-alcoholic steatohepatitis. Journal of hepatology 2007;47:571-579.

[77] Wree A, Broderick L, Canbay A, Hoffman HM, Feldstein AE. From NAFLD to NASH to cirrhosis-new insights into disease mechanisms. Nature reviews Gastroenterology & hepatology 2013;10:627-636.

[78] Malhi H, Barreyro FJ, Isomoto H, Bronk SF, Gores GJ. Free fatty acids sensitise hepatocytes to TRAIL mediated cytotoxicity. Gut 2007;56:1124-1131.

[79] Feldstein AE, Canbay A, Angulo P, Taniai M, Burgart LJ, Lindor KD, et al. Hepatocyte apoptosis and fas expression are prominent features of human nonalcoholic steatohepatitis. Gastroenterology 2003;125:437-443.

[80] Crespo J, Cayon A, Fernandez-Gil P, Hernandez-Guerra M, Mayorga M, Dominguez-Diez A, et al. Gene expression of tumor necrosis factor alpha and TNF-receptors, p55 and p75, in nonalcoholic steatohepatitis patients. Hepatology 2001;34:1158-1163.

[81] Li Z, Berk M, McIntyre TM, Gores GJ, Feldstein AE. The lysosomal-mitochondrial axis in free fatty acid-induced hepatic lipotoxicity. Hepatology 2008;47:1495-1503.

[82] Malhi H, Guicciardi ME, Gores GJ. Hepatocyte death: a clear and present danger. Physiological reviews 2010;90:1165-1194.

[83] Szabo G, Petrasek J. Inflammasome activation and function in liver disease. Nature reviews Gastroenterology & hepatology 2015;12:387-400.

[84] Carpino G, Renzi A, Onori P, Gaudio E. Role of hepatic progenitor cells in nonalcoholic fatty liver disease development: cellular cross-talks and molecular networks. International journal of molecular sciences 2013;14:20112-20130.

[85] Leclercq IA, Farrell GC, Schriemer R, Robertson GR. Leptin is essential for the hepatic fibrogenic response to chronic liver injury. Journal of hepatology 2002;37:206-213.

[86] Ding X, Saxena NK, Lin S, Xu A, Srinivasan S, Anania FA. The roles of leptin and adiponectin: a novel paradigm in adipocytokine regulation of liver fibrosis and stellate cell biology. The American journal of pathology 2005;166:1655-1669.

[87] Wang J, Leclercq I, Brymora JM, Xu N, Ramezani-Moghadam M, London RM, et al. Kupffer cells mediate leptin-induced liver fibrosis. Gastroenterology 2009;137:713-723.

[88] Tilg H, Moschen AR. Evolution of inflammation in nonalcoholic fatty liver disease: the multiple parallel hits hypothesis. Hepatology 2010;52:1836-1846.

[89] Weltman MD, Farrell GC, Liddle C. Increased hepatocyte CYP2E1 expression in a rat nutritional model of hepatic steatosis with inflammation. Gastroenterology 1996;111:1645-1653.

[90] Yao ZM, Vance DE. Reduction in VLDL, but not HDL, in plasma of rats deficient in choline. Biochemistry and cell biology = Biochimie et biologie cellulaire 1990;68:552-558.

[91] Larter CZ, Yeh MM, Williams J, Bell-Anderson KS, Farrell GC. MCD-induced steatohepatitis is associated with hepatic adiponectin resistance and adipogenic transformation of hepatocytes. Journal of hepatology 2008;49:407-416.

[92] Hebbard L, George J. Animal models of nonalcoholic fatty liver disease. Nature reviews Gastroenterology & hepatology 2011;8:35-44.

[93] Zhang J, Burrington CM, Davenport SK, Johnson AK, Horsman MJ, Chowdhry S, et al. PKCdelta regulates hepatic triglyceride accumulation and insulin signaling in Lepr(db/db) mice. Biochemical and biophysical research communications 2014;450:1619-1625.

[94] Bray GA, Paeratakul S, Popkin BM. Dietary fat and obesity: a review of animal, clinical and epidemiological studies. Physiology & behavior 2004;83:549-555.

[95] Buettner R, Scholmerich J, Bollheimer LC. High-fat diets: modeling the metabolic disorders of human obesity in rodents. Obesity 2007;15:798-808.

[96] Kanuri G, Bergheim I. In vitro and in vivo models of non-alcoholic fatty liver disease (NAFLD). International journal of molecular sciences 2013;14:11963-11980.

[97] Hill-Baskin AE, Markiewski MM, Buchner DA, Shao H, DeSantis D, Hsiao G, et al. Diet-induced hepatocellular carcinoma in genetically predisposed mice. Human molecular genetics 2009;18:2975-2988.

[98] Ito M, Suzuki J, Sasaki M, Watanabe K, Tsujioka S, Takahashi Y, et al. Development of nonalcoholic steatohepatitis model through combination of high-fat diet and tetracycline with morbid obesity in mice. Hepatology research : the official journal of the Japan Society of Hepatology 2006;34:92-98.

[99] Ito M, Suzuki J, Tsujioka S, Sasaki M, Gomori A, Shirakura T, et al. Longitudinal analysis of murine steatohepatitis model induced by chronic exposure to high-fat diet. Hepatology research : the official journal of the Japan Society of Hepatology 2007;37:50-57.

[100] Tsukamoto H, French SW, Benson N, Delgado G, Rao GA, Larkin EC, et al. Severe and progressive steatosis and focal necrosis in rat liver induced by continuous intragastric infusion of ethanol and low fat diet. Hepatology 1985;5:224-232.

[101] Deng QG, She H, Cheng JH, French SW, Koop DR, Xiong S, et al. Steatohepatitis induced by intragastric overfeeding in mice. Hepatology 2005;42:905-914.

[102] Leamy AK, Egnatchik RA, Young JD. Molecular mechanisms and the role of saturated fatty acids in the progression of non-alcoholic fatty liver disease. Progress in lipid research 2013;52:165-174.

[103] Yasutake K, Kohjima M, Kotoh K, Nakashima M, Nakamuta M, Enjoji M. Dietary habits and behaviors associated with nonalcoholic fatty liver disease. World journal of gastroenterology 2014;20:1756-1767.

[104] Machado RM, Stefano JT, Oliveira CP, Mello ES, Ferreira FD, Nunes VS, et al. Intake of trans fatty acids causes nonalcoholic steatohepatitis and reduces adipose tissue fat content. The Journal of nutrition 2010;140:1127-1132.

[105] Obara N, Fukushima K, Ueno Y, Wakui Y, Kimura O, Tamai K, et al. Possible involvement and the mechanisms of excess trans-fatty acid consumption in severe NAFLD in mice. Journal of hepatology 2010;53:326-334.

[106] Estadella D, da Penha Oller do Nascimento CM, Oyama LM, Ribeiro EB, Damaso AR, de Piano A. Lipotoxicity: effects of dietary saturated and transfatty acids. Mediators of inflammation 2013;2013:137579.

[107] Lottenberg AM, Afonso Mda S, Lavrador MS, Machado RM, Nakandakare ER. The role of dietary fatty acids in the pathology of metabolic syndrome. The Journal of nutritional biochemistry 2012;23:1027-1040.

[108] Assy N, Nassar F, Nasser G, Grosovski M. Olive oil consumption and non-alcoholic fatty liver disease. World journal of gastroenterology 2009;15:1809-1815.

[109] Zivkovic AM, German JB, Sanyal AJ. Comparative review of diets for the metabolic syndrome: implications for nonalcoholic fatty liver disease. The American journal of clinical nutrition 2007;86:285-300.

[110] Paniagua JA, de la Sacristana AG, Sanchez E, Romero I, Vidal-Puig A, Berral FJ, et al. A MUFA-rich diet improves posprandial glucose, lipid and GLP-1 responses in insulin-resistant subjects. Journal of the American College of Nutrition 2007;26:434-444.

[111] Ryan MC, Itsiopoulos C, Thodis T, Ward G, Trost N, Hofferberth S, et al. The Mediterranean diet improves hepatic steatosis and insulin sensitivity in individuals with non-alcoholic fatty liver disease. Journal of hepatology 2013;59:138-143.

[112] Lee JY, Moon JH, Park JS, Lee BW, Kang ES, Ahn CW, et al. Dietary oleate has beneficial effects on every step of non-alcoholic Fatty liver disease progression in a methionine- and choline-deficient diet-fed animal model. Diabetes & metabolism journal 2011;35:489-496.

[113] Hua J, Ma X, Webb T, Potter JJ, Oelke M, Li Z. Dietary fatty acids modulate antigen presentation to hepatic NKT cells in nonalcoholic fatty liver disease. Journal of lipid research 2010;51:1696-1703.

[114] Yuan F, Wang H, Tian Y, Li Q, He L, Li N, et al. Fish oil alleviated high-fat diet-induced non-alcoholic fatty liver disease via regulating hepatic lipids metabolism and metaflammation: a transcriptomic study. Lipids in health and disease 2016;15:20.

[115] Di Minno MN, Russolillo A, Lupoli R, Ambrosino P, Di Minno A, Tarantino G. Omega-3 fatty acids for the treatment of non-alcoholic fatty liver disease. World journal of gastroenterology 2012;18:5839-5847.

[116] Parker HM, Johnson NA, Burdon CA, Cohn JS, O'Connor HT, George J. Omega-3 supplementation and non-alcoholic fatty liver disease: a systematic review and meta-analysis. Journal of hepatology 2012;56:944-951.

[117] Ganz M, Szabo G. Immune and inflammatory pathways in NASH. Hepatology international 2013;7 Suppl 2:771-781.

[118] van Buul VJ, Tappy L, Brouns FJ. Misconceptions about fructose-containing sugars and their role in the obesity epidemic. Nutrition research reviews 2014;27:119-130.

[119] Bergheim I, Weber S, Vos M, Kramer S, Volynets V, Kaserouni S, et al. Antibiotics protect against fructose-induced hepatic lipid accumulation in mice: role of endotoxin. Journal of hepatology 2008;48:983-992.

[120] Spruss A, Kanuri G, Wagnerberger S, Haub S, Bischoff SC, Bergheim I. Toll-like receptor 4 is involved in the development of fructose-induced hepatic steatosis in mice. Hepatology 2009;50:1094-1104.

[121] Schultz A, Neil D, Aguila MB, Mandarim-de-Lacerda CA. Hepatic adverse effects of fructose consumption independent of overweight/obesity. International journal of molecular sciences 2013;14:21873-21886.

[122] Lim JS, Mietus-Snyder M, Valente A, Schwarz JM, Lustig RH. The role of fructose in the pathogenesis of NAFLD and the metabolic syndrome. Nature reviews Gastroenterology & hepatology 2010;7:251-264.

[123] Alisi A, Manco M, Pezzullo M, Nobili V. Fructose at the center of necroinflammation and fibrosis in nonalcoholic steatohepatitis. Hepatology 2011;53:372-373.

[124] du Plessis J, van Pelt J, Korf H, Mathieu C, van der Schueren B, Lannoo M, et al. Association of Adipose Tissue Inflammation With Histologic Severity of Nonalcoholic Fatty Liver Disease. Gastroenterology 2015;149:635-648 e614.

[125] Wouters K, van Gorp PJ, Bieghs V, Gijbels MJ, Duimel H, Lutjohann D, et al. Dietary cholesterol, rather than liver steatosis, leads to hepatic inflammation in hyperlipidemic mouse models of nonalcoholic steatohepatitis. Hepatology 2008;48:474-486.

[126] Sanches SC, Ramalho LN, Augusto MJ, da Silva DM, Ramalho FS. Nonalcoholic Steatohepatitis: A Search for Factual Animal Models. BioMed research international 2015;2015:574832.

[127] Matsuzawa N, Takamura T, Kurita S, Misu H, Ota T, Ando H, et al. Lipid-induced oxidative stress causes steatohepatitis in mice fed an atherogenic diet. Hepatology 2007;46:1392-1403.

[128] Ahima RS, Flier JS. Leptin. Annual review of physiology 2000;62:413-437.

[129] Kucera O, Cervinkova Z. Experimental models of non-alcoholic fatty liver disease in rats. World journal of gastroenterology 2014;20:8364-8376.

[130] Diehl AM. Lessons from animal models of NASH. Hepatology research : the official journal of the Japan Society of Hepatology 2005;33:138-144.

[131] Chalasani N, Crabb DW, Cummings OW, Kwo PY, Asghar A, Pandya PK, et al. Does leptin play a role in the pathogenesis of human nonalcoholic steatohepatitis? The American journal of gastroenterology 2003;98:2771-2776.

[132] Hummel KP, Dickie MM, Coleman DL. Diabetes, a new mutation in the mouse. Science 1966;153:1127-1128.

[133] Sahai A, Malladi P, Pan X, Paul R, Melin-Aldana H, Green RM, et al. Obese and diabetic db/db mice develop marked liver fibrosis in a model of nonalcoholic steatohepatitis: role of short-form leptin receptors and osteopontin. American journal of physiology Gastrointestinal and liver physiology 2004;287:G1035-1043.

[134] Yamashita T, Murakami T, Iida M, Kuwajima M, Shima K. Leptin receptor of Zucker fatty rat performs reduced signal transduction. Diabetes 1997;46:1077-1080.

[135] Godbole V, York DA. Lipogenesis in situ in the genetically obese Zucker fatty rat (fa/fa): role of hyperphagia and hyperinsulinaemia. Diabetologia 1978;14:191-197.

[136] Liao W, Angelin B, Rudling M. Lipoprotein metabolism in the fat Zucker rat: reduced basal expression but normal regulation of hepatic low density lipoprotein receptors. Endocrinology 1997;138:3276-3282.

[137] Soltys K, Dikdan G, Koneru B. Oxidative stress in fatty livers of obese Zucker rats: rapid amelioration and improved tolerance to warm ischemia with tocopherol. Hepatology 2001;34:13-18.

[138] Carmiel-Haggai M, Cederbaum AI, Nieto N. A high-fat diet leads to the progression of non-alcoholic fatty liver disease in obese rats. FASEB journal : official publication of the Federation of American Societies for Experimental Biology 2005;19:136-138.

[139] Shimomura I, Hammer RE, Richardson JA, Ikemoto S, Bashmakov Y, Goldstein JL, et al. Insulin resistance and diabetes mellitus in transgenic mice expressing nuclear SREBP-1c in adipose tissue: model for congenital generalized lipodystrophy. Genes & development 1998;12:3182-3194.

[140] Nakayama H, Otabe S, Ueno T, Hirota N, Yuan X, Fukutani T, et al. Transgenic mice expressing nuclear sterol regulatory element-binding protein 1c in adipose tissue exhibit liver

histology similar to nonalcoholic steatohepatitis. Metabolism: clinical and experimental 2007;56:470-475.

[141] Ludwig J, McGill DB, Lindor KD. Review: nonalcoholic steatohepatitis. Journal of gastroenterology and hepatology 1997;12:398-403.

[142] Depner CM, Philbrick KA, Jump DB. Docosahexaenoic acid attenuates hepatic inflammation, oxidative stress, and fibrosis without decreasing hepatosteatosis in a Ldlr(-/-) mouse model of western diet-induced nonalcoholic steatohepatitis. The Journal of nutrition 2013;143:315-323.

[143] Bieghs V, Van Gorp PJ, Wouters K, Hendrikx T, Gijbels MJ, van Bilsen M, et al. LDL receptor knock-out mice are a physiological model particularly vulnerable to study the onset of inflammation in non-alcoholic fatty liver disease. PloS one 2012;7:e30668.

[144] Subramanian S, Goodspeed L, Wang S, Kim J, Zeng L, Ioannou GN, et al. Dietary cholesterol exacerbates hepatic steatosis and inflammation in obese LDL receptor-deficient mice. Journal of lipid research 2011;52:1626-1635.

[145] Gupte AA, Liu JZ, Ren Y, Minze LJ, Wiles JR, Collins AR, et al. Rosiglitazone attenuates age- and diet-associated nonalcoholic steatohepatitis in male low-density lipoprotein receptor knockout mice. Hepatology 2010;52:2001-2011.

[146] Subramanian S, Han CY, Chiba T, McMillen TS, Wang SA, Haw A, 3rd, et al. Dietary cholesterol worsens adipose tissue macrophage accumulation and atherosclerosis in obese LDL receptor-deficient mice. Arteriosclerosis, thrombosis, and vascular biology 2008;28:685-691.

[147] Schreyer SA, Vick C, Lystig TC, Mystkowski P, LeBoeuf RC. LDL receptor but not apolipoprotein E deficiency increases diet-induced obesity and diabetes in mice. American journal of physiology Endocrinology and metabolism 2002;282:E207-214.

[148] Ozsolak F, Milos PM. RNA sequencing: advances, challenges and opportunities. Nature reviews Genetics 2011;12:87-98.

[149] Wang Z, Gerstein M, Snyder M. RNA-Seq: a revolutionary tool for transcriptomics. Nature reviews Genetics 2009;10:57-63.

[150] Morozova O, Marra MA. Applications of next-generation sequencing technologies in functional genomics. Genomics 2008;92:255-264.

[151] Trapnell C, Hendrickson DG, Sauvageau M, Goff L, Rinn JL, Pachter L. Differential analysis of gene regulation at transcript resolution with RNA-seq. Nature biotechnology 2013;31:46-53.

[152] Oshlack A, Robinson MD, Young MD. From RNA-seq reads to differential expression results. Genome biology 2010;11:220.

[153] Tarazona S, Garcia-Alcalde F, Dopazo J, Ferrer A, Conesa A. Differential expression in RNA-seq: a matter of depth. Genome research 2011;21:2213-2223.

[154] Trapnell C, Roberts A, Goff L, Pertea G, Kim D, Kelley DR, et al. Differential gene and transcript expression analysis of RNA-seq experiments with TopHat and Cufflinks. Nature protocols 2012;7:562-578.

[155] Wang ET, Sandberg R, Luo S, Khrebtukova I, Zhang L, Mayr C, et al. Alternative isoform regulation in human tissue transcriptomes. Nature 2008;456:470-476.

[156] Denoeud F, Aury JM, Da Silva C, Noel B, Rogier O, Delledonne M, et al. Annotating genomes with massive-scale RNA sequencing. Genome biology 2008;9:R175.

[157] Maher CA, Kumar-Sinha C, Cao X, Kalyana-Sundaram S, Han B, Jing X, et al. Transcriptome sequencing to detect gene fusions in cancer. Nature 2009;458:97-101.

[158] Griffith M, Griffith OL, Mwenifumbo J, Goya R, Morrissy AS, Morin RD, et al. Alternative expression analysis by RNA sequencing. Nature methods 2010;7:843-847.

[159] Nagalakshmi U, Wang Z, Waern K, Shou C, Raha D, Gerstein M, et al. The transcriptional landscape of the yeast genome defined by RNA sequencing. Science 2008;320:1344-1349.

[160] Cloonan N, Forrest AR, Kolle G, Gardiner BB, Faulkner GJ, Brown MK, et al. Stem cell transcriptome profiling via massive-scale mRNA sequencing. Nature methods 2008;5:613-619.

[161] Holt CL, Schroy PC, 3rd. A new paradigm for increasing use of open-access screening colonoscopy. Clinical gastroenterology and hepatology : the official clinical practice journal of the American Gastroenterological Association 2008;6:377-378.

[162] Griffith M, Walker JR, Spies NC, Ainscough BJ, Griffith OL. Informatics for RNA Sequencing: A Web Resource for Analysis on the Cloud. PLoS computational biology 2015;11:e1004393.

[163] Cray C, Zaias J, Altman NH. Acute phase response in animals: a review. Comparative medicine 2009;59:517-526.

[164] Janeway CA TP, Walport M, Shlomchik MJ. Immunobiology 5th ed. 2001:732.

[165] Tecles F, Spiranelli E, Bonfanti U, Ceron JJ, Paltrinieri S. Preliminary studies of serum acute-phase protein concentrations in hematologic and neoplastic diseases of the dog. Journal of veterinary internal medicine / American College of Veterinary Internal Medicine 2005;19:865-870.

[166] Horadagoda NU, Knox KM, Gibbs HA, Reid SW, Horadagoda A, Edwards SE, et al. Acute phase proteins in cattle: discrimination between acute and chronic inflammation. The Veterinary record 1999;144:437-441.

[167] Petersen HH, Nielsen JP, Heegaard PM. Application of acute phase protein measurements in veterinary clinical chemistry. Veterinary research 2004;35:163-187.

[168] Devaraj S, Singh U, Jialal I. The evolving role of C-reactive protein in atherothrombosis. Clinical chemistry 2009;55:229-238.

[169] Zhong W, Zen Q, Tebo J, Schlottmann K, Coggeshall M, Mortensen RF. Effect of human C-reactive protein on chemokine and chemotactic factor-induced neutrophil chemotaxis and signaling. Journal of immunology 1998;161:2533-2540.

[170] Murata H, Shimada N, Yoshioka M. Current research on acute phase proteins in veterinary diagnosis: an overview. Veterinary journal 2004;168:28-40.

[171] Huang Z, Ung T. Effect of alpha-1-acid glycoprotein binding on pharmacokinetics and pharmacodynamics. Current drug metabolism 2013;14:226-238.

[172] Tothova C, Nagy O, Kovac G. Acute phase proteins and their use in the diagnosis of diseases in ruminants: a review. Vet Med-Czech 2014;59:163-180.

[173] Kaplan J, Jordan I, Sturrock A. Regulation of the transferrin-independent iron transport system in cultured cells. The Journal of biological chemistry 1991;266:2997-3004.

[174] Tokita K, Schmid K. Variants of Alpha-1-Acid Glycoprotein. Nature 1963;200:266.

[175] Fournier T, Medjoubi NN, Porquet D. Alpha-1-acid glycoprotein. Biochimica et biophysica acta 2000;1482:157-171.

[176] Hochepied T, Berger FG, Baumann H, Libert C. Alpha(1)-acid glycoprotein: an acute phase protein with inflammatory and immunomodulating properties. Cytokine & growth factor reviews 2003;14:25-34.

[177] Dente L, Pizza MG, Metspalu A, Cortese R. Structure and expression of the genes coding for human alpha 1-acid glycoprotein. The EMBO journal 1987;6:2289-2296.

[178] Luo Z, Lei H, Sun Y, Liu X, Su DF. Orosomucoid, an acute response protein with multiple modulating activities. J Physiol Biochem 2015;71:329-340.

[179] Abboud FM, Mark AL, Heistad DD, Eckberg DL, Schimid PG. Selectivity of autonomic control of the peripheral circulation in man. Transactions of the American Clinical and Climatological Association 1975;86:184-197.

[180] Ricca GA, Hamilton RW, McLean JW, Conn A, Kalinyak JE, Taylor JM. Rat alpha 1-acid glycoprotein mRNA. Cloning of double-stranded cDNA and kinetics of induction of mRNA levels following acute inflammation. The Journal of biological chemistry 1981;256:10362-10368.

[181] Baumann H, Gauldie J. Regulation of hepatic acute phase plasma protein genes by hepatocyte stimulating factors and other mediators of inflammation. Molecular biology & medicine 1990;7:147-159.

[182] Alam T, Papaconstantinou J. Interaction of acute-phase-inducible and liver-enriched nuclear factors with the promoter region of the mouse alpha 1-acid glycoprotein gene-1. Biochemistry 1992;31:1928-1936.

[183] Wigmore SJ, Fearon KC, Maingay JP, Lai PB, Ross JA. Interleukin-8 can mediate acute-phase protein production by isolated human hepatocytes. The American journal of physiology 1997;273:E720-726.

[184] Lin TH, Sugiyama Y, Sawada Y, Suzuki Y, Iga T, Hanano M. Effect of surgery on serum alpha 1-acid glycoprotein concentration and serum protein binding of DL-propranolol in phenobarbital-treated and untreated rats. Drug metabolism and disposition: the biological fate of chemicals 1987;15:138-140.

[185] Mouthiers A, Mejdoubi N, Baillet A, Amelie PA, Porquet D. Retinoids increase alpha-1 acid glycoprotein expression at the transcriptional level through two distinct DR1 retinoic acid responsive elements. Biochimica et biophysica acta 2004;1678:135-144.

[186] Lefebvre P, Cariou B, Lien F, Kuipers F, Staels B. Role of bile acids and bile acid receptors in metabolic regulation. Physiological reviews 2009;89:147-191.

[187] Porez G, Gross B, Prawitt J, Gheeraert C, Berrabah W, Alexandre J, et al. The hepatic orosomucoid/alpha1-acid glycoprotein gene cluster is regulated by the nuclear bile acid receptor FXR. Endocrinology 2013;154:3690-3701.

[188] Spiller F, Carlos D, Souto FO, de Freitas A, Soares FS, Vieira SM, et al. alpha1-Acid glycoprotein decreases neutrophil migration and increases susceptibility to sepsis in diabetic mice. Diabetes 2012;61:1584-1591.

[189] Elg SA, Mayer AR, Carson LF, Twiggs LB, Hill RB, Ramakrishnan S. Alpha-1 acid glycoprotein is an immunosuppressive factor found in ascites from ovaria carcinoma. Cancer 1997;80:1448-1456.

[190] Gemelli C, Martello A, Montanari M, Zanocco Marani T, Salsi V, Zappavigna V, et al. The Orosomucoid 1 protein is involved in the vitamin D - mediated macrophage de-activation process. Experimental cell research 2013;319:3201-3213.

[191] Komori H, Watanabe H, Shuto T, Kodama A, Maeda H, Watanabe K, et al. alpha(1)-Acid glycoprotein up-regulates CD163 via TLR4/CD14 protein pathway: possible protection against hemolysis-induced oxidative stress. The Journal of biological chemistry 2012;287:30688-30700.

[192] Nakamura K, Ito I, Kobayashi M, Herndon DN, Suzuki F. Orosomucoid 1 drives opportunistic infections through the polarization of monocytes to the M2b phenotype. Cytokine 2015;73:8-15.

[193] Tilg H, Vannier E, Vachino G, Dinarello CA, Mier JW. Antiinflammatory properties of hepatic acute phase proteins: preferential induction of interleukin 1 (IL-1) receptor antagonist over IL-1 beta synthesis by human peripheral blood mononuclear cells. The Journal of experimental medicine 1993;178:1629-1636.

[194] Libert C, Brouckaert P, Fiers W. Protection by alpha 1-acid glycoprotein against tumor necrosis factor-induced lethality. The Journal of experimental medicine 1994;180:1571-1575.

[195] Van Molle W, Libert C, Fiers W, Brouckaert P. Alpha 1-acid glycoprotein and alpha 1-antitrypsin inhibit TNF-induced but not anti-Fas-induced apoptosis of hepatocytes in mice. Journal of immunology 1997;159:3555-3564.

[196] Hochepied T, Wullaert A, Berger FG, Baumann H, Brouckaert P, Steidler L, et al. Overexpression of alpha(1)-acid glycoprotein in transgenic mice leads to sensitisation to acute colitis. Gut 2002;51:398-404.

[197] Paxton JW. Alpha 1 -acid glycoprotein and binding of basic drugs. Methods and findings in experimental and clinical pharmacology 1983;5:635-648.

[198] Lee YS, Choi JW, Hwang I, Lee JW, Lee JH, Kim AY, et al. Adipocytokine orosomucoid integrates inflammatory and metabolic signals to preserve energy homeostasis by resolving immoderate inflammation. The Journal of biological chemistry 2010;285:22174-22185.

[199] Sun Y, Yang Y, Qin Z, Cai J, Guo X, Tang Y, et al. The Acute-Phase Protein Orosomucoid Regulates Food Intake and Energy Homeostasis via Leptin Receptor Signaling Pathway. Diabetes 2016;65:1630-1641.

[200] Alfadda AA, Fatma S, Chishti MA, Al-Naami MY, Elawad R, Mendoza CD, et al. Orosomucoid serum concentrations and fat depot-specific mRNA and protein expression in humans. Molecules and cells 2012;33:35-41.

[201] Wiklund PK, Pekkala S, Autio R, Munukka E, Xu L, Saltevo J, et al. Serum metabolic profiles in overweight and obese women with and without metabolic syndrome. Diabetology & metabolic syndrome 2014;6:40.

[202] Jung Y, Diehl AM. Non-alcoholic steatohepatitis pathogenesis: role of repair in regulating the disease progression. Digestive diseases 2010;28:225-228.

[203] Qureshi K, Abrams GA. Metabolic liver disease of obesity and role of adipose tissue in the pathogenesis of nonalcoholic fatty liver disease. World journal of gastroenterology 2007;13:3540-3553.

[204] Gastaldelli A, Harrison SA, Belfort-Aguilar R, Hardies LJ, Balas B, Schenker S, et al. Importance of changes in adipose tissue insulin resistance to histological response during thiazolidinedione treatment of patients with nonalcoholic steatohepatitis. Hepatology 2009;50:1087-1093.

[205] Duval C, Thissen U, Keshtkar S, Accart B, Stienstra R, Boekschoten MV, et al. Adipose tissue dysfunction signals progression of hepatic steatosis towards nonalcoholic steatohepatitis in C57BL/6 mice. Diabetes 2010;59:3181-3191.

[206] Welsh JA, Sharma A, Abramson JL, Vaccarino V, Gillespie C, Vos MB. Caloric sweetener consumption and dyslipidemia among US adults. Jama 2010;303:1490-1497.

[207] Reedy J, Krebs-Smith SM. Dietary sources of energy, solid fats, and added sugars among children and adolescents in the United States. Journal of the American Dietetic Association 2010;110:1477-1484.

[208] Abdelmalek MF, Suzuki A, Guy C, Unalp-Arida A, Colvin R, Johnson RJ, et al. Increased fructose consumption is associated with fibrosis severity in patients with nonalcoholic fatty liver disease. Hepatology 2010;51:1961-1971.

[209] Ekstedt M, Franzen LE, Mathiesen UL, Thorelius L, Holmqvist M, Bodemar G, et al. Long-term follow-up of patients with NAFLD and elevated liver enzymes. Hepatology 2006;44:865-873.

[210] Machado MV, Michelotti GA, Xie G, Almeida Pereira T, Boursier J, Bohnic B, et al. Mouse models of diet-induced nonalcoholic steatohepatitis reproduce the heterogeneity of the human disease. PloS one 2015;10:e0127991.

[211] Lighton JR, Turner RJ. The hygric hypothesis does not hold water: abolition of discontinuous gas exchange cycles does not affect water loss in the ant Camponotus vicinus. The Journal of experimental biology 2008;211:563-567.

[212] Weir JB. New methods for calculating metabolic rate with special reference to protein metabolism. The Journal of physiology 1949;109:1-9.

[213] Marklund S, Marklund G. Involvement of the superoxide anion radical in the autoxidation of pyrogallol and a convenient assay for superoxide dismutase. European journal of biochemistry / FEBS 1974;47:469-474.

[214] Kaiyala KJ SC, Podolsky RH, McGuinness O. MMPC Energy Expenditure Analysis Page.https://www.mmpc.org/shared/regression.aspx.

[215] Sumiyoshi M, Sakanaka M, Kimura Y. Chronic intake of high-fat and high-sucrose diets differentially affects glucose intolerance in mice. The Journal of nutrition 2006;136:582-587.

[216] Syn WK, Yang L, Chiang DJ, Qian Y, Jung Y, Karaca G, et al. Genetic differences in oxidative stress and inflammatory responses to diet-induced obesity do not alter liver fibrosis in

mice. Liver international : official journal of the International Association for the Study of the Liver 2009;29:1262-1272.

[217] Mehta K, Van Thiel DH, Shah N, Mobarhan S. Nonalcoholic fatty liver disease: pathogenesis and the role of antioxidants. Nutrition reviews 2002;60:289-293.

[218] Voigt A, Agnew K, van Schothorst EM, Keijer J, Klaus S. Short-term, high fat feeding-induced changes in white adipose tissue gene expression are highly predictive for long-term changes. Molecular nutrition & food research 2013;57:1423-1434.

[219] Weisberg SP, McCann D, Desai M, Rosenbaum M, Leibel RL, Ferrante AW, Jr. Obesity is associated with macrophage accumulation in adipose tissue. The Journal of clinical investigation 2003;112:1796-1808.

[220] Rombouts K, Marra F. Molecular mechanisms of hepatic fibrosis in non-alcoholic steatohepatitis. Digestive diseases 2010;28:229-235.

[221] Parlee SD, Lentz SI, Mori H, MacDougald OA. Quantifying size and number of adipocytes in adipose tissue. Methods in enzymology 2014;537:93-122.

[222] Parlee SD, Simon BR, Scheller EL, Alejandro EU, Learman BS, Krishnan V, et al. Administration of saccharin to neonatal mice influences body composition of adult males and reduces body weight of females. Endocrinology 2014;155:1313-1326.

[223] Simon BR, Learman BS, Parlee SD, Scheller EL, Mori H, Cawthorn WP, et al. Sweet taste receptor deficient mice have decreased adiposity and increased bone mass. PloS one 2014;9:e86454.

[224] Khan T, Muise ES, Iyengar P, Wang ZV, Chandalia M, Abate N, et al. Metabolic dysregulation and adipose tissue fibrosis: role of collagen VI. Molecular and cellular biology 2009;29:1575-1591.

[225] Sun K, Kusminski CM, Scherer PE. Adipose tissue remodeling and obesity. The Journal of clinical investigation 2011;121:2094-2101.

[226] Halberg N, Khan T, Trujillo ME, Wernstedt-Asterholm I, Attie AD, Sherwani S, et al. Hypoxia-inducible factor 1alpha induces fibrosis and insulin resistance in white adipose tissue. Molecular and cellular biology 2009;29:4467-4483.

[227] Sun K, Tordjman J, Clement K, Scherer PE. Fibrosis and adipose tissue dysfunction. Cell metabolism 2013;18:470-477.

[228] Pendergast JS, Branecky KL, Yang W, Ellacott KL, Niswender KD, Yamazaki S. High-fat diet acutely affects circadian organisation and eating behavior. The European journal of neuroscience 2013;37:1350-1356.

[229] Almind K, Kahn CR. Genetic determinants of energy expenditure and insulin resistance in diet-induced obesity in mice. Diabetes 2004;53:3274-3285.

[230] Hoevenaars FP, Keijer J, Swarts HJ, Snaas-Alders S, Bekkenkamp-Grovenstein M, van Schothorst EM. Effects of dietary history on energy metabolism and physiological parameters in C57BL/6J mice. Experimental physiology 2013;98:1053-1062.

[231] van Beek L, van Klinken JB, Pronk AC, van Dam AD, Dirven E, Rensen PC, et al. The limited storage capacity of gonadal adipose tissue directs the development of metabolic disorders in male C57Bl/6J mice. Diabetologia 2015;58:1601-1609.

[232] Gray SL, Nora ED, Grosse J, Manieri M, Stoeger T, Medina-Gomez G, et al. Leptin deficiency unmasks the deleterious effects of impaired peroxisome proliferator-activated receptor gamma function (P465L PPARgamma) in mice. Diabetes 2006;55:2669-2677.

[233] Kim JY, van de Wall E, Laplante M, Azzara A, Trujillo ME, Hofmann SM, et al. Obesity-associated improvements in metabolic profile through expansion of adipose tissue. The Journal of clinical investigation 2007;117:2621-2637.

[234] Dhingra R, Sullivan L, Jacques PF, Wang TJ, Fox CS, Meigs JB, et al. Soft drink consumption and risk of developing cardiometabolic risk factors and the metabolic syndrome in middle-aged adults in the community. Circulation 2007;116:480-488.

[235] Stanhope KL, Schwarz JM, Keim NL, Griffen SC, Bremer AA, Graham JL, et al. Consuming fructose-sweetened, not glucose-sweetened, beverages increases visceral adiposity and lipids and decreases insulin sensitivity in overweight/obese humans. The Journal of clinical investigation 2009;119:1322-1334.

[236] Sarjeant K, Stephens JM. Adipogenesis. Cold Spring Harbor perspectives in biology 2012;4:a008417.

[237] Duffaut C, Galitzky J, Lafontan M, Bouloumie A. Unexpected trafficking of immune cells within the adipose tissue during the onset of obesity. Biochemical and biophysical research communications 2009;384:482-485.

[238] Strissel KJ, DeFuria J, Shaul ME, Bennett G, Greenberg AS, Obin MS. T-cell recruitment and Th1 polarization in adipose tissue during diet-induced obesity in C57BL/6 mice. Obesity 2010;18:1918-1925.

[239] Gatselis NK, Ntaios G, Makaritsis K, Dalekos GN. Adiponectin: a key playmaker adipocytokine in non-alcoholic fatty liver disease. Clinical and experimental medicine 2014;14:121-131.

[240] Loomba R, Sanyal AJ. The global NAFLD epidemic. Nature reviews Gastroenterology & hepatology 2013;10:686-690.

[241] Vos MB, Lavine JE. Dietary fructose in nonalcoholic fatty liver disease. Hepatology 2013;57:2525-2531.

[242] Luo Y, Burrington CM, Graff EC, Zhang J, Judd RL, Suksaranjit P, et al. Metabolic phenotype and adipose and liver features in a high-fat Western diet-induced mouse model of obesity-linked NAFLD. American journal of physiology Endocrinology and metabolism 2016;310:E418-439.

[243] Nishikawa S, Sugimoto J, Okada M, Sakairi T, Takagi S. Gene expression in livers of BALB/C and C57BL/6J mice fed a high-fat diet. Toxicologic pathology 2012;40:71-82.

[244] Oh HY, Shin SK, Heo HS, Ahn JS, Kwon EY, Park JH, et al. Time-dependent network analysis reveals molecular targets underlying the development of diet-induced obesity and non-alcoholic steatohepatitis. Genes & nutrition 2013;8:301-316.

[245] Sreekumar R, Rosado B, Rasmussen D, Charlton M. Hepatic gene expression in histologically progressive nonalcoholic steatohepatitis. Hepatology 2003;38:244-251.

[246] Younossi ZM, Baranova A, Ziegler K, Del Giacco L, Schlauch K, Born TL, et al. A genomic and proteomic study of the spectrum of nonalcoholic fatty liver disease. Hepatology 2005;42:665-674.

[247] Younossi ZM, Gorreta F, Ong JP, Schlauch K, Del Giacco L, Elariny H, et al. Hepatic gene expression in patients with obesity-related non-alcoholic steatohepatitis. Liver international : official journal of the International Association for the Study of the Liver 2005;25:760-771.

[248] Liang W, Menke AL, Driessen A, Koek GH, Lindeman JH, Stoop R, et al. Establishment of a general NAFLD scoring system for rodent models and comparison to human liver pathology. PloS one 2014;9:e115922.

[249] Langmead B, Trapnell C, Pop M, Salzberg SL. Ultrafast and memory-efficient alignment of short DNA sequences to the human genome. Genome biology 2009;10:1.

[250] Trapnell C, Pachter L, Salzberg SL. TopHat: discovering splice junctions with RNA-Seq. Bioinformatics 2009;25:1105-1111.

[251] Li H, Handsaker B, Wysoker A, Fennell T, Ruan J, Homer N, et al. The sequence alignment/map format and SAMtools. Bioinformatics 2009;25:2078-2079.

[252] Robinson MD, Oshlack A. A scaling normalization method for differential expression analysis of RNA-seq data. Genome biology 2010;11:1.

[253] Benjamini Y, Hochberg Y. Controlling the false discovery rate: a practical and powerful approach to multiple testing. Journal of the royal statistical society Series B (Methodological) 1995:289-300.

[254] Gene Ontology C, Blake JA, Dolan M, Drabkin H, Hill DP, Li N, et al. Gene Ontology annotations and resources. Nucleic acids research 2013;41:D530-535.

[255] Kanehisa M, Goto S. KEGG: kyoto encyclopedia of genes and genomes. Nucleic acids research 2000;28:27-30.

[256] Thomas PD, Kejariwal A, Campbell MJ, Mi H, Diemer K, Guo N, et al. PANTHER: a browsable database of gene products organized by biological function, using curated protein family and subfamily classification. Nucleic acids research 2003;31:334-341.

[257] Livak KJ, Schmittgen TD. Analysis of relative gene expression data using real-time quantitative PCR and the 2(-Delta Delta C(T)) Method. Methods 2001;25:402-408.

[258] Tiniakos DG, Vos MB, Brunt EM. Nonalcoholic fatty liver disease: pathology and pathogenesis. Annual review of pathology 2010;5:145-171.

[259] Powell AE, Wang Y, Li Y, Poulin EJ, Means AL, Washington MK, et al. The pan-ErbB negative regulator Lrig1 is an intestinal stem cell marker that functions as a tumor suppressor. Cell 2012;149:146-158.

[260] Lehto M, Olkkonen VM. The OSBP-related proteins: a novel protein family involved in vesicle transport, cellular lipid metabolism, and cell signalling. Biochimica et biophysica acta 2003;1631:1-11.

[261] Zhou Z, Yon Toh S, Chen Z, Guo K, Ng CP, Ponniah S, et al. Cidea-deficient mice have lean phenotype and are resistant to obesity. Nature genetics 2003;35:49-56.

[262] Zangar RC, Novak RF. Effects of fatty acids and ketone bodies on cytochromes P450 2B, 4A, and 2E1 expression in primary cultured rat hepatocytes. Archives of biochemistry and biophysics 1997;337:217-224.

[263] Collison KS, Maqbool ZM, Inglis AL, Makhoul NJ, Saleh SM, Bakheet RH, et al. Effect of dietary monosodium glutamate on HFCS-induced hepatic steatosis: expression profiles in the liver and visceral fat. Obesity 2010;18:1122-1134.

[264] Zhou L, Xu L, Ye J, Li D, Wang W, Li X, et al. Cidea promotes hepatic steatosis by sensing dietary fatty acids. Hepatology 2012;56:95-107.

[265] Bijl N, Sokolovic M, Vrins C, Langeveld M, Moerland PD, Ottenhoff R, et al. Modulation of glycosphingolipid metabolism significantly improves hepatic insulin sensitivity and reverses hepatic steatosis in mice. Hepatology 2009;50:1431-1441.

[266] Crispe IN. Hepatic T cells and liver tolerance. Nature reviews Immunology 2003;3:51-62.

[267] Harte AL, da Silva NF, Creely SJ, McGee KC, Billyard T, Youssef-Elabd EM, et al. Elevated endotoxin levels in non-alcoholic fatty liver disease. Journal of inflammation 2010;7:15.

[268] Tosello-Trampont AC, Landes SG, Nguyen V, Novobrantseva TI, Hahn YS. Kuppfer cells trigger nonalcoholic steatohepatitis development in diet-induced mouse model through tumor necrosis factor-alpha production. The Journal of biological chemistry 2012;287:40161-40172.

[269] Sutti S, Jindal A, Locatelli I, Vacchiano M, Gigliotti L, Bozzola C, et al. Adaptive immune responses triggered by oxidative stress contribute to hepatic inflammation in NASH. Hepatology 2014;59:886-897.

[270] Gadd VL, Skoien R, Powell EE, Fagan KJ, Winterford C, Horsfall L, et al. The portal inflammatory infiltrate and ductular reaction in human nonalcoholic fatty liver disease. Hepatology 2014;59:1393-1405.

[271] Sell S. Heterogeneity and plasticity of hepatocyte lineage cells. Hepatology 2001;33:738-750.

[272] Roskams T, Yang SQ, Koteish A, Durnez A, DeVos R, Huang X, et al. Oxidative stress and oval cell accumulation in mice and humans with alcoholic and nonalcoholic fatty liver disease. The American journal of pathology 2003;163:1301-1311.

[273] Nobili V, Carpino G, Alisi A, Franchitto A, Alpini G, De Vito R, et al. Hepatic progenitor cells activation, fibrosis, and adipokines production in pediatric nonalcoholic fatty liver disease. Hepatology 2012;56:2142-2153.

[274] Richardson MM, Jonsson JR, Powell EE, Brunt EM, Neuschwander-Tetri BA, Bhathal PS, et al. Progressive fibrosis in nonalcoholic steatohepatitis: association with altered regeneration and a ductular reaction. Gastroenterology 2007;133:80-90.

[275] Michelotti GA, Machado MV, Diehl AM. NAFLD, NASH and liver cancer. Nature reviews Gastroenterology & hepatology 2013;10:656-665.

[276] Zhang F, Xu X, Zhang Y, Zhou B, He Z, Zhai Q. Gene expression profile analysis of type 2 diabetic mouse liver. PloS one 2013;8:e57766.

[277] Starmann J, Falth M, Spindelbock W, Lanz KL, Lackner C, Zatloukal K, et al. Gene expression profiling unravels cancer-related hepatic molecular signatures in steatohepatitis but not in steatosis. PloS one 2012;7:e46584.

[278] Whittaker S, Marais R, Zhu AX. The role of signaling pathways in the development and treatment of hepatocellular carcinoma. Oncogene 2010;29:4989-5005.

[279] Mas VR, Maluf DG, Archer KJ, Yanek KC, Fisher RA. Angiogenesis soluble factors as hepatocellular carcinoma noninvasive markers for monitoring hepatitis C virus cirrhotic patients awaiting liver transplantation. Transplantation 2007;84:1262-1271.

[280] Fischer AN, Fuchs E, Mikula M, Huber H, Beug H, Mikulits W. PDGF essentially links TGF-beta signaling to nuclear beta-catenin accumulation in hepatocellular carcinoma progression. Oncogene 2007;26:3395-3405.

[281] Trayhurn P. Hypoxia and adipose tissue function and dysfunction in obesity. Physiological reviews 2013;93:1-21.

[282] Arias-Loste MT, Fabrega E, Lopez-Hoyos M, Crespo J. The Crosstalk between Hypoxia and Innate Immunity in the Development of Obesity-Related Nonalcoholic Fatty Liver Disease. BioMed research international 2015;2015:319745.

[283] Liu CY, Xu JY, Shi XY, Huang W, Ruan TY, Xie P, et al. M2-polarized tumor-associated macrophages promoted epithelial-mesenchymal transition in pancreatic cancer cells, partially through TLR4/IL-10 signaling pathway. Laboratory investigation; a journal of technical methods and pathology 2013;93:844-854.

[284] Lo KA, Labadorf A, Kennedy NJ, Han MS, Yap YS, Matthews B, et al. Analysis of in vitro insulin-resistance models and their physiological relevance to in vivo diet-induced adipose insulin resistance. Cell Rep 2013;5:259-270.

[285] Range H, Poitou C, Boillot A, Ciangura C, Katsahian S, Lacorte JM, et al. Orosomucoid, a new biomarker in the association between obesity and periodontitis. PloS one 2013;8:e57645.

[286] Dandona P, Aljada A, Bandyopadhyay A. Inflammation: the link between insulin resistance, obesity and diabetes. Trends in immunology 2004;25:4-7.

[287] Dalmas E, Clement K, Guerre-Millo M. Defining macrophage phenotype and function in adipose tissue. Trends in immunology 2011;32:307-314.

[288] Lanthier N, Molendi-Coste O, Horsmans Y, van Rooijen N, Cani PD, Leclercq IA. Kupffer cell activation is a causal factor for hepatic insulin resistance. American journal of physiology Gastrointestinal and liver physiology 2010;298:G107-116.

[289] Gunnarsson P, Levander L, Pahlsson P, Grenegard M. The acute-phase protein alpha 1-acid glycoprotein (AGP) induces rises in cytosolic Ca2+ in neutrophil granulocytes via sialic acid binding immunoglobulin-like lectins (siglecs). FASEB journal : official publication of the Federation of American Societies for Experimental Biology 2007;21:4059-4069.

[290] Atemezem A, Mbemba E, Vassy R, Slimani H, Saffar L, Gattegno L. Human alpha1-acid glycoprotein binds to CCR5 expressed on the plasma membrane of human primary macrophages. The Biochemical journal 2001;356:121-128.

Appendix 1

Supplemental Table 1. Hepatic gene expression in mice fed diets for 2 weeks

	LFWD		HFWD			LFWD + F/S			HFWD + F/S					
Gene	Fold	SE	Fold	SE†	p value	Fold	SE	p value	Fold	SE	p value	Function		
BCL2	1.0	0.06	0.96	0.08	0.835	0.84	0.06	0.088	0.76	0.07	0.020*	Apoptosis		
BCL6	1.0	0.21	0.38	0.10	0.026	0.50	0.11	0.041	0.61	0.21	0.248	Apoptosis		
BNIP3	1.0	0.07	0.88	0.07	0.257	1.06	0.05	0.619	0.90	0.09	0.485	Apoptosis		
FASL	1.0	0.13	0.54	0.13	0.033	0.44	0.08	0.007	0.52	0.08	0.011	Apoptosis		
TNFa	1.0	0.17	0.97	0.25	0.578	0.88	0.25	0.579	1.73	0.51	0.184	Apoptosis		
TNFSF10	1.0	0.10	0.95	0.08	0.618	1.02	0.08	0.952	0.85	0.06	0.157	Apoptosis		
p21	1.0	0.18	1.25	0.29	0.246	2.13	0.62	0.046	1.57	0.31	0.059	Cell cycle (G1/S transition)		
Cyclin D1	1.0	0.13	1.23	0.16	0.265	1.82	0.18	0.001	1.03	0.11	0.893	Cell cycle (G1/S transition)		
p27	1.0	0.04	1.61	0.84	0.560	1.54	0.80	0.407	1.62	0.84	0.585	Cell cycle (G1/S transition)		
GADD45	1.0	0.11	0.59	0.11	0.057	0.72	0.10	0.084	0.57	0.10	0.027	Cell cycle (G2 arrest)/DNA repair		
CEBPb	1.0	0.09	0.80	0.08	0.113	0.91	0.10	0.515	0.73	0.07	0.034	fibrosis		
Collagen 1	1.0	0.13	0.80	0.09	0.148	0.71	0.07	0.041	0.77	0.08	0.104	fibrosis		
Collagen 3	1.0	0.14	0.81	0.09	0.204	0.78	0.09	0.159	0.97	0.11	0.749	fibrosis		
TGFb	1.0	0.05	1.14	0.12	0.154	1.24	0.10	0.043	1.07	0.06	0.353	fibrosis		
Il10	1.0	0.28	0.74	0.28	0.272	0.94	0.34	0.459	1.24	0.45	0.862	fibrosis (anti)		
Il13ra2	1.0	0.14	0.95	0.16	0.696	0.84	0.16	0.428	0.62	0.15	0.207	fibrosis (anti)		
Actin a2	1.0	0.17	1.39	0.23	0.681	1.10	0.23	0.947	1.65	0.29	0.356	fibrosis (pro)		
Agt	1.0	0.11	1.74	0.19	0.001	1.63	0.24	0.014	1.26	0.14	0.143	fibrosis (pro)		
MIP1	1.0	0.18	0.97	0.33	0.743	1.72	0.44	0.095	0.91	0.31	0.851	fibrosis (pro)		
G6P	1.0	0.15	0.95	0.16	0.745	1.31	0.17	0.282	1.20	0.20	0.469	glucose metabolism		
PCK	1.0	0.08	0.64	0.10	0.013	1.00	0.13	0.745	0.67	0.04	0.001	glucose metabolism		
FAS	1.0	0.07	1.48	0.08	0.000	1.69	0.22	0.005	1.33	0.12	0.007	Inflammation		
Il1a	1.0	0.11	1.10	0.12	0.779	0.87	0.09	0.273	0.97	0.10	0.628	Inflammation		
Il1b	1.0	0.20	0.86	0.19	0.694	0.67	0.11	0.144	1.03	0.22	0.956	Inflammation		
PAI-1	1.0	0.16	1.12	0.23	0.768	1.09	0.18	0.884	1.28	0.26	0.462	Inflammation		
IGFBP1	1.0	0.14	0.63	0.15	0.275	1.05	0.23	0.642	0.49	0.14	0.089	insulin/IGF signaling		
PTPB1	1.0	0.10	1.32	0.20	0.068	1.87	0.30	0.007	1.36	0.15	0.040	insulin/IGF signaling		

TRIB3	1.0	0.12	0.64	0.10	0.026	0.53	0.07	0.005	0.45	0.08	0.003	insulin/IGF signaling	
ACC1	1.0	0.08	0.83	0.07	0.130	0.92	0.11	0.704	0.98	0.08	0.782	Lipid metabolism	
Acox1	1.0	0.09	1.95	0.16	0.000	2.05	0.21	0.000	2.00	0.19	0.000	Lipid metabolism	
IRS-2	1.0	0.05	0.82	0.07	0.061	0.95	0.09	0.780	0.72	0.08	0.017	lipid metabolism	
Mttp	1.0	0.06	1.19	0.06	0.010	1.18	0.04	0.006	1.20	0.04	0.001	Lipid metabolism	
PPARa	1.0	0.07	0.99	0.06	0.930	1.04	0.09	0.556	0.96	0.05	0.533	Lipid metabolism	
PGC-1a	1.0	0.09	0.57	0.08	0.008	0.79	0.06	0.036	0.58	0.06	0.001	Lipid metabolism	
Scd1	1.0	0.09	0.53	0.09	0.011	0.88	0.13	0.585	0.99	0.09	0.856	Lipid metabolism	
SREBP-1	1.0	0.11	1.10	0.12	0.582	1.17	0.11	0.400	0.86	0.09	0.280	Lipid metabolism	
SREBP-2	1.0	0.11	1.11	0.17	0.353	1.58	0.27	0.019	1.22	0.14	0.150	Lipid metabolism	
Apo C-III	1.0	0.06	0.92	0.04	0.191	0.94	0.04	0.284	0.86	0.04	0.049	Lipid Metabolism	
Apo E	1.0	0.10	1.35	0.13	0.021	1.46	0.16	0.013	1.03	0.10	0.826	Oxid Stress - Responsive genes	
Hmox1	1.0	0.05	1.29	0.14	0.045	1.18	0.12	0.139	1.28	0.13	0.043	Oxid Stress - Responsive genes	
Cat	1.0	0.04	0.95	0.05	0.462	0.84	0.04	0.032	0.77	0.03	0.002	Oxid Stress - ROS detoxification	
CuZnSOD	1.0	0.04	0.97	0.05	0.660	0.99	0.05	0.920	0.87	0.05	0.078	Oxid Stress - ROS metabolism	
MnSOD	1.0	0.06	1.10	0.05	0.215	1.08	0.06	0.390	0.98	0.06	0.811	Oxid Stress - ROS metabolism	
EC-SOD	1.0	0.05	0.39	0.31	0.895	1.16	0.07	0.063	1.05	0.04	0.478	Oxid Stress - ROS metabolism	
p22 phox	1.0	0.04	1.04	0.09	0.704	1.09	0.11	0.455	0.98	0.08	0.828	Oxid Stress - Superoxide metabolism	
gp91 phox	1.0	0.07	1.02	0.08	0.807	1.06	0.12	0.486	1.02	0.07	0.805	Oxid Stress - Superoxide metabolism	
p47 phox	1.0	0.07	1.26	0.14	0.077	1.39	0.16	0.034	1.25	0.14	0.094	Oxid Stress - Superoxide metabolism	
p67 phox	1.0	0.06	1.10	0.08	0.298	1.18	0.13	0.179	1.21	0.09	0.068	Oxid Stress - Superoxide metabolism	
iNos	1.0	0.20	0.74	0.15	0.215	1.29	0.32	0.543	1.05	0.29	0.912	Oxid Stress - Superoxide metabolism	
Nox4	1.0	0.05	0.84	0.05	0.077	0.89	0.05	0.220	0.76	0.05	0.024	Oxid Stress - Superoxide metabolism	
PKCa	1.0	0.07	0.79	0.07	0.041	0.72	0.06	0.008	0.72	0.06	0.007	PKC isoforms	
PKCb	1.0	0.06	0.82	0.06	0.075	0.73	0.05	0.012	0.84	0.12	0.564	PKC isoforms	
PKCd	1.0	0.06	1.37	0.14	0.017	1.51	0.13	0.001	1.08	0.08	0.488	PKC isoforms	
PKCe	1.0	0.07	1.36	0.09	0.002	1.35	0.11	0.007	1.10	0.07	0.295	PKC isoforms	
PKCq	1.0	0.07	0.92	0.04	0.192	1.05	0.06	0.515	1.05	0.06	0.528	PKC isoforms	
PKCl	1.0	0.09	0.93	0.11	0.667	0.89	0.09	0.370	0.75	0.10	0.113	PKC isoforms	
PKCz	1.0	0.06	1.46	0.07	0.000	1.45	0.10	0.000	1.14	0.05	0.045	PKC isoforms	

†Standard Error (SE)
* $p > 0.05$ are written in red

Supplemental Table 2. Hepatic gene expression in mice fed diets for 12 weeks

	LFWD		HFWD			LFWD + F/S			HFWD + F/S					
Gene	Fold	SE	Fold	SE	p-value	Fold	SE	p-value	Fold	SE	p-value	Function		
BCL2	1.0	0.08	0.92	0.12	0.524	1.16	0.17	0.373	0.90	0.13	0.601	Apoptosis		
BCL6	1.0	0.29	1.46	0.37	0.285	1.39	0.59	0.249	0.68	0.22	0.498	Apoptosis		
BNIP3	1.0	0.14	1.42	0.16	0.042	1.54	0.13	0.002	1.30	0.12	0.072	Apoptosis		
FASL	1.0	0.14	0.37	0.13	0.035	0.74	0.11	0.209	0.74	0.12	0.223	Apoptosis		
TNFa	1.0	0.31	2.03	0.44	0.043	2.24	0.37	0.008	3.54	0.73	0.025	Apoptosis		
TNFSF10	1.0	0.04	1.12	0.08	0.243	0.98	0.05	0.828	0.87	0.07	0.286	Apoptosis		
p21	1.0	0.71	2.59	1.36	0.637	1.23	0.66	0.625	3.75	1.93	0.272	Cell cycle (G1/S transition)		
Cyclin D1	1.0	0.19	0.94	0.18	0.768	0.87	0.17	0.580	1.23	0.24	0.411	Cell cycle (G1/S transition)		
p27	1.0	0.05	1.09	0.06	0.257	1.11	0.06	0.214	0.85	0.04	0.033	Cell cycle (G1/S transition)		
GADD45	1.0	0.19	1.98	0.38	0.036	1.70	0.35	0.139	1.73	0.34	0.117	Cell cycle (G2 arrest)/DNA repair		
CEBPb	1.0	0.14	0.78	0.09	0.152	1.14	0.16	0.479	0.96	0.12	0.906	fibrosis		
Collagen 1	1.0	0.09	1.30	0.18	0.173	1.31	0.20	0.287	3.44	0.48	0.005	fibrosis		
Collagen 3	1.0	0.07	1.45	0.20	0.086	1.13	0.11	0.322	3.57	0.37	0.001	fibrosis		
TGFb	1.0	0.08	1.00	0.06	0.981	1.19	0.08	0.087	1.42	0.10	0.006	fibrosis		
Il10	1.0	0.31	1.37	0.40	0.515	0.96	0.40	0.697	2.12	0.56	0.105	fibrosis (anti)		
Il13ra2	1.0	0.30	1.15	0.37	0.944	2.51	0.83	0.078	0.78	0.27	0.386	fibrosis (anti)		
Actin a2	1.0	0.21	1.66	0.36	0.120	1.04	0.22	0.980	2.03	0.63	0.171	fibrosis (pro)		
Agt	1.0	0.13	1.27	0.13	0.089	1.18	0.11	0.205	1.10	0.12	0.454	fibrosis (pro)		
MIP1	1.0	0.29	1.11	0.53	0.333	0.92	0.27	0.896	3.97	0.93	0.006	fibrosis (pro)		
G6P	1.0	0.10	0.53	0.07	0.003	0.76	0.13	0.440	0.10	0.12	0.002	glucose metabolism		
PCK	1.0	0.18	0.55	0.08	0.018	1.27	0.18	0.277	0.69	0.07	0.033	glucose metabolism		
FAS	1.0	0.09	0.81	0.08	0.137	1.06	0.12	0.695	1.24	0.12	0.113	Inflammation		
Il1a	1.0	0.25	1.03	0.29	0.568	0.87	0.28	0.439	0.98	0.30	0.627	Inflammation		
Il1b	1.0	0.14	1.52	0.28	0.157	0.96	0.18	0.919	3.22	0.81	0.052	Inflammation		
PAI-1	1.0	0.09	0.34	0.31	0.779	0.98	0.09	0.968	1.13	0.14	0.441	Inflammation		
IGFBP1	1.0	0.28	0.52	0.16	0.136	0.97	0.35	0.797	1.27	0.34	0.692	insulin/IGF signaling		
PTPB1	1.0	0.15	0.95	0.10	0.657	0.99	0.12	0.994	0.99	0.13	0.977	insulin/IGF signaling		
TRIB3	1.0	0.11	1.18	0.14	0.273	1.44	0.33	0.171	0.78	0.11	0.300	insulin/IGF signaling		
ACC1	1.0	0.14	1.06	0.11	0.799	0.94	0.10	0.644	0.97	0.19	0.816	Lipid metabolism		
Acox1	1.0	0.18	1.50	0.19	0.033	1.33	0.23	0.276	1.27	0.16	0.214	Lipid metabolism		
IRS-2	1.0	0.11	0.84	0.13	0.262	1.10	0.18	0.783	0.51	0.08	0.009	Lipid metabolism		
Mttp	1.0	0.11	1.20	0.04	0.006	1.21	0.07	0.034	1.04	0.03	0.349	Lipid metabolism		
PPARa	1.0	0.12	1.30	0.11	0.021	1.53	0.14	0.003	1.25	0.13	0.125	Lipid metabolism		
PGC-1a	1.0	0.12	0.71	0.07	0.018	1.32	0.14	0.084	1.03	0.10	0.769	Lipid metabolism		
Scd1	1.0	0.16	1.01	0.18	0.659	1.02	0.17	0.650	1.03	0.17	0.598	Lipid metabolism		

SREBP-1	1.0	0.08	0.94	0.07	0.452	0.84	0.09	0.225	0.63	0.08	0.012	Lipid metabolism	
SREBP-2	1.0	0.13	1.17	0.10	0.205	1.63	0.19	0.016	1.70	0.14	0.000	Lipid metabolism	
Apo C-III	1.0	0.08	1.09	0.05	0.125	1.23	0.05	0.002	1.01	0.06	0.827	Lipid Metabolism	
Apo E	1.0	0.12	1.17	0.11	0.212	1.03	0.10	0.869	0.92	0.09	0.419	Oxid Stress - Responsive genes	
Hmox1	1.0	0.14	1.06	0.09	0.653	1.21	0.11	0.146	1.56	0.21	0.052	Oxid Stress - Responsive genes	
Cat	1.0	0.07	1.17	0.08	0.110	1.53	0.11	0.001	1.12	0.12	0.373	Oxid Stress - ROS detoxification	
CuZnSOD	1.0	0.08	1.17	0.06	0.039	1.20	0.07	0.036	0.93	0.06	0.485	Oxid Stress - ROS metabolism	
MnSOD	1.0	0.10	1.07	0.08	0.524	1.13	0.10	0.283	0.95	0.07	0.501	Oxid Stress - ROS metabolism	
EC-SOD	1.0	0.11	1.16	0.09	0.174	1.21	0.09	0.128	1.57	0.14	0.007	Oxid Stress - ROS metabolism	
p22 phox	1.0	0.09	0.94	0.06	0.493	0.94	0.08	0.711	1.16	0.07	0.098	Oxid Stress - Superoxide metabolism	
gp91 phox	1.0	0.12	0.89	0.08	0.340	1.15	0.12	0.315	1.35	0.13	0.034	Oxid Stress - Superoxide metabolism	
p47 phox	1.0	0.13	0.88	0.09	0.353	1.10	0.12	0.518	1.23	0.11	0.102	Oxid Stress - Superoxide metabolism	
p67 phox	1.0	0.11	1.03	0.07	0.759	1.09	0.10	0.482	1.43	0.13	0.018	Oxid Stress - Superoxide metabolism	
iNos	1.0	0.30	1.16	0.19	0.425	0.92	0.14	0.893	1.35	0.19	0.125	Oxid Stress - Superoxide metabolism	
Nox4	1.0	0.09	1.01	0.08	0.861	1.25	0.08	0.034	0.62	0.07	0.006	Oxid Stress - Superoxide metabolism	
PKCa	1.0	0.02	1.08	0.06	0.349	1.15	0.08	0.148	1.40	0.12	0.028	PKC isoforms	
PKCb	1.0	0.10	1.10	0.07	0.295	1.32	0.13	0.074	1.36	0.10	0.011	PKC isoforms	
PKCd	1.0	0.12	1.02	0.09	0.957	1.04	0.10	0.825	0.98	0.10	0.820	PKC isoforms	
PKCe	1.0	0.11	1.27	0.10	0.046	1.31	0.10	0.026	1.16	0.14	0.290	PKC isoforms	
PKCq	1.0	0.09	1.09	0.08	0.386	1.20	0.10	0.111	1.11	0.09	0.323	PKC isoforms	
PKCl	1.0	0.12	1.12	0.11	0.363	1.56	0.16	0.019	1.14	0.09	0.261	PKC isoforms	
PKCz	1.0	0.07	0.93	0.09	0.614	0.91	0.06	0.281	0.69	0.05	0.003	PKC isoforms	

†Standard Error (SE)
* $p > 0.05$ are written in red

Supplemental Table 3. Adipose tissue gene expression in mice fed diets for 2 weeks

	LFWD 2 wk		HFWD 2 wk			LFWD + S 2 wk			HFWD + S 2 wk			
Gene	Fold	SE	Fold	SE	p-value	Fold	SE	p-value	Fold	SE	p-value	Function
Adipoq	1.0	0.09	1.74	0.19	0.007	1.23	0.21	0.300	1.22	0.12	0.365	Adipokines
Bcl2l11	1.0	0.11	1.83	0.33	0.029	3.24	1.13	0.036	1.84	0.47	0.055	Apoptosis
Bcl6	1.0	0.13	1.22	0.14	0.361	0.65	0.13	0.117	1.05	0.16	0.755	Apoptosis
Bnip3	1.0	0.09	1.86	0.29	0.003	2.01	0.29	0.001	1.31	0.26	0.156	Apoptosis
Fasn	1.0	0.28	0.35	0.05	0.000	0.65	0.15	0.214	0.35	0.02	0.000	Apoptosis
Tnfsf10	1.0	0.10	1.08	0.14	0.617	1.60	0.38	0.040	1.06	0.16	0.608	Apoptosis
Cyclin D1	1.0	0.16	1.74	0.32	0.138	2.86	0.74	0.010	1.59	0.33	0.188	Cell Cycle
p21	1.0	0.12	1.75	0.24	0.006	0.75	0.09	0.128	2.72	0.25	0.000	Cell Cycle
p27	1.0	0.06	1.42	0.19	0.043	2.01	0.41	0.013	1.10	0.22	0.386	Cell Cycle
Gadd45a	1.0	0.09	1.74	0.17	0.002	1.91	0.28	0.002	1.46	0.14	0.025	Cell Cycle
Cebpa	1.0	0.07	1.12	0.19	0.241	1.48	0.43	0.076	0.87	0.13	0.807	Differentiation
Cebpb	1.0	0.08	1.11	0.12	0.366	0.86	0.06	0.188	1.03	0.05	0.883	Differentiation
Pparg	1.0	0.07	1.34	0.16	0.025	1.98	0.57	0.024	1.03	0.16	0.557	Differentiation
Srebf1	1.0	0.09	0.90	0.08	0.353	0.57	0.17	0.131	0.70	0.08	0.016	Differentiation
Agt	1.0	0.12	1.39	0.23	0.363	0.55	0.24	0.609	0.94	0.16	0.700	Inflammation
MIP1a	1.0	0.17	1.39	0.31	0.580	1.55	0.45	0.283	1.23	0.35	0.574	Inflammation
Il1b	1.0	0.16	1.43	0.33	0.430	1.69	0.38	0.191	1.47	0.28	0.413	Inflammation
Il6	1.0	0.16	2.49	0.95	0.026	3.11	0.89	0.006	2.11	0.50	0.026	Inflammation
PAI-1	1.0	0.21	1.60	0.32	0.233	1.91	0.43	0.062	1.56	0.49	0.136	Inflammation
Tnfa	1.0	0.13	1.33	0.19	0.456	0.69	0.21	0.313	1.54	0.24	0.119	Inflammation
Acaca	1.0	0.13	0.28	0.06	0.000	0.52	0.07	0.002	0.21	0.02	0.000	Lipogenesis
Acox1	1.0	0.07	1.25	0.14	0.069	1.26	0.12	0.045	0.98	0.08	0.870	Lipogenesis
Dgat1	1.0	0.09	1.21	0.08	0.170	0.94	0.14	0.820	0.87	0.08	0.262	Lipogenesis
Fabp4	1.0	0.06	1.73	0.21	0.002	3.11	1.15	0.027	1.39	0.31	0.093	Lipogenesis
Fasl	1.0	0.14	2.23	0.74	0.405	4.26	1.82	0.080	1.55	0.60	0.559	Lipogenesis
Gpam	1.0	0.10	0.73	0.08	0.025	0.65	0.05	0.002	0.45	0.02	0.000	Lipogenesis
Scd1	1.0	0.11	0.72	0.10	0.056	1.13	0.24	0.282	0.51	0.08	0.002	Lipogenesis
Srebf2	1.0	0.12	1.24	0.19	0.471	0.56	0.30	0.969	0.93	0.18	0.792	Lipogenesis
Irf4	1.0	0.24	1.01	0.24	0.797	0.87	0.24	0.674	0.85	0.14	0.466	Lipolysis
Pnpla2	1.0	0.09	0.91	0.12	0.666	0.78	0.09	0.144	0.59	0.05	0.002	Lipolysis
Sirt1	1.0	0.07	1.55	0.15	0.011	2.02	0.32	0.002	1.23	0.15	0.230	Lipolysis
Acacb	1.0	0.11	0.39	0.07	0.001	0.44	0.08	0.002	0.24	0.02	0.000	Lipid Oxidation
Cpt1a	1.0	0.06	1.89	0.19	0.001	1.68	0.34	0.059	1.75	0.26	0.010	Lipid Oxidation
Pdk4	1.0	0.08	1.34	0.23	0.135	1.86	0.43	0.010	1.15	0.16	0.398	Lipid Oxidation
Ppara	1.0	0.09	0.87	0.13	0.506	0.82	0.17	0.591	0.58	0.07	0.011	Lipid Oxidation
Ppargc1a	1.0	0.12	1.10	0.19	0.924	1.19	0.17	0.763	0.76	0.12	0.245	Lipid Oxidation
Cat	1.0	0.07	1.51	0.20	0.010	1.85	0.41	0.014	1.29	0.21	0.110	Oxidative Stress
p22 phox	1.0	0.07	1.98	0.24	0.002	1.78	0.23	0.011	1.98	0.42	0.023	Oxidative Stress

gp91 phox	1.0	0.08	1.69	0.15	0.001	1.84	0.20	0.001	1.33	0.17	0.073	Oxidative Stress
Gclc	1.0	0.11	1.45	0.17	0.135	2.18	0.44	0.007	1.36	0.26	0.202	Oxidative Stress
Gpx1	1.0	0.09	1.97	0.38	0.008	3.40	1.20	0.019	1.76	0.49	0.064	Oxidative Stress
Gsr	1.0	0.08	1.29	0.13	0.119	0.96	0.23	0.687	1.00	0.10	0.944	Oxidative Stress
Hmox1	1.0	0.08	1.52	0.15	0.022	1.47	0.13	0.033	1.64	0.16	0.005	Oxidative Stress
Ncf1	1.0	0.09	1.76	0.21	0.007	1.70	0.32	0.028	1.63	0.23	0.016	Oxidative Stress
Ncf2	1.0	0.34	1.84	0.36	0.696	2.08	0.64	0.343	1.73	0.43	0.613	Oxidative Stress
Nfe2l2	1.0	0.07	1.61	0.16	0.004	1.82	0.21	0.001	1.36	0.12	0.040	Oxidative Stress
Nos2	1.0	0.09	1.14	0.15	0.297	0.81	0.10	0.162	0.68	0.10	0.018	Oxidative Stress
Sod1	1.0	0.07	2.58	1.40	0.131	2.40	0.65	0.014	1.25	0.29	0.199	Oxidative Stress
Sod2	1.0	0.08	1.41	0.20	0.047	2.53	0.90	0.027	1.61	0.33	0.042	Oxidative Stress
PKCa	1.0	0.09	1.66	0.17	0.001	2.07	0.38	0.003	1.40	0.15	0.028	PKC isoforms
PKCb	1.0	0.06	1.17	0.18	0.313	1.92	0.48	0.037	1.24	0.21	0.206	PKC isoforms
PKCd	1.0	0.09	1.89	0.28	0.007	1.35	0.20	0.180	1.77	0.20	0.007	PKC isoforms
PKCe	1.0	0.08	0.92	0.11	0.705	0.75	0.10	0.073	0.61	0.04	0.000	PKC isoforms
PKCq	1.0	0.10	1.74	0.30	0.019	1.97	0.34	0.004	1.31	0.21	0.360	PKC isoforms
PKCl	1.0	0.20	2.26	1.13	0.052	1.32	0.23	0.861	1.18	0.26	0.910	PKC isoforms
PKCz	1.0	0.25	1.71	0.44	0.493	1.98	0.57	0.252	1.50	0.37	0.637	PKC isoforms
GLUT4	1.0	0.11	0.67	0.09	0.012	0.58	0.06	0.000	0.41	0.05	0.000	Signaling
Trib3	1.0	0.10	0.92	0.16	0.923	0.79	0.11	0.205	0.70	0.07	0.038	Signaling

†Standard Error (SE)
* $p > 0.05$ are written in red

Supplemental Table 4. Adipose tissue gene expression in mice fed diets for 12 weeks

	LFWD 2 wk		HFWD 2 wk			LFWD + S 2 wk			HFWD + S 2 wk			
Gene	Fold	SE	Fold	SE	p-value	Fold	SE	p-value	Fold	SE	p-value	Function
Adipoq	1.0	0.15	0.86	0.13	0.405	0.92	0.16	0.669	0.43	0.06	0.004	Adipokines
Bcl2l11	1.0	0.08	1.80	0.33	0.053	1.09	0.19	0.757	2.24	0.45	0.056	Apoptosis
Bcl6	1.0	0.30	1.01	0.20	0.845	0.75	0.19	0.483	0.98	0.18	0.658	Apoptosis
Bnip3	1.0	0.13	1.04	0.20	0.873	1.14	0.23	0.821	0.74	0.14	0.175	Apoptosis
Fasn	1.0	0.21	0.37	0.05	0.002	0.72	0.14	0.278	0.32	0.05	0.001	Apoptosis
Tnfsf10	1.0	0.19	1.16	0.18	0.535	1.24	0.26	0.304	1.20	0.21	0.438	Apoptosis
Cyclin D1	1.0	0.18	1.32	0.21	0.210	1.04	0.16	0.808	1.96	0.34	0.025	Cell Cycle
p21	1.0	0.31	2.61	0.43	0.001	1.06	0.21	0.916	2.20	0.38	0.005	Cell Cycle
p27	1.0	0.14	1.17	0.12	0.287	0.98	0.19	0.779	1.04	0.10	0.840	Cell Cycle
Gadd45a	1.0	0.15	1.28	0.07	0.007	1.03	0.13	0.650	1.10	0.12	0.451	Cell Cycle
Cebpa	1.0	0.13	0.78	0.07	0.097	0.92	0.09	0.570	0.67	0.07	0.025	Differentiation
Cebpb	1.0	0.22	0.94	0.10	0.557	0.77	0.11	0.159	1.16	0.13	0.355	Differentiation
Pparg	1.0	0.09	0.83	0.10	0.264	0.96	0.11	0.642	0.66	0.09	0.056	Differentiation
Srebf1	1.0	0.14	0.78	0.08	0.085	0.78	0.07	0.072	0.51	0.06	0.002	Differentiation
Agt	1.0	0.18	0.51	0.11	0.040	0.82	0.19	0.693	0.19	0.04	0.001	Inflammation
MIP1a	1.0	0.27	5.24	1.33	0.014	1.13	0.26	0.599	16.99	3.88	0.003	Inflammation
Il1b	1.0	0.17	2.19	0.34	0.005	1.15	0.23	0.390	2.60	0.65	0.024	Inflammation
Il6	1.0	0.15	1.40	0.31	0.233	0.66	0.11	0.081	2.00	0.59	0.121	Inflammation
PAI-1	1.0	0.43	0.70	0.24	0.237	1.01	0.43	0.855	1.88	0.64	0.385	Inflammation
Tnfa	1.0	0.26	2.76	0.62	0.024	0.95	0.16	0.810	4.83	1.12	0.012	Inflammation
Acaca	1.0	0.15	0.33	0.04	0.000	0.84	0.13	0.469	0.26	0.04	0.000	Lipogenesis
Acox1	1.0	0.15	1.15	0.12	0.302	1.01	0.14	0.789	0.92	0.11	0.657	Lipogenesis
Dgat1	1.0	0.13	0.89	0.12	0.461	0.91	0.11	0.410	0.69	0.09	0.069	Lipogenesis
Fabp4	1.0	0.11	1.23	0.24	0.825	1.20	0.24	0.872	0.78	0.17	0.296	Lipogenesis
Fasl	1.0	0.22	1.08	0.25	0.891	0.63	0.20	0.370	1.57	0.35	0.203	Lipogenesis
Gpam	1.0	0.19	0.65	0.09	0.023	0.87	0.10	0.411	0.51	0.06	0.001	Lipogenesis
Scd1	1.0	0.08	0.63	0.12	0.098	0.97	0.11	0.628	0.22	0.06	0.002	Lipogenesis
Srebf2	1.0	0.18	1.46	0.15	0.050	0.84	0.12	0.503	1.46	0.19	0.046	Lipogenesis
Irf4	1.0	0.26	0.99	0.13	0.872	0.94	0.36	0.513	0.76	0.11	0.189	Lipolysis
Pnpla2	1.0	0.23	0.81	0.14	0.347	0.95	0.19	0.979	0.50	0.08	0.006	Lipolysis
Sirt1	1.0	0.11	1.13	0.12	0.452	0.96	0.15	0.892	1.01	0.12	0.985	Lipolysis
Acacb	1.0	0.13	0.57	0.11	0.059	1.09	0.24	0.707	0.45	0.08	0.018	Oxidation
Cpt1a	1.0	0.19	1.38	0.11	0.013	0.96	0.17	0.865	1.82	0.17	0.001	Oxidation
Pdk4	1.0	0.26	2.69	0.49	0.003	1.71	0.47	0.096	2.06	0.35	0.010	Oxidation
Ppara	1.0	0.15	0.60	0.09	0.016	0.84	0.12	0.338	0.47	0.09	0.012	Oxidation
Ppargc1a	1.0	0.18	0.83	0.17	0.356	1.19	0.26	0.759	0.85	0.20	0.598	Oxidation

Cat	1.0	0.11	1.07	0.15	0.794	1.11	0.14	0.656	0.86	0.12	0.366	Oxidative Stress
p22 phox	1.0	0.15	2.79	0.41	0.003	0.96	0.15	0.884	4.51	1.01	0.019	Oxidative Stress
gp91 phox	1.0	0.21	2.52	0.38	0.005	0.85	0.19	0.782	4.14	0.83	0.005	Oxidative Stress
Gclc	1.0	0.12	1.14	0.14	0.489	1.05	0.15	0.762	0.99	0.13	0.869	Oxidative Stress
Gpx1	1.0	0.11	1.43	0.24	0.227	1.16	0.26	0.621	1.21	0.27	0.551	Oxidative Stress
Gsr	1.0	0.16	1.18	0.09	0.139	0.94	0.11	0.816	1.04	0.08	0.681	Oxidative Stress
Hmox1	1.0	0.20	2.17	0.38	0.050	1.01	0.20	0.615	3.90	0.45	0.000	Oxidative Stress
Ncf1	1.0	0.26	2.40	0.44	0.025	0.83	0.22	0.695	3.47	0.75	0.007	Oxidative Stress
Ncf2	1.0	0.18	2.97	0.45	0.004	0.96	0.14	0.899	4.43	0.98	0.023	Oxidative Stress
Nfe2l2	1.0	0.17	1.30	0.12	0.040	0.92	0.13	0.774	1.31	0.15	0.083	Oxidative Stress
Nos2	1.0	0.19	0.95	0.09	0.706	0.95	0.10	0.734	0.87	0.14	0.710	Oxidative Stress
Sod1	1.0	0.07	1.02	0.18	0.755	1.08	0.19	0.937	0.65	0.12	0.130	Oxidative Stress
Sod2	1.0	0.11	1.44	0.19	0.097	0.95	0.11	0.622	1.27	0.18	0.264	Oxidative Stress
PKCa	1.0	0.16	0.98	0.10	0.963	1.00	0.11	0.826	0.53	0.05	0.000	PKC isoforms
PKCb	1.0	0.15	1.93	0.26	0.022	0.88	0.14	0.680	3.65	0.63	0.003	PKC isoforms
PKCd	1.0	0.17	2.18	0.33	0.008	0.87	0.10	0.393	2.71	0.52	0.023	PKC isoforms
PKCe	1.0	0.21	0.81	0.08	0.122	0.96	0.15	0.992	0.76	0.12	0.219	PKC isoforms
PKCq	1.0	0.15	1.07	0.06	0.427	1.06	0.14	0.449	0.73	0.04	0.002	PKC isoforms
PKCl	1.0	0.32	1.87	0.45	0.310	0.78	0.27	0.535	1.71	0.44	0.432	PKC isoforms
PKCz	1.0	0.38	1.22	0.34	0.728	1.06	0.36	0.776	0.81	0.24	0.682	PKC isoforms
GLUT4	1.0	0.18	0.69	0.10	0.064	0.80	0.05	0.027	0.32	0.05	0.000	Signaling
Trib3	1.0	0.19	1.16	0.11	0.284	1.20	0.21	0.228	1.22	0.12	0.155	Signaling

†Standard Error (SE)
* $p > 0.05$ are written in red